Fatty acid ethanolamine derivatives: metabolism and function

Nahed Sail Alharthi, MSc.

Thesis submitted to the University of Nottingham for the degree of Doctor of Philosophy

December 2018

Abstract

Anandamide is the most recognised member of the *N*-acylethanolamines, NAEs group. It was the first identified endogenous cannabinoid and TRPV1 agonist as well as acting through PPARs. A wide range of endogenous NAE analogues has been detected in tissues and shown to play a role in many physiological properties. The main aim of this thesis was to investigate the profile of a series of saturated, monounsaturated and polyunsaturated NAEs as substrates for FAAH and to investigate their actions on cannabinoids, TRPV1 and PPARs receptors in *vitro*.

A novel nonradioactive assay was optimised and utilised for measurement of FAAH activity based on ethanolamine detection produced from hydrolysis of NAEs in rat liver microsomal preparations. CHO cells stably transfected with human recombinant CB_1 and CB_2 receptors were exposed to NAEs in rapid response assays, such as ERK phosphorylation and $[Ca^{2+}]_i$. This range of NAEs was also tested in DRG neurons using a calcium imaging technique. Selected NAEs were investigated for potential modulatory effects on inflammatory markers.

In the FAAH assay, the majority of n-3 and n-6 NAEs showed high affinities and maximal rates of hydrolysis while the saturated and monounsaturated NAEs examined all exhibited low affinities and slower rates of hydrolysis. In signal transduction assays of CB receptor activation, the n-6 NAEs of C20:4, C22:5 and C22:4 elicited responses in both ERK and calcium ion assays of CB_1 and CB_2 receptor while n-3 NAEs activated CB_2 receptors in calcium ion assay. Both n-6 and n-3 but not saturated or monounsaturated NAEs, were able to elicit calcium responses in rat DRG neurones, which were inhibited in the presence of capsazepine. Besides these, n-3 NAE derivatives (including C22:5 and C20:5) and n-6 NAE derivatives (including C20:4 and C22:5) as well as PEA inhibited LPS elevation of IL-1β expression in human immune cells. The PEA effect was blocked by GW6471 a PPARα antagonist in human monocytes.

The data presented demonstrate that saturated and monounsaturated NAEs appear inactive as endocannabinoids or endovanilloids (at least, under the conditions assessed here) and their relatively high levels in tissues may result from their low affinity and

slow rates of hydrolysis compared to the n-3 and n-6 PUFA NAEs. The n-6 NAEs as C22:4 and C22:5 as well as C20:4 appear to be ‘genuine’ endocannabinoids and endovanilloids. The n-3 NAEs are less effective at CB_1 receptors but seem to be equally effective as the n-6 NAE at CB_2 cannabinoids receptors, suggesting they act as endocannabinoids with a CB_2 preference as well as endovanilloids. Therefore, the anti-inflammatory properties of n-3NAEs may be mediated by CB_2 receptors. A resulting hypothesis from these studies is that part of the beneficial effect of long-term dietary intake of n-3 PUFAs may result, at least in part, from a selective activation of CB_2 receptors compared to CB_1 receptors.

Declaration

The research presented in this thesis is a bona fide original work carried out by the author: .Nahed Sail Alharthi, at the University of Nottingham. All the experiments were performed by the author under supervision of Dr. Stephen Alexander and Dr Andrew Bennett, at the University of Nottingham, UK.

Acknowledgements

- **Dr. Stephen Alexander**, who provided constant guidance, laboratory support and encouragement throughout all stages of this study.

- **Dr. Andrew Bennett**, who provided guidance, support and encouragement during the study.

- **Dr. Luisa Martínez-Pomares**, who gave me access to her laboratory and research facilities to conduct part of my work.

- **Dr. Michael Garle, Paul Millns and Mrs Monika Owen**, Faculty of Medicine and Health Sciences, Queen's Medical Centre at University of Nottingham, for their technical support.

- **Prince Sattam bin Abdulaziz University**, for their financial support for this project.

- All colleagues who have directly or indirectly contributed to this research.

- Finally, I am sincerely grateful to my mother who give me a great support and encouragement and my dear brother and sisters who stood beside me and gave me love and support.

Dissemination of Results

Poster

N Alharthi, MJ Garle, SPH Alexander (2014). **A novel fluorescence-based assay for fatty acid amide hydrolase activity based on quantification of ethanolamine production**. *British Pharmacological Society winter Meeting* 14-18th December 2014 London- UK.

N Alharthi, MJ Garle, SPH Alexander (2015). **Novel fluorescence-based assay for amide hydrolysis: anandamide and N-arachidonoyl-glycine as substrates**. *International Cannabinoid Research Society Meeting* 28th June-3rd July 2015 Halifax-Canada.

N Alharthi, SPH Alexander (2015). **Polyunsaturated fatty acid ethanolamines may be hydrolysed by Fatty Acid Amide Hydrolase**. *British Pharmacological Society winter Meeting* 15th -17th December 2015 London- UK.

N Alharthi, SPH Alexander (2016). **Polyunsaturated fatty acid ethanolamines as endogenous cannabinoids**. *International Cannabinoid Research Society Meeting* 27th -30rd June 2016 Bukowina Tatrzańska-Poland.

N Alharthi, SPH Alexander (2017). **PUFA N-acylethanolamines increase intracellular calcium through cannabinoid and TRPV1 receptors**. 8th European workshop on *Cannabinoid research* 31 August-2nd September 2017, University of Roehampton –London.

Article

Nahed Alharthi, Peter Christensen, Wafa Hourani, Catherine Ortori, David A Barrett, Andrew J Bennett, Victoria Chapman and Stephen PH Alexander (2018). **n-3 polyunsaturated N-acylethanolamines as are CB_2 cannabinoid receptor-preferring metabolites endocannabinoids.**
This article has been puplished to the Molecular and Lipid Metabolism section of Biochimica et Biophysica Acta.

Contents

Declaration III
Acknowledgements IV
Dissemination of Results V
Contents VI
List of figures XI
List of tables XIV
Abbreviation XV

Chapter 1-General introduction

1.1 Cannabis 1
1.2 Cannabinoid Receptor Ligands 2
1.2.1 Classical Cannabinoids 2
1.2.2 Non-Classical Cannabinoids 2
1.2.3 Aminoalkylindoles 3
1.2.4 Diarylpyrazoles 3
1.2.5 Endogenous Ligands 5
1.2.6 Biosynthesis 7
1.2.7 Catabolism and Transformation 9
1.2.7.1 Fatty Acid Amide Hydrolase 9
1.2.7.2 Other Hydrolytic Enzymes 10
1.2.7.3 FAAH Inhibitors 11
1.2.7.4 Clinical evaluation of FAAH inhibitors 13
1.2.7.5 Oxidative Metabolism 15
1.3 Molecular Targets of Anandamide 17
1.3.1 Cannabinoid Receptors 17
1.3.2 Transient Receptor Potential Vanilloid 1 24
1.3.3 Peroxisome proliferator-activated receptor 26
1.4 Other Bioactive N-acylethanolamines 29
1.4.1 n-6 Fatty Acid Derivatives of Ethanolamine 29
1.4.1 n-3 Fatty acid Derivatives of Ethanolamine 31
1.4.2 Monounsaturated and Saturated Fatty acid Derivatives of Ethanolamine 33

1.5 Aims and Objectives of the Project 36

Chapter 2-Methods and Materials

2.1 Materials 37

2.1.1 Chemicals 37

2.1.2 Antibodies and Enzymes 37

2.1.3 Vectors and Primers 38

2.2 Methods 39

2.2.1 Measurement of FAAH activity 39

2.2.1.1 Assay Development 39

2.2.1.2 Tissue preparation 39

2.2.1.3 Assay application 40

2.2.2 Validation 42

2.2.3 Intracellular signalling assay 43

2.2.3.1 Chinese Hamster Ovary culture 43

2.2.3.2 In-cell Western assay 44

2.2.3.3 Intracellular calcium FlexStation 45

2.2.3.4 Intracellular calcium imaging 46

2.2.3.4.1 Dorsal root ganglia (DRG) cell culture 46

2.2.3.4.2 Calcium imaging 47

2.2.4 Cloning and protein expression 48

2.2.4.1 Designing the cloning primers 48

2.2.4.2 Polymerase Chain Reaction 50

2.2.4.3 Agarose gel electrophoresis 50

2.2.4.4 Digestion and ligation of DNA into vector 50

2.2.4.5 Bacterial Culture 51

2.2.5 Cyclooxygenase activity measurement 55

2.2.6 Transient transfection and luciferase report gene assay 57

2.2.7 Gene expression for inflammatory cytokines 58

2.2.7.1 Isolation of peripheral blood mononuclear cells (PBMCs) from human blood 58

2.2.7.1.1 Monocyte purification 59

2.2.7.1.2 Monocyte and macrophage culture and treatment 59

2.2.7.2 Quantitative Real Time PCR (q-PCR) 60
2.2.7.2.1 RNA extraction 60
2.2.7.2.2 Complementary DNA synthesis 61
2.2.7.2.3 Pre-amplification procedure 61
2.2.7.2.4 Primer and probe design 62
2.2.7.2.5 TaqMan real-time quantitative PCR 64
2.2.8 Nitric oxide measurement 65
2.3 Statistical and Data analysis 66

Chapter 3-Development of a novel fluorescence assay based on quantification of ethanolamine to measure activity of FAAH enzyme

3.1 Introduction 67
3.1.1 FAAH enzyme activity measurements 69
3.2 Aim 71
3.3 Results 72
3.3.1 FAAH assay development 72
3.3.1.1 Measurement of ethanolamine 72
3.3.1.2 Optimization of ethanolamine quantification 74
3.3.1.3 Application of assay 79
3.3.2 Assay validation 85
3.3.3 FAAH-mediated hydrolysis of fatty acid ethanolamines 87
3.4 Quantification of amino acids 92
3.5 Discussion 95
3.6 Conclusion 102

Chapter 4-Functional effects of fatty acid ethanolamines at human CB_1 and CB_2 cannabinoid receptors

4.1 Introduction 103
4.2 Aim 106
4.3 Results 107
4.3.1 Investigation of ERK phosphorylation in human CB_1 transfected CHO cells 107
4.3.2 Investigation of intracellular calcium mobilisation in CHO-hCB_1 cells 115

4.3.2.1 Effect of an allosteric modulator of CB_1 receptors on intracellular calcium…….....124

4.3.3 Effects of fatty acid ethanolamine ligands on intracellular calcium mobilisation in human CB_2-transfected CHO cells 126

4.3 Discussion.....136

4.4 Conclusion 141

Chapter 5-Functional effects of fatty acid ethanolamines at rat transient receptor potential vanilloid 1 (TRPV1) channels

5.1 Introduction.....142

5.2 Aim 143

5.3 Results.....144

5.3.1 Effects of fatty acid ethanolamine ligands on intracellular calcium responses in DRG neuros.....144

5.3.1.2 Effect of a TRPV1 antagonist on fatty acid ethanolamine induced increases in intracellular calcium in rat DRG neurons.....156

5.4 Discussion.....164

5.5 Conclusion 168

Chapter 6-Expression of human recombinant peroxisome proliferator-activated receptors (PPARs)

6.1 Introduction.....169

6.2 Aim 171

6.3 Results.....172

6.3.1 Construction of pET28a(+)-human PPAR-LBD 172

6.3.2 Protein expression and solubility test 176

6.4 Discussion.....181

Chapter 7-Evaluation of fatty acid ethanolamine ligands in an immune system model *in vitro*

7.1 Introduction.....183

7.2 Aim 184

7.3 Results.....185

7.3.1 Fatty acid ethanolamine ligands effects on inflammatory markers.....185

7.3.1.1 Human iNOS activity in mouse macrophage cells.....185

7.3.1.2 Inflammatory markers in primary human cells 192

7.3.1.2.1 Measurement of Nitric oxide 192
7.3.1.2.2 Cytokines gene expression 195
7.3.2 Cyclooxygenase-2 activity 205
7.4 Discussion 207
7.4.1 Effect of NAEs on human iNOS activity in RAW246.7 cells 207
7.4.2 Effect of NAEs on NO production and cytokine expression in human monocytes and macrophages 209
7.5 Conclusion 211
Chapter 8-General Discussion
8.1 Discussion 212
8.2 Future directions and points to consider 216
8.3 Conclusion 217
Chapter 9-Appendices
9.1 Effect of URB597 on FAAH-catalysed hydrolysis of fatty acids ethanolamine 218
9.2 ERK phosphorylation assay optimisation 219
9.3 COX activity assay optimisation 221
10 References 225

List of figures

Figure 1.1 Structures of several example cannabinoid receptor ligands from classical, non-classical, aminoalkylindoles and diarylpyrazoles classes. 4
Figure 1.2 Chemical structures of the two main endocannabinoids that have been widely studied. 5
Figure 1.3 The major pathway for biosynthesis of AEA in the cell membrane. 8
Figure 1.4 Chemical structure of URB597 12
Figure 1.5 Oxidative metabolism of AEA by cyclooxygenase-2 and lipoxygenase (12- and 15-LOX) 15
Figure 1.7 Chemical structure of Organon compounds positive allosteric modulators 23
Figure 1.8 Structure of peroxisome proliferator–activated receptors 27
Figure 1.10 Chemical structures of n-6 fatty acid derivatives of ethanolamine 31
Figure 1.11 Chemical structures of n-3 fatty acid derivatives of ethanolamine 33
Figure 2.1 pEt28a(+) vector (Invitrogen) 38
Figure 2.2 pcDNA3.1/Zeo vectors circle map (Invitrogen) 38
Figure 2.3 TaqMan Real-time PCR standard curve for reference gene. RNA polymerase in human monocytes 65
Figure 3.1 Effect of URB597 (0.3 mg/kg, single dose) on the levels of NAEs using LC-MS in lung and testes of rat 68
Figure 3.2 Anandamide hydrolysis by fatty acid amide hydrolase (FAAH) 70
Figure 3.3 Quantification of ethanolamine and ammonium sulphate using NDC as fluorescent reagent. 73
Figure 3.4 Stability of fluorescence production of ethanolamine reaction over time. 74
Figure 3.5 Effects of different dilutions of stopping reagents (PCA and TCA) on ethanolamine quantification. 76
Figure 3.6 Effect of pH of borate developing buffer on the quantification of ethanolamine. . 78
Figure 3.7 Time course of FAAH activity in rat liver microsomes. 80
Figure 3.8 (A) The effect of BSA on FAAH-catalysed hydrolysis of PEA at 8 μM in rat liver microsomal preparations. 81
Figure 3.9 The effect of protein concentration on FAAH-catalysed hydrolysis in different rat liver microsomal preparations. 83
Figure 3.10 Hydrolysis of AEA by rat liver microsomes 84
Figure 3.11 Radiometric assay used in inhibition of FAAH activity-catalysed by AEA in rat liver microsomal at 10 μg/ml. 86
Figure 3.12 N-acylethanolamines hydrolysis in rat liver microsomes (A) n-6 NAEs (B) n-3 NAEs (C) n-9 and saturated NAEs. 88
Figure 3.13 Concentration-dependence of URB597 inhibition of fatty acid ethanolamine hydrolysis by rat liver microsomes. 91
Figure 3.14 Representative standard curve of glycine. 92
Figure 4.1 Time course of ERK phosphorylation induced by cannabinoid agonists in CHO-hCB_1cells 108
Figure 4.2 Immunofluorescence images showing the effect of fatty acids ethanolamine ligands at 10 μM on ERK phosphorylation in in CHO-hCB_1 cells. 110
Figure 4.3 Effect of fatty acid ethanolamine ligands on ERK phosphorylation in CHO-hCB_1 cells. 111
Figure 4.4 The effect of the CB_1 antagonist AM251 on fatty acid ethanolamine-induced increases in ERK phosphorylation. 113
Figure 4.5 Inhibition of fatty acid ethanolamine ligand-induced increases in ERK phosphorylation in CHO-hCB_1 in the presence of PTX. 114
Figure 4.6 Effect of BSA upon agonist-evoked calcium mobilisation 115

Figure 4.7 Representative curves showing the time courses of intracellular calcium mobilisation responses to the positive controls (HU210, ATP), agonist ligands of n-6 PUFA-ethanolamides and vehicle (ethanol and DMSO)..... 117
Figure 4.8 Changes in intracellular Ca^{2+} levels stimulated by fatty acids ethanolamine ligands in CHO-hCB_1 cells..... 119
Figure 4.9 The effect of the CB_1 antagonist AM251 on intracellular calcium mobilisation in response to agonist stimulation of CHO-hCB_1 cells..... 120
Figure 4.11 Inhibition of n-6 fatty acid ethanolamines and HU210 induced Ca^{2+} elevation by pertussis toxin in CHO-hCB_1 cells..... 123
Figure 4.12 Effect of a CB_1 positive allosteric modulator on intracellular Ca^{2+} mobilisation peak (A) and area under the curve (B) responses in CHO-hCB_1. 125
Figure 4.13 Representative curves showing the time courses of intracellular calcium mobilisation responses to the positive controls (JWH015, ATP), n-6 NAEs and ethanol as vehicle (A) and n-3 NAEs (B) 128
Figure 4.14 The maximum peak of intracellular Ca^{2+} mobilisation stimulation in response to fatty acid ethanolamines dissolved in ethanol (A) and DMSO (B) in CHO-hCB_2. 129
Figure 4.15 Inhibition of fatty acid ethanolamine ligands induced intracellular calcium mobilisation using CB_2 antagonist in CHO-hCB_2 cells. 132
Figure 4.16 Effect of CB_2 antagonist (AM630) on the latency to peak of calcium mobilisation response to activation CHO-hCB_2 cells stimulated by tested NAEs ligands. 134
Figure 4.17 Intracellular calcium mobilisation in response to n-3 and n-6 fatty acid ethanolamines in the presence of PTX in CHO-hCB_2. 135
Figure 5.1 Stimulation of DRG neurons expressing TRPV1 in response to the vanilloid agonist, capsaicin. 146
Figure 5.2 (A) C20:4 NAE (10 μM) evoked increases in intracellular calcium in DRG neurons. 147
Figure 5.3 (A) C22:4 NAE evoked changes in $[Ca^{2+}]_i$ in rat DRG neurons expressing TRPV1 148
Figure 5.4 (A) C22:5, n-6 NAE (10 μM) evoked increases $[Ca^{2+}]$i in rat DRG neurons expressing TRPV1. 149
Figure 5.5 Effect of C22:6 NAE on intracellular calcium in DRG neurons expressed TRPV1 150
Figure 5.6 (A) C22:5 n-3 NAE elicited increase in $[Ca^{2+}]$i in DRG neurons..... 151
Figure 5.7 Elevation of intracellular calcium levels in rat DRG neurons using calcium imaging. 152
Figure 5.8 Comparison of fatty acid ethanolamine-induced intracellular calcium ion levels measured using calcium imaging, with rat dorsal root ganglion neurones in vitro. 154
Figure 5.9 Area under the curve summaries of intracellular calcium response induced by 2 min exposure to NAE ligands 155
Figure 5.10 Comparison of evoked increases in $[Ca^{2+}]_i$ in adult rat DRG neurons to repeated application of C20:4 NAE. 157
Figure 5.11 Inhibition of C20:4 ethanolamine-induced increases in intracellular calcium mediated via the TRPV1 receptor in DRG neurons..... 159
Figure 5.12 Effect of TRPV1 antagonist on C22:5, n-6 ethanolamine-induced $[Ca^{2+}]_i$ in sensory neurons..... 160
Figure 5.13 (A) TRPV1 receptor mediated intracellular calcium elevations induced by C22:4 ethanolamine. 161
Figure 5.14 The functional activity of TRPV1 on increase in intracellular calcium stimulated by C22:6 ethanolamine ligand. 162
Figure 5.15 (A) TRPV1 receptor effects of C22:5, n-3 ethanolamine stimulated intracellular calcium increase in DRG neurons..... 163

Figure 5.16 Conformational analysis of several N-acylethanolamines using MacroModel in Movahed and co-workers study 167
Figure 6.1 Construction of ligand binding domain-activation factors (LBD-AF2) of human PPARs into pE28a (+) vector 173
Figure 6.2 Amplification of LBD-AF2 domain of human PPAR α, β, and γ. 174
Figure 6.3 Cloning the LBD-AF-2 domain of human PPARα, β and γ into pET28 a (+) vector. 175
Figure 6.4 His-tagged human PPARγ LBD-AF-2 expression but not α and β, in cell lysates of E.coli stable 21 (D3). 177
Figure 6.5 The sites of rare codons in the protein expression sequences of hPPAR (A) α and (B) β 179
Figure 6.6 Expression of His-tagged hPPAR LBD-AF-2 formed in inclusion bodies (A) α, (B) β, (C) γ. 180
Figure 7.1 LPS effects on hiNOS production in RAW46.7 cells 186
Figure 7.2 The effect of C20:4 NAE on LPS-induced production in RAW246.7 cells. 187
Figure 7.3 Palmitoylethanolamin (C16:0 NAE) effects on hiNOS activity stimulated by LPS in RAW246.7 cells. 188
Figure 7.4 DHEA (C22:6 NAE) effects on hiNOS activity stimulated by LPS in RAW246.7 cells. 189
Figure 7.5 Candidate receptors effects on hiNOS activity stimulated by LPS in RAW246.7 cells 191
Figure 7.6 Images for primary monocytes and macrophage from human blood cultured in RPMI1460 media. 193
Figure 7.7 Effect of NAEs on LPS-stimulated NO production in human monocytes and macrophages. 194
Figure 7.8 Stability of candidate reference genes expression (GAPDH, B2M, β-actin, TBP) among groups of LPS concentrations in human monocytes. 196
Figure 7.9 Effect of palmitoylethanolamine (PEA) on the expression levels of IL-1β, IL-10 and TNF-α in human monocytes stimulated by various LPS concentrations. 198
Figure 7.10 The effect of NAEs on LPS-induced inflammatory cytokine expression (IL-1β and TNF-α) and anti-inflammatory cytokine expression (interleukin-10) in human monocytes. 199
Figure 7.11 Inhibition of LPS evoked inflammatory cytokine (IL-1β) in the presence of NAEs in human macrophages. 200
Figure 7.12 Peroxisome proliferator activated receptor (α, β, γ) expression in human monocytes 202
Figure 7.13 Peroxisome proliferator activated receptor (α, β, γ) expression in human macrophages 203
Figure 7.14 A pilot experiment for investigate the effect of PPAR α receptor inhibition on IL-1β expression stimulated by LPS in human monocytes 204
Figure 7.15 Scheme of COX activity detection using Amplex red. The cyclooxygenase reaction converts arachidonic acid to prostaglandin G2 (PGG2). 205
Figure 9.1 URB597-evoked inhibition of NAE hydrolysis by rat liver microsomes. 218
Figure 9.2.1 Effect of cell seeding density on HU210induced ERK phosphorylation. 219
Figure 9.2.2 Effect of apyrase on HU210 stimulated ERK phosphorylation at various starvation times. 220
Figure 9.4 Western blot analysis showing COX-2 expression in whole cell lysates of BV-2 (20 µg protein) stimulated by 1 µg/ml LPS at various times 222
Figure 9.5 Optimisation of peroxidase activity assay in mouse microglia cells (BV-2) stimulated with 1µg/ml LPS 223
Figure 9.6 Effect of ibuprofen in inhibition COX activity in human platelet. 224

List of tables

Table 1.1 Binding of AEA to cannabinoid receptors 6
Table 2.1. Sequences of primers designed for cloning. 49
Table 2.2 Composition of solutions used in SDS PAGE. 54
Table 2.3 Primers and probes sequences for TaqMan gene expression analysis 63
Table 2.4 Primers and probes sequences for TaqMan gene expression analysis 64
Table 3.1 Enzyme kinetics of AEA hydrolysis in different rat liver microsomal preparations 82
Table 3.2 Enzyme kinetics of fatty acid ethanolamine hydrolysis by rat liver microsomes. .. 89
Table 3.3. The potency of URB597 in hydrolysis of tested ligands. 90
Table 3.4. Representative kinetics of AEA hydrolysis in tissue preparations 99
Table 3.5 Potency of URB597 reported in previous studies. 100

Abbreviation

µM	Micromolar
12-(S)-HPETE	12-(S)-hydroperoxyeicosatetraenoyl acid
2-AG	2-Arachidonoylglycerol
7TM	seven transmembrane
ACTB	actin, beta
AE	*N*-Arachidoylethanolamine
AEA	anandamide
ATP	adenosine triphosphate
AUC	area under the curve
B2M	β-microglobulin
BSA	bovine serum albumin
Ca^{2+}	calcium
cAMP	cyclic adenosine monophosphate
CB_1	cannabinoid type 1 receptor
CB_2	cannabinoid type 2 receptor
CBD	cannabidiol
CBN	cannabinol
cDNA	complementary DNA
CGRP	calcitonin-gene-related peptide
CHO	chinese hamster ovary cells
CNS	central nervous system
COXs	cyclooxygenases
CYP450	cytochromes P450
Czp	capsazepine
DAG	diacylglycerol
DHA	docosahexaenoic acid
DHEA	*N*-docosahexaenoylethanolamide
DMEM/F12	Dulbecco's Modified Eagle Medium: Mixture F12
DOEA	*N*-Docosaneoylethanolamine

DPEA	*N*-docosapentaenoylethanolamine
DRG	dorsal root ganglia
DTEA	*N*-docosatetraenoylethanolamide
DTT	dithiothreitol
E.coli	*Escherichia coli*
EA	Ethanolamide
EC_{50}	maximal effective concentration
EDTA	ethylenediaminetetraacetic acid
EETs	epoxyeicosatrienoic acids
EFM-19	human breast cancer
EPA	eicosapentaenoic acid
EPEA	*N*-eicosapentaenoylethanlamine
ERK	extracellular signal-regulated
FAAH	fatty acid amide hydrolase
FBS	foetal bovine serum
GAPDH	glyceraldehyde-3-phosphate dehydrogenase
GDE4	glycerophosphodiesterase
GDNF	glial cell line derived neurotrophic factor
GPCRs	G protein-coupled receptors
GTPγS	guanosine 5'-O-[gamma-thio]triphosphate
HEPES	4-(2-hydroxyethyl)-1-piperazineethanesulfonic acid
HL-60 cells	human promyelocytic leukaemia cells
HpETEs	hydroperoxyeicosatetranoicacids
HTS	high-throughput screening
IC_{50}	an index of drug potency
IFN	interferon
IL	interleukin
iNOS	inducible nitric oxide synthase
IP3	inositol 1,4,5-trisphosphate
IPTG	isopropyl β-D thiogalactoside
K*i*	inhibition constant of substrate

K_m	michaelis-Menten constant
LBD	ligand binding domain
LEA	linoleoyl ethanolamide
LOXs	lipoxygenases
LPA	lysophosphatidic acid
LPS	lipopolysaccharide
LTB4	leukotriene B4
MACS	magnetic cell separation
MAPK	mitogen-activated protein kinase
M-CSF	macrophage colony stimulating factor
mg/ml	milligrams per millilitre
mM	millimolar
NAAA	N-acylethanolamine-hydrolysing acid amidase
N-acyl PEs	N-acyl phosphatidylethanolamines
NAEs	N-acylethanolamines
NAPE	N-acylphosphatidylethanolamine
NAPE-PLD	N-acylphosphatidylethanolamine phospholipase D
NAT	*N*-acyltransferase
NDC	Naphthalene 2,3-dicarboxaldehyde
NEA	N-Nervonoylethanolamine
NGF	nerve growth factor
nM	nanomolar
nmole/min/mg	nanomole per minute per milligram
NO	nitric oxide
OEA	*N*-oleoylethanolamine
PA	phosphatidic acid
PAGE	polyacrylamide gel electrophoresis
PBMCs	peripheral blood mononuclear cells
PBS	phosphate buffer saline
PC	1-arachidonoyl-phosphatidylcholine
PC-12 cells	rat pheochromocytoma

PCA	perchloric acid
PCR	polymerase chain reaction
PE	phosphatidylethanolamine
PEA	*N*-palmitoylethanolamine
PI3K	phosphoinositol 3-kinase
PIP2	phosphoinositol 4,5-bisphosphate
PKA	protein kinase A
PKC	protein kinase C
PLC	phospholipase C
PMSF	phenylmethylsulfonylfluoride
PPARs	peroxisome proliferator-activated receptors
PPAR-α$^{-/-}$	PPARα-knockout mice
PTX	pertussis toxin
PUFAs	polyunsaturated fatty acids
RFU	relative fluorescence units
ROS	reactive oxygen species
RT-PCR	Real Time PCR
RTX	resiniferatoxin
SDS	Sodium dodecyl sulphate
SEA	*N*-stearoylethanolamine
SEM	standard error of the mean
TAE	tris accetic acid EDTA
TB	terrific Broth
TBP	TATA-binding protein
TCA	trichloroacetic acid
TNF-α	tumour necrosis factor
TRPV1	transient receptor potential vanilloid 1
V_{max}	maximal rate of enzyme activity
α LEA	linolenoyl ethanolamine
Δ^9-THC	Δ^9-tetrahydrocannabinol
µg/mL	microgram per milliter

Chapter 1
General introduction

1.1 Cannabis

Cannabis sativa, is a flowering plant, which has been used in medicine, for religious ceremonies and recreationally, stretching back for more than a thousand years (Pertwee, 2006). *Cannabis* is the source for at least 66 compounds now known as cannabinoids, the best known being Δ^9-tetrahydrocannabinol (Δ^9-THC), cannabinol (CBN) and cannabidiol (CBD). In 1964, the principle psychoactive compound (Δ^9-THC) was first identified and elucidated and this was the first step to challenging the notion of cannabinoid non-specific functionality. Due to its highly lipophilic nature, it was thought that the effects of Δ^9-THC were exerted by interfering with the plasma cell membrane, stimulating or inhibiting membrane-associated enzymes and altering the physical state of various ion channels (Pertwee, 2006).

Continued research efforts and the development of novel techniques have helped in the identification of Δ^9-THC-binding sites, where it acts on two major receptors belonging to the superfamily of G protein-coupled receptors (GPCRs) also known as seven transmembrane (7TM) receptors, to produce its pharmacological and biomedical effects. These are the cannabinoid receptors, CB_1 and CB_2 (Matsuda *et al.*, 1990).

Since the discovery of the chemical structure of Δ^9-THC, many cannabinoid receptor ligands have been synthesised. These ligands have been classified based on the chemical classes and pharmacological activity.

1.2 Cannabinoid Receptor Ligands

1.2.1 Classical Cannabinoids

Compounds contain ABC-tricyclic dibenzopyran derivatives may be referred to as classical cannabinoid. The classical cannabinoid compounds are either naturally occurring phytocannabinoids in the *Cannabis* sativa plant or synthetic analogues of these natural compounds. Δ^9-THC is the exemplar agonist often identified in this group. Δ^9-THC exhibits similar affinity for cannabinoid receptors (CB_1 and CB_2) where it act as a partial agonist at the CB_1 receptor (Howlett *et al.*, 2002).

HU-210 (11-hydroy-Δ^9-THC-dimethylheptyl) is one of the most widely used synthetic analogues of this class (**Figure 1.1**). HU210 acts as a full agonist at both CB receptor types and is reported to have a higher affinity for the CB_1 and CB_2 receptors than Δ^9-THC (Howlett *et al.*, 2002). Most of the compounds of this group are non-selective for the CB receptors; however, a few compounds which exhibit CB_2 receptor selectivity such as HU-308, JWN-051 and L-759633 have been developed (Pertwee, 2005).

1.2.2 Non-Classical Cannabinoids

Compounds in this group lack the dihydropyran ring structure, with either bi- or tri-cyclic analogues. CP 55, 940, (2-[(1R,2R,5R)-5-hydroxy-2-(3-hydroxypropyl) cyclohexyl]-5-(2-methyloctan-2-yl) phenol, **Figure 1.1**), is the best-known compound in this group. It exhibits similar affinity for both CB_1 and CB_2 receptors but it is reported as having a slightly lower affinity than HU-210 (Howlett *et al.*, 2002). CP55940 is routinely used as a reference agonist or radiolabelled tracer in CB receptor binding assays. Other examples of compounds in this class are CP 47,497 and CP 55,244 which

are reported to have high potency and affinity at both receptor types (Howlett *et al.*, 2002).

1.2.3 Aminoalkylindoles

Compounds in this group structurally differ from classical and non-classical cannabinoids. The best-known compound from this group is R-(+)-WIN55212-2 (**Figure 1.1**), which has modest CB_2 selectivity and exhibits high affinity for CB receptor. There are other synthetic aminoalkylindole compounds that have been developed with greater CB_2 selectivity such as JWH015 and L-768242 (Howlett *et al.*, 2002, Showalter *et al.*, 1996).

1.2.4 Diarylpyrazoles

The main compounds of this group of diarylpyrazoles are inverse agonists and antagonists. Rimonabant (SR141716) was the first compound identified in this group and was reported to have high affinity, with a measure of selectivity and inverse agonist properties at CB_1 receptor (Huestis *et al.*, 2001). Further synthetic analogues of rimonabant have been developed as high selectivity antagonists at the CB_1 receptors, such as AM 251 and AM 281 (Lan *et al.*, 1999). Unlike CB_1 receptors, selective CB_2 antagonists including SR144528 and AM 630, exhibit higher selectivity toward CB_2 (Howlett *et al.*, 2002, Ross *et al.*, 1999).

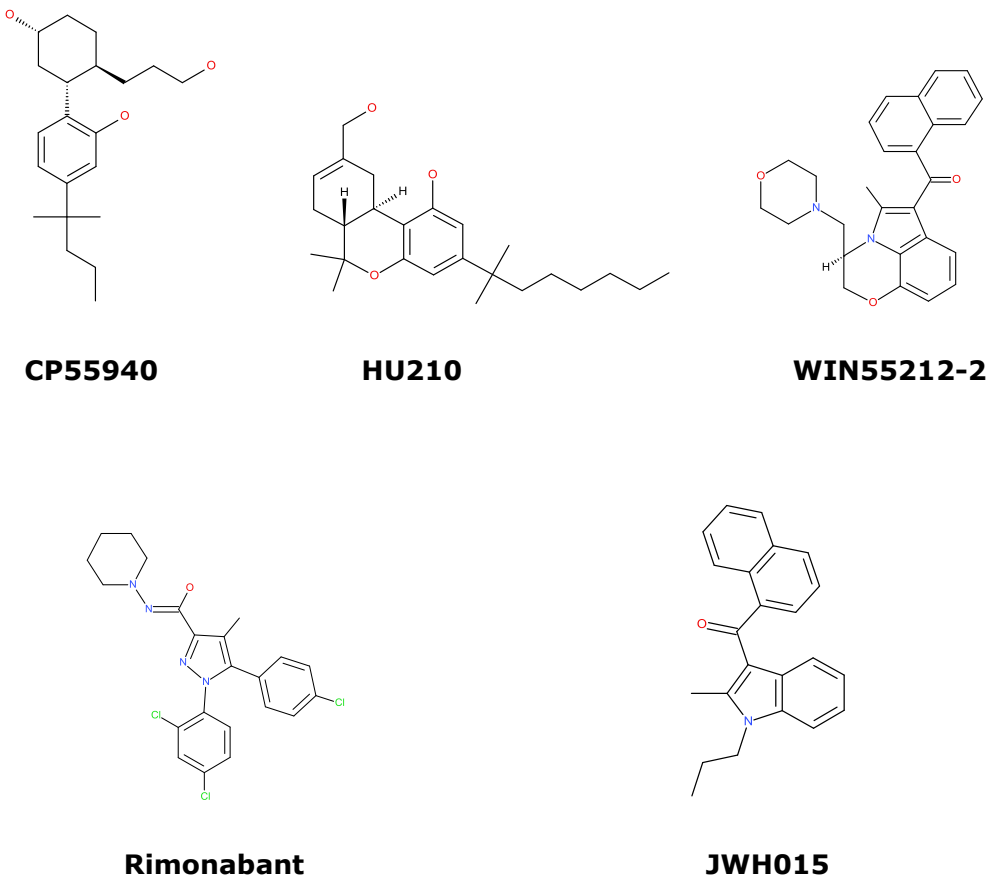
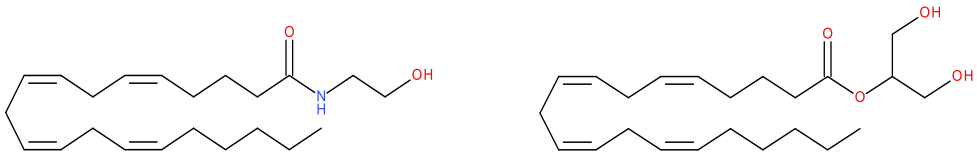


Figure 1.1 Structures of several example cannabinoid receptor ligands from classical, non-classical, aminoalkylindoles and diarylpyrazoles classes.

1.2.5 Endogenous Ligands

The discovery of cannabinoid receptors drove researchers to recognize lipid signalling mediators known as endocannabinoids (Devane *et al.*, 1992). Endocannabinoids are fatty acids conjugated either with ethanolamine to form N-acylethanolamines (NAEs), such as *N*-arachidonoylethanolamine (AEA, C20:4 NAE) or with glycerol to form monoacylgycerols, such as 2- arachidonoylglycerol (2-AG) (**Figure 1.2)**.

The two main well characterised endogenous cannabinoid receptor ligands or endocannabinoids are eicosanoids; anandamide (AEA) and 2-AG. Anandamide was isolated first as an endogenous ligand for cannabinoid receptors from porcine brain. The name AEA is derived from the Sanskrit word ‘ananda’, meaning ‘bliss’ (Devane *et al.*, 1992).



***N*-Arachidonoylethanolamine** **2-Arachidonoylgycerol**

Figure 1.2 Chemical structures of the two main endocannabinoids that have been widely studied.

AEA has been shown to bind to CB_1 and CB_2 receptors with moderate affinity *in vitro* by displacement of radioligand in the nanomolar range (see in **Table 1.1)**. In addition, it appears as a partial agonist in a number of *in vitro* functional assays and shows modest (~5 fold) CB_1 receptor selectivity (Howlett *et al.*, 2002).

Table 1.1 Binding of AEA to cannabinoid receptors adapted from (Howlett *et al.*, 2002).

	K*i* (nM), CB_1 receptor	**K*i* (nM), CB_2 receptor**
Rat brain	39.2 61[a] 71.7[a] 252	279[a]
Mouse brain		1930[a]
Recombinant human receptor	543 89[a]	581 1940 371[a]

[a] with phenylmethylsulfonyl fluoride

Anandamide (AEA, C20:4), the amide product of arachidonic acid and ethanolamine is found throughout the rat brain, and in regions of the human brain such as the hippocampus, thalamus, medulla, cortex, cerebrum, brainstem, striatum, limbic forebrain, diencephalon, cerebellum and mesencephalon (Sugiura *et al.*, 2002). Besides the brain, AEA was detected in bovine retina as well as peripheral tissues, including the heart and spleen of rat, (and human) and the liver, kidney, thymus, testes and skin of

rat and mouse uterus (Bisogno *et al.*, 1999). In addition, AEA presents in tumour cells, such as EFM-19 (human breast cancer), PC-12 cells (rat pheochromocytoma), in human neuroblastoma CH100 cells, lymphoma U937 cells and in meningioma (Sugiura *et al.*, 2002).

AEA exhibits the same pharmacological activities as cannabinoid ligands although they are different in structure (Sugiura *et al.*, 2002). AEA can indeed mediate diverse physiological processes including anxiety (Gaetani *et al.*, 2003), appetite (Rodriguez de Fonseca *et al.*, 2001), nociception (Walker *et al.*, 1999), and learning and memory (Lichtman *et al.*, 2002). Furthermore, AEA inhibits breast cancer cell proliferation (De Petrocellis *et al.*, 1998a). Moreover, AEA has been implicated in acute and inflammatory pain (Zygmunt *et al.*, 1999).

1.2.6 Biosynthesis

Anandamide is thought to be synthesised 'on demand' from lipid precursors which are ubiquitous in the cell membrane. The major biosynthetic pathway (**Figure 1.3**) involves *N*-acyltransferase (NAT) in the formation of *N*-acylphosphatidylethanolamine (NAPE) by transfer of a fatty acyl chain from the sn-1 position of one phospholipid to the amino group of phosphatidylethanolamine. This process has been described to be catalysed by a calcium-dependent membrane-associated NAT. The NAEs and phosphatidic acid (PA) are formed by hydrolysis of NAPE, via NAPE-selective phospholipase D (NAPE-PLD) (Bisogno, 2008). This enzyme activity can be regulated by a number of neurotransmitters or membrane depolarization (Giuffrida *et al.*, 1999, Kim *et al.*, 2002, Varma *et al.*, 2001). In 2015, a glycerophosphodiesterase (GDE4) was found to be a novel lysophospholipase D enzyme found in mouse brain, stomach, testis and colon,

and is involved in the generation of NAEs and lysophosphatidic acid (LPA) (Tsuboi *et al.*, 2015).

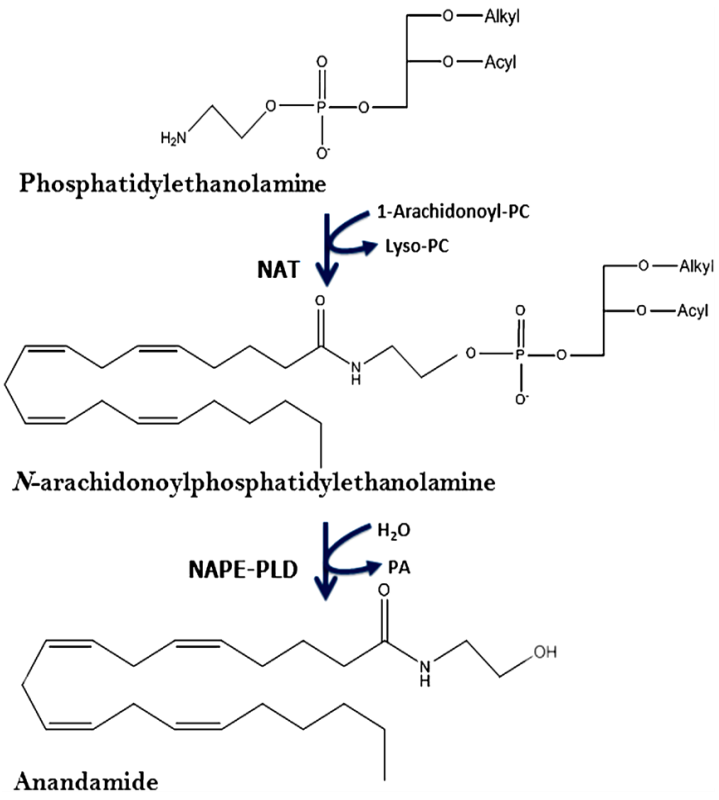


Figure 1.3 The major pathway for biosynthesis of AEA in the cell membrane. The arachidonic acid transfer from 1-arachidonoyl-phosphatidylcholine (PC) to phosphatidylethanolamine (PE) is catalysed by an *N*-acyltransferase to form a lipid precursor (NAPE), followed by cleavage by NAPE-specific phospholipase D (NAPE-PLD) to release AEA and phosphatidic acid (PA). Adapted from (Fonseca *et al.*, 2013).

1.2.7 Catabolism and Transformation

There are two major enzymatic pathways identified for modification of endocannabinoids which are the hydrolysis and oxidation pathways.

1.2.7.1 Fatty Acid Amide Hydrolase

Endocannabinoids are rapidly eliminated by fatty acid amide hydrolase (FAAH) to generate free fatty acids and ethanolamine. FAAH is a membrane-bound protein highly abundant in microsomal fractions of rat liver and brain. It is also found in different tissues such as testis, small intestine and spleen; however, it was not detected in the heart and skeletal muscle of rats (Sugiura *et al.*, 2002). The catalytic triad of FAAH structure is characterized as serine-serine-lysine with an alkaline optimal pH 8.5-10 (Ueda *et al.*, 2000).

Schmid and co-workers investigated the enzyme responsible for AEA hydrolysis in rat liver (Schmid *et al.*, 1985). However, the first description for enzymatic degradation of AEA was in 1993 by an enzyme initially entitled 'anandamide amidase' in several cell lines such as glioma and neuroblastoma cells and also in several rat tissues (Deutsch and Chin, 1993b). In 1996, this enzyme was renamed FAAH due to its capability for recognizing the majority of fatty acid amides (Cravatt *et al.*, 1996) but AEA is hydrolysed more rapidly than other fatty acid amides, thus AEA appears to be a preferred substrate (Giang and Cravatt, 1997).

FAAH enzyme was first cloned from rat (Cravatt *et al.*, 1996), then in human and mouse liver (Giang and Cravatt, 1997) and pig brain (Goparaju *et al.*, 1999). All these enzymes

are made up of 579 amino acids in length and share sequence homologies ranging from 81 to 91%.

1.2.7.2 Other Hydrolytic Enzymes

A second fatty acid amide hydrolase (FAAH-2) in human but not murids (mice and rat) has been described. It was found mainly in brain, liver, kidney, prostate, ovaries lung, and heart. In addition, it is localised in lipid droplets and therefore, it is suggested that this enzyme has a different physiological role to FAAH-1 (Wei *et al.*, 2006). Interestingly, it was shown that FAAH-2 localises in the opposite orientation to FAAH-1 in cell membranes, where FAAH-1 is proposed to have a cytoplasmic activity, while FAAH-2 faces the luminal contents (Wei *et al.*, 2006). This enzyme works at alkaline pH and has reactivity toward oleamide rather than AEA and other NAEs (Kaczocha *et al.*, 2010).

A third enzyme, *N*-acylethanolamine-hydrolysing acid amidase (NAAA), is a lysosomal enzyme that also hydrolyses AEA, but it appears to prefer palmitoylethanolamine (Ueda *et al.*, 2001). It belongs to the choloylglycine hydrolase family, which cleaves carbon-nitrogen bonds in linear amides, other than peptide bonds (Oinonen and Rouvinen, 2000). NAAA is expressed in rat lung, spleen, small intestine, thymus and cecum, with exceptionally high expression in rat alveolar macrophages (Ueda *et al.*, 2010). It catalyses the same reaction as FAAH, at the optimal pH range of 4.5-5 (Zhao *et al.*, 2007).

1.2.7.3 FAAH Inhibitors

In recent years, much attention has been given to the pharmacological manipulation of the endocannabinoid system and in particular FAAH inhibition in order to increase the intracellular levels of endocannabinoids and therefore, enhance their activity.

There are many reports linking AEA and FAAH as a therapeutic targets in a variety of pathophysiological conditions such as pain (Walker *et al.*, 1999), multiple sclerosis (Molina-Holgado *et al.*, 1998), Parkinson's disease(Di Marzo *et al.*, 2000), cancer (De Petrocellis *et al.*, 1998b) and inflammation (Berdyshev *et al.*, 1997). Therefore, the FAAH enzyme is potentially a promising drug target for treatment of many diseases.

A number of FAAH inhibitors have been described since the discovery of anandamide. Phenylmethylsulfonylfluoride (PMSF) was discovered serendipitously to be an inhibitor of FAAH when this compound was added to rat brain homogenates to protect the FAAH enzyme from proteolytic degradation (Deutsch and Chin, 1993a). Subsequently, several classes of FAAH inhibitors have been reported, including reversibly (such as trifluoromethyl ketonesα or ketoheterocycles) or irreversibly (such as fluorophosphonates, carbamates and ureas) acting agents (Ueda *et al.*, 1995b, Hillard *et al.*, 1995).

URB597 (cyclohexyl carbamic acid 3’-carbamoyl-biphenyl-3-yl ester, **Figure 1.5**) is a potent and selective FAAH and human FAAH-2 inhibitor *in vitro* and *in vivo* (Wei *et al.*, 2006). It belongs to the alkylcarbamic acid aryl ester family, with two hydrogen bond donors and five hydrogen bond acceptors. It is a crystalline white solid (MW 338.4 g/mol) soluble in phosphate buffer saline (pH 7.4) and stable in various conditions such

as heat, acid, peroxide, light, and simulated gastric fluid, making it a very useful agent for characterization of FAAH activity (Piomelli *et al.*, 2006).

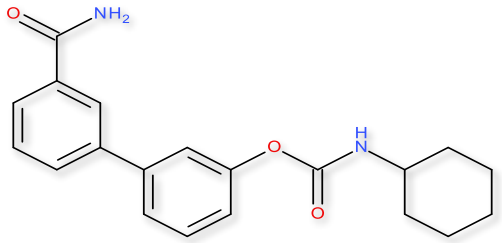


Figure 1.4 Chemical structure of URB597 (Mor *et al.*, 2004).

A study has reported that URB597 caused the augmentation of AEA levels in rat liver tissue (Fegley *et al.*, 2005), in brain membrane, with an IC_{50}= 4 nM and in rat cortical neurons, with an IC_{50}= 0.50 nM (Kathuria *et al.*, 2003) while this effect was absent in FAAH null mice (Fegley *et al.*, 2005). A further, a study demonstrated that FAAH inhibition by URB597 reduced oedema formation in carrageenan-induced hind paw inflammation (Holt *et al.*, 2005). Additionally, it was reported that URB597 exhibited benzodiazepine-like properties (anxioly) at doses consistent with FAAH inhibition in vivo where this effect was accompanied by an elevation of anandamide levels in the brain (Kathuria *et al.*, 2003). Similarly, oral administration of URB597 (at 0.3 mg/kg) exerted antidepressant-like effects in an animal model of depression with enhanced AEA signalling in brain (Bortolato *et al.*, 2007).

1.2.7.4 Clinical evaluation of FAAH inhibitors

Significant advances have continued in the development of FAAH inhibitors but no inhibitors have been approved for therapeutic use. There are many clinical trials that have been conducted to investigate the efficacy of several FAAH inhibitors that have been developed and to identify dose-limiting toxicity.

BIA 10–2474 3-(1-(cyclohexyl (methyl)carbamoyl)-1H-imidazol-4-yl)pyridine 1-oxide is a novel FAAH inhibitor developed by the Portuguese pharmaceutical company Bial-Portela & Ca. SA. Recently, Portugal's Bial Pharmaceuticals conducted Phase I clinical trials in France with BIA 10–2474 in healthy human volunteers for neuropathic pain. The adverse effects observed in those healthy volunteers who were subjected to multiple increasing doses of drug included brain damage and deep cerebral haemorrhage, as well as one subject dying (Kaur *et al.*, 2016). Toxicology studies for BIA 10–2474 were conducted in cynomolgus monkeys where it was observed that the dose for the inhibitor to damage the medulla oblongata was 100 mg/kg for 24 h. However, there has not yet been published a full investigation of the dosage and toxicity of BIA 10–2474 (Kaur *et al.*, 2016). In 2017, a study revealed that BIA 10–2474 inhibits lipases which cause alteration in the lipid network in the cortical neurons of human which therefore might lead to dysregulation in the nerve system (van Esbroeck *et al.*, 2017).

There are other clinical trials that have been conducted on FAAH inhibitors such as PF-04457845 (Johnson *et al.*, 2011) and V158866 (Pawsey *et al.*, 2016) that have not reported any adverse effect in volunteers and they were considered safe in humans. **PF-04457845,** (N-pyridazin-3-yl-4-(3-[5-(trifluoromethyl)-2 pyridyloxy] benzylidene)

piperidine-1-carboxamide), is a piperidine urea FAAH inhibitor which is highly potent and selective compared with that of the previously reported piperidine ureas inhibitors such as **PF-3845 and PF-750,** as well as URB597 (Ahn *et al.*, 2011, Johnson *et al.*, 2011).

Li and co-workers reported that this inhibitor was well tolerated in healthy humans at doses which cause maximal inhibition of FAAH activity and elevation of endocannabinoids levels (Li *et al.*, 2012). A study demonstrated that oral administration of PF-04457845 to rats reduced FAAH activity and elevated AEA levels in plasma and brain and also reduced the hyperalgesic inflammatory condition in rat pain models and was suggested to be a useful clinical candidate for the treatment of pain and central nervous system (CNS) disorders (Ahn *et al.*, 2011). Another study of Phase II trails to investigate the PF-04457845 effect in osteoarthritis patients identified that the analgesic effect of FAAH1 inhibition was lacking in humans (Huggins *et al.*, 2012). In 2016, Pawsey and co-workers described V158866 (FAAH inhibitor) and its tolerance in single and multiple doses and safety in healthy humans but there is no further investigation published on this inhibitor (Pawsey *et al.*, 2016).

1.2.7.5 Oxidative Metabolism

Much evidence has emerged indicating that oxygenases including cyclooxygenases, lipoxygenases and cytochrome P450s induce the oxidation of the arachidonic acid moiety of endocannabinoids. There are three enzymes involved in the oxidation of endocannabinoids as shown in **Figure 1.4**.

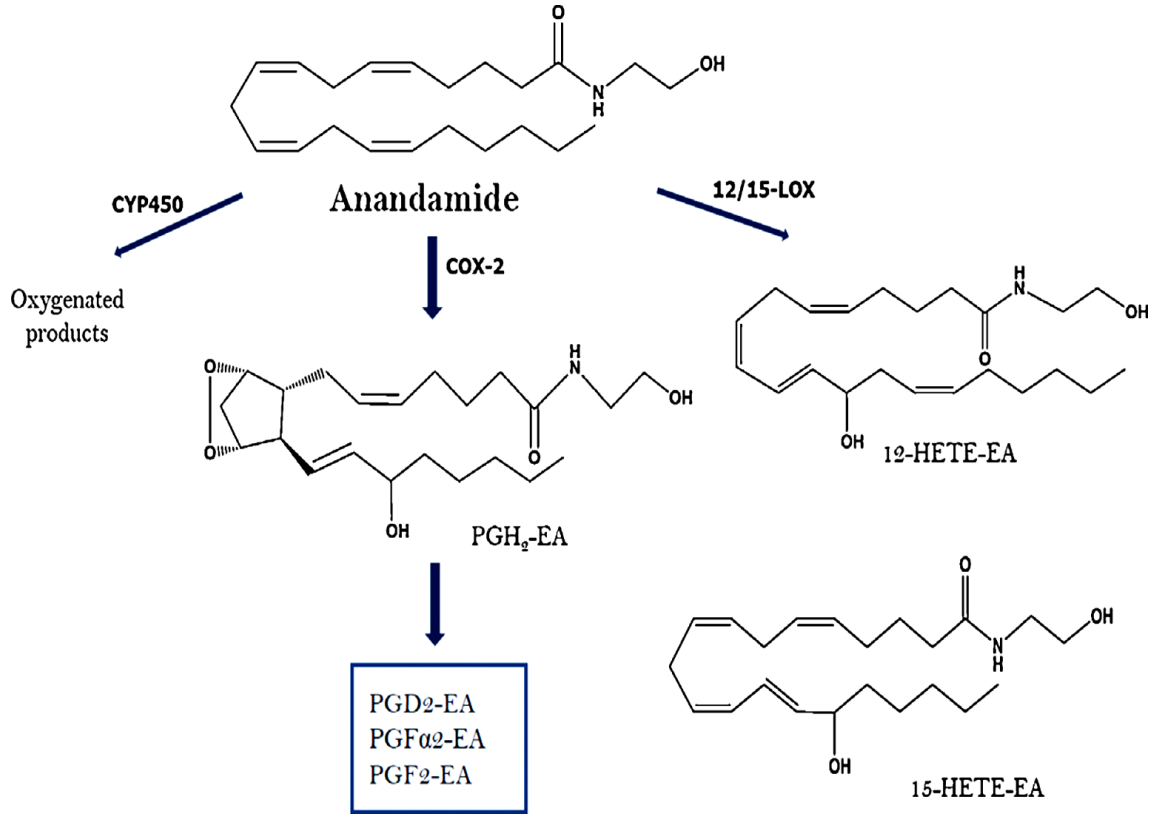


Figure 1.5 Oxidative metabolism of AEA by cyclooxygenase-2 and lipoxygenase (12- and 15-LOX) to produce ethanolamide (EA) derivatives and cytochrome 450 to yield hydroxyanandamides (epoxyeicosatrienoic acids). Adapt from (Fonseca *et al.*, 2013).

Cyclooxygenases (COXs; prostaglandin endoperoxide synthases) catalyse the rate-determining step in the production of prostanoids (including prostaglandins, PGs and thromboxane) from arachidonic acid (Hamberg and Samuelsson, 1973). There are two isoforms of COX, COX-1 and COX-2. It was thought that COX acts only on free fatty acids but AEA has been reported to be metabolised by COX-2 to yield prostaglandin E2 ethanolamide (Yu *et al.*, 1997). Moreover, it was suggested that prostaglandin ethanolamides possibly bind novel receptors to regulate several biological functions, including intraocular blood pressure (Woodward *et al.*, 2001).

Lipoxygenases (LOXs) are a family of non-heme iron-containing enzymes that catalyse the addition of a single molecule of oxygen to polyunsaturated fatty acids and derivatives Arachidonate, for example, is metabolised by LOX to produce hydroperoxyeicosatetranoic acids (HpETEs), which are metabolised to lipid mediators. Human LOXs has been identified to catalyse the region- and stereospecific oxygenation at C5, C12 and C15 of arachidonic acid (Hampson *et al.*, 1995). The incubation of AEA with 12-LOX purified from porcine leukocytes and rat brain and 15-LOX from rabbit reticulocytes produced 12- and 15- HpETEs, respectively (Hampson *et al.*, 1995). In contrast, 12-LOX purified from human platelets has less activity with AEA while 5-LOX was inactive (porcine leukocytes) (Ueda *et al.*, 1995a).

Cytochrome P450 (CYP450) isoforms are able to metabolise both exogenous and endogenous compounds. Some isoforms can oxidize arachidonic acid to form epoxyeicosatrienoic acids (EETs), which play important roles in blood pressure regulation and inflammation (Smith *et al.*, 2005, Hye Khan *et al.*, 2014). At least 10 different metabolic alternatives for AEA with murine hepatic CYP450s were observed

due to sequential metabolism, yielding mono-and dihydroxylated products as well as epoxides and combinations (Bornheim *et al.*, 1995).

1.3 Molecular Targets of Anandamide

After biosynthesis, endocannabinoids can be released into the extracelular space (through a mechanism not yet defined) to activate CB receptors or transport them from the extracellular space back in to the intracellular space to activate non-CB_1/CB_2 receptors such as Transient receptor potential vanilloid or peroxisome proliferator-activated receptors.

1.3.1 Cannabinoid Receptors

1.3.1.1 Tissue Distribution

There are two main cannabinoid receptors, which transduce the effects of cannabinoids. First cannabinoids receptor (CB_1 receptor) was isolated from a rat cerebral cortex and later from testes, human and mouse brain. It is highly abundant in regions of the brain such as the cerebellum, the basal ganglia, and the hippocampus (Di Marzo *et al.*, 2000, Matsuda *et al.*, 1990, Demuth and Molleman, 2006). Initially, it was believed to be localised predominantly in brain tissue, however, CB_1 has also been identified in peripheral tissues, including in the reproductive the cardiovascular and immune system, and the gastrointestinal tract, the spleen, as well as the liver (Svizenska *et al.*, 2008).

The second cannabinoid receptor (CB_2 receptor) was cloned from human promyelocytic leukaemia cells (HL-60 cells) in 1993 (Munro *et al.*, 1993). Expression of CB_2 is mainly restricted to immune cells (T-cells, B-cells, monocytes) (Munro *et al.*, 1993, Galiegue *et al.*, 1995). In addition, there is evidence showing expression of

CB_2 receptors in the culture of nervous cells and CNS, particularly in neurons and microglia (Svizenska *et al.*, 2008).

1.3.1.2 Signal Transduction Mechanisms

CB_1 and CB_2 receptors are members of the rhodopsin-like G protein-coupled receptor (GPCR) family (Joost and Methner, 2002). Both receptors subtypes are coupled predominantly to $G_{i/o,}$ where activation of CB receptors via endogenous or synthetic agonists leads to the dissociation of the $G_{i/o}$ subunit from $G_{\beta\gamma}$ subunits and consequent interaction with numerous intracellular signalling pathways (Howlett *et al.*, 2002), **see Figure 1.6**.

- **Inhibition of Adenylyl Cyclase**

The first characterisation of CB_1 receptors showed coupling to $G_{i/o}$ proteins, and the consequent inhibition of adenylyl cyclase and cyclic adenosine monophosphate (cAMP)-dependent protein kinase (PKA) (Demuth and Molleman, 2006). Anandamide inhibits forskolin-stimulated cAMP production in mouse N18TG2 neuroblastoma cells (Vogel *et al.*, 1993) and rat cerebellar membranes (Childers *et al.*, 1994). This response was pertussis toxin (PTX)-sensitive in transfected CHO cells expressing exogenous CB_1 receptors (Felder *et al.*, 1993a). In addition, cAMP accumulation was inhibited by CB_2 receptor activation in CHO expressing CB_2 receptors (Felder *et al.*, 1995). The modulation of cAMP concentration regulates a major cellular activity such as gene regulation as a result of phosphorylation by PKA which is important in synaptic plasticity and phosphorylation/dephosphorylation of voltage-K^+-dependent channels

that is important in postsynaptic or presynaptic functions of neurons (Childers and Deadwyler, 1996).

- **Mitogen-activated protein kinase**

Mitogen-activated protein kinase (MAPK) family members regulate biological functions by phosphorylation of specific target molecules and is involved in many cellular responses such as cell growth, transformation, gene expression, cell proliferation and apoptosis (Pearson *et al.*, 2001).

The cannabinoid receptors have been shown to be coupled positively to mitogen-activated protein kinase, mainly extracellular signal-regulated (ERK). ERK phosphorylation activated via CB_1 receptors has been described in several cells such as transfected CHO cells (Galve-Roperh *et al.*, 2002), murine neuroblastoma cell lines (Graham *et al.*, 2006), U373MG human astrocytoma (Bouaboula *et al.*, 1995), and also via CB_2 receptors in HL-60 cells (Kobayashi *et al.*, 2001). These responses were PTX-sensitive, suggesting the involvement of $G_{i/o}$ proteins or activation of β-arrestin-1 (Delgado-Peraza *et al.*, 2016)

The mechanisms of MAPK activation have not been fully elucidated; however, there are a number of pathways that have been suggested. Previous studies have suggested activation of phosphatidylinositol 3-kinase (PI3K) (Galve-Roperh *et al.*, 2002) and ceramide (lipid second messenger), with consequent activation of Raf, which is an upstream mediator of the ERK signalling cascade (Sánchez *et al.*, 1998). Furthermore, indirect actions of ERK activation has been suggested to be through effects on cAMP accumulation (Melck *et al.*, 1999) and at least one report of modulation via Gq proteins (Asimaki and Mangoura, 2011).

Previous reports have shown ERK1/2 phosphorylation to have a role in modulating endothelial growth, proliferation in human vascular endothelium cells (Liu *et al.*, 2000) and anti-proliferation in human breast cancer (Melck *et al.*, 1999), where these responses were blocked by rimonabant (CB_1 antagonist). Moreover, CB_1 receptor-mediated ERK activation is believed to play an important role in synaptic plasticity and neuroprotection (Rueda *et al.*, 2002). There are relatively few studies about CB_2 receptors in the activation of ERK1/2 signalling pathways. Functionally, CB_2 receptor-activated ERK phosphorylation in the regulation of inflammatory processes have been reported in several studies (Merighi *et al.*, 2012, Adhikary *et al.*, 2012).

- **Modulation of ion channels**

The activation of cannabinoid receptors can modulate calcium and potassium ion channels positively or negatively depending on the type of channel. In cell lines expressing CB_1 receptors, AEA inhibited the N-type Ca^{2+} channel (Mackie *et al.*, 1993), Q-type Ca^{2+} current in ATT20 transfected cells (Mackie *et al.*, 1995), where its effect was PTX-sensitive, suggesting that it was mediated by $G_{i/o}$ protein and cAMP-independent (Mackie *et al.*, 1993).

L-type Ca^{2+} channels have also been shown to be negatively regulated by CB_1 receptors in cerebral vessels in response to AEA (Gebremedhin *et al.*, 1999). In contrast to CB_1 receptors, CB_2 receptors have not been demonstrated, as yet, in the regulation of ion channels. In the modulation of potassium channel activity, CB_1 activation has been demonstrated to be coupled positively with inwardly rectifying K_{ir} channels, which is PTX-dependent in AtT20 transfected cells (Mackie *et al.*, 1995).

- **Intracellular calcium regulation**

Cannabinoid receptors activation is able to increase the concentration of intracellular calcium $[Ca^{2+}]_i$ by promoting calcium release from internal stores. Endocannabinoid activation of intracellular Ca^{2+} release has been reported in undifferentiated N18TG2 neuroblastoma and NG108-15 neuroblastoma-glioma hybrid cells (Sugiura *et al.*, 1996, Sugiura *et al.*, 1997). This effect was blocked by rimonabant, suggesting the involvement of CB_1 receptor (Sugiura *et al.*, 1999). The main mechanism by which cannabinoid receptors activate intracellular calcium release is believed to be from the cleavage of phosphatidylinositol 4,5-bisphosphate (PIP_2) to diacylglycerol (DAG) and inositol 1,4,5-trisphosphate (IP3) via phospholipase C (PLC). IP_3 then activates IP_3 receptors on the endoplasmic reticulum to release $[Ca^{2+}]$ into the cytoplasmic.

The mechanism of AEA-induced intracellular Ca^{2+} release has been reported in transfected HEK293 cells, where it was abolished by a CB_1 antagonist and IP3 blockers (xestospongin C and heparin) (Brailoiu *et al.*, 2011). These data indicate that the CB_1 receptor is coupled to $G_{i/o}$ protein to mediate calcium mobilisation via PLC signalling pathways. Similar to the CB_1 receptor, AEA-activated CB_2 receptor promoted release of intracellular Ca^{2+} has been reported in calf pulmonary endothelial cells via PLC signalling pathway (Zoratti *et al.*, 2003). Another pathway to be described for the release of intracellular Ca^{2+} downstream of CB_1 receptor is IP_3-independent and coupled to $G_{q/11}$ protein (Lauckner *et al.*, 2005) (**Figure 1.6**).

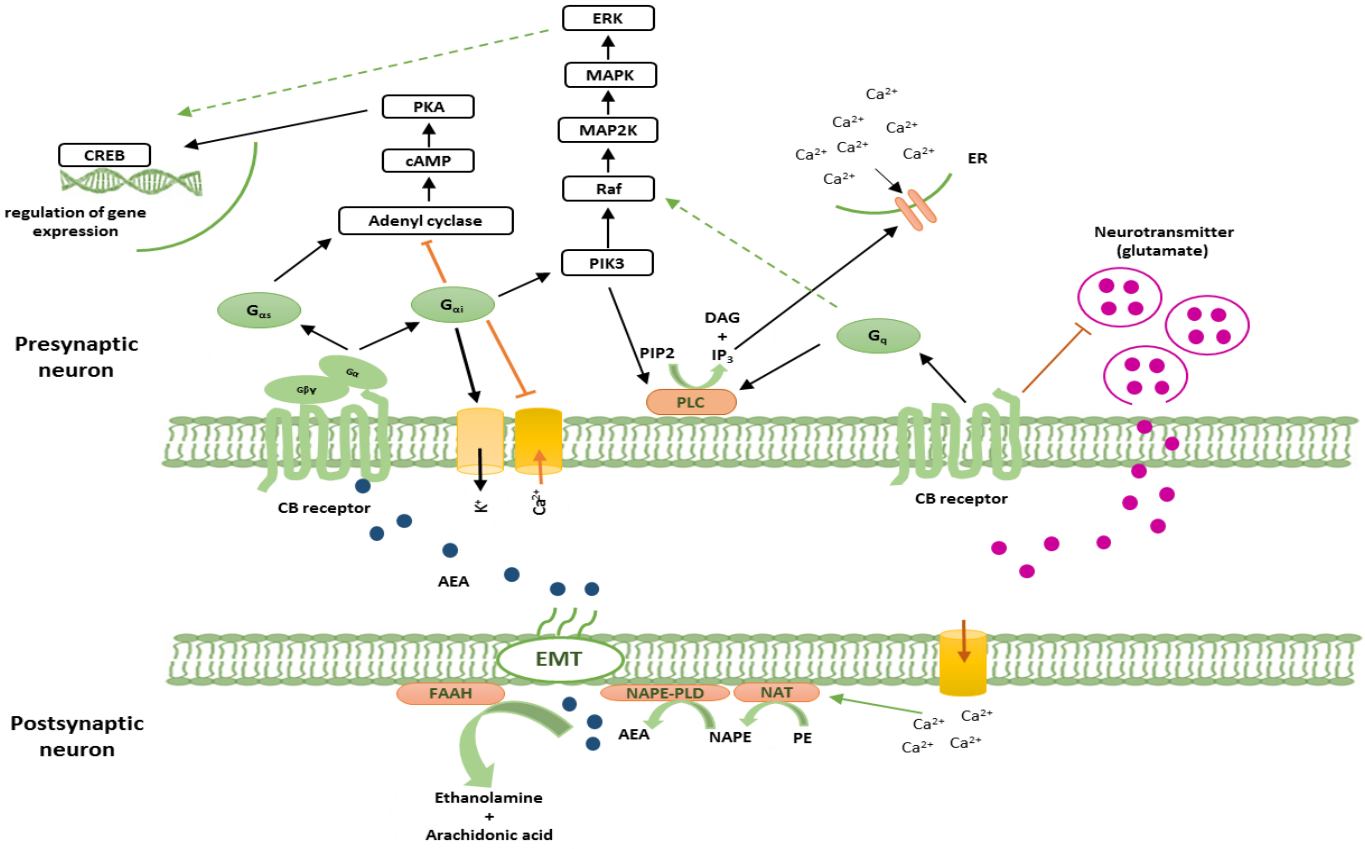


Figure 1.6 Schematic representation of the endocannabinoid system in pre- and postsynaptic neurons. CB receptors couple positively to ERK phosphorylation through $G_{i/o}$ or G_q proteins. CB receptor can regulate neuronal excitability and neurotransmitter release such as glutamate (toxic) via $G_{i/o}$ protein-dependent modulation of various potassium and calcium ion channels, in line with anandamide (AEA)' role as retrograde neurotra smitters [which is synthesis from membrane phospholipid-associated precursors (NAPEs)] and via endocannabinoid membrane transporter (EMT) release to extracellular space to activate CB receptors, resulting in inhibition pre-synaptic neuronal activity or release intracellular space to hydrolse AEA to arachidonic acid and ethanolamine through FAAH. In certain cases, the CB receptor has couple to other G proteins, including G_s, which, in contrast to $G_{i/o}$, activates AC, and G_q protein, which activates phospholipase C (PLC) that lead to release of calcium ions from intracellular store (endoplasmic reticulum).

1.3.1.3 Cannabinoid Receptor Allosteric Modulators

The interaction of CB_1 receptors and allosteric modulator compounds has been reported. The interaction of these modulators with a distinct binding site on the CB_1 receptor which is different to the binding site of endogenous agonist, hence 'orthosteric binding site', is suggested to alter the efficacy and binding of orthosteric agonists (Christopoulos and Kenakin, 2002).

A series of allosteric compounds synthesised by 'Organon' has been characterised at CB_1 receptors (**Figure 1.7**) (Price *et al.*, 2005) such as **Org 29647** (5-chloro-3-ethyl-1*H*-indole-2-carboxylic acid (1-benzyl-pyrrolidin-3-yl)-amide, 2-enedioicacid salt), **Org 27569** (5-chloro-3-ethyl-1*H*-indole-2-carboxylic acid [2-(4-piperidin-1-yl-phenyl)-ethyl]-amide), and **Org 27759** (3-ethyl-5-fluoro-1*H*-indole-2-carboxylic acid (2-94-dimethylamino-phenyl)-ethyl]-amide).

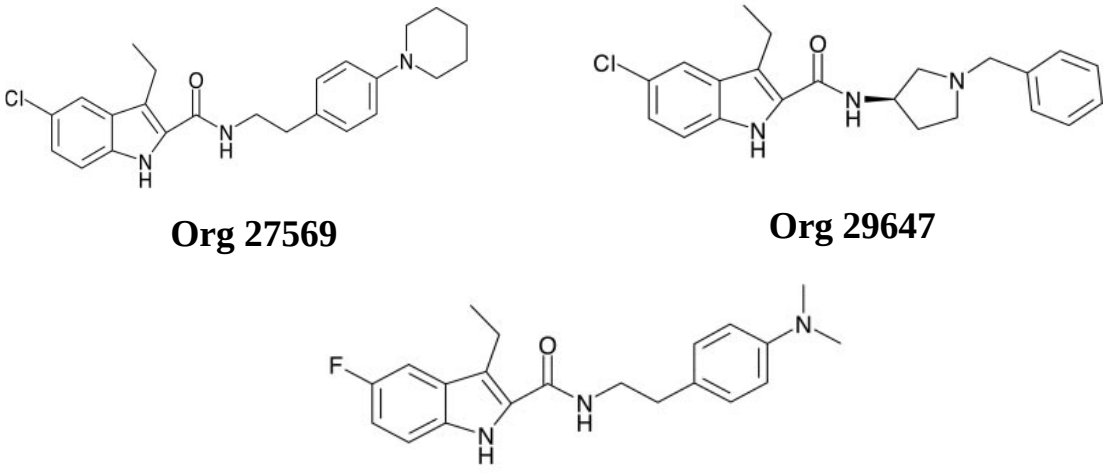


Figure 1.7 Chemical structure of Organon compounds positive allosteric modulators. Adapted from (Price *et al.*, 2005).

In mouse brain, these modulators were shown to significantly decrease the efficacy of AEA induced-[^{35}S]GTPγS binding (Price *et al.*, 2005) and β-arrestin in HEK- 293 hCB_1 (Baillie *et al.*, 2013).

In 2007, 4-chlorophenyl)-3-[3-(6-pyrrolidin-1-ylpyridin-2-yl)phenyl]urea (PSNCBAM-1) was described as a negative allosteric modulator having similar results to Organon compounds, suggesting similar effects on binding site and signalling pathways (Horswill *et al.*, 2007). However, Org 27569 and PSNCBAM-1 appear to be ligand dependent where PSNCBAM-1 had high potency for CP55940 compared with WIN55212 in mouse brain (Baillie *et al.*, 2013).

1.3.2 Transient Receptor Potential Vanilloid 1

1.3.2.1 Expression

Transient receptor potential vanilloid 1 (TRPV1) receptor is a nonselective cation channel, that, when activated, allows the influx of cations, predominantly Ca^{2+}. TRPV1 is an afferent neuron nociceptive receptor which is highly expressed in sensory neurons originating from the CNS including dorsal root and trigeminal ganglia (Schicho *et al.*, 2004).

Many studies have confirmed that TRPV1 channel is expressed in non-neuronal cell, such as smooth muscle (Jaggar *et al.*, 2001), liver, keratinocytes, mast cells, macrophage human umbilical vein endothelial cells (Himi *et al.*, 2012), leukocytes (Saunders *et al.*, 2007) and microglia (Kim *et al.*, 2006).

1.3.2.2 TRPV1 Receptor ligands

The TRPV1 receptor is activated by multiple noxious stimuli such as capsaicin, vanilloids, resiniferatoxin (RTX), heat, hydrogen ions (Tominaga *et al.*, 1998, Caterina *et al.*, 1997) and also some putative endogenous ligands such as lipoxygenase product of arachidonic acids metabolism 12-(S)-hydroperoxyeicosatetraenoyl acid (12-(S)-HPETE), 5-(S)HETE and leukotriene B4 (LTB4) (Hwang *et al.*, 2000). Furthermore, AEA has shown to be an endogenous ligand for TRPV1 receptor where its sensitivity to AEA suggests it to be a cannabinoid receptor (Zygmunt *et al.*, 1999, Tucker *et al.*, 2001).

- **Sensitisation and Desensitisation of TRPV1 receptors**

TRPV1 receptor activity can be sensitised by phosphorylation with protein kinase C (PKC) and protein kinase A (PKA) and these can be triggered by activation of receptors associated with inflammation for example prostaglandins, leukotrienes and calcitonin-gene-related peptide (CGRP) (Bhave *et al.*, 2002). Moreover, AEA, bradykinin, and NGF which stimulate phospholipase C (PLC) can sensitise TRPV1 receptor through diacylglycerol (DAG) hydrolysed from PIP_2 (Prescott and Julius, 2003).

Prolonged exposure or repeat application of agonist evoked intracellular calcium leading to desensitisation of TRPV1 to subsequent agonist where this process protects cells from excitotoxicity (Bhave *et al.*, 2002). The desensitisation of TRPV1 to capsaicin has been demonstrated in many studies (Docherty *et al.*, 1996, Liu *et al.*, 2005). Previous reports showed that AEA exerted anti-nociceptive effects through TRPV1 receptor (Horvath *et al.*, 2008), suggesting that desensitisation of TRPV1 is one

possible mode of action. In CHO-hTRPV1 cells and skeletal muscle arterioles of rat, AEA caused complete desensitisation of TRPV1 (Lizanecz *et al.*, 2006), this is postulated to be a therapeutic alternative to manipulate TRPV1 activity.

1.3.2.3 TRPV1 Receptor Functions

TRPV1 receptor activation is involved in either the pathogenesis, or disease progression, of problems such as neuropathic pain and neurogenic inflammation. The interaction between AEA and TRPV1 receptors has been reported in pain (Di Marzo *et al.*, 2002) and cardiovascular pathways (Pacher *et al.*, 2005, Parolaro *et al.*, 2002). Vanilloids play an integral role in apoptosis of immune cells through TRPV1-dependent and independent mechanisms. AEA has been shown to induce apoptosis in cervical carcinoma cell lines (Contassot *et al.*, 2004b), human glioma cells (Contassot *et al.*, 2004a), neuroblastoma cells CHP100 and lymphoma U937 cells (Maccarrone *et al.*, 2000), which is TRPV1-dependent involving the increase of intracellular calcium, mitochondrial uncoupling, release of cytochrome c and activation of caspase-9 or -3. Furthermore, capsaicin, a TRPV1 receptor agonist, was found to inhibit reactive oxygen species (ROS) in microglia (Schilling and Eder, 2009).

1.3.3 Peroxisome proliferator-activated receptor

Peroxisome proliferator-activated receptors (PPARs) belonging to the nuclear receptor family are composed of three isoforms α, β and γ. Members form heterodimers with retinoid X receptors (**Figure 1.8**), and bind to specific DNA sequences called PPAR response elements leading to changes in the transcription of target genes upon ligand

activation (O'Sullivan, 2007). The target genes of PPARs are involved in the regulation of inflammation, cell differentiation, metabolism and energy homeostasis.

PPARα is distributed in different tissues such as the liver, heart and skeletal muscle. With regard to PPARγ, there are three isoforms: PPARγ1, PPARγ2, and PPARγ3, which are expressed, in adipose tissues and in macrophages. PPAR β/δ is a powerful metabolic regulator, and is ubiquitously expressed.

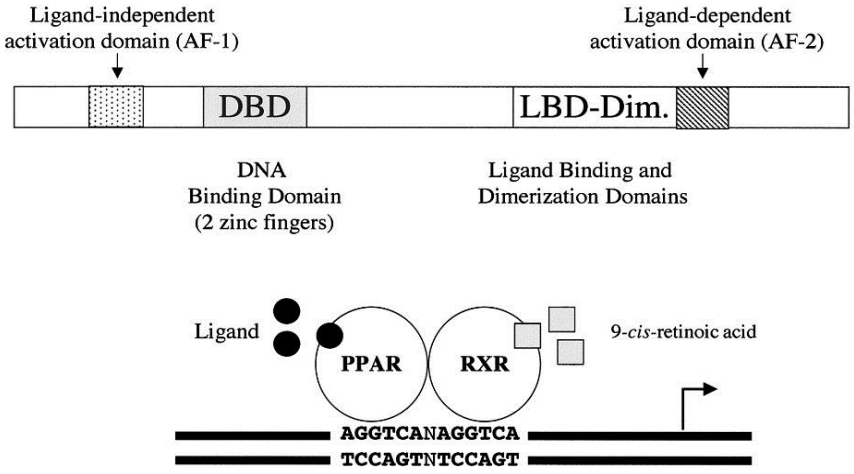


Figure 1.8 Structure of peroxisome proliferator–activated receptors. Adapted from (Ferré, 2004).

1.3.3.1 Activation of PPARs

PPARs have a ligand-binding domain that can be activated by a number of chemical structures including plant extracts. The naturally occurring ligands of PPARy including unsaturated fatty acids such as linolenic acid, linoleic acid and arachidonic acid, as well as other eicosanoids (15-deoxy-$\Delta^{12,14}$-PGJ2 (15d-PGJ2) and 8S-HETE were also found

to be activators of PPARγ (Xu *et al.*, 1999). PPARα has been found to be activated by a wide range of saturated and unsaturated fatty acids, such as oleic acid, palmitic acid, linoleic acid, and arachidonic acid with micromolar affinities (Göttlicher *et al.*, 1992) as well as the lipoxygenase metabolite 8(S)-HETE (Yu *et al.*, 1995). Like PPARα and PPARγ, a wide range of unsaturated and saturated fatty acids act as ligands for PPAR β (Forman *et al.*, 1997).

Since 2002, evidence has accumulated showing that endogenous ligands such as endocannabinoids can bind to and activate PPARs and this link has been identified through various studies, including reporter gene assays, binding studies and the use of antagonists (O'Sullivan, 2016). The interaction between endocannabinoids and PPARs has been reported in many studies. AEA has been shown to bind and increase PPARα driven transcription activity in HeLa cells (Sun *et al.*, 2007). Furthermore, the metabolites of AEA have also been shown to activate PPARβ in the brain (Yu *et al.*, 2014) while a few studies have reported that AEA activates PPARγ (Bouaboula *et al.*, 2005, Rockwell and Kaminski, 2004).

1.3.3.2 PPAR Functions

Clinically, agonists at PPARα and PPARγ are useful for manipulating lipid metabolism such as fenofibrate and thiazolidinediones, respectively (Oliver *et al.*, 2001, Willson *et al.*, 1996). The PPAR receptor can be a target for endocannabinoids, where there is potential for their therapeutic effects such as anti-inflammatory, analgesic effects.

The PPAR- mediated anti-inflammatory effects of AEA have been reported in several studies. AEA has been shown to inhibit the release of pro-inflammatory cytokines

interleukin-2 (IL-2) which was prevented by an antagonist of PPARγ (Rockwell and Kaminski, 2004). Rockwell *et al.* (2004) have shown that AEA-induced inhibition of the pro-inflammatory cytokine IL-2 is PPAR-α-mediated and activated by the COX-2 metabolite of AEA. The endocannabinoids exert neuroprotective properties against excitotoxicity which is mediated by PPARγ in a model of multiple sclerosis (Loría *et al.*, 2010).

1.4 Other Bioactive N-acylethanolamines

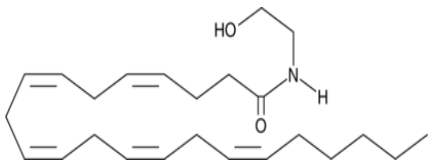
Previous studies have identified a wide range of NAEs in rat and human tissues (Giuffrida *et al.*, 2000, Joosten *et al.*, 2010). There appears to be a correlation between different NAEs in various tissues of rats and the fatty acid composition of their diets, dependent on the presence of saturated fats, polyunsaturated fats or monounsaturated fats (Artmann *et al.*, 2008a). Therefore, the presence of the wide range of NAEs from different lengths of fatty acids and degrees of saturation in mammalian tissues suggests that NAEs can be synthesised on the basis of the availability of precursor fatty acids. Much research focuses on unsaturated fatty acids that are more abundant in animals, in particular arachidonic acid (20:4, n-6). There is a wide variety of fatty acid derivatives in nature but their biological significance or pharmacological potential have not been fully elucidated.

1.4.1 n-6 Fatty Acid Derivatives of Ethanolamine

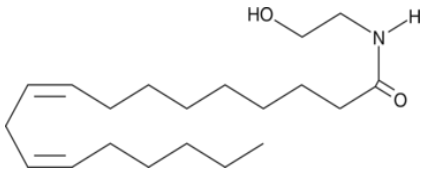
There are few studies focused on n-6 NAEs other than AEA (**Figure 1.10**). For example**, *N*-docosatetraenoylethanolamide (DTEA, C22:4 NAE)** is a reported CB_1 agonist that is rarely studied in comparison to C20:4. It is reported to inhibit electrically

evoked contraction of vasa deferentia, with an IC_{50} values= 96 nM and 53 nM for DTEA and AEA, respectively (Pertwee *et al.*, 1994). DTEA was also identified and isolated from porcine brain (Hanus *et al.*, 1993) and shown to inhibit the specific binding of [^{3}H] HU-243 to CB_1 receptor in COS-7 cells transfected with CB_1 receptor to inhibit adenylate cyclase activity in CHO-rCB_1 receptor, in a PTX-dependent manner (Barg *et al.*, 1995).

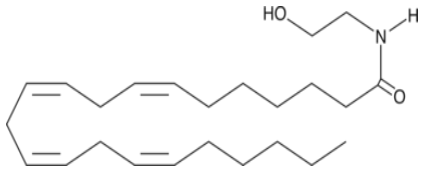
In 1993, ***N*-linoleoylethanolamine (LEA, C18:2 NAE)**, was detected in porcine brain and murine peritoneal macrophages (Hanus *et al.*, 1993) and mouse peritoneal macrophages (Schmid *et al.*, 1997). Another study demonstrated that C18:2 NAE was synthesised from a NAPE precursor in mouse J774 macrophages and N18 neuroblastoma cells (Di Marzo *et al.*, 1996). In 2013, linoleoylethanolamine was shown to be more effective in the suppression of tumour necrosis (TNF-α) damage compared to dipotassium glycrrhizinate which is widely used for skin care treatment (Ishida *et al.*, 2013), and the authors proposed LEA to be a new therapeutic agent against contactdermatitis. Besides these compounds, it was observed that ***N*-docosapentaenoylethanolamine (DPEA, C22:5 NAE)** was significantly increased in the hippocampus of mice during dietary n-3 fatty acids deficiency while AEA levels were unaffected (Kim *et al.*, 2011).



***N*-Docosapentaenoylethanolamine**



***N*-Linoleoylethanolamine**



***N*- Docosatetraenoylethanolamine**

Figure 1.10 Chemical structures of n-6 fatty acid derivatives of ethanolamine.

1.4.1 n-3 Fatty acid Derivatives of Ethanolamine

Existing research suggests a critical role played by dietary-essential n-3 polyunsaturated fatty acids (**Figure 1.11**), mainly from fish oils, in the human diet. They are reported to have significant health benefits, such as reducing the risk of cardiovascular diseases, potentially cancer and anti-inflammation, for review, see (Laye *et al.*, 2018, Endo and Arita, 2016). A previous study showed that ***N*-docosahexaenoylethanolamide (DHEA, C22:6 NAE)** can be detected in human plasma (Wood *et al.*, 2008). Furthermore, the biosynthesis of DHEA and ***N*-eicosapentaenoylethanlamine (EPEA, C20:5 NAE)** increases after exposure to docosahexaenoic acid (DHA) and eicosapentaenoic acid (EPA) with anti-inflammatory properties; however the explicit mechanism behind these effects has not been fully investigated (Balvers *et al.*, 2010). Similarly, DHEA and EPEA are present in prostate

and breast cancer cells expressing CB receptors (Brown *et al.*, 2011). The anti-proliferation effects of DHEA and EPEA in cancer cell lines were mediated through CB receptors and also potencies of these effects were enhanced by inhibition of FAAH in prostate cancer cells (Brown *et al.*, 2010). Furthermore, it has been shown that DHEA was involved in neuritogenesis and synaptogenesis, was highly enriched in the brain and also improved glucose uptake, therefore reducing insulin sensitivity, compared to AEA (Kim *et al.*, 2014, Kim *et al.*, 2011).

In 2013, Figueroa *et al.* (2013) showed that consumption of n-3 PUFA leads to the accumulation of ***N*-docosapentaenoylethanolamine (DPEA, C22:5 NAE**) in addition to DHEA and EPEA. This biosynthesis correlated with a reduction in hyperalgesia and inflammation. Recently, it has been shown that the n-3 NAEs epoxides derived from EPA and DEA inhibited pro-inflammatory cytokine (IL-6) and nitrite levels but increased anti-inflammatory cytokines (IL-10) in BV-2 microglia (McDougle *et al.*, 2017). In addition, Sheskin and co-workers examined the binding of a series of n-3 NAEs to the brain CB_1 receptors and it appeared that ***N*-linolenoyl ethanolamine (LEA, C18:3 NAE)** was inactive (Sheskin *et al.*, 1997).

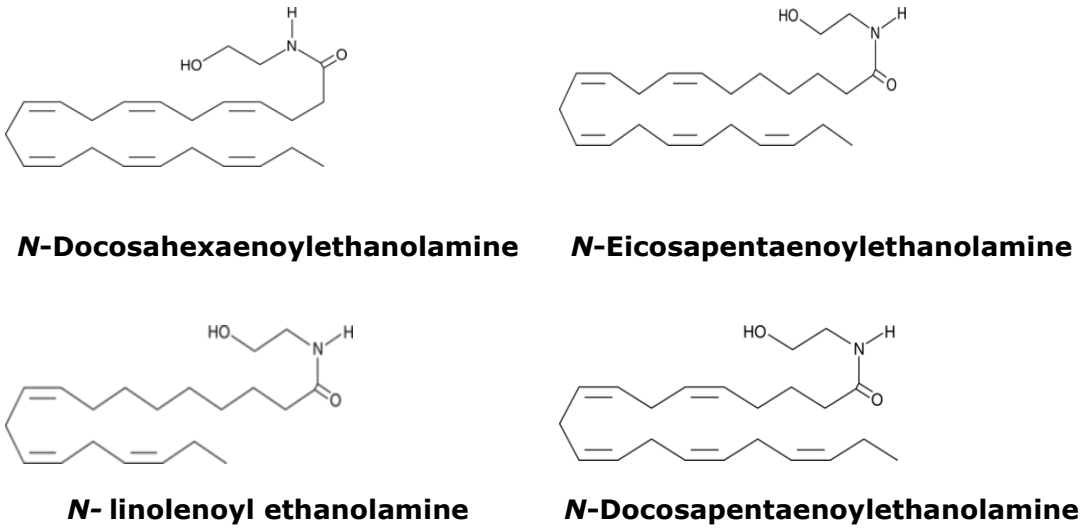


Figure 1.11 Chemical structures of n-3 fatty acid derivatives of ethanolamine.

1.4.2 Monounsaturated and Saturated Fatty acid Derivatives of Ethanolamine

In 2005, a study showed that ***N*-docosaenoylethanolamide (DOEA, C22:1 NAE)** and ***N*-arachidoylethanolamine (AE, C20:0 NAE)** (**Figure 1.12**) inhibited depolarisation-induced Ca^{2+} efflux mediated by voltage-gated Ca^{2+} channels in rabbit skeletal muscle and were able to inhibit the specific binding of [^{3}H]isradipine in membranes (Oz *et al.*, 2005). In addition, C22:1 ethanolamine has been detected in mouse brain but whether this ligand acts as a substrate for CB_1 and CB_2 receptors has not been reported yet (Saghatelian *et al.*, 2004b).

***N*-nervonoylethanolamine** (C24:1 ethanolamide) has been previously identified in mouse brains (Leung *et al.*, 2006). Furthermore, C24:1 NAE and C20:0 NAE were biosynthesised via NAPE-PLD in mouse brain tissue as levels were reduced following

the disruption of the NAPE-PLD gene (Leung *et al.*, 2006). A further study by Saghatelian and co-workers suggested that C24:1 ethanolamine is a substrate for FAAH (Saghatelian *et al.*, 2004a) but its activation of CB_1 and CB_2 receptors has not been reported yet.

Another monounsaturated fatty acid ethanolamine has been extensively investigated as seen in (**Figure 1.10)**. ***N*-oleoylethanolamine (OEA, C18:1 NAE)** has been shown to modulate feeding behaviour, induce satiety and reduce body weight by increasing the transcription activity of PPARα (Fu *et al.*, 2003). Moreover, OEA induced lipolysis and reduced triacylglycerol in liver and adipose tissue but not in obese PPAR-$\alpha^{-/-}$ mice (lacking PPAR-α) (Guzman *et al.*, 2004). OEA also has analgesic properties in models of visceral and inflammation pain in rat and mice (Suardíaz *et al.*, 2007). In terms of a stroke model, OEA reduces infarct volume from the middle cerebral artery occlusion in mice which is absent in PPAR-$\alpha^{-/-}$ mice (Sun *et al.*, 2007). Moreover, appetite suppressant activity of OEA might be through its action on the G protein-coupled receptor 119 (GPR119), which is a potential target for treating obesity and metabolism disorders via OEA, although AEA does not activate this receptor (Overton *et al.*, 2006).

On the other hand, there is evidence indicating that saturated fatty acid ethanolamines such as ***N*-palmitoylethanolamine (PEA, C16:0 NAE)** and ***N*-stearoylethanolamine (SEA, C18:0 NAE)** modulate inflammation. A previous study reported that SEA was capable of being down-regulated in skin inflammation of a murine model of passive IgE-induced cutaneous anaphylaxis (Dalle Carbonare *et al.*, 2008) but was not mediated via CB_1 and CB_2 receptors. SEA was unable to displace [^{3}H]CP55.940 binding to CB_1 and CB_2 receptors, in the brain and spleen of mice(Maccarrone *et al.*, 2002).

PEA has been shown to be effective in reducing acute inflammation (Costa *et al.*, 2002) and has been found to exert antinociceptive effects (Gingold and Bergasa, 2003) and neuroprotective effects (Conti *et al.*, 2002). It has been reported that it is not a ligand at CB_1 receptors in rat brain (Sheskin *et al.*, 1997). PEA along with AEA and OEA, has been shown to be present in human seminal plasma, mid-cycle oviductal fluid, follicular fluid, amniotic fluid, milk and fluids from malignant ovarian cysts (Schuel *et al.*, 2002).

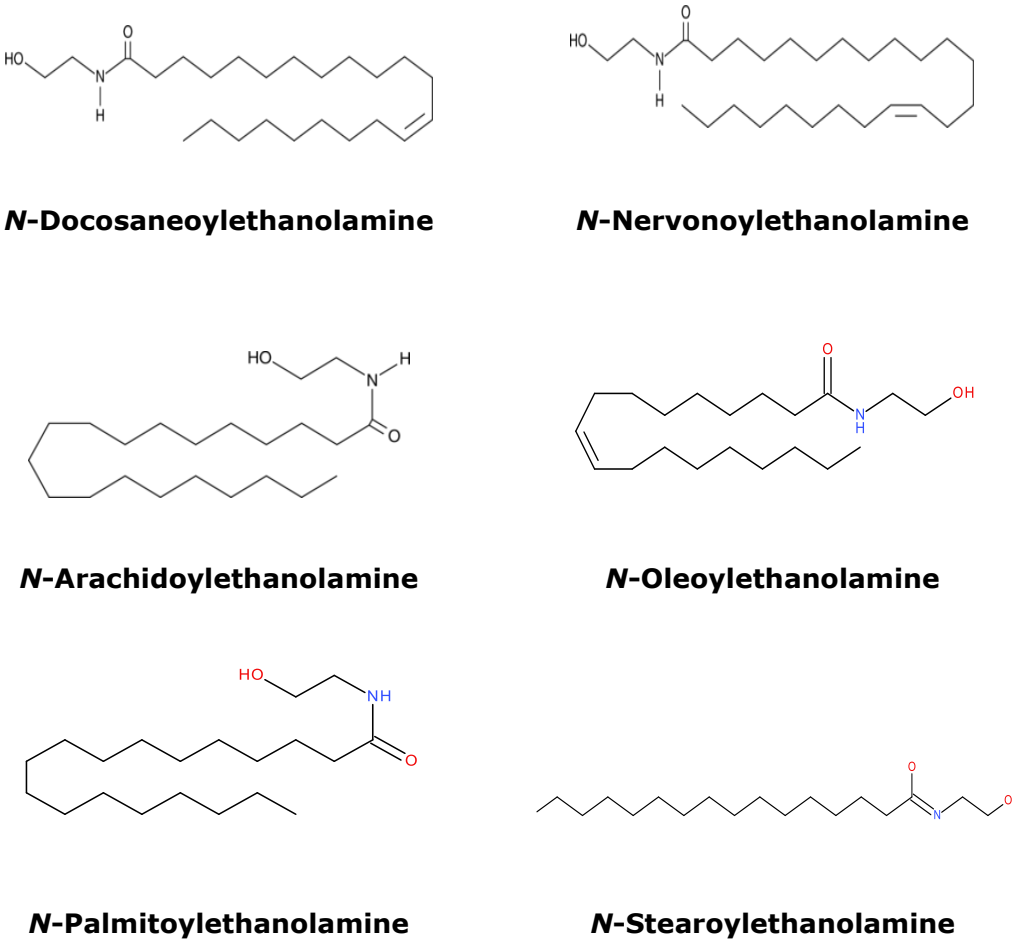


Figure 1.12 Chemical structures of mono-unsaturated and saturated fatty acid derivatives of ethanolamine.

1.5 Aims and Objectives of the Project

Although most of the research on endocannabinoids has focused on AEA (and 2-AG), there is a possibility that the biological effects in this system are not limited to this compound. There are other NAEs which probably act as endocannabinoids, in particular, polyunsaturated fatty acid ethanolamines, which have been studied only superficially.

The main aim of this project was to gain an increased understanding of the roles of multiple NAEs, particularly the conjugates of PUFAs, as endogenous signalling molecules.

More specifically, the objectives of this study were to examine:

- The metabolism of different NAEs by FAAH in rat liver microsomes
- The actions of multiple NAEs at human recombinant CB_1 and CB_2 cannabinoid receptors
- The action of multiple NAEs at rat dorsal root ganglion TRPV1 receptors.
- The action of multiple NAEs at human recombinant PPARs.
- The anti-inflammatory impact of NAEs in vitro.

Chapter 2
Methods and Materials

2.1 Materials

2.1.1 Chemicals

All chemicals were obtained from Sigma-Aldrich (Poole, Dorset, UK) or BDH Laboratory Supplies (Poole, Dorset, UK), unless otherwise stated. Fluo-4AM, Fura-2AM, Amplex red and Neurobasal medium (NBM, Gibco) were from Life Technologies. All cannabinoids, AEA and URB597 were obtained from Tocris Bioscience (Bristol, UK), unless otherwise stated. PEA, SEA, OEA were synthesised in the School of Chemistry, University of Nottingham by Dr S.P.H. Alexander. Other NAEs and heme were purchased from Cayman Chemicals (Cambridge Biosciences, Cambridge, UK). TaqMan Fast Universal PCR Master Mix was purchased from Agilent.

2.1.2 Antibodies and Enzymes

The primary antibodies, anti-ERK1/2 rabbit (#9102) and anti-phospho-ERK1/2 (Thr202/Tyr204) monoclonal mouse (#9106) were purchased from Cell Signalling Technology (Boston, USA). COX-2 (mouse) monoclonal antibody was from Abcam Biochemicals® (Bristol, UK). Sal1 and NdeI enzymes**,** Pfu DNA polymerase, Taq DNA polymerase and T4 DNA ligase were obtained from New England Biolabs (NEB). All standard molecular weight markers were purchased from Bio-Rad laboratories Ltd. (UK).

2.1.3 Vectors and Primers

All vectors used were purchased from Invitrogen (Carlsbad, CA). Primers and probers were obtained from Eurofins (Munich Germany).

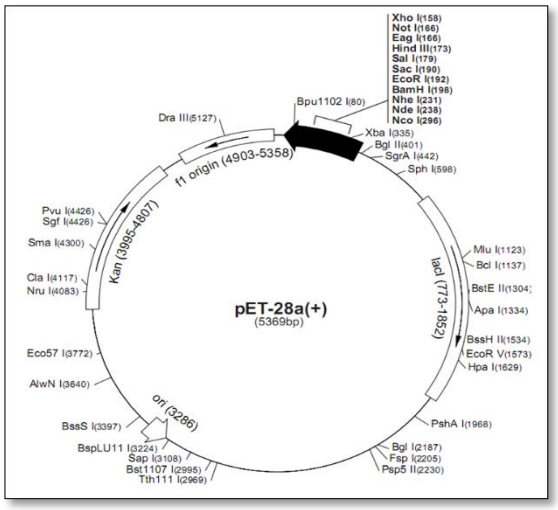


Figure 2.1 pEt28a(+) vector (Invitrogen)



Figure 2.2 pcDNA3.1/Zeo vectors circle map (Invitrogen)

2.2 Methods

2.2.1 Measurement of FAAH activity

2.2.1.1 Assay Development

Ethanolamine is a common product of hydrolysis of all N-acylethanolamines by fatty acid amide hydrolase. Following an initial identification of naphthalene 2,3-dicarboxaldehyde (NDC) as a reagent to generate a fluorescent adduct with ethanolamine, several factors were investigated to optimise ethanolamine quantification. The latency and stability of the fluorescent adduct over time and the optimum pH of the borate development buffer for mixing with NDC were assessed. Different dilutions of trichloroacetic acid (TCA) and perchloric acid (PCA) (5, 10, 20) as stopping reagents for the assay were also investigated.

Serial dilutions of ethanolamine were prepared in phosphate buffer (0.2 M K_2PO_4, 0.05 M KH_2PO_4 and 1 mM ethylenediaminetetracetic acid (EDTA), supplemented with 1 mg/ml defatted bovine albumin serum, adjusted to pH 7.4). Stopping reagent was added followed by vortexing. Standard solutions were then treated exactly as test solutions (see below) for development and quantification of the fluorescent product.

2.2.1.2 Tissue preparation

Rat liver crude particulate fractions were prepared according to the method of De-Bank et al., (2005) with several modifications. Fresh liver was dissected from Wistar rats (6-9 weeks old and 1.50 - 2.50 g weight), and weighed after washing in 0.05M potassium phosphate buffer, pH 7.4. Prior to homogenising, liver was roughly chopped with scissors in homogenising buffer. Tissue was then homogenized in 1:10 (w/v) of

phosphate buffer using a Polytron homogeniser before being centrifuged at 10,000 x g for 20 min at 4 °C (unless otherwise stated).

The pellet containing the nucleus and un-homogenised material was discarded and the supernatant layer was re-centrifuged at 30,000 x g at 4 °C for 60 min. The membrane pellet was resuspended in 2 volumes of original wet weight in phosphate buffer. The protein concentration was determined by standard methods (Lowry et al. 1951). The tissue protein concentration was adjusted to 10 µg/ml and stored as aliquots at -80 ºC until required.

2.2.1.3 Assay application

The particulate preparation was diluted 100-fold in assay buffer containing 1 mg/ml BSA. Assay reaction was initiated by adding 5µl of substrate to 500 µl of tissue/BSA mixture in 1.5 ml Eppendorf tubes, incubating at 37 °C for 15 min. Inhibitors, such as URB597, were pre-incubated with the tissue at 37 °C for 15 min before addition of the substrate.

The reaction was stopped by 250 µl of 10 % (w/v) TCA before centrifuging at 3000 x g for 5 min to clear the protein. The supernatant layer was removed and used in the detection step. NDC was made up to 1 mg/mL in acetonitrile at this time and then diluted 1:4 in 0.2 M tetraborate buffer (pH 11.0). 50 µl of the supernatant layer was distributed into individual wells of a 96-well plate followed by 150 µl of the NDC developing buffer. The plate was shaken for a second and the fluorescence was quantified at 418 nm excitation and 480 nm emission in a microtitre plate fluorimeter

(FLUOstar Galaxy). Alongside the samples, serial dilution of ethanolamine was freshly prepared to allow calculation of ethanolamine production from each reaction. Blanks in the absence of substrate or tissue were measured in parallel. All substrates and URB597 were dissolved in ethanol or DMSO and then diluted in assay buffer to the desired concentration so that the vehicle concentration never exceeded 0.1%. The enzyme activity was expressed as nmol/min/mg of protein.

For FAAH activity calculation, the fluorescence value for each well was plotted against the standard curve of ethanolamine to measure the amount of ethanolamine produced from each reaction where the data were fitted by non-linear regression (one-site binding) analysis using GraphPad Prism software (GraphPad 6.0). The rate of hydrolysis for each ligand concentration was calculated based on this equation:

$$\left[\frac{\textbf{amount of ethanolamine (nanomoles)}}{\textbf{incubation time} \times \textbf{protein (mg)}}\right]$$

, Volumes were adjusted for sampling of the supernatant layer to calculate the total amount of ethanolamine generated. Kinetic values (K_m and V_{max}) for enzyme activity were calculated using a Michaelis-Menten equation fitted in GraphPad Prism7 ($\mathbf{K_m}$ is the substrate concentration at which the reaction rate is half the maximum velocity and $\mathbf{V_{max}}$ is the maximum rate). The negative logarithm (pIC_{50}) of URB597 that resulted in a 50% inhibition of FAAH activity was calculated by non-linear regression using GraphPad Prism6 using the four parameter logistic equation. The mean ± SEM of these data were calculated from at least three experiments.

2.2.2 Validation

The current 'Gold Standard' assay for FAAH activity relies on the measurement of rates of hydrolysis of radiolabelled AEA, and so an analysis was conducted to compare kinetic estimates from the novel assay with the established methodology.

2.2.2.1 Radiometric assay

The AEA hydrolysis assay is based on the presence of a label in the ethanolamide moiety (*N*-arachidonoyl-[^{3}H]-ethanolamine) and was adapted from published methods (Holt *et al.*, 2005, Boldrup *et al.*, 2004). Rat liver microsomal fractions were diluted to 10 μg/ml protein in Tris-EDTA buffer containing BSA (1 mg/ml).

AEA (400 μM in ethanol) was diluted 100-fold dilution in BSA (1 mg/ml) and then tracer amounts 2 μl [3H]-AEA (to 50-100 000 dpm/assay) were added, before vortexing and incubating in a final volume of 100 μl for 15 min at 37 °C. Where indicated, inhibitors were added to the tissue/BSA/buffer mix and pre-incubated for 15 min at 37 °C. Blanks were incubated in parallel in the absence of tissue or the absence of substrate. To stop the reaction, 400 μl activated charcoal (4% w/v in 0.5 M HCl) was added, following by vortexing and centrifugation at 13000 rpm for 5 min. 200 μl aliquots of supernatant layers were then mixed with 3 mL scintillation fluid (Emulsifier-Safe, PerkinElmer, Waltham, CA/USA) and counted in the tritium channel for a (minimum of 3 min), with quench correction using a scintillation analyzer (Tri-Carb, PACKARD, Palo Alto, CA/USA). Total available substrate was measured by adding the tritiated substrate directly to 3 ml scintillation fluid. The enzyme activity was expressed as nmol/min/mg of protein.

2.2.3 Intracellular signalling assay

2.2.3.1 Chinese Hamster Ovary culture

Chines Hamster Ovary (CHO) cells, stably transfected with either human recombinant cannabinoid type 1 receptors or type 2 receptors, were provided by Pfizer-Neusentis (Cambridge, UK). The stable transfection of Chinese hamster ovary (CHO) cells with human CB receptors is well characterised for investigation of responses to cannabinoid ligands allowing many signalling pathways to be measured as well as environmental manipulations such as pertussis toxin exposure. Therefore, it was the model chosen for studying the functional effects of ethanolamine derivatives of various fatty acids at cannabinoid receptors.

Cells were grown as monolayers in Dulbecco's Modified Eagle Medium: Mixture F12 (DMEM/F12) supplemented with 10% heat-inactivated foetal bovine serum (FBS), 2 mM L-glutamine, 400 and 500 μg/ml G418 for CB_1 and CB_2, respectively, in 75 cm^2 flask and maintained in a 5 % CO_2 humidified incubator at 37 °C. At 95% confluency, cells were washed once with phosphate buffer saline (PBS) and incubated with trypsin/EDTA solution for approximately 3 min until most of the cells were detached the culture flask. The cell suspension was diluted in culture medium to prevented further trypsin action and then cells were collected by centrifugation at 300 x g for 5 min. The culture medium was aspirated and the cell pellet was re-suspended in fresh medium. The cells were counted using an Automated Cell Counter (Bio-Rad TC10™) using Trypan Blue. The cells were seeded in a new culture flask (1.5 million per flask) and passaged every 2-3 days. The cells were cultured under sterile condition and all reagents culture were warmed at 37 °C before use.

2.2.3.2 In-cell Western assay

The signalling of MAP kinase phosphorylation was investigated in CHO-hCB_1 using an In-cell western assay. This is a quantitative fluorescent immunoassay where proteins are immunocytochemically labelled in fixed cultured cells *in situ*. Cells were cultured into 96-well plate ($4x10^4$ cells/well) in DMEM F-12 culture medium at room temperature for 1 hour. Previous experiments in the group had established that this step helped to reduce an edge effect on the assay plate. Cells were incubated overnight at 37 °C, 5% CO_2. 30 min prior to starting the experiment, culture medium was removed by aspiration and replaced with serum-free medium containing 1 mg/ml BSA. Where indicated, PTX or receptor antagonists were incubated with cells before adding ligands.

Suitable concertation of ligands were performed in serum-free media, 20 µl of which was added to each well to make up a final volume to 200 µl/well. The assay plate was incubated for 5 min with ligands at 37 °C, 5% CO_2 and then were rapidly aspirated. Cells were fixed with 4% paraformaldehyde in PBS (150 µl/well) for 20 min at room temperature. Cells were permeabilised using 0.1% (v/v) Triton X-100 in PBS (150 µl /well) for 20 min at room temperature. Non-specific binding sites were blocked with 5 % (w/v) of milk in PBS for 20 min at room temperature.

Primary antibodies directed against total and phosphorylated ERK1/2 were dissolved in blocking agent. Wells were incubated with primary antibody solution (80 µl/ well) overnight at 4 °C with gentle rocking. The antibody concentrations were 1:400 rabbit anti-ERK-1/2 and 1:500 mouse monoclonal anti-phospho-ERK1/2 (Thr202/Tyr204). Control wells were incubated with blocking solution only and without primary antibody to measure non-specific binding of the secondary antibody. The next day,

the primary antibody solution was aspirated and then each well was washed three times with BSA (1 mg/ml) containing PBS for 5 min each time at room temperature with gentle rocking. LI-COR IRDye secondary antibodies were incubated with cells (100 µl/well) in darkness at 37 °C for 60 min after dilution in blocking agent. The secondary antibodies were then aspirated and the wells were washed three times with PBS.

The plate was imaged using LI-COR Odyssey® NIR Imaging System (software v3.0.) at 129 µm resolution scanning simultaneously at 700 and 800 nm, with settings of medium quality and focus offset of 4.0 mm, The secondary antibody non-specific response was subtracted from levels in other wells. Levels of phospho-ERK were normalised as a ratio to the total ERK in each individual well. Thereafter, values in the presence of ligands were compared to vehicle responses.

2.2.3.3 Intracellular calcium FlexStation

Changes in intracellular calcium concentration were determined in CHO-hCB_1 and CHO-hCB_2 using a FLEXstation with the calcium-sensitive dye Fluo-4. Cells were cultured in 96-well black-walled plates for 24 h at 37 °C, 5 % CO_2. Fluo-4 AM was solubilised in 10% pluronic acid and DMSO and then was diluted to 2 µM in DMEM Ham-F12 medium containing 2.5 mM probenecid. The organic anion transport inhibitor probenecid was added to reduce leakage of the de-esterified indicator.

Cells were loaded with dye (100µl/well) and incubated for 45 min at 37 °C. Cells were washed twice with HEPES-buffered saline solution containing (HBSS) 2.5 mM probenecid (25mM HBSS, 2 mM sodium pyruvate, 1.3 mM $CaCl_2$, 10 mM glucose.

and 1mM $MgSO_4$, adjusted to pH 7.4) to remove excess dye and incubated for 30 min at 37 °C. Treatment with PTX or antagonist, where indicated was conducted before addition of ligands.

Ligands were prepared in HBSS buffer from stock aliquots (10 mM) at the required concentration and loaded to the corresponding compound wells (ethanol and DMSO concentration never exceeded 0.1 %). The assay and compound plates were loaded into the fluorimetric reader (FlexStation, Molecular Devices, Sunnyvale, CA/USA) and analysed using FLUO protocol. The fluorescence response for individual well was measured at an excitation wavelength of 485 nm and emission wavelength of 515 nm. The peak calcium response for each ligand was calculated by subtracting the basal levels from the maximum response. Area under the curve (AUC) of response to ligand versus time was calculated. The latency of peak response was calculated by subtracting the time of ligand addition from the time point of the peak. ATP was used as a positive control and to normalize responses between experiments.

2.2.3.4 Intracellular calcium imaging

2.2.3.4.1 Dorsal root ganglia (DRG) cell culture

Rats were killed by asphyxiation and were then dissected to collect the spinal cord. The dorsal root ganglia (DRG) cells of rats (Lumbar 5 and 6) were collected in Hank's Balanced salt solution supplemented with HEPES. The ganglia were incubated in neurobasal medium containing 2.5 mg/ml collagenase supplemented with horse serum for 90 min. Ganglia were then washed three times to remove any medium residues and then were incubated in PBS containing 2.5 mg/ml of porcine trypsin for 30 min. DRG neurons were suspended in 1 ml 15% (w/v) bovine albumin serum solution to which

was slowly added 3 ml of the remaining bovine serum albumin to form a bilayer. The DRG neurons were collected by centrifugation of the bilayer at 500 x g for 5 min and the pelleted cells were then re-suspended in 1 ml neurobasal medium supplemented with horse serum, 2 mM L-glutamine, 200 units⁄ml penicillin, 200 ng⁄ml streptomycin, 50 ng/ml nerve growth factor (NGF) and glial cell line derived neurotrophic factor (GDNF). The cell suspension ~ 150 µl was pipetted on sterilized glass coverslips and incubated overnight at 37 °C, 5 % CO_2 prior to intracellular calcium imaging.

2.2.3.4.2 Calcium imaging

DRG neurons, following overnight culture, were washed three times in HEPES-buffered saline solution (145 mM NaCl, 5 mM KCl, 2 mM $CaCl_2$, 1 mM $MgSO_4.7H_2O$, 10 mM HEPES and 10 mM glucose, adjusted to pH 7.4). Cells were incubated with Fura-2 AM for 45 min at 37 °C in the dark and then were washed three times with HEPES buffer to remove excess dye for at least 20 min prior to imaging and recording. For imaging, a coverslip was placed in the recording chamber using glue to prevent tissue movement and then placed under the microscope. The image was captured by a digital camera (Q-Imaging ROLERA-XR or ANDOR Xion) at an interval time which was normally set to 5 s. DRG neurons were superfused with ligand at high concertation (10 µM) for 2 min and then allowed to recover for 45 min prior to the addition of capsaicin (10 µM). Where indicated, 10 µM capsazepine was incubated with cells for 20 min followed immediately by ligand addition. Fura-2 was measured based on the excitation light filtered through 340 and 380nm band pass filters and emission light was registered at 500 nm. Andro iQ software was used to analyse the response for individual DRG neurones. These are predominantly C-type nociceptor neurones as they exhibited

an average equatorial somal diameter ≤ 30 µm. The peak of the calcium response then was calculated using Excel, subtracting the basal response identified as the mean fluorescence for the six frames (at intervals of 5 s) immediately prior to the addition of ligand. Data were normalised to the capsaicin response from each neurone.

2.2.4 Cloning and protein expression

2.2.4.1 Designing the cloning primers

Cloning primers for the target genes were designed manually according to a database sequence that was retrieved from NCBI online database search www.ncbi.nlm.nih.gov. The cloning primers were designed based on restriction sites in vectors used. All primers were examined by blasting using NCBI BLAST to ensure that the chosen sequence was specific for the gene of interest and analysed using Integrated DNA Technologies to calculate melt point, their guanine-cytosine (GC) and their suitability to hairpin structure. Primers were dissolved to 100pmol/ml in DPEC-water autoclaved.according to the manufacturer's protocol provided with the primers. Forward and reverse primers were diluted in 1/10 as stock to carry on polymerase chain reaction (PCR). All primers are listed in **Table 2.1.**

Table 2.1. Sequences of primers designed for cloning.

Human Gene	Sequences	Tm	Gene bank accession NO.	Product size (bp)
PPARα	**Forward:** 5'CAC**CATATG**CGCAGCTGCAAGATCCAGAA- 3' **Reverse:** 5'-GTG**GTCGAC**TCAGTACATGTCCCTGTAGA-3'	61 °C 55 °C	**NM_001001928.2**	987
PPARβ/δ	**Forward:** 5'- CAC**CATATG**TTCCAGCAGCTACACAGAC-3' **Reverse:** 5'- GTG**GTCGAC**TTAGTACATGTCCTTGTAGATCT-3'	57 °C 54 °C	**NM_001171818.1**	1215
PPARγ	**Forward:** 5'-CAC**CATATG**TGTCGGATCCACAAAAAAAGTA-3' **Reverse:** 5'-GTG**GTCGAC**CTAGTACAAGTCCTTGTAGATCTCC-3'	56 °C 58 °C	**NM_005037.5**	981

2.2.4.2 Polymerase Chain Reaction

All DNA amplification were performed by the DNA thermocycler using Advantage^{TM} 2 PCR kit (Cat no. 639207). Cycle conditions were a follow: an initial denaturation step of 30 second at 98 °C, followed by 30 cycles of: 95 °C for 10 seconds, 55, 54, 61 °C for 30 seconds for hPPARα, β, γ, respectively and final extension at 72 °C for 1 min.

2.2.4.3 Agarose gel electrophoresis

1% agarose gel electrophoresis was prepared in 0.5x TAE electrophoresis buffer and heated the mixture in a microwave oven until melted. After the mixture had dissolved and cooled to around 55 °C, ethidium bromide was added to mixture and was then poured in casting tray containing comb. After the gel had solidified, the comb was removed and put in electrophoresis chamber covered with 0.5x TAE. DNA samples containing loading buffer were loaded in each well and current (5V/cm) is applied. The gel was visualized by an ultraviolet transilluminator.

2.2.4.4 Digestion and ligation of DNA into vector

The insert and pET28a (+) vector to be used were digested using appropriate restriction enzymes and appropriate buffer after recovering DNA fragment by using MinElute Gel Extraction Kit (Qiagen, 28604). Samples were incubated at 37 °C for 2 hours and then were heat inactivated for 20 min at 65 °C to complete digestion. The digestion results were confirmed by agarose electrophoresis. The products were purified and estimated the concentration by visualisation on agarose gel for further process. A 20 µl ligation reaction was prepared using an approximate 3:1 molar ratio of insert to plasmid with 2

µl 10x ligation buffer and 1µl of T4 DNA ligase. The reaction was incubated at 4 °C overnight.

2.2.4.5 Bacterial Culture

2.2.4.5.1 Transformation of competent cells using calcium chloride

Transformation of competent cells *E.coli* cells was performed by using calcium chloride. Prior to transformation, *E.coli* were streaked out on LB agar plate with free antibiotic for 16-20 h at 37 °C. A single colony was picked from a plate and inoculated in 250 µl ice-cold calcium chloride (100 mM) and flicking the tube the until colony disappeared. For transformation, 100 ng of plasmid was added into cell suspension and incubated on ice for 10 min. The cells then were heat-shocked at 42 °C for 30 s and 800 µl LB medium (20 g tryptone, 5g yeast extract, 10mM NaCl per liter) was added. The mixture was incubated for 1 h at 37 °C with vigorous shaking to allow the bacteria to recover and to express the antibiotic resistance marker encoded by the plasmid. The bacterial cells were recovered by centrifugation at 1000 x g speed for 10 min. The supernatant layer was discarded and the pellet re-suspended with 100 µl medium. 100 µl of transformed competent cells were transferred onto an agar plate containing appropriate antibiotic and were then incubated overnight at 37 °C until the transformed colonies appeared.

2.2.4.5.2 Plasmid DNA Mini-Prep using alkaline lysis

A single colony of transformed bacteria was inoculated into 5ml of LB containing the appropriate antibiotic and incubated overnight at 37 °C with vigorous shaking. The

bacterial pellet was recovered from 1.5ml overnight culture by centrifugation at 10,000 x g for 10 min. The pellet was re-suspended in 200 µl of ice-cold solution I (50 mM glucose, 25 mM Tris-Cl (pH 8.0), 10 mM EDTA (pH 8.0) by vigorous vortexing. Solution II (0.2N NaOH, 1% (w/v) SDS) was freshly prepared and then 400 µl was added and mix by inverting. The mixture was incubated for 5 min on ice. 400 µl of ice-cold solution III (5M CH_3COOK, 11.5% (v/v) glacial acetic acid) was added to the mixture and kept on ice for 5 min. The cell lysate was collected by centrifugation at maximum speed for 5 min at 4 °C. The supernatant layer was transferred to a fresh tube and then 2 µl RNAse was added before being incubated for 1 hour at 37 °C. An equal volume of phenol:chloroform:isoamyl alcohol then was added and mixed by vortexing for few seconds and the emulsion was centrifuged at maximum speed for 3 min at 4 °C. The aqueous upper layer was transferred to a fresh tube and 2 volumes of ethanol were added to precipitate nucleic acid at room temperature. The precipitation was recovered by centrifugation at 13,000 rpm for 5 min at 4 °C and then the pellet was washed with 70% of ethanol. The pellet was dried from ethanol by leaving the open tube for 5-10 min and then it was dissolved in 50µl HPLC autoclaved water and stored at -20 °C until required.

2.2.4.5.3 Induction of protein expression in host bacteria

The recombinant plasmid containing hPPARs-LBD was transformed into host bacteria. A single colony was inoculated into 5 ml of medium containing appropriate antibiotics and grow overnight at 37 °C. The bacteria culture then was diluted 1:100 into LB

medium or Terrific Broth (TB) medium (1.2 g tryptone, 2.4 g yeast extract, 10 ml glycerol per 90 ml H_2O and add 10 ml phosphate buffer) until it reached an appropriate optical density at 600 nm. The dilution culture was induced with appropriate concentration of IPTG and incubated in shaker at 18 or 25°C.

The bacteria culture (1.5 ml) was collected by centrifugation at maximum speed for 5 min and then was lysed by using cell lytic (Sigma) or native lysis buffer (0.5% (w/v) Brij58, 0.5 %.(v/v) Tween-20, 300 mM KCl, 50 mM KH_2PO_4 and 5 mM imidazole). The soluble and insoluble fragments were electrophoresed on SDS-PAGE to evaluate protein expression.

2.2.4.5.4 SDS polyacrylamide gel electrophoresis (SDS PAGE)

The gel and buffers were prepared as described in **Table 2.2.** 10% Gel was run in 1x running buffer at 100Am until observed the dye in the bottom of the gel. Gel were transferred and rinsed with staining solution in a developing tray for 1 hour with gentle agitation at room temperature. The gel was then destained by using destaining solution until band was clear and visible.

Table 2.2 Composition of solutions used in SDS PAGE.

Solution	Preparation
4×Separation gel buffer	1.5 M Tris-HCl 0.4% (w/v) SDS
4× Stacking gel buffer	0.5 M Tris-HCl 0.4 % (w/v) SDS
Separation gel	6.7 ml 30% (w/v) acrylamide 5 ml 4×separation gel buffer 200 µl 10% (w/v) ammonium persulphate 20 µl TEMED 8.3 ml H_2O
Stacking gel	1 ml 30% (w/v) acrylamide 2.5 ml 4×stacking gel buffer 100 µl 10% (w/v) ammonium persulphate 10 µl TEMED 6.5 ml H_2O
10× running buffer	144 g glycine 30 g Tris base 100 ml 10% (w/v) SDS in 1000ml H_2O
Staining solution	0.2 % (w/v) Coomassie Brilliant Blue 45 % (v/v) methanol 10 % (v/v) acetic acid
Destaining solution	20 % (v/v) methanol 10 % (v/v) acetic acid

2.2.5 Cyclooxygenase activity measurement

2.2.5.1.1 Microglial cell culture and enzyme preparation

BV-2 cells, a mouse microglial cell line, were grown in Dulbecco's Modified Eagle Medium: Mixture F12 (DMEM/F12) supplemented with 10% heat-inactivated foetal bovine serum, 2 mM L-glutamine in 75 c m^2 flasks and maintained in a 5 % CO_2 humidified incubator at 37 °C. The cells were passaged every 2-3 days and all cell culture conditions were performed under sterile condition.

BV-2 cells were treated for 6 h with 1 µg/ml Lipopolysaccharide (LPS) at 85% confluency. After incubation, cells were washed with PBS and detached from the culture flask by scraping. The cell suspension was collected by centrifugation at 300 x g for 5 min at 4 °C and then re-suspended in ice-cold homogenisation buffer (50 mM Tris base and 1 mM EDTA, adjusted to pH 7.8). The cell pellet was sonicated on ice in three 10 s burst to avoid heating and then was centrifuged at 30,000 x g for 30 min at 4 °C. The supernatant layer was removed and pellet was re-suspended in homogenisation buffer and protein concentration was determined by established methods (Lowry et al., 1951). The sample was stored at 80 °C until required.

2.2.5.1.2 Isolation of human platelets from whole blood

Human platelet samples were kindly provided by Nuha Alnajri from our research group using procedures approved by the Faculty of Medicine Ethics Committee. The protein content was determined by established methods (Lowry *et al.*, 1951) and stored at 80 °C until required.

2.2.5.1.3 Immunoblotting

BV-2 cells were plated ($5x10^5$) in 6 well plates for 24 h. Cells were treated at 80% confluency either with fresh media or bacterial lipopolysaccharide (LPS, 1 µg/ml) for the indicated times to induce COX-2 expression. Cells were washed twice with cold PBS and then suspended in cold lysis buffer (50 mM Tris-HCl, pH 8.0; 150 mM NaCl and 1% NP-40) containing 1 tablet of protease inhibitor cocktail (4-(2- aminoethyl) benzenesulfonyl fluoride hydrochloride, bestatin hydrochloride, leupeptin, E-64, aprotinin, pepstatin A, and phosphoramidon disodium salt; Sigma) for 15 min on ice. The cell lysate was centrifuged at 13,000 x g for 3 min and the pellet re-suspended in assay buffer. The protein concentration was determined using Lowry protein assay (Lowry *et al.*, 1951).

2.2.5.1.4 Assay application

The COX-2 activity method is a fluorescence-based assay based on detection of peroxidase activity utilizing Amplex Red reagent. This method was developed according to the procedure used in a COX-2 activity kit (Cayman, USA).

The tissue sample was diluted in assay buffer (100 mM Tris base, pH8) and initially incubated with heme (1.4 µM) for a minute to increase activity of COX-2. Assay reaction (200 µl) was made up in 96 well plates containing the tissue sample by adding 20 µl of Amplex red (100 µM) and then 5 µl of arachidonic acid (4 mM) was immediately added. The plate was gently shaken for at least 5 min at 37 °C or 25 °C to allow equilibrium prior to placing in a spectrophotometer (where indicated, tissue samples were pre-incubated with inhibitor for 5 min at room temperature). Absorbance

was automatically measured at 590-610 nm every 30 s up to 30 min. Data were obtained from three independent experiments, unless otherwise stated.

2.2.6 Transient transfection and luciferase reporter gene assay

RAW264.7, a mouse macrophage cell line, was grown in Dulbecco's Modified Eagle Medium supplemented with 10 % heat-inactivated foetal bovine serum, 2 mM L-glutamine, 1 mM sodium pyruvate and penicillin (5000 U/ml) streptomycin (5000 µg/ml) mixture. RAW246.7 cells were plated in 48 well plates and transiently transfected at 60-70 % confluency with a luciferase reporter gene construct containing promoter sequence with human iNOS (inducible nitric oxide synthase) plasmid (0.3 µg) or empty vector (pcDNA3.1) per well. Human iNOS promoter were kindly provided by Dr Dawson from University of Nottingham.

Transient transfection was carried out by using Roche Xtreme Gene transfection method with Xtreme gene reagent. The transfection complex was prepared in serum free medium using 3:1 ratio (µl reagent to µg plasmid). Prior to transfection for 20 min, growth media were removed and replaced with fresh culture medium. The transfection mixture was added in each well (plasmid amount 0.3 µg/well) and then incubated for 24 h. After the incubation period, transfected cells were pre-treated with ligands for 30 min and then treated with LPS for 6 h at 10 ng/ml. All ligands were prepared in serum-free medium at the required concentration. Ethanol and DMSO concentrations never exceeded 0.1% in each well.

The luciferase gene expression was measured using the Luciferase Assay System (Promega) and a luminometer (TD-20/20, Turner Biosystems). After the incubation period, growth medium was removed and then cells washed once with PBS. The cells were harvested and lysed using 1X cell lysis buffer. 20 µl of cell lysate was pipetted into luminometer tubes containing 100 µl of luciferase assay reagent and then vortexed briefly. The tube was placed in the luminometer and a recording was made. Each transfection experiment was done in triplicates and each experiment was repeated at least three times. Data were expressed as the mean ± SEM of relative luciferase activity normalized to protein concentration.

2.2.7 Gene expression for inflammatory cytokines

2.2.7.1 Isolation of peripheral blood mononuclear cells (PBMCs) from human blood

All procedures were approved by the Faculty of Medicine Ethics Committee. Blood sample was collected from healthy donors in EDTA vacutainer (BD Diagnostics-Pre analytical Systems, UK) after obtaining consent. Blood was homogenised gently and diluted in an equal volume of Hank's balanced salt solution and gently overlayed on Histopaque -1077 in 50 ml Falcon tubes. The samples were centrifuged at 800 g, with slow acceleration for 30 min at room temperature. PBMCs were removed from the Ficoll interface using a sterile plastic Pasteur pipette and washed twice with Hank's balanced salt solution. The supernatant layer was discarded and the pellet was kept on ice for the next step.

2.2.7.1.1 Monocyte purification

Monocytes were purified from PBMCs by cluster of differentiation (CD) 14 microbeads using magnetic cell separation (MACS) (Miltenyi Biotec). PBMCs were resuspended in cold MACS buffer consisting of 2 mM EDTA, 0.5% FBS in 50 ml PBS and then 20 µl of CD14 beads were added per 10^{-7} PBMCs. The solution was mixed well and incubated at 4 °C in the dark for 15 min. In the meantime, a MS column and magnet were prepared with a pre-separation filter on a MS column and placed into a MACS separator to prevent cell clumps and blocking the column. The column was rinsed three times to be wetted with MACS buffer before applying the suspension. The cells were washed out once with MACS buffer after incubation and centrifuged at 350 x g for 5 min (acceleration=3). 500 µl of the suspension was applied to the wet MS column and washed three times with MACS buffer to facilitate pass CD14 cell through filter.

The column then was put in 15 ml falcon tube and the plunger provided was used to flush 1 ml of MACS buffer through the column. The monocytes were collected after washing and centrifugation at 350 x g at 4 °C for 5 min. Monocytes were re-suspended in RPMI1460 supplemented with 10 % human AB serum, 2 mM L-glutamine, 100 U/ml penicillin, 100 µg/ml streptomycin and 10 mM HEPES to use as described in the next section.

2.2.7.1.2 Monocyte and macrophage culture and treatment

Monocytes were cultured in 96 well tissue culture plates (~$50x10^4$ cells/well) in culture medium including GM-CSF (50 ng/ml) for differentiation to macrophages. The culture

was fed with fresh medium every 3 days and cell differentiation was monitored by light microscopy. Following 7 days of differentiation, cells were pre-treated with 10 µM ligand for 30 min. and then 10 ng/ml LPS was added for another 6 h. For monocyte culture, cells were cultured in 96 well tissue culture plate at 5 x 10^4 cells/well in culture medium and treated as described in macrophage treatment. Where indicated, the PPARα antagonist, GW6471 (10 µM) was added prior to NAEs treatment for 30 min. All incubation period for treatment were performed under 37 °C. All ligands were prepared from 10 mM stocks in serum free medium and solvent was never in excess of 0.1%. Cells were then harvested in Tri-reagent for RNA extraction and medium was collected for nitric oxide quantification.

2.2.7.2 Quantitative Real Time PCR (q-PCR)

2.2.7.2.1 RNA extraction

RNA was isolated from primary cultured human monocytes and macrophages using Tri-reagent® (Sigma, UK). Cells were washed with PBS, homogenised in lysis reagent and incubated for 5 min on ice to dissociate the nucleoprotein complexes completely. To separate the mixture into RNA aqueous, 1-bromo-3-chloro-propane (BCP) was added to samples and centrifuged at 10,000 x g for 15 min at 4 °C. The upper aqueous phase (RNA phase) was transferred to a new tube and isopropanol added with 1 µl glycogen to precipitate RNA.

The RNA precipitation was collected by centrifugation at 10,000 x g for 10 min at 4 °C and the pellet was washed twice with 70 % ethanol. The pellet was dissolved in 87.5 µl DPEC-water and incubated at 65 °C for 5 min to make RNA linear and then DNAase

was added to eliminate DNA. RNA was extracted by adding phenol/chloroform/isoamyl/alcohol and centrifuged at 10,000 x g for 15 min at 4 °C. 40 µl of 3 M sodium acetate and 2 volumes of absolute ethanol was added to precipitate RNA. RNA was collected by centrifugation at 10,000 x g for 15 min at 4 °C and washed twice with 70 % ethanol. The purity and concentration of RNA were measured by using NanoDrop (ND-1000 Spectrophotometer, NanoDrop Technologies, USA) at 260 nm.

2.2.7.2.2 Complementary DNA synthesis

Complementary DNA (cDNA) was produced from 100 ng total RNA using superscript III reverse transcriptase (Invitrogen, UK). The following were added in PCR tube: 3 µl of random primer (100ng/ml) was added to 100ng total RNA and incubated for 5 min at 65 °C. After incubation, 6.3 µl of mixture were added to make up the final reaction volume of 20.5µl (2 µl 10x affinity script RT buffer, 2 µl of 100 mM DTT, 0.8 µl of 100 mM dNTP, with 1 µl of RT for samples or DPEC-water for negative control. The mixture was incubated for 20 min. at 37 °C then 60 min at 50 °C and 70 °C for 15 min. cDNA synthesized was kept at -20 °C for future use. No Template control (NTC) and No Rtase Control (NEC) were also included.

2.2.7.2.3 Pre-amplification procedure

The principle of TaqMan® Pre-amplification technique aims to increase the copy number of the target gene prior to real time PCR. The cDNA for target genes were pre-amplified by pre-amplification reaction. The reaction conditions were based on the amplification of 6.25 µl cDNA in a 25 µl reaction containing 12.5 µl TaqMan® master Mix and 6.25 µl pooled primers mix, where primers for targeting genes listed in **Table**

2.3 were pooled together to prepare mixture containing 0.2 pmol of each primer in Tris-EDTA buffer. The cDNA pre-amplification was then performed in a thermocycler with the following conditions: an initial denaturation step at 96 °C of 10 min, followed by 10 cycles of amplification (95 °C for 15 seconds and 60 °C for 4 min). The pre-amplified product was keep at -20 °C until use.

2.2.7.2.4 Primer and probe design

Primers and probes for Taqman assay were designed from the NCBI database using Primer express (Perkin Elmer, PE) III software (ABI Applied Biosystems). The best probes and primers for target genes were selected to suit PE criteria for Taqman assay (**see Table 2.3**). To ensure specificity of target genes, primers were blasted by using NCBI. Primers and Probes were prepared as described in **section 2.2.4.1**.

Table 2.3 Primers and probes sequences for TaqMan gene expression analysis

Human Gene	Sequences (5'-3')
IL-1ß	**Forward** CCTAAACAGATGAAGTGCTCCTT **Reverse** GGTGGTCGGAGATTCGTAGCT **Probe** CTGGACCTCTGCCCTCTGGATGGC
IL-10	**Forward** TTGCTGGAGGACTTTAAGGGTTAC **Reverse** GTCTGGGTCTTGGTTCTCAGCTT **probe** TTGCCAAGCCTTGTCTGAGATGATCCA
TNF-alpha	**Forward** CCCAGGGACCTCTCTCTAATCA **Reverse** GGTTTGCTACAACATGGGCTACA **probe** CTCTGGCCCAGGCAGTCAGATCATCT
PPARα	**Forward** TCATCACGGACACGCTTTCA **Reverse** TCCCCGCAGATTCTACATTCG **probe** CTCGGTGACTZATCCTGTGGTCCC
PPARβ	**Forward** CATCCTCACCGGCAAAGC **Reverse** CCTTCTCTGCCTGCCACAAT **probe** ACACGGCGCCCTTTGTGATCCA
PPARγ	**Forward** GTGGAGACCGCCCAGGTT **Reverse** ACTCAGGGTGGTTCAGCTTCA **probe** ACAACCTGCTACAAGCCCTGGAGCTCC
B2M	**Forward** CGCTCCGTGGCCTTAGC **Reverse** AATCTTTGGAGTACGCTGGATAGC **probe** TGCTCGCGCTACTCTCTCTTTCTGGC
ACTB	**Forward** CCTGGCACCCAGCACAAT **Reverse** GCCGATCCACACGGAGTACT **probe** ATCAAGATCATTGCTCCTCCTGAGCGC
GAPDH	**Forward** CAA CAG CCT CAA GAT CAT CAG C **Reverse** TGG CAT GGA CTG TGG TCA TGA G **probe** CCT GGC CAA GGT CAT CCA TGA CAA C
TBP	**Forward** ATCCACAGTGAATCTTGGTTGTAAACT **Reverse** AAACCGCTTGGGATTATATTCG **probe** AGACCATTGCACGTGCCCGA

2.2.7.2.5 TaqMan real-time quantitative PCR

The mRNA expression levels of selected genes in **Table 2.3** were performed using the automated AirMax software, Real Time PCR (RT-PCR) system (Agilent, UK). Data were analysed based the relative standard curve method. The standard curve consisted of 4-fold serial dilutions of synthesised cDNA for all samples studied. The reaction mixture was made up **according to Table 2.4**.

Table 2.4 Primers and probes sequences for TaqMan gene expression analysis

Reagent	Volume (µl)
TaqMan® Brilliant lll Ultra Fast PCR Master Mix with low ROX	10
Forward primer (10 µM)	0.8
Reverse primer (10 µM)	0.8
Probe (150 nM)	0.4
HPLC H_2O	3
cDNA	5
Total volume	20

All standards, samples and negative control were distributed into optical 96 well plate in triplicate. PCR conditions were performed following the manufacturer's instructions, an initial step (**melting temperature**) at 95 °C for 3 min, followed by 40 cycles (**annealing temperature**) at 95 °C for 5 s and 60 °C for 10 s.

The standard curve was plotted as threshold cycle (Ct value) versus the logarithm of the serial cDNA dilutions, where Ct is the point at which fluorescence is generated and rises to a signal significantly above background. The slope of standard curve should be between -3.2 to 3.6 and efficiency (90% - 100%), see **Figure 2.3.** The data were

normalised to B2M as reference gene. Data are presented as means ± SEM of three independent experiment.

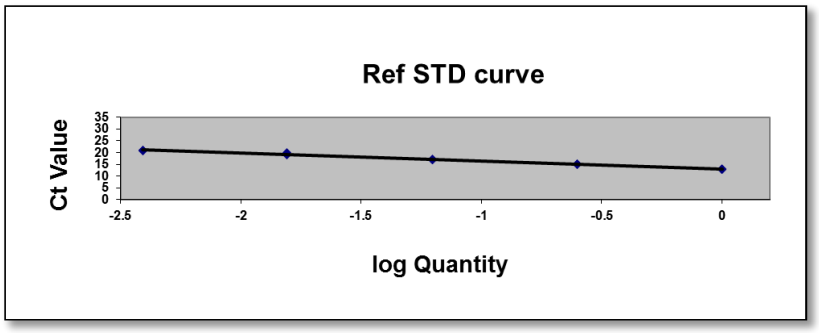


Figure 2.3 TaqMan Real-time PCR standard curve for reference gene. RNA polymerase in human monocytes representing the slope value (-3. 35) and correlation co-efficient (r2) value (0.99).

2.2.8 Nitric oxide measurement

Nitrite accumulation in culture medium for human monocytes and macrophages was monitored as nitric oxide (NO) production using Griess method (Green *et al.*, 1982). After the incubated period with compounds, 100 µl of the cell culture medium from each well was mixed with an equal volume of Griess reagent (2% sulfanilamide and 0.1% naphthylethylenediamine dihydrochloride in 1mM HCl) and then incubated for 10 min at room temperature. A serial dilution of sodium nitrite was prepared as a standard curve for NO formation. Absorbance was determined at 540 nm spectrophotometrically.

2.3 Statistical and Data analysis

All data were collected from at least three or more independent experiments in triplicate, unless otherwise stated. Data were analysed using GraphPad Prism Version 6.0 Software (GraphPad Software, Inc.,SanDiego CA, USA) and are expressed as the standard error of the mean (SEM).

Statistical normality test was conducted on all data. Parametric data (Functional activity of hCB_1 and CB_2, URB597 effects, DRG neurons responses, hiNOS promoter activity, gene expression levels of cytokines, NO production) were analysed by one-way and Two-way analysis of variance (ANOVA) followed by a Dunnett's test for multiple comparisons or student's un-paired or paired t-test for direct comparisons between two variable. $P<0.05$ was considered statistically significant.

Chapter 3
Development of a novel fluorescence assay based on quantification of ethanolamine to measure activity of FAAH enzyme

3.1 Introduction

Fatty acid amides occur in nature in multiple forms; from ceramide as a major component of sphingolipids to the N-acyl constituent of proteins. Glycerophospholipids with amide bonds are present only in trace amounts, and include N-acyl phosphatidylethanolamines (N-acyl PEs) and N-acyl phosphatidylserines (N-acyl-PSs) (Astarita *et al.*, 2008). Although N-acyl PEs and N-acyl-PS might have other functions in biological membranes, a major interest in N-acyl PEs derives from their precursor function for N-acylethanolamines.

Following the discovery of AEA as the first endogenous cannabinoid, less attention has been paid to the other NAEs, especially n-3 and n-6 long-chain polyunsaturated fatty acids ethanolamines, to examine the biological relevance of these ligands. Existing research suggests a critical role played by n-3 and n-6 polyunsaturated fatty acids, mainly from fish oils, in the human diet that are reported to have significant health benefits, such as reducing the risk of cardiovascular diseases, potentially reducing cancer and evoking an anti-inflammatory response. The explicit mechanisms behind these effects remain unknown (Balvers *et al.*, 2010). The reason for this absence of information might be a lack of understanding of the metabolism of these compounds.

FAAH is a membrane-bound protein localised predominantly to the microsomal fraction of rat liver and brain (Deutsch and Chin, 1993a, Desarnaud *et al.*, 1995). A previous study investigating the levels of NAEs in different rat tissue (Pete Christensen, PhD 2009) observed significantly elevated levels of C22:5, C22:4, C18:2. NAEs in liver and brain after 5 h post-mortem alongside with C20:4, C16:0 and C18:1. Furthermore,

URB597, a selective FAAH inhibitor, significantly increased levels of saturated and monounsaturated NAEs in rat lung, but not testes as seen in **Figure 3.1**. Given the biological importance of NAEs, all these observations raised further questions concerning the hydrolytic cleavage of these NAEs by FAAH.

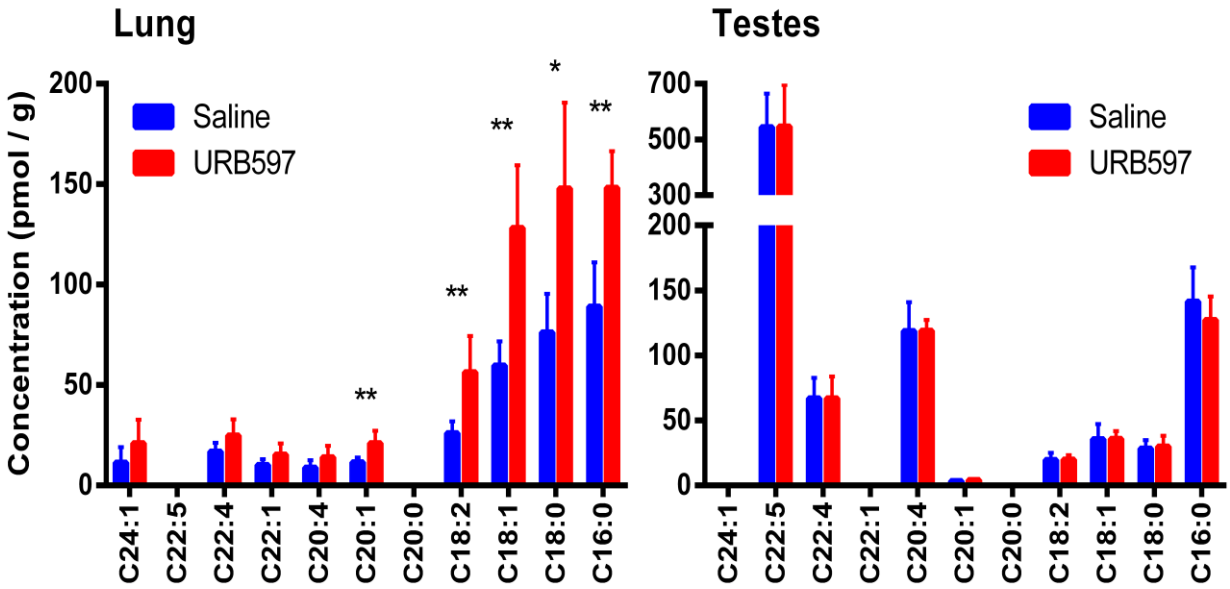


Figure 3.1 Effect of URB597 (0.3 mg/kg, single dose) on the levels of NAEs using LC-MS in lung and testes of rat. Data are from Pete Christensen and are mean ± SEM of 5-6 animals. *p< 0.05, ** p< 0.01, non-parametric Mann-Whitney test (Christensen PhD, 2009).

In Pete's study (2009), the average concentration of NAEs in sample tissues which is mix of heterogeneous cells, with unknown subcellular distribution was measured. In addition, the levels of NAEs are synthesised on demand from their precursors and act locally, suggesting that their levels are likely to be constantly fluctuating. Therefore, the 'real' concentration of NAEs is difficult to predict. It can be assumed that 10 µM is

an optimal concentration of NAEs which could be used for receptors studies in the following chapters such as cannabinoids (CB_1 and CB_2) and TRPV1 receptors. Moreover, the potency of AEA in activation of these receptors has been reported in previous studies with pEC50 values of 6.6 (Priestley *et al.*, 2017b, Movahed *et al.*, 2005).

3.1.1 FAAH enzyme activity measurements

Since the discovery of FAAH as a potential therapeutic target, research has multiplied considerably to find a simple assay to measure activity of FAAH. In fact, there are various methods to monitor FAAH activity. Up until recently, conventional assays required radiolabelled substrates and/or involve the use of chromatographic techniques.

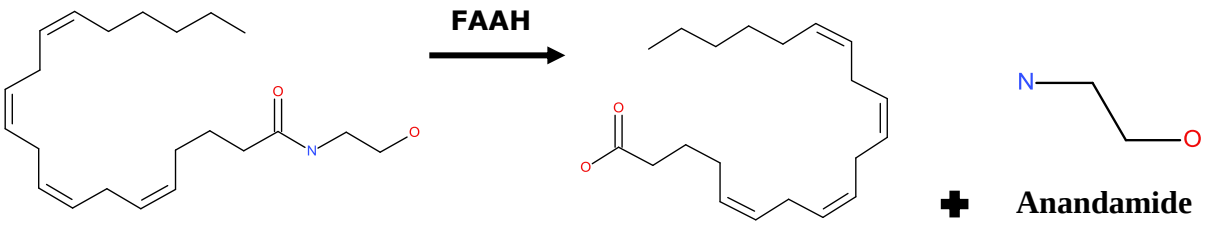
Thin-layer chromatography was the first method for separating the radioactive arachidonic acid that results from AEA (*N*-^{3}H-arachidonoylethanolamine) hydrolysis (Deutsch and Chin, 1993b). However, there are drawbacks associated with the use of radioactivity and to overcome that, an alternative method made use of high-performance liquid chromatography and non-labelled AEA as a substrate (Lang *et al.*, 1996). However, it was not sufficient for low FAAH activity detection.

A further version of the FAAH assay used chloroform extraction to separate the water-soluble radioactive ethanolamine product of AEA (*N*-arachidonoyl-^{3}H-ethanolamine) hydrolysis (Maurelli *et al.*, 1995). This assay could not be adapted to a high-throughput screening (HTS) format due to the cumbersome physical manipulations of the method and handling restrictions. In 1997, a fluorescence displacement assay was described which measured FAAH activity indirectly by detecting the displacement of a bound

fluorescent fatty acid analogue by free fatty acid generated upon hydrolysis of AEA (Thumser *et al.*, 1997b).

In 2005, a "simple, sensitive and high throughput" FAAH assay was described using arachidonic acid conjugated to a coumarin as substrate, which generated a fluorescent product (Ramarao *et al.*, 2005) In the same year, an enzyme coupled spectrophotometric assay was reported, which made use of one of the natural substrates for FAAH, oleamide (De Bank *et al.*, 2005). Scaling for HTS was described, however, the assay has disadvantages of being a destructive (rather than accumulative) method and also through the coincidence of the detection wavelength (340 nm) with many of the potential inhibitors of the enzyme.

Prior to investigate FAAH activity in NAE hydrolysis, a fluorescence assay was generated in our lab at the University of Nottingham (described in further detail below). This assay is based on quantification of ethanolamine released from hydrolysis of NAEs (**Figure 3.2**), which is cost effective, avoids handling radioisotopes and is amenable for medium-throughput screening.



Arachidonic acid **Ethanolamine**

Figure 3.2 Anandamide hydrolysis by fatty acid amide hydrolase (FAAH).

3.2 Aim

The aim of this Chapter was to generate a validated assay of NAE hydrolysis. The specific objectives were to:

1. Develop a novel fluorescence assay based on ethanolamine quantification.
2. Determine the enzyme kinetics (K_m and V_{max}) of FAAH activity towards various NAEs using a rat liver microsomal preparation.
3. Validate the NAE hydrolysis assay by determining the potency of URB597 as a selective inhibitor of FAAH activity.

3.3 Results

3.3.1 FAAH assay development

3.3.1.1 Measurement of ethanolamine

FAAH, the enzyme responsible for hydrolysis of AEA and other *N*-acylethanolamines, generates ethanolamine and free fatty acids. Therefore, ethanolamine was considered the optimal candidate molecule to measure to quantify this enzyme. Before applying the assay to measure FAAH activity, it was necessary to determine whether the ethanolamine generated by *N*-acylethanolamine hydrolysis could be detected by this assay, using NDC and acetonitrile (1 mg/ml) which react with ethanolamine to yield a strong fluorescence adduct at alkaline buffer (borate buffer at pH 11) (Miralles *et al.*, 1997).

A serial dilution of ethanolamine was prepared (0-10) mM and diluted in potassium phosphate buffer, pH 7. TCA (10%) was added before serially diluting ethanolamine concentrations 3-fold in NDC/acetonitrile/borate mix, and reading the plate at 420 nm excitation and 480 nm emission in a fluorescence spectrometer (FLUOstar Galaxy application). To test the selectivity of this assay, serial dilutions of ammonium sulphate were prepared using the same range of concentrations of ethanolamine. The standard curve of fluorescence values against ethanolamine and ammonium sulphate concentrations were plotted (**Figure 3.3)**. The ethanolamine curve was concentrations-dependent and saturable at concentrations above 25 μM under these assay conditions. In comparison, the plot with ammonium sulphate was essentially flat over the same concentration range.

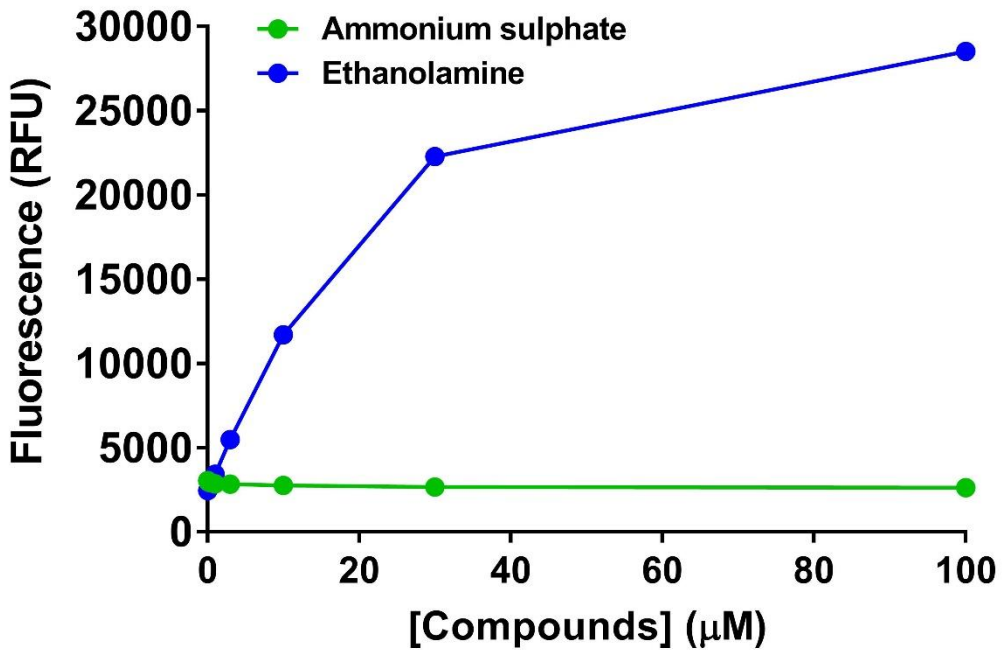


Figure 3.3 Quantification of ethanolamine and ammonium sulphate using NDC as fluorescence developing reagent. Serial concentrations of ethanolamine and ammonium sulphate were prepared in phosphate buffer at pH 7.4 and then 'stopped' using 10% TCA. The fluorescence was measured using a fluorimeter (FLUOstar Galaxy) set at 418 nm excitation and 480 nm emission. Data are mean ± SEM of fluorescence readings from four independent experiments.

3.3.1.2 Optimization of ethanolamine quantification

3.3.1.2.1 Latency and stability of the fluorescent adduct

In order to assess the viability of the fluorescent adduct, an experiment was conducted with various ethanolamine concentrations prepared at pH 7.4 and these were followed over time (**Figure 3.4**).

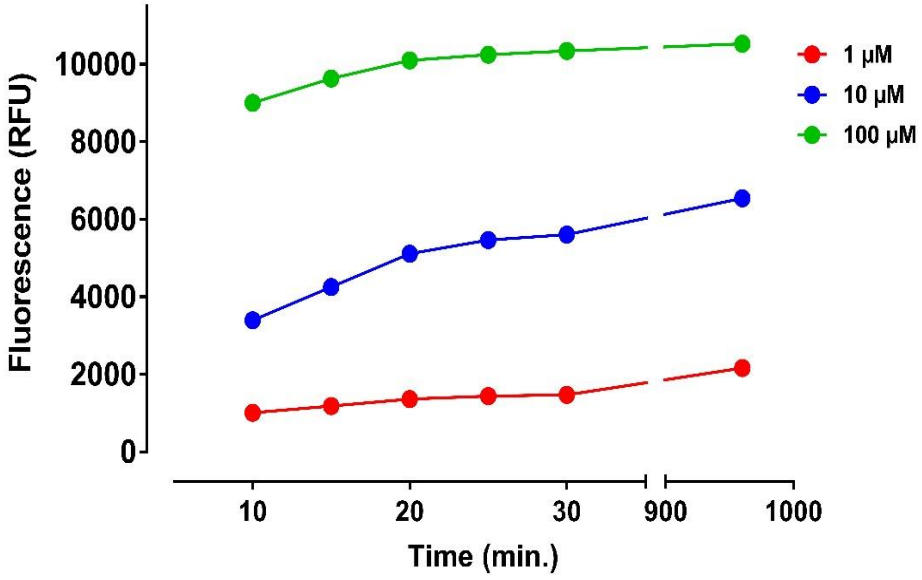


Figure 3.4 Stability of fluorescence production of ethanolamine reaction over time. The fluorescence produced by three ethanolamine concentrations was monitored using a fluorimeter set at 418 nm excitation and 480 nm emission (n=1).

Results of varying development times on the fluorescent adduct of ethanolamine can be seen in **Figure 3.4**. Rates of reactions were dependent on ethanolamine concentrations. All three concentrations were shown to be reasonably stable and distinguishable from each other over the time period examined.

3.3.1.2.2 Effect of TCA and PCA

In many different enzyme assays, perchloric acid (PCA) and trichloroacetic acid (TCA) act as stopping reagents, as they are effective at precipitating protein. The influence of different PCA and TCA concentrations, 20%, 10%, 5% (w/v), were therefore compared for their effects on ethanolamine quantification (**Figure 3.5**). It appeared that there were no differences in the observed fluorescence products of ethanolamine between different concentrations of TCA and PCA. However, it was noticeable that the blank was slightly lower in the presence of TCA than PCA.

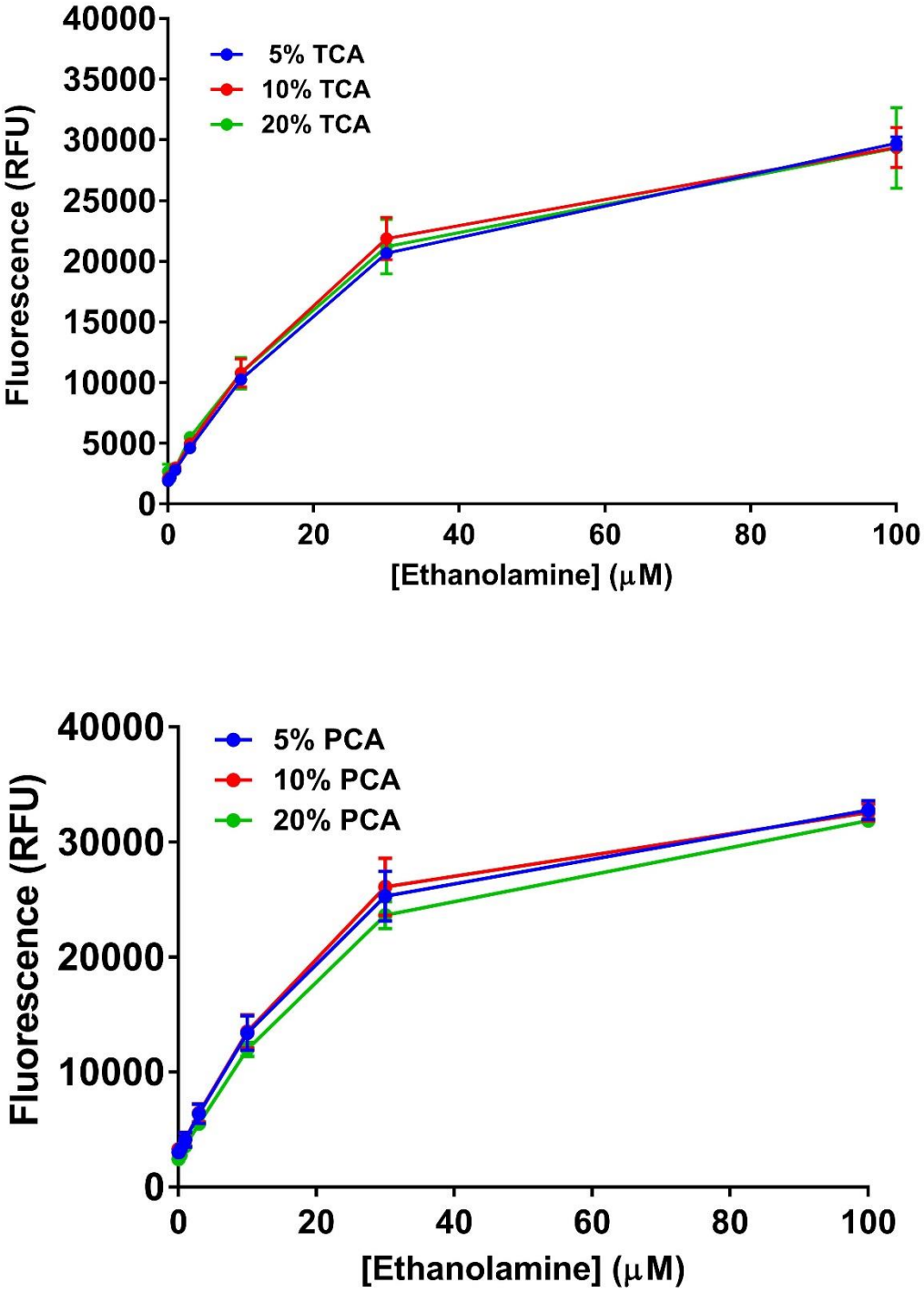


Figure 3.5 Effects of stopping reagents (PCA and TCA) dilutions on ethanolamine quantification. Ethanolamine concentrations were prepared at serial dilutions in phosphate assay buffer at pH 7.4. The reaction was stopped with different PCA and TCA dilutions. The fluorescence produced was measured at 418 nm excitation and 480 nm emission Data are means ± SEM of fluorescent readings from three independent experiments.

3.3.1.2.3 Effect of pH of borate buffer

The NDC/acetonitrile mix reacts with ethanolamine in the presence of an alkaline borate buffer to generate a strong fluorescent adduct (possibly 1-cyanoisoindole) (Miralles *et al.*, 1997). The optimization of borate buffers on ethanolamine quantification at alkaline pH ranging between 10.1, 10.5, 11 and 11.5 was investigated (**Figure 3.6**).

There were no obvious differences in the fluorescence of ethanolamine production between different pH values of borate buffers (**Figure 3.6**). Good sensitivity of fluorescence was achieved at pH 11 (Miralles *et al.*, 1997). On the basis of the results obtained from these experiment, borate buffer pH 11 was chosen for all subsequent experiments.

All of the results described above demonstrate that the novel assay can measure ethanolamine production. The next step was then to apply the novel assay to measure ethanolamine production from hydrolysis of fatty acid ethanolamine.

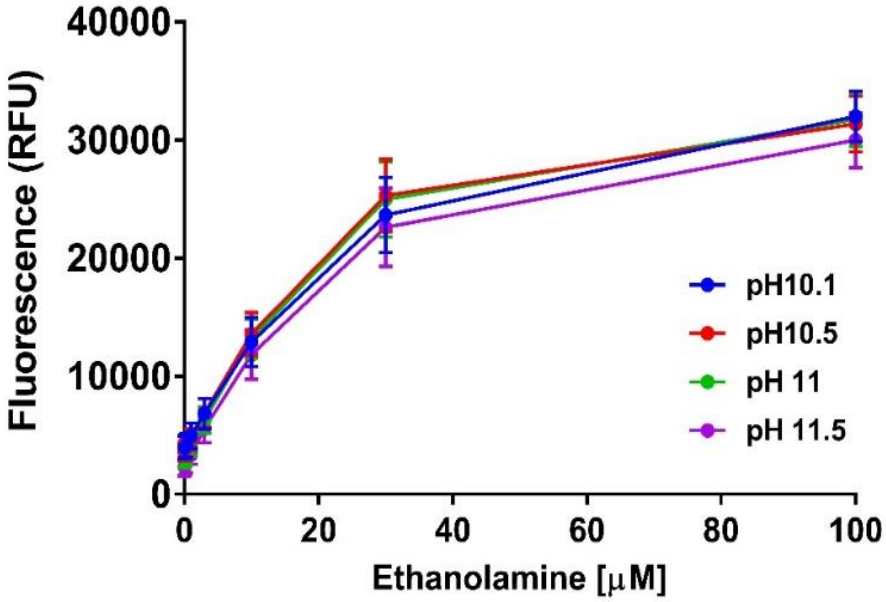


Figure 3.6 Effect of pH of borate developing buffer on the quantification of ethanolamine. Serial concentration of ethanolamine were prepared in assay buffer (pH 7.4) and stopped the reaction using 10% TCA. The fluoresce reagent (NDC) were dissolved in acetonitrile (1:1) followed by then mixed with different pH of borate buffer. The fluorescent product was measured at 418 nm excitation and 480 nm emission. Data are means ± SEM of fluorescent readings from four independent experiments conducted in triplicate.

3.3.1.3 Application of assay

FAAH is a membrane bound enzyme which is highly expressed in liver and brain tissue (Schmid *et al.*, 1985) therefore, rat liver microsomes were chosen as a source of FAAH activity. In order to generate an assay of FAAH activity, there are several factors which must be examined that might affected enzyme activity.

- **Incubation time**

An enzyme assay requires an incubation period sufficient to allow the production of a considerable amount of detectable and measurable ethanolamine. However, an extended time may mean that the catalytic activity of the enzyme may be lost due to denaturation. Enzyme activity was, therefore, investigated for up to 60 min with a range of OEA concentrations (**Figure 3.7**).

OEA hydrolysis was observed to be almost directly proportional to the incubation time up to 30 min, with linear regression analysis showing $r^2 = 0.9764$ and $p < 0.0001$ (**Figure 3.7**). For further investigation, a time point of 15 min was chosen to measure FAAH activity.

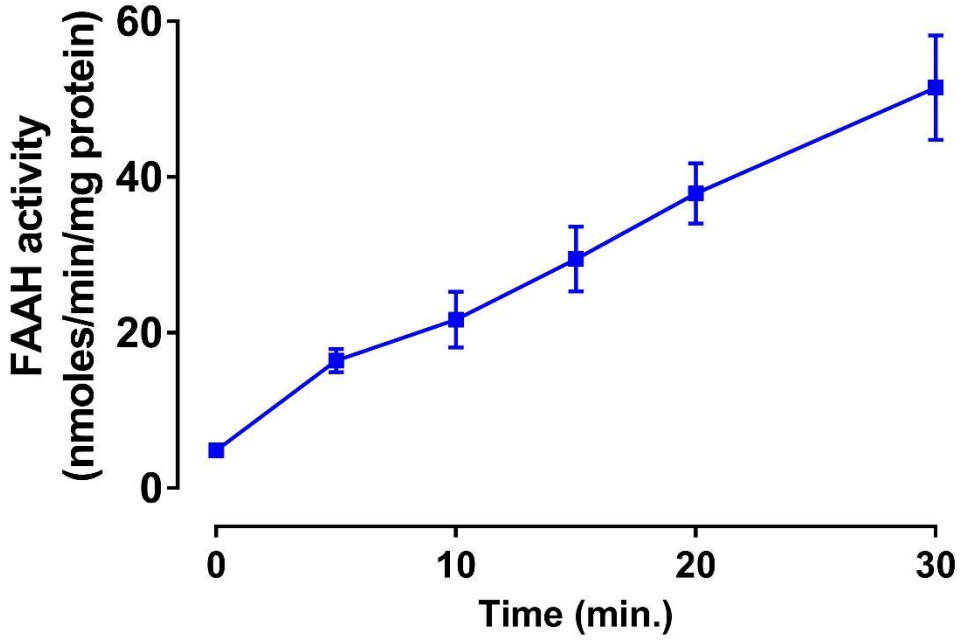


Figure 3.7 Time course of FAAH activity in rat liver microsomes. At different time point of incubation, 100-fold dilution of tissue in assay buffer was incubated with OEA (100 µM) at 37 °C at various times. Data are mean ± SEM of enzyme activity in nmol/min/mg protein from three independent rat microsomal preparations.

- **Effect of Bovine Serum Albumin on FAAH activity**

Bovine serum albumin (BSA) acts as a weak antioxidant to stabilize many enzyme activities and prevents adhesion of the enzyme/ligands to the reaction vessel. In addition, it is a major transport protein for many compounds, including fatty acids and N-acylethanolamides (Demuth and Molleman, 2006). The influence of BSA on FAAH activity was, therefore, investigated.

The effects of varying BSA concentrations on FAAH activity can be seen in **Figure 3.8 A**. It appeared that BSA significantly increased of rat liver hydrolysis of PEA at 8 μM (one-way ANOVA followed by post-hoc Dunnett's test; *p<0.05). Therefore, 1 mg/ml BSA was chosen for subsequent experiments.

A range of substrate concentrations was; also investigated (**Figure 3.8 B**). The rates of OEA hydrolysis were dependent on OEA concentrations and the presence of BSA (1 mg/ml). It appeared that the presence of BSA had more of an effect on the V_{max} without altering the affinity (K_m), where K_m for OEA with and without BSA were 12 μM but V_{max} were 72 and 96 nmol/min/mg, respectively. It is apparent that BSA does not alter substrate presentation but somehow increases FAAH activity.

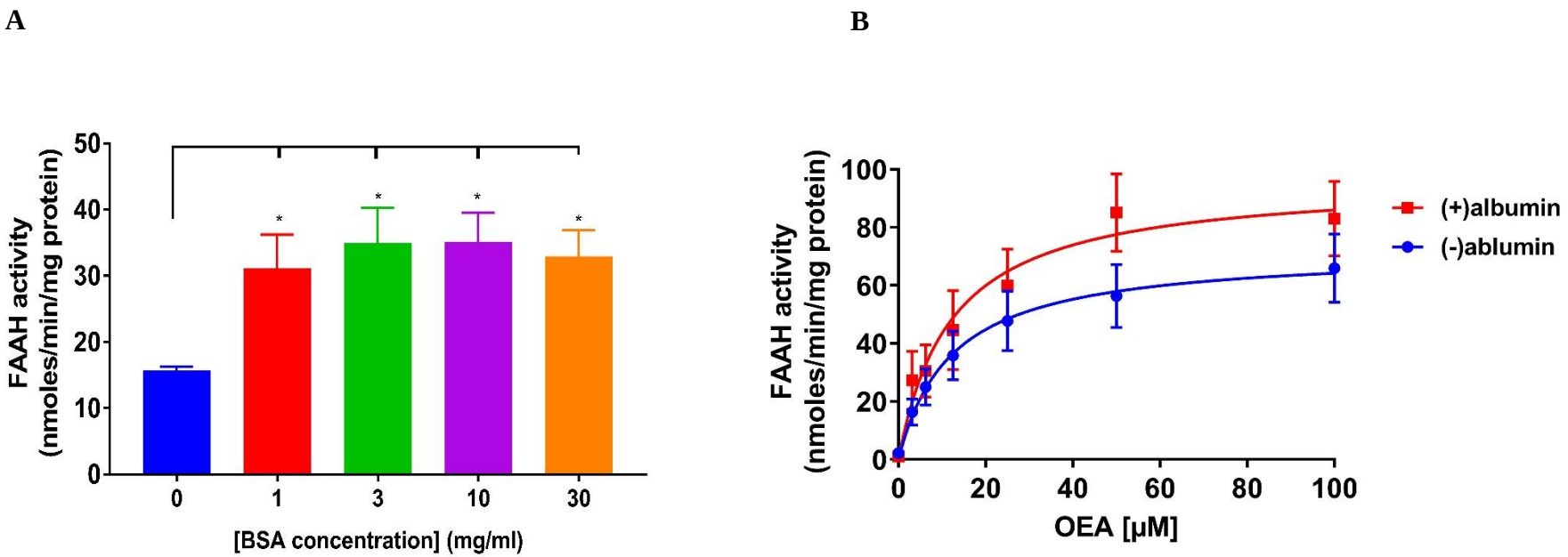


Figure 3.8 (A) The effect of BSA on FAAH-catalysed hydrolysis of PEA at 8 µM in rat liver microsomal preparations. Statistical analysis was determined using one-way ANOVA followed by post-hoc Dunnett's test; *p<0.05. **(B)** 1 mg/ml of BSA enhanced the maximal velocity of FAAH activity mediated OEA hydrolysis. Data are mean ± SEM of four different liver microsome preparations.

- **Protein concertation**

Analysis from multiple determinations suggested that there were variations in K_m values in different preparations of rat liver **(Table 3.1)**. Therefore, the influence of serial dilution of tissue on FAAH activity was investigated, as seen in **Figure 3.9**. There were differences in FAAH activity at the highest concentration of protein, while at the low concentrations (~ 10 µg/ml) there were similarities in activities between different liver microsomal preparations. Therefore, 10 µg/ml of protein was used for subsequent experiments.

Table 3.1 Enzyme kinetics of AEA hydrolysis in different rat liver microsomal preparations (n= 4)

Liver microsomes	Protein (µg/ml)	K_m (µM)	V_{max} (nmol/min/mg)
1	33.4	14.4	43.4
2	51.2	50.9	73.42
3	58.8	50.9	83.0
4	27.4	7.0	46.5

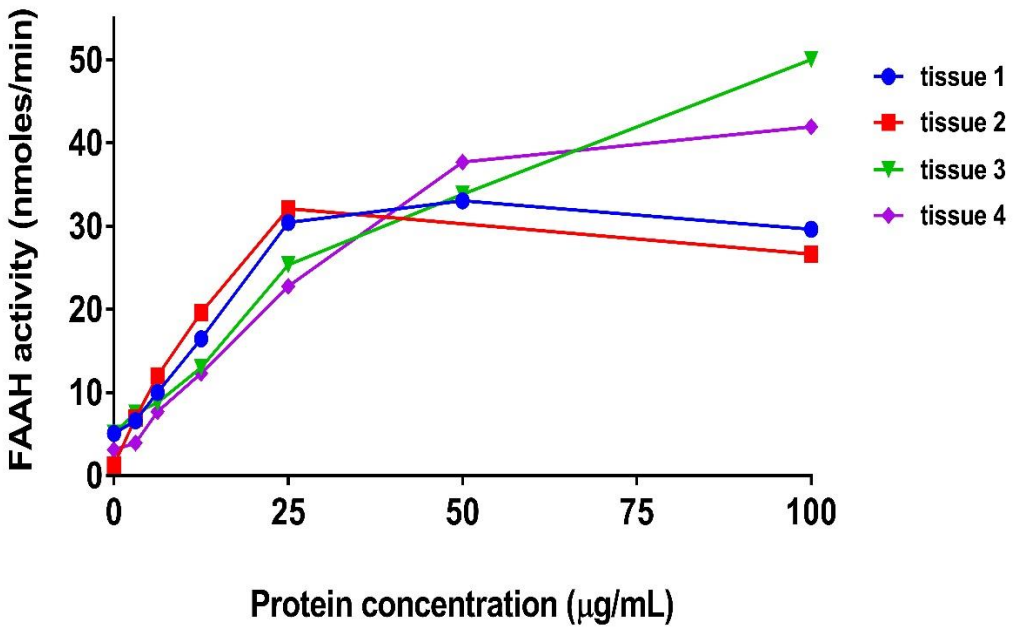


Figure 3.9 The effect of protein concentration on FAAH-catalysed hydrolysis in different rat liver microsomal preparations. Serial dilutions of proteins were prepared in assay buffer (pH 7.4) and incubated with 1 mM PEA at 37 °C for 15 min.

- **FAAH activity mediated AEA hydrolysis in liver microsomes**

AEA hydrolase activity in rat liver microsomes at 10 µg/ml protein was measured using the fluorescence assay (**Figure 3.10).** AEA hydrolysis was concentration-dependent with K_m (2 ± 0.6 µM) and V_{max} values (183 ± 9 nmol/min/mg protein) calculated from fitting the Michaelis–Menten equation.

These results indicated that this assay was effective as a measure of FAAH activity, and so the next step was to complete the validation process.

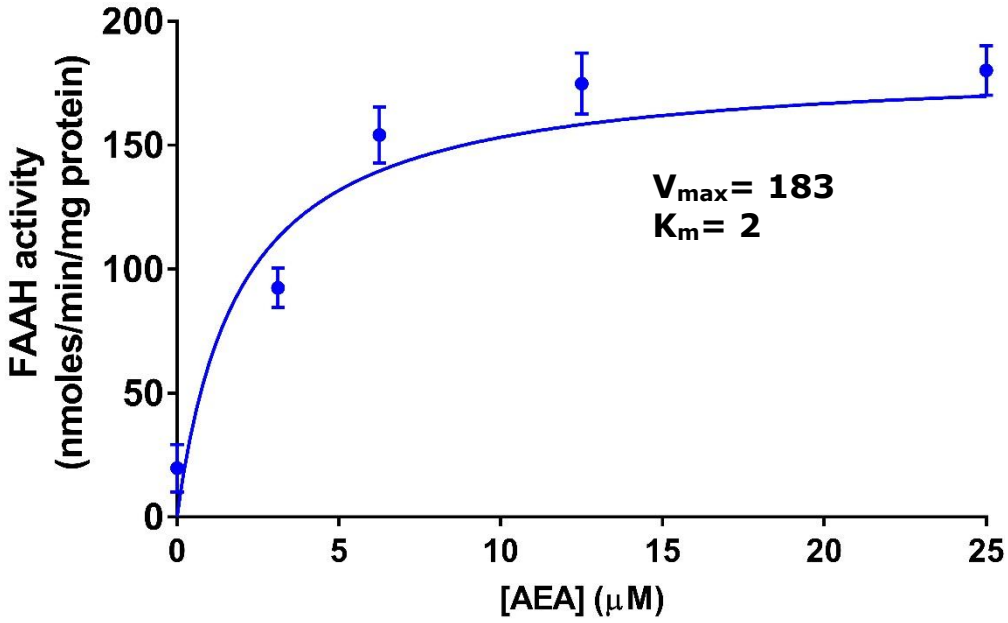


Figure 3.10 Hydrolysis of AEA by rat liver microsomes. Serial dilutions of AEA were prepared and incubated with 10 µg/ml liver microsomes in assay buffer (pH 7.4) containing 1 mg/ml BSA at 37 °C for 15 min. Data are mean ± SEM values of three different liver tissue preparations.

3.3.2 Assay validation

The previous results demonstrated that the novel fluorescence assay could measure AEA hydrolysis in rat liver preparations; to confirm the involvement of FAAH in this activity, parallel experiments were conducted with the 'Gold Standard' assay and inhibitor of FAAH activity (**Figure 3.11**) Thus, the effect of the FAAH selective inhibitor URB597 on AEA hydrolysis in liver microsomes (at 10 µg/ml protein) was examined using the fluorescence assay and, in direct parallel using the same preparations and solutions, the radiometric assay.

AEA hydrolysis was inhibited by URB597 in a concentration dependent manner using the novel fluorescence assay and classical radiometric assay. The pIC_{50} values of URB597 for inhibition of FAAH activity using the novel fluorescence assay was 9.9 ± 0.01, Hill slope= -0.5 ± 0.05 and minimum inhibition= 5 ± 0.3. The same parameters were 9.8 ± 0.2, Hill slope= -0.7 ± 0.2 and minimum inhibition= -6 ± 4 using the radiometric assay.

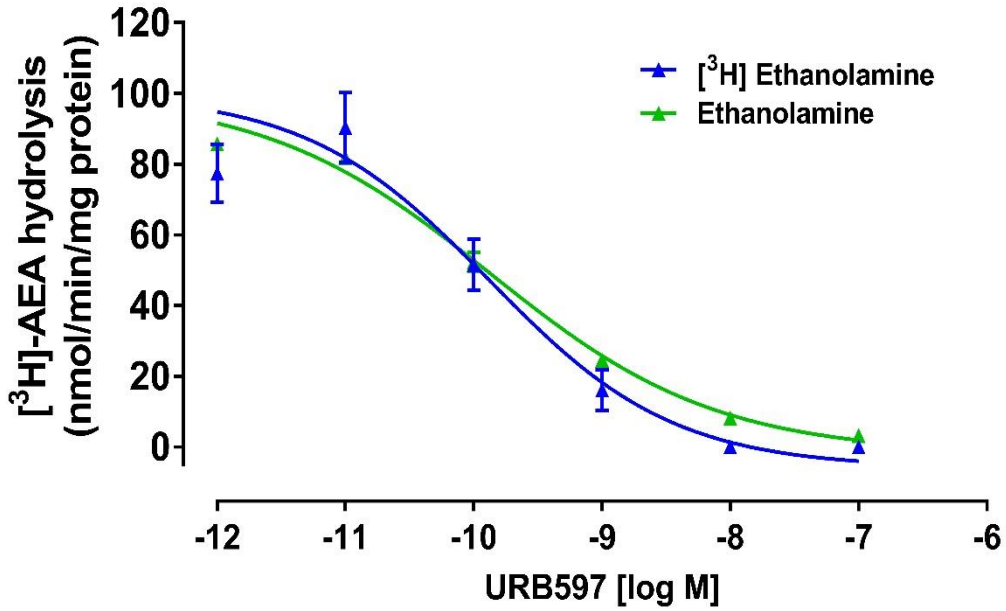


Figure 3.11 Radiometric assay used in inhibition of FAAH activity-catalysed by AEA in rat liver microsomal at 10 µg/ml. URB597 concentrations were pre-incubated with tissue at 10 µg/ml for 15 min in Tris-EDTA buffer at pH 7.4 buffer. Following incubation with AEA at 5 µM for 15 min. at 37 °C. FAAH activity hydrolysed AEA from each assay was measured and calculated as described in method section. Data are shown as mean ± SEM values from liver microsomal preparations.

3.3.3 FAAH-mediated hydrolysis of fatty acid ethanolamines

The novel fluorescence assay based on ethanolamine quantification was utilised to investigate the hydrolysis of a number of commercially available fatty acid ethanolamines in rat liver microsomes.

The data shows that rat liver membranes hydrolysed all of the NAEs in a concentration-dependent manner. The enzyme kinetic values (**K_m** and **V_{max})** of each compound were calculated according to the Michaelis-Menten equation. The affinities (K_m) of tested fatty acid ethanolamines can be divided into higher affinity (2-7 µM) and low affinity (12-18 µM) (as seen in **Table 3.2)**. All NAEs with two or more unsaturations showed higher affinity while the group exemplified by all the saturated and monounsaturated NAEs showed low affinity, with the exception of C22:1, n-9 which exhibited high affinity. The maximal velocities of hydrolysis (V_{max}) can be grouped similarly to the affinity classification. Most NAEs which exhibited low affinity showed lower maximal rates while not all higher affinity substrates had high V_{max} values, where the maximal rates of C22:5, n-6 and C22:6, n-3 NAEs hydrolysis appeared low.

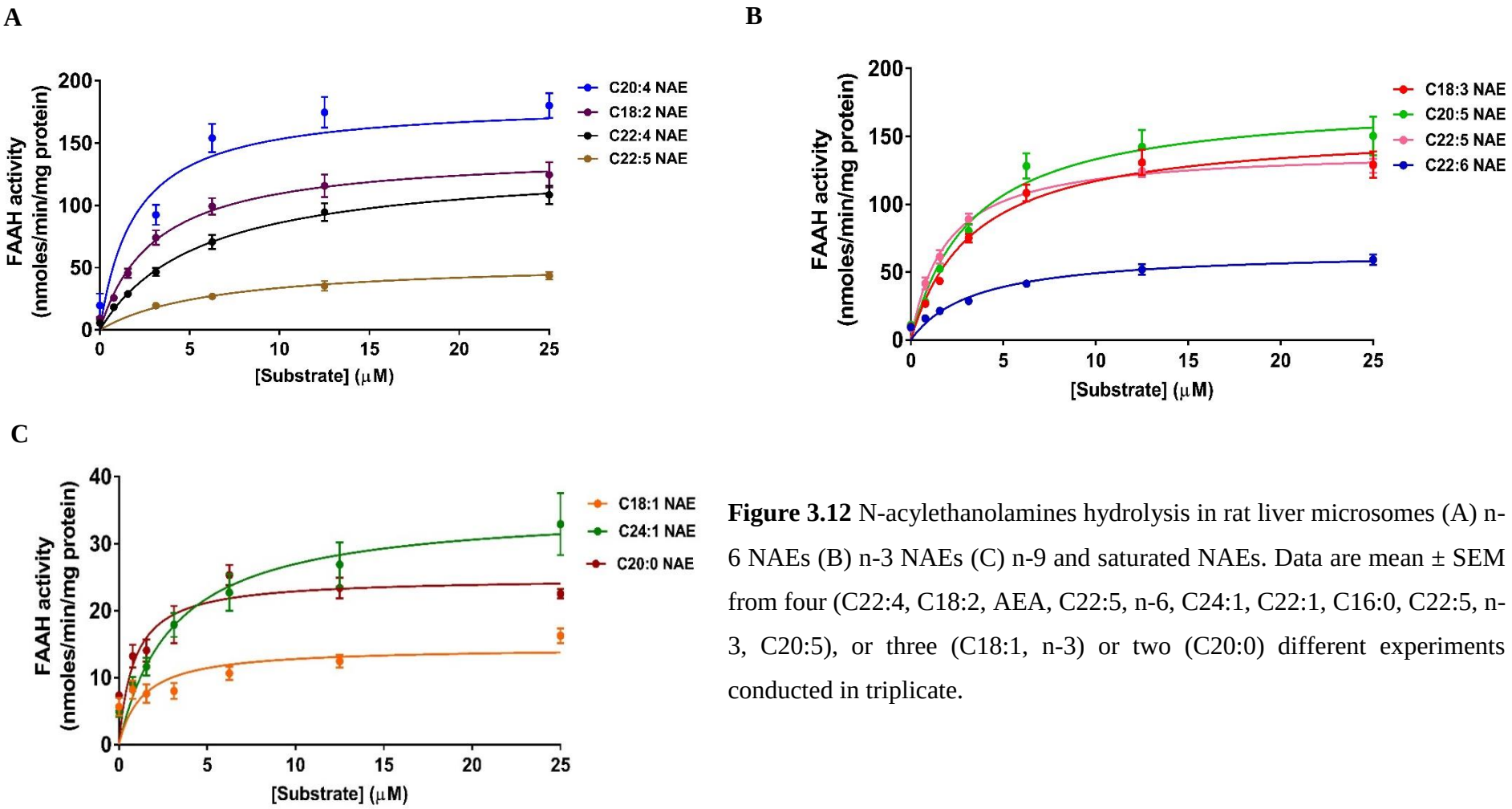


Figure 3.12 N-acylethanolamines hydrolysis in rat liver microsomes (A) n-6 NAEs (B) n-3 NAEs (C) n-9 and saturated NAEs. Data are mean ± SEM from four (C22:4, C18:2, AEA, C22:5, n-6, C24:1, C22:1, C16:0, C22:5, n-3, C20:5), or three (C18:1, n-3) or two (C20:0) different experiments conducted in triplicate.

Table 3.2 Enzyme kinetics of fatty acid ethanolamine hydrolysis by rat liver microsomes.

NAEs	K_m (μM)	V_{max} (nmol/min/mg)	Relative rate (% AEA V_{max})
C20:4, n-6	2 ± 0.6	183 ± 8	100%
C 20:5, n-3	3 ± 0.2	177 ± 16	97%
C18:3,n-3	4 ± 0.2	153 ± 13	83%
C 18:2, n-6	4 ± 0.2	142 ± 16	78%
C22:5, n-3	2 ± 0.5	136 ± 11	74%
C 22:4, n-6	7 ± 0.7	132 ± 17	72%
C22:6, n-3	7 ± 0.8	64 ± 7	35%
C22:5, n-6	2 ± 0.2	56 ± 8	31%
C18:1, n-9	15 ± 5	42 ± 6	23%
C16:0	18 ± 6	41 ± 5	22%
C22:1, n-9	3 ± 0.8	36 ± 13	20%
C18:0	12 ± 4	32 ± 5	18%
C20:0	13 ± 1	16 ± 4	13%
C24:1, n-9	16 ± 2	14 ± 1	8%

To confirm the role of FAAH activity in mediating the hydrolysis these ligands, serial dilutions of URB597 were pre-incubated with tissue for 15 min prior to substrate incubation (**Figure 3.13**). The results revealed that URB597 inhibited fatty acid ethanolamine hydrolysis of all the substrates tested in a concentration dependent manner. The potencies (pIC_{50} values) of URB597 inhibition of NAE hydrolysis were similar to the URB597 potency for inhibition of AEA hydrolysis, as seen in **Table 3.3**. Hydrolysis of other fatty acid ethanolamines, C22:5, n-3, C 20:5 n-3 and C22:1, was also inhibited by 1 μM URB597, as seen in **Appendices**.

Table 3.3. The potency of URB597 in hydrolysis of tested ligands. Data are shown as mean ± SEM values from four separated experiments in triplicates from different preparation of liver microsomes.

NAEs	minimum response (nmoles/min/ mg protein)	maximum response (nmoles/min/ mg protein)	$LogIC_{50}$	Hill Slope
C18:3, n-3	-6 ± 2	95 ± 5	-9.6 ± 0.1	-0.8 ± 0.1
C 18:2, n-6	-6 ± 2	103 ± 15	-9.9± 0.3	-0.7 ± 0.1
C 22:4, n-6	-2 ± 3	101 ± 4	-9.7 ± 0.1	-0.9 ± 0.03
C22:6, n-3	-0.03 ± 1	100 ± 3	-9.8 ± 0.1	-1 ± 0.1
C22:5, n-6	-3 ± 3	44 ± 4	-10 ± 0.2	-1.3 ± 0.3
C22:1, n-6	-7 ± 3	44 ± 17	-9.7 ± 0.3	-1 ± 0.1

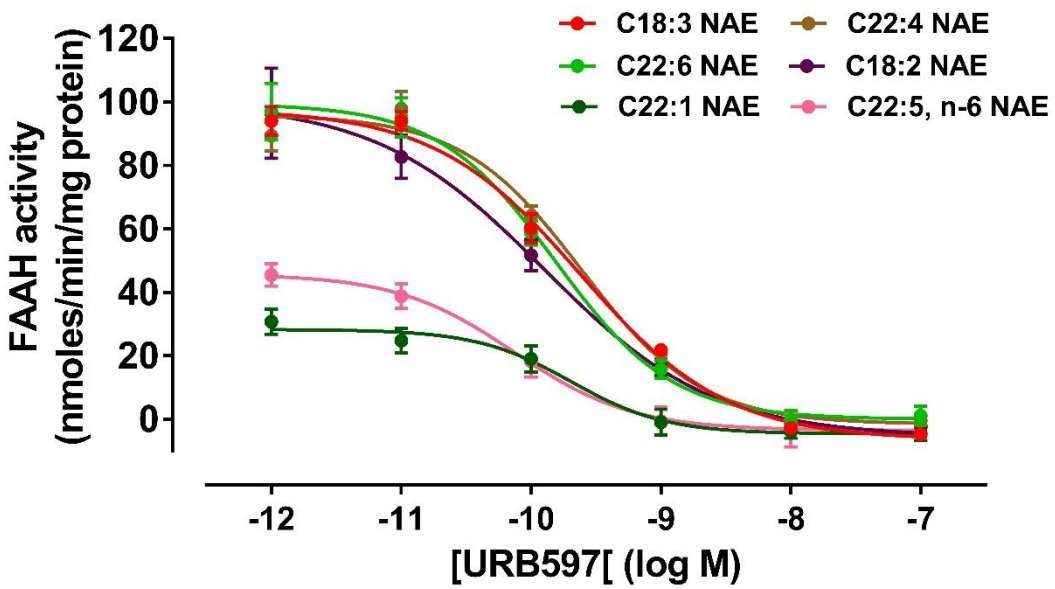


Figure 3.13 Concentration-dependence of URB597 inhibition of fatty acid ethanolamine hydrolysis by rat liver microsomes. URB597 was pre-incubated with tissue (10 µg/ml) for 15 min at 37 °C prior to incubation with substrate at a concentration twice the K_m value.

3.4 Quantification of amino acids

The novel fluorescence assay that has been described above for ethanolamine detection was adapted for detection of glycine (**Figure 3.14**). The results showed that the glycine detection curve was concentration-dependent under the same conditions. Therefore, it can be applied to measure hydrolysis of N-arachidonoyl-glycine (NAGly).

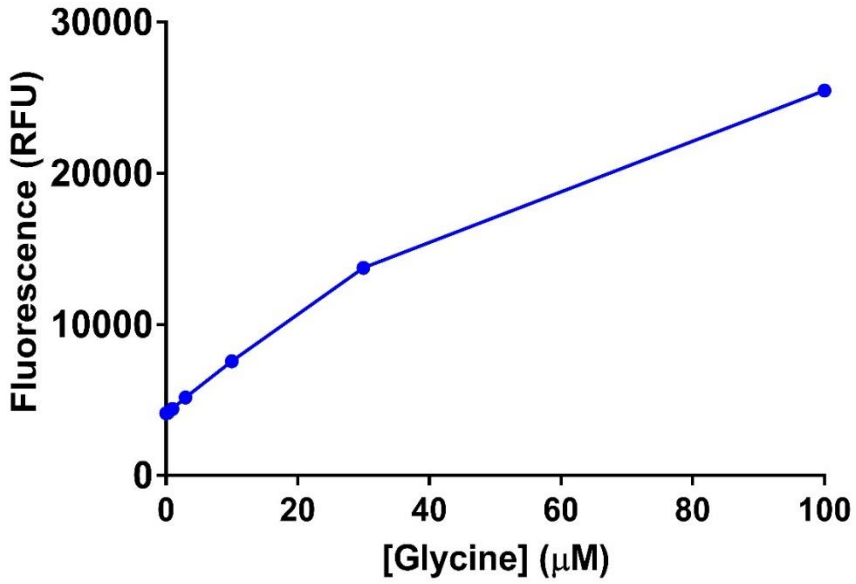


Figure 3.14 Representative standard curve of glycine. Glycine was prepared at serial dilutions in phosphate buffer (pH 7.4) followed by "stopping the reaction" by adding 10% TCA. Glycine was detected following reaction with NDC in 0.2 M borate buffer, pH 11 and the resulting fluorescence was monitored with excitation at 420 nm and emission at 480 nm. Data are expressed as mean ± SEM of four independent experiments.

The hydrolysis of NAGly in rat liver microsomes at 10 µg/ml protein was investigated (**Figure 3.15 A**). NAGly hydrolysis was concentration-dependent, with K_m (12 ± 3 µM) and V_{max} values (62 ± 12 nmol/min/mg protein) calculated from fitting the Michaelis-Menten equation.

Serial concentrations of URB597 were used to confirm the role of FAAH activity in mediating the NAGly hydrolysis. URB597 inhibited NAGly hydrolysis in a concentration dependent manner, with a pIC_{50} value of -9.3 (**Figure 3.15 B**).

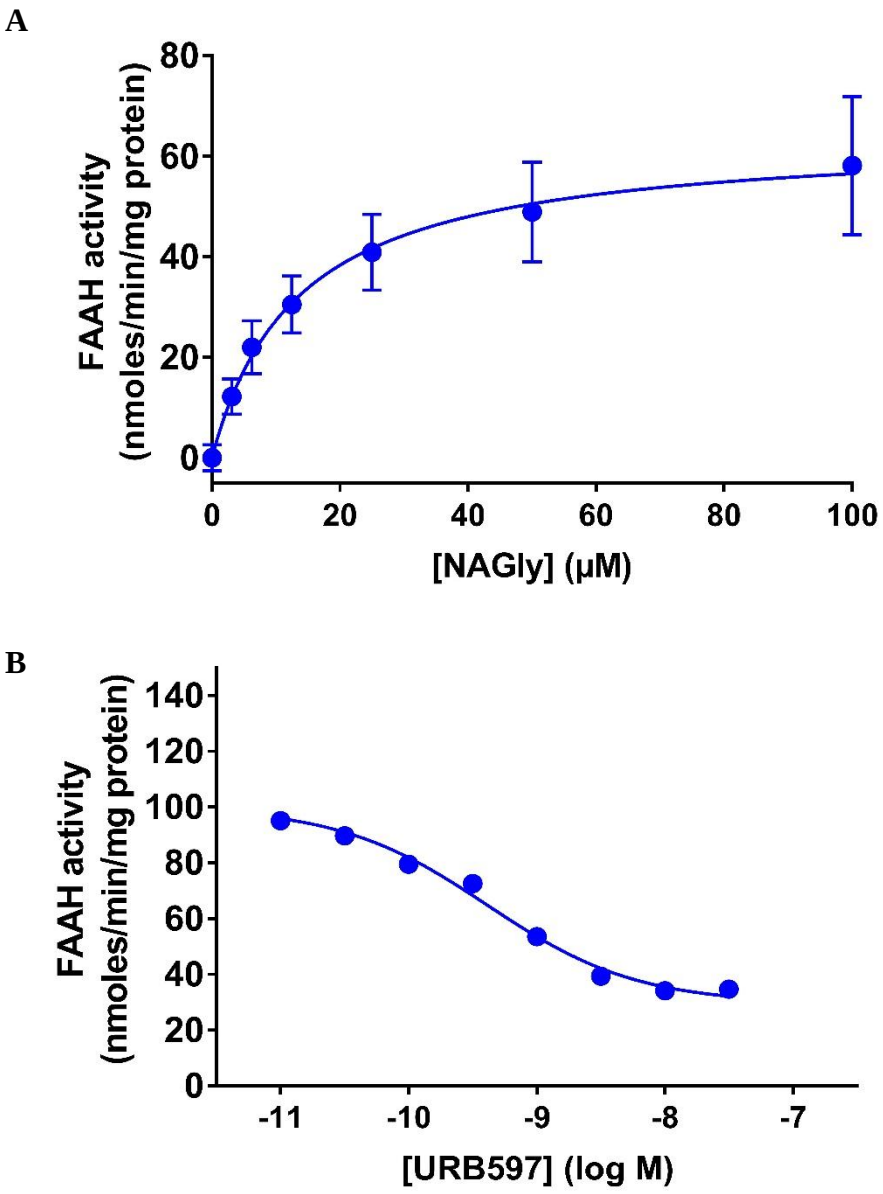


Figure 3.15 (A) The hydrolysis of N-arachidonylglycine in rat liver microsomes. **(B)** The effect of URB597 on FAAH mediated NAGly hydrolysis in liver microsomes. Data are mean ± SEM of four independent experiments.

3.5 Discussion

The aim of this chapter was to develop and validate an assay for FAAH activity-mediated hydrolysis of fatty acid ethanolamines in rat liver microsomes. The final assay is simple and inexpensive, as well as bypassing the drawbacks associated with the use of radiochemicals and laborious chromatographic techniques. In addition, it provides a secondary assay with a distinct methodology as a follow-up to high throughput screening of compound libraries of potential FAAH inhibitors.

3.5.1 Optimisation of novel fluorescence assay

This assay is based on ethanolamine quantification generated from NAE hydrolysis. The basic principles for this assay have been described by Miralles et al. (1997), who used cyanide to react with *O*-phthaladehyde (OPA) as a reagent to produce the fluorescent 1- cyano-2-alkyl-isoindole. However, NDC as a reagent is more stable than OPA and therefore the assay was adapted accordingly. Ethanolamine was reacted with NDC and methyl cyanide (acetonitrile) to produce a strong fluorescent product under alkaline conditions.

This product is an as yet uncharacterized fluorescent derivative (possibly 1-cyanoisoindole), allowing for fluorescence to be measured at 420 nm excitation and 480 nm emission. The product showed reasonable stability over time. Replacing the ethanolamine with ammonium sulphate, failed to generate fluorescence under these same assay conditions (**Figure 3.3)**, therefore, ethanolamine could be measurable and used to measure FAAH activity with some degree of selectivity.

However, it was necessary to conduct optimization for ethanolamine detection, including assessing the effect of different pH borate buffers, as well as the alternatives of TCA and PCA as stopping reagents. This assay required a borate buffer at alkaline pH which combines with acetonitrile to stabilize the reaction however there was no difference in ethanolamine detection at pH 10.1, 10.5, 11.0 or 11.5 of borate buffer. A study suggested that a combination of acetonitrile and borate buffer would be optimal at pH 11 (Bantan-Polak *et al.*, 2001). This pH was, therefore, adopted for subsequent methodologies.

Stopping solutions are used to halt the chemical reactions in biochemical assays and should be rapid and complete in order to ensure consistency of measurement. TCA and PCA are widely used as stopping reagents to precipitate proteins and halt reactions. Although there was no obvious difference between various concentrations of PCA and TCA on ethanolamine production, the blank in the presence of TCA was lower than with PCA. A previous report indicated that protein precipitation was higher in the presence of TCA than PCA, which may explain this difference (Rajalingam *et al.*, 2009). Given that the detection element of the assay required developing of fluorescence in an alkaline medium, it meant that the amount of TCA should be optimised for stopping reactions. Therefore, 10% TCA was chosen to avoid mixing an excess amount of TCA with the alkaline developing solution (borate buffer).

In addition to measuring ethanolamine, this assay was applied to measure *N*-acylamino acid hydrolysis by MSc students conducting a research project under my partial supervision. *N*-arachidonoylglycine is an examples of an endogenous fatty acid derivative with distinct molecular targets to the NAEs, possibly including GPR18,

which has potential for future therapeutic exploitation. Currently, the knowledge of mechanism/s of *N*-acylamino acid turnover is only superficial, so a future aim would be to extend the assay to measure *N*-acylamino acid hydrolysis.

3.5.2 FAAH activity in rat liver microsomal

Previous reports demonstrated FAAH activity was higher in microsomes rather than mitochondria or other tissue fractions (Desarnaud *et al.*, 1995, Schmid *et al.*, 1985). Therefore, microsomes of rat liver were used to investigate the hydrolysis of a panel of fatty acid ethanolamines by FAAH activity. Prior to of this part of the investigation, there were several factors requiring optimisation such as time, protein concentration and the presence of BSA. The hydrolytic activity of FAAH enzyme in rat liver is time-dependent up to 30 min (**Figure 3.7)**. This is consistent with a previous study, which showed a linear relationship between time and hydrolysis of AEA up to 30 min by FAAH (Maccarrone *et al.*, 1999). It is apparent that 10 to 15 min is sufficient for assessing activity of the FAAH enzyme and this was used subsequently.

Application of the novel fluorescence-based assay to measure FAAH activity-catalysed hydrolysis of AEA was successful and allowed determination of K_m and V_{max} values. The AEA affinity value to FAAH enzyme obtained from novel fluorescence assay (2 µM) was similar magnitude affinity to FAAH in rat and human brain but higher affinity compared with other tissues (**Table 3.4).** Most published methods for measuring AEA hydrolysis use radiolabelled compounds, and thin layer chromatography (TLC) or high performance liquid chromatography (HPLC) to separate the product. Potentially, the differences in K_m might be due to pH (many studies use a more alkaline pH closer to

the optimum for FAAH) and temperature which could alter kinetic parameters. In addition, protein concentration may affect the results as the methods described in the literature involve protein concentrations from 100-200 µg. The investigation of this possibility is observed in our results as seen in **Table 3.4.**

Although FAAH is highly expressed in liver (Deutsch and Chin, 1993a), there is no comparable study to examine the enzyme kinetics in rat liver microsomes (K_m and V_{max} values). Our data demonstrate that the maximal velocity of enzyme hydrolysis i.e. V_{max} value is higher than that of other tissues (**Table 3.4)**. The variation in V_{max} values probably reflects the degree of purification of the preparation; for example, whether microsomes were prepared compared to total homogenates or total particulate preparations. The inclusion of BSA in the assay was also influential on the V_{max} determined. It has been suggested that BSA acts as a transporter which might increase availability of AEA to bind with FAAH and also to remove fatty acid products from the enzyme, thereby increasing the apparent maximal velocity of reaction (**Figure 3.8 B)**.

Table 3.4. Representative kinetics of AEA hydrolysis in tissue preparations

Tissue	Km (μM)	Vmax (nmol/min/mg)	Procedure	Citation
Rat brain microsomes	12.7	5.63	Radiometric assay	(Desarnaud *et al.*, 1995)
Human brain	2.0	0.80	Reversed phase-high performance liquid chromatography (HPLC)	(Maccarrone *et al.*, 1998)
Rat brain microsomes	8.6	0.362 ± 16	High performance liquid chromatography (HPLC)	(Lang *et al.*, 1996)
Rabbit brain (microsome)	2.8	5.5 ± 1.3	A Fluorescence Displacement Assay	(Thumser *et al.*, 1997a)
Rat brain membranes	3.4	2.2	Thin layer chromatography (TLC)	(Hillard *et al.*, 1995)
Porcine brain	60	0.37	Radiometric assay	(Ueda *et al.*, 1995b)
Human brain	3.2	680	Radiometric assay	(Erdozain *et al.*, 2015)

In the validation process, the novel assay was shown to exhibit concentration-dependent inhibition of AEA hydrolysis in liver microsomes by a widely-used FAAH inhibitor (URB597). In comparing URB597 potency for hydrolysis of AEA (5 µM), we observed discrepancies in IC_{50} values measured in the novel fluorescence assay compared with several studies described in the literature (**Table 3.5)**.

Table 3.5 Potency of URB597 reported in previous studies.

Tissue	[AEA]	Protein content	IC_{50}	Reference
rat liver	100 µM	13.7 µg	70 nM	(Sun *et al.*, 2005)
brain membranes	100 nM	50 µg	4.6 nM	(Mor *et al.*, 2004)
rat liver	10 µM	100 µg	4.7 nM	(Clapper *et al.*, 2006)

These discrepancies in potency can be explained as mentioned previously that kinetics of inhibition in AEA hydrolysis may have been affected by the conditions of each assay such as temperature, pH and protein content. In addition, period of pre-incubation for URB597 with FAAH may influence the results of IC_{50}. Therefore, pre-incubation for a longer time may be caused increasing inhibition and thus lower IC_{50} values.

To circumvent any variations in assay conditions, identical conditions were applied in the classical radiometric assay (same volumes, protein and BSA concentrations, buffers and incubation periods of URB597). Under these conditions, the pIC_{50} value obtained was not different to the pIC_{50} observed in the novel assay. Thus, although the novel assay does not have the high sensitivity of the radiometric version, the development of

the novel fluorescence assay was successfully applied to measure FAAH activity with inexpensive materials and with reasonable rapidity.

3.5.3 FAAH activity mediated fatty acids ethanolamine

The novel fluorescence assay was expanded to measure FAAH activity with various fatty acid ethanolamines. The substrate specificity of FAAH has been examined in a limited fashion in various enzyme preparations, primarily because of the lack of a single unifying assay. Often anandamide is used as substrate and alternative substrates defined by their ability to reduce substrate conversion. The AEA analogues examined in the present study could be hydrolysed by FAAH in rat liver microsomes, however the maximal rate of AEA hydrolysis was the highest. This observation suggests that AEA is indeed a preferred substrate for FAAH as described in other studies (Desarnaud *et al.*, 1995, Maccarrone *et al.*, 1998).

Although the affinities of many of the fatty acid ethanolamines tested were similar, long chain monounsaturated and saturated NAEs were hydrolysed at much lower maximal rates than polyunsaturated fatty acids of ethanolamine. This is in line with Desarnaud and co-workers (1995), who reported the FAAH activity is selective to AEA in rat brain and also observed the low activity of FAAH in catalysing PEA (C16:0 NAE) hydrolysis. Bisogno *et al.* (1997) demonstrated that catalytic efficiency of C18:2, C20:4 NAEs hydrolysis was highest in leukocytes compared to long chain NAEs such as C22:1 NAE. Although most of the ligands tested in the present study have not previously been reported, several articles supported the idea that the structure of the

fatty acid amide such as the degree of saturation and length chain might play an important role in their hydrolysis (Bisogno *et al.*, 1997, Desarnaud *et al.*, 1995).

The inhibition of FAAH activity on hydrolysis of a panel of fatty acid ethanolamine ligands was investigated using the selective inhibitor for FAAH, URB597. The effect of URB597 on AEA hydrolysis has been reported in several tissues, as shown in **Table 3.4**. The similar potencies for URB597 against the fatty acid ethanolamines tested in present study confirmed the involvement of FAAH in their hydrolysis; a novel observation since this had not been directly investigated. At least one report described nervonoylethanolamine (C24:1) to accumulate in the brains of mice with a disrupted gene encoding FAAH (Leung *et al.*, 2006).

3.6 Conclusion

This Chapter described the development and validation of a novel assay which was used to demonstrate the hydrolysis of a panel of fatty acid ethanolamine by FAAH in rat liver. Rat liver FAAH enzyme activity was able to discriminate with the fatty acid structure of NAEs where activity increased with increasing unsaturation and decreasing chain length. These data may open the way to future investigations of the activity of these fatty acids ethanolamine in intact cells and also investigate their signalling on molecular targets that are related to the endocannabinoid system.

Chapter 4

Functional effects of fatty acid ethanolamines at human CB_1 and CB_2 cannabinoid receptors

4.1 Introduction

Endocannabinoids have numerous pharmacological effects through classical cannabinoid receptors, including analgesia, anti-inflammation, and neuroprotection (Di Marzo *et al.*, 1994, Harris *et al.*, 2000, Strangman *et al.*, 1998, Molina-Holgado *et al.*, 1998). Effects of fatty acid ethanolamine derivatives mirror many of the reported effects of established synthetic cannabinoids and endocannabinoids in many studies on various mammalian cell types. However, there remains a paucity of evidence for the action of the extended family of fatty acid ethanolamines on CB receptor signalling.

A limited number of fatty acid ethanolamine ligands other than anandamide have been shown to bind and activate CB receptors. Homo-γ linolenoylethanolamine (C20:3 NAE) and docosatetraethanolamine (C22:4 NAE) were isolated from pig brain and were found to be able to bind to CB_1 receptors with K_i values of 34 and 53 nM, respectively (Hanus *et al.*, 1993). Furthermore, n-3 fatty acid ethanolamine such as C22:6 and C20:5 are reported to regulate cell growth and proliferation in cancer cells and may be involved in neurogenesis and synaptogenesis via CB receptors (Kim *et al.*, 2011, Brown *et al.*, 2010).

Fatty acids in the human diet, even in short term feeding, can regulate the level of NAEs and endocannabinoids in various tissues (Artmann *et al.*, 2008b). It has also been observed that n-3 PUFA consumption contributes to the appearance of ethanolamine derivatives, including docosapentaenoylethanolamine (C22:5 NAE) that possesses anti-inflammatory properties (Figueroa *et al.*, 2013). In addition to polyunsaturated fatty acids derivatives, saturated and monounsaturated fatty acids such as

nervonoylethanolamine (C24:1 NAE), arachidoylethanolamine (C20:0 NAE) and docosaneoylethanolamine (erucylethanolamine, C22:1 NAE) have been identified in mouse brain and were observed to inhibit depolarisation induced calcium fluxes (Oz *et al.*, 2005). Nevertheless, the mechanisms underlying these effects are not fully understood. Biosynthesis of the majority of fatty acid ethanolamines appears to involve a similar pathway to AEA (C20:4 NAE) biosynthesis; the Ca^{2+}-dependent *N*-acyltransferase forming *N*-acylphosphatidylethanolamines in the membrane phospholipid (Okamoto *et al.*, 2004).

Inhibition of adenylyl cyclase was the first characterised CB_1 and CB_2 receptors activation, which is mediated via $G_{i/o}$ protein (Howlett and Fleming, 1984, Howlett *et al.*, 1986). CB_1 receptor-mediated inhibition of forskolin stimulated cAMP formation has been shown in transfected CHO cells (Felder *et al.*, 1995, Felder *et al.*, 1993a), rat cerebellar membranes (Childers *et al.*, 1994) and N18TG2 membranes in the presence of a PMSF inhibitor (Pinto *et al.*, 1994) and via CB_2 receptors in transfected CHO cells (Felder *et al.*, 1995). Hillard and co-workers observed that AEA inhibited forskolin stimulated-cAMP mediated through hCB_1 and CB_2 receptors in CHO cells within 30 min of AEA incubation in the presence of PMSF (Hillard *et al.*, 1999). This effect of AEA was mediated through $G_{i/o}$ proteins (Felder *et al.*, 1993b). Furthermore, AEA over 2 h was able to stimulate [^{35}S]GTPγS binding to G proteins, with an EC_{50} value of 390 nM in rat cerebellar membrane in the presence of PMSF to inhibit FAAH activity (Breivogel *et al.*, 1998, Hillard *et al.*, 1999) and an EC_{50} value of 850 nM in mouse brains (Burkey *et al.*, 1997).

Activation of CB_1 and CB_2 receptors also results in phosphorylation of p42 (ERK2) and p44 (ERK1) almost universally in cells either with' endogenous or recombinant expression. Bouaboula *et al.* (1995), with a peak of CB_1 receptor activation of ERK signalling between 6 and 10 min. Furthermore, AEA has been shown to activate ERK1/2 phosphorylation within 5 min in human vascular endothelial cells (Liu *et al.*, 2000) and HEK293 cells expressing CB_1 receptors (Daigle *et al.*, 2008).

Raising intracellular free Ca^{2+} levels is one of the characterised mechanisms which has been shown to be a CB_1 and CB_2 receptor-mediated response. Endogenous cannabinoids have been shown to give a rapid (within seconds) and transient increase in intracellular Ca^{2+} in various cells, such as in human umbilical vein-derived EA.hy926 (Mombouli *et al.*, 1999), NG108-15 neuroblastoma-glioma (Sugiura *et al.*, 1996), N18TG2 neuroblastoma (Sugiura *et al.*, 1997) and in calf pulmonary endothelial cells (CPAE) (Zoratti *et al.*, 2003).

Largely, research has been confined to arachidonic acid derivatives in examining these receptors and signalling pathways. To date, there are limited signal transduction data available for the wider range of fatty acid ethanolamine derivatives on classical cannabinoid receptors.

4.2 Aim

The aim of this Chapter was to investigate the range of commercially-available fatty acid ethanolamine ligands for functional responses in CHO cells heterologously expressing human CB_1 and CB_2 receptors by selecting two robust signal transductions pathways mediated through CB receptors, focussing on rapid assays to avoid any ligand metabolism effects.

At maximum concentration of NAEs (10 μM) possible to activate CB receptors and also to avoid the low solubility due to nature of NAEs, were assessed:

1. The effects of a variety of saturated, mono- and polyunsaturated fatty acid ethanolamines on MAP kinase (ERK) signalling pathway in CHO-hCB cells.

2. The effects of a variety of saturated, mono- and polyunsaturated fatty acids on intracellular calcium levels in CHO-hCB cells.

4.3 Results

4.3.1 Investigation of ERK phosphorylation in human CB_1 transfected CHO cells

ERK phosphorylation assays were designed to elicit responses for a panel of fatty acid ethanolamine ligands. For optimisation of the experimental conditions and to confirm the methodological validation of the assay to detect the ligand-mediated pERK stimulation in CHO cells expressing human CB_1 receptors, a set of initial experiments was conducted (see the Appendices) using the cannabinoid agonist, HU210, at a concentration of 1 μM. On the basis of the results obtained from these experiments, a cell seeding density of 40,000 cells/well and serum-starvation time of 6 h were chosen as optimised conditions for all subsequent experiments.

The time course of ERK activation was investigated for determining the optimum period for p-ERK stimulation for subsequent experiments. CHO-hCB_1 cells were treated with HU210 or AEA (C20:4 NAE) at various time points from 0-60 min. Both agonists produced a rapid increase in phospho-ERK levels with maximum response achieved at 5 min (**Figure 4.1**). After this time period, levels of ERK were decreased and remained constant up to 60 min.

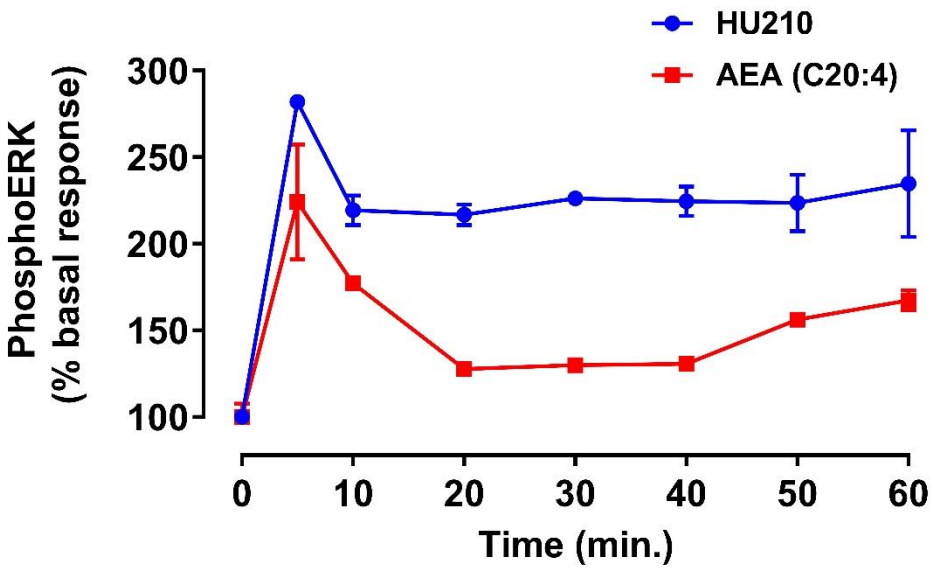


Figure 4.1 Time course of ERK phosphorylation induced by cannabinoid agonists in CHO-hCB$_1$cells. Cells were cultured for 24 h followed by serum starvation for 6 h. Cells were stimulated with 10 µM of each ligand at various time points (0-60 min). ERK phosphorylation values were normalized to the corresponding total-ERK values.

4.3.1.1 Effect of fatty acid ethanolamine ligands on ERK phosphorylation (p-ERK) in CHO-hCB$_1$ cells

CHO-hCB$_1$ were stimulated with various concentrations of HU210 and AEA for 5 min which was conducted by our research group. Both agonists produced a concentration-dependent increase in phospho-ERK levels, with pEC50 value of 9.3 and 6.6 for HU210 and AEA, respectively (Priestley *et al.*, 2017b). Therefore, a maximum concentration of ligand (at 10 µM) was used which possible activate ERK phosphorylation.

Cells were treated with 10 µM of each of the fatty acid ethanolamine ligands, AEA (C20:4, n-6), DTEA (C22:4), 4DPEA (C22:5, n-6), LEA (C18:2, n-6), 7DPEA (C22:5, n-3), ALEA (C18:3, n-3), EPEA (C20:5, n-3), DOEA (C22:1,n-9), NEA (C24:1,n-9), AE (C20:0), OEA (C18:1,n-9), PEA (C16:0), SEA (C18:0) and cannabinoid agonist (HU210) for 5 min to compare peak responses for phospho-ERK level generation (**Figure 4.2 and 4.3**).

The long chain n-6 fatty acids ethanolamine ligands were able to evoke a response comparable to AEA-induced phospho-ERK (**Figure 4.3,** one-way ANOVA, Dunnett's test, $p<0.05$) The shorter chain n-6 fatty acids as C18:2, n-6, all long chain of n-3 fatty acids (C22:5, C20:5, C22:6, C18:3) and mono-saturated and saturated fatty acids NAEs failed to elicit pERK responses (one-way ANOVA, Dunnett's test, $p>0.05$).

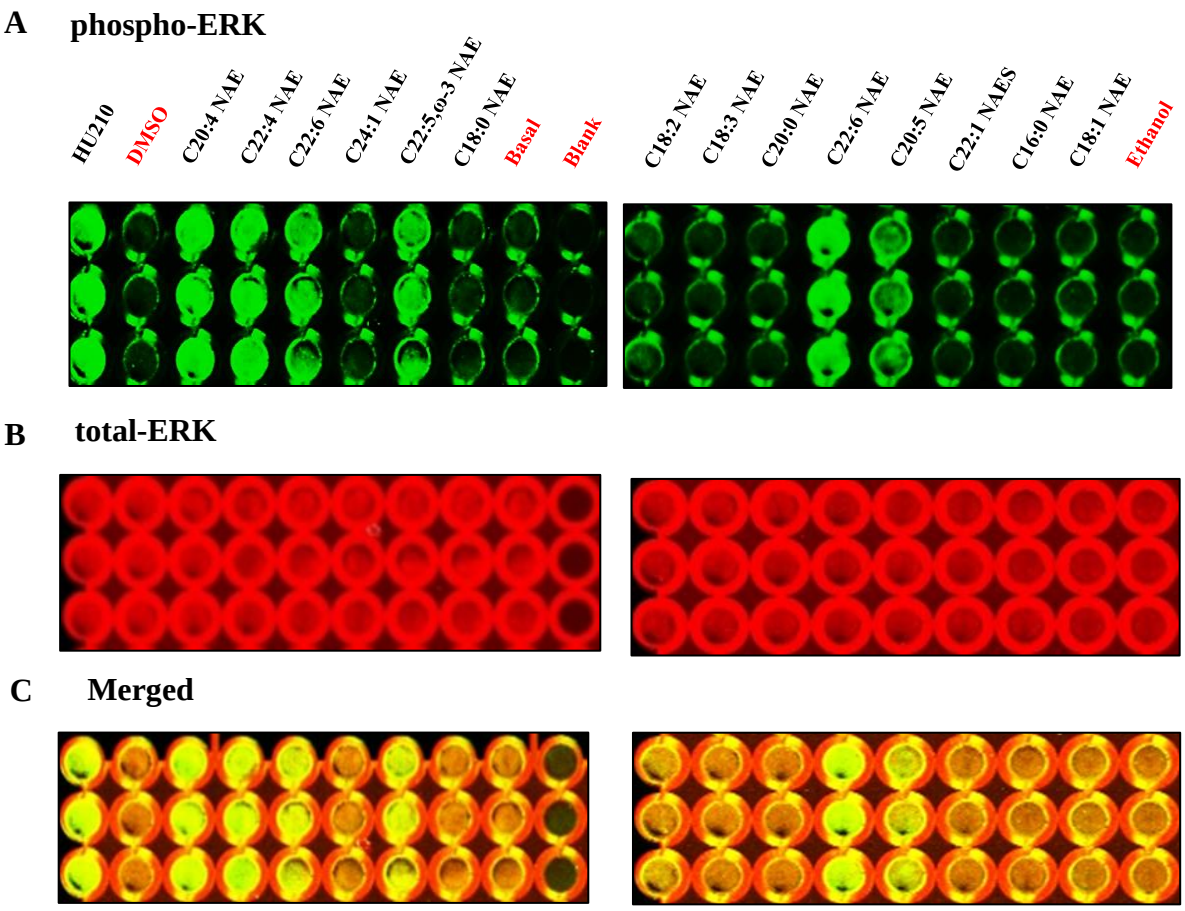


Figure 4.2 Immunofluorescence images showing the effect of fatty acids ethanolamine ligands at 10 μM on ERK phosphorylation in in CHO-hCB$_1$ cells. The images were captured by LI-COR Odyssey® NIR Imaging System at 129 μM resolution (A) phospho-ERK (green channel) were scanned at 800 nm. (B) total ERK (red channel) were scanned at 700 nm. (C) Merged. The data are from a single experiment conducted in triplicate.

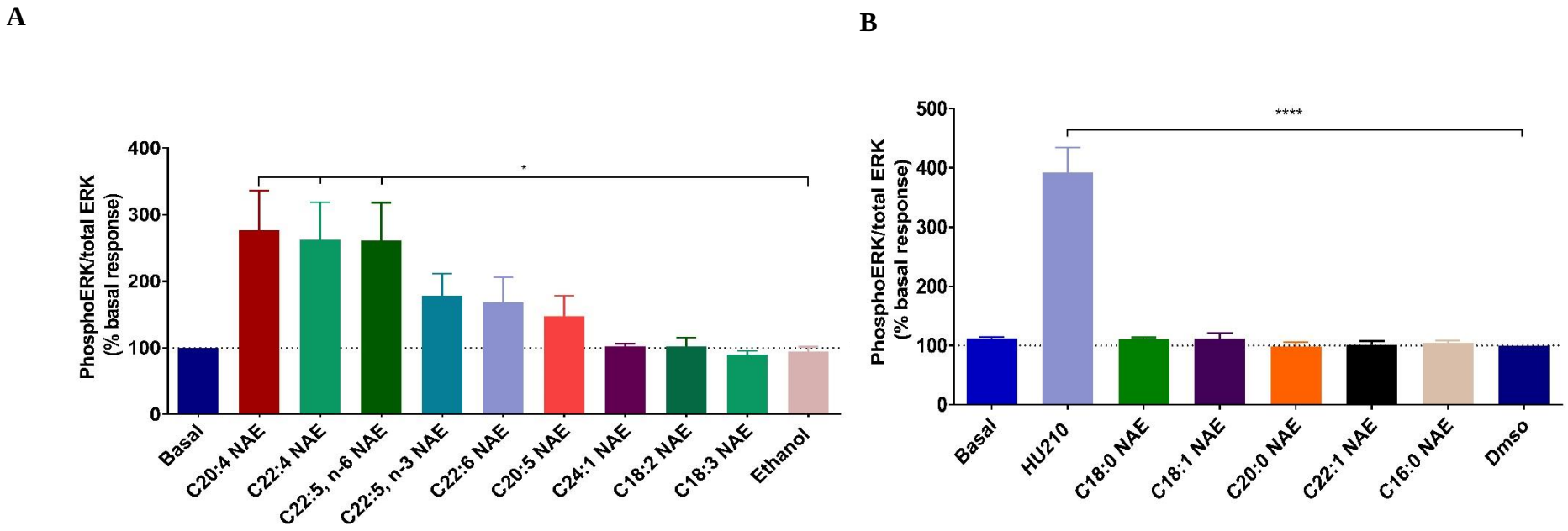


Figure 4.3 Effect of fatty acid ethanolamine ligands on ERK phosphorylation in CHO-hCB$_1$ cells. Cells were cultured for 24 h followed by serum starvation for 6 h. Cells were stimulated with 10 µM of each ligand for 5 min at 37 °C. **(A)** ERK phosphorylation for ligands dissolved in ethanol. **(B)** ERK phosphorylation for ligands dissolved in DMSO. ERK phosphorylation values were normalized to the corresponding total-ERK values. Data are expressed as mean ± SEM values from four independent experiments performed in triplicate using different passages. Statistical analysis was conducted using one-way ANOVA followed by post-hoc Dunnett's test; *p<0.05; ***p<0.0001; compared to vehicle (either ethanol or DMSO).

In order to confirm the role of CB_1 receptors on ERK stimulation, the responses to n-6 fatty acid ethanolamine ligands were examined using the CB_1 receptor selective antagonist (AM251) (Lan *et al.*, 1999). At 100 nM AM251, there was a significant blockade of ERK stimulation in response to n-6 fatty acid ethanolamines, as shown in **Figure 4.4** (paired, two-tailed t-test; $p < 0.05$) using 10 µM ATP and 10% (v/v) FBS as positive controls. Interestingly, AM251 (100 nM) had a similar effect on ATP-induced ERK phosphorylation which appeared similar to the effect of NAEs (**Figure 4.4**, paired, two-tailed t-test; $p < 0.05$).

The role of $G_{i/o}$ proteins coupled to CB_1 receptors in mediated ERK response was investigated using PTX which inactivates G_i protein. Pre-treatment of cells with PTX (600 ng/ml) for 6 h inhibited the PUFA ethanolamine ligand-induced increase in ERK phosphorylation (**Figure 4.5**).

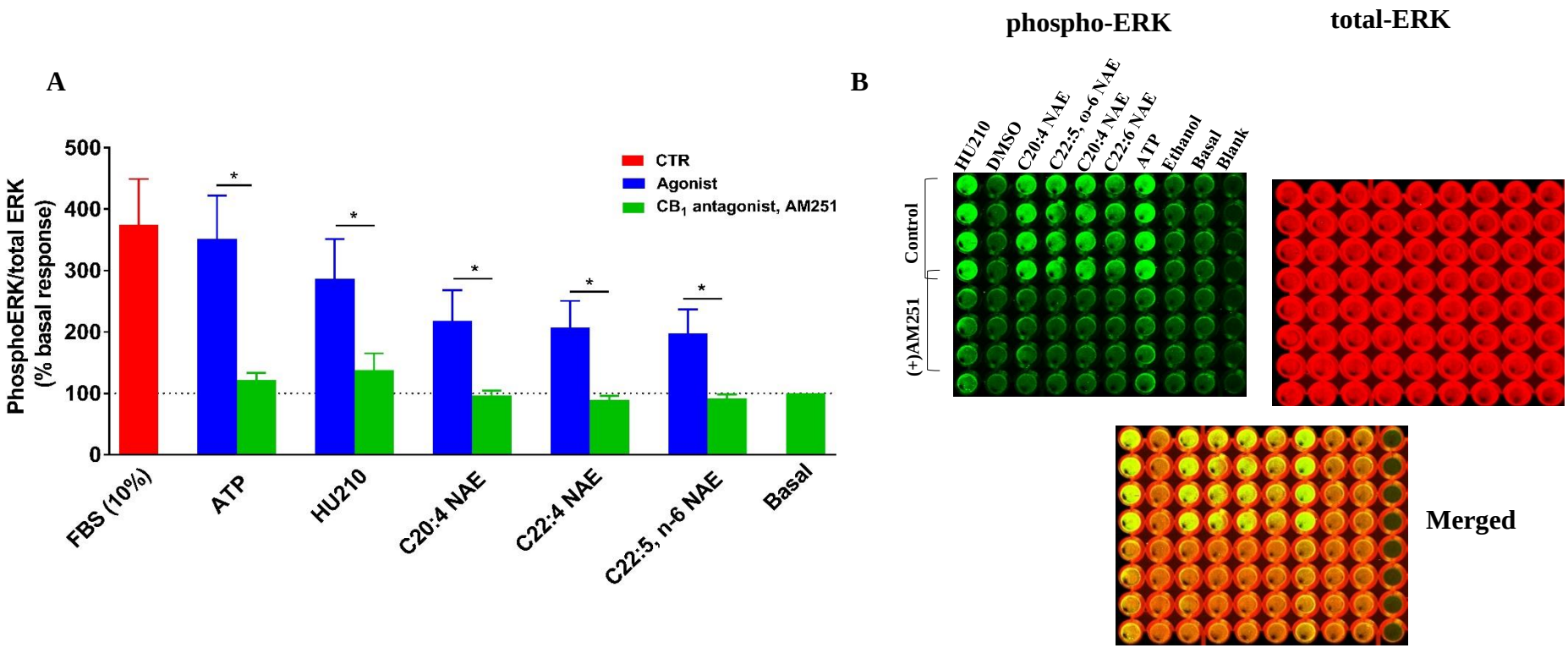


Figure 4.4 The effect of the CB_1 antagonist AM251 on fatty acid ethanolamine-induced increases in ERK phosphorylation. CHO-hCB_1 cells were cultured for 24 h in 96 well plate followed by a serum starvation period for 6 h. Cells were pre-treated with AM251 for 30 min. prior to p-ERK stimulation with 10 µM agonist for 5 min at 37 °C using 10% FBS used as positive control (CTR). The plate was imaged by LI-COR Odyssey® NIR Imaging System at 129 µM resolution. **(A)** ERK phosphorylation values of agonist were normalized to the corresponding basal response Data are expressed as mean ± SEM values from 6 separate experiments using different passages performed in triplicate. Statistical analysis was conducted data by comparing agonist in the absence (blue column) and presence (green column) of AM251 using paired, two-tailed, *t*-test *p<0.05; **(B)** Immunofluorescence images for phospho-ERK were measured at 800 nm, total ERK at 700nm and Merged.

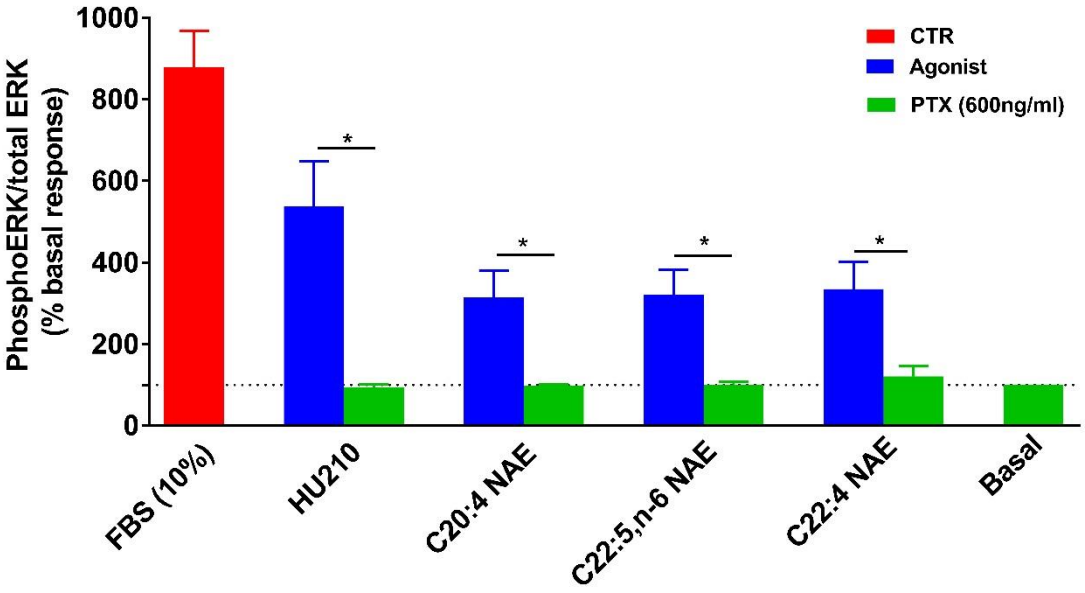


Figure 4.5 Inhibition of fatty acid ethanolamine ligand-induced increases in ERK phosphorylation in CHO-hCB$_1$ in the presence of PTX. Cells were incubated with 600 ng/ml PTX for 6 h at 37 °C prior to stimulation with agonists at 10 µM for 5 min. Data are mean± SEM from four independent experiments using cells from different passages performed in triplicate. Data are presented as percentage of the basal response and were analysed as the raw data using paired, two-tailed, *t*-test *p<0.05, agonist in the absence (blue column) compared with in presence of PTX (green column).

4.3.2 Investigation of intracellular calcium mobilisation in CHO-hCB$_1$ cells

The fatty acid ethanolamine effect on intracellular calcium mobilisation via the human CB_1 receptor was investigated in CHO-hCB_1 using a FlexStation and Fluo-4. A preliminary experiment was performed to determine the effect of fatty acid-free BSA on calcium mobilisation (**Figure 4.6)**. The inclusion of BSA (1 mg/ml) in the assay buffer did not alter the intracellular calcium response elicited by 10 µM AEA, HU210 or ATP induced calcium mobilisation (paired, two-tailed *t*-test, $p > 0.05$).

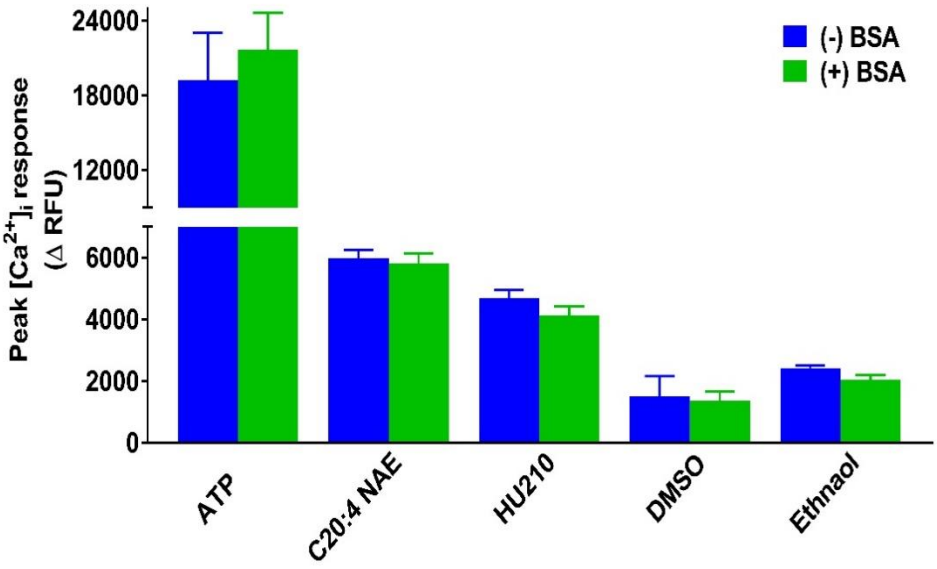


Figure 4.6 Effect of BSA upon agonist-evoked calcium mobilisation. CHO-hCB_1 cells were stimulated with 10 µM ATP, HU210 or AEA in the presence or absence of 1 mg/ml BSA. Data are mean ± SEM from three independent experiments using cells from different passages performed in triplicate. Statistical analysis was conducted on the raw data using a paired, two-tailed, *t*- test, $p > 0.05$, 10 µM agonist in the presence of BSA compared with absence of BSA.

Cells were exposed to NAEs, CB_1 receptor agonist (HU210) or ATP at concentrations of 10 μM. The time course of intracellular calcium increases in CHO-hCB_1 cells in response to ligands was recorded over 3 min (**Figure 4.7**). Following a baseline recording for 20 s, there was a rapid rise in intracellular calcium in CHO-hCB_1 cells stimulated by HU210, C20:4 NAE and C22:4 NAE as well as the positive control ATP, followed by a gradual decline in Ca^{2+} response (for HU210, C20:4 NAE and C22:4 NAE). The ethanol or DMSO vehicles did not produce any response over time.

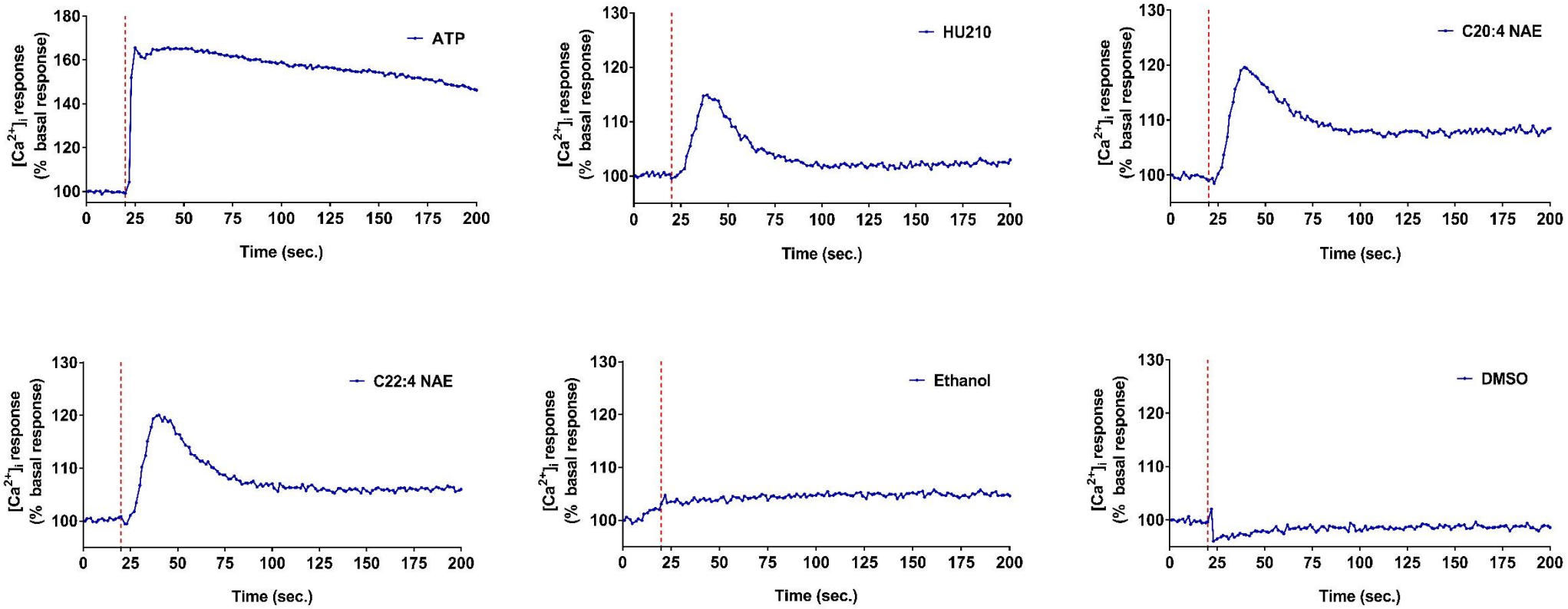


Figure 4.7 Representative curves showing the time courses of intracellular calcium mobilisation responses to the positive controls (HU210, ATP), agonist ligands of n-6 PUFA-ethanolamides and vehicle (ethanol and DMSO) measured by Fluo4 fluorescence in CHO-hCB_1 cells with red dashed line indicating the time of agonist addition.

HU210 and the long chain fatty acid ethanolamines derived from n-6 conjugates (C20:4, n-6, C22:5, n-6, C22:4, n-6) were able to elicit a significant elevation of $[Ca^{2+}]_i$ response in CHO-hCB_1 cells (**Figure 4.8**, one way ANOVA, Dunnett's test; $p < 0.05$). At the concentration used (10 µM), all the other NAEs failed to evoke a significant change in $[Ca^{2+}]_i$. level (one way ANOVA, Dunnett's test*;* $p > 0.05$).

To confirm the involvement of the CB_1 receptor in mediating the calcium responses elicited by long chain n-6 fatty acids ethanolamine, the effect of the CB_1 receptor antagonist AM251 on calcium responses was investigated in CHO-hCB_1 cells. Statistical analysis revealed that pre-incubation of the cells with 100 nM AM251 significantly reduced the peak (maximum) calcium response evoked by C20:4, n-6 NAE and HU210 to 66 ± 7 % and 58 ± 4 % of control (**Figure 4.9 A**), respectively but had no effect on the AUC of the total calcium over 3 min. (**Figure 4.9 B**). Similarly, AM251 did not affect AUC and the maximum peak induced by C22:5, n-6 and C22:4 NAEs while the antagonist significantly reduced the $[Ca^{2+}]_i$ response stimulated by ATP from 2.47 ± 0.24 to 1.98 ± 0.15 RFU.

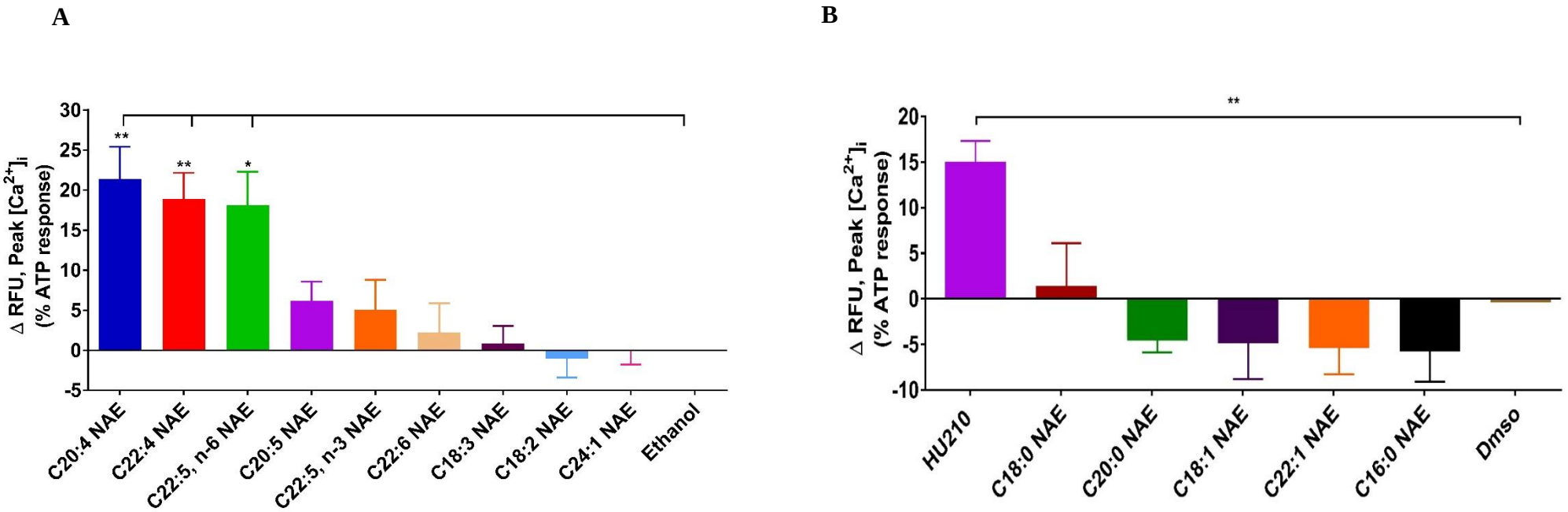


Figure 4.8 Changes in intracellular Ca^{2+} levels stimulated by fatty acids ethanolamine ligands in CHO-hCB_1 cells. Cells were cultured for 24 hrs and then stimulated with agonist (10 µM) at 37 °C (A) Ligands dissolved in ethanol. (B) Ligands dissolved in DMSO. Data are presented as percentage of the ATP response as means ±SEM of triplicate determinations from six independent experiments. The untransformed data were analysed using one-way ANOVA, followed by post-hoc Dunnett's test; *p<0.05, **p<0.01, comparing agonist with vehicle.

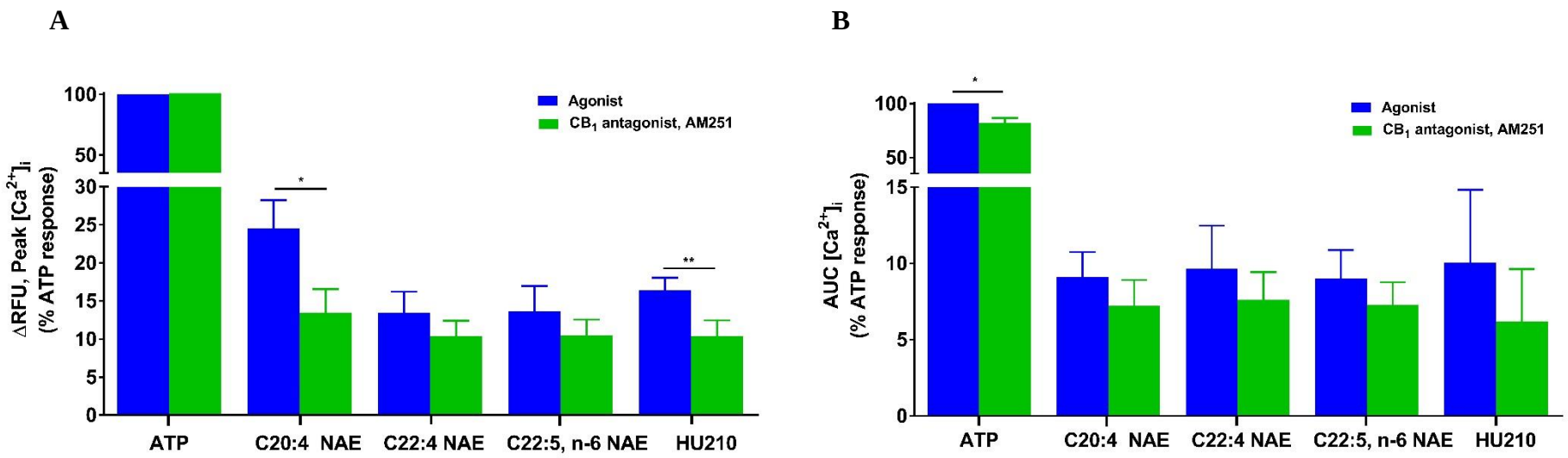
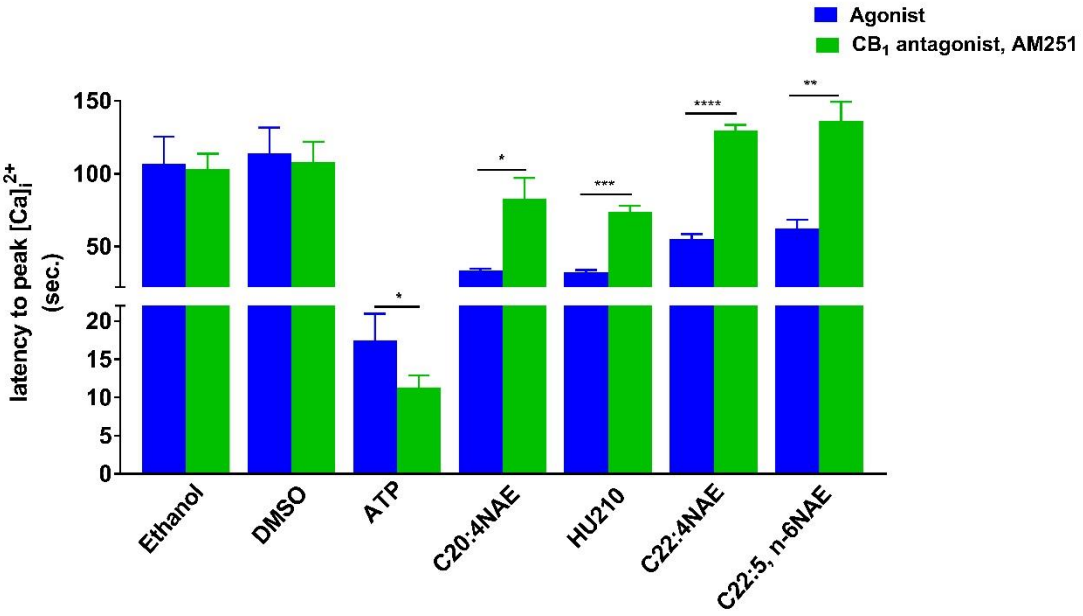


Figure 4.9 The effect of the CB_1 antagonist AM251 on intracellular calcium mobilisation in response to agonist stimulation of CHO-hCB_1 cells, measuring (A) the peak response and (B) the area under the curve (AUC). CHO-hCB_1 cells were pre-treated with 100 nM AM251 at 37 °C followed by adding of agonists and measured by Fluo4 fluorescence. All data shown are mean values ± SEM from four independent experiments performed in triplicate. Data analysis was conducted on untransformed data using paired, two-tailed t-test., *p<0.05, **p<0.01, comparing agonist in absence and presence of AM251.

The latency to peak for all ligands tested in presence of 100 nM AM251 are shown in **Figure 4.10**. AM251 increased significantly the latency to peak of HU210, C20:4 NAE, C22:4 NAE and C22:5, n-6 NAE-induced $[Ca^{2+}]_i$. Notably, AM251 reduced significantly the latency to peak of ATP from 18 ± 3 to 12 ± 2 s (paired, two-tailed, *t*-test, $p< 0.05$).

The effect of pertussis toxin treatment on CB_1 receptor mediated intracellular calcium was assessed to test the involvement of G_i protein (**Figure 4.11**). Treatment of CHO-hCB_1 cells with PTX (600 ng/ml) for 6 h at 37 °C evoked a significant decrease in peak $[Ca^{2+}]_i$ response to C20:4 NAE,C22:4 NAE and HU210 (paired, *t*-test two-tailed; $p<0.05$). Similarly, PTX had a significant effect on total calcium levels (AUC over 3 min) induced by HU210, C20:4 NAE and C22:4 NAE (**Figure 4.11 B**).



Fig**ure 4.10** The effect of AM251 on the latency-to-peak for changes in $[Ca^{2+}]i$ levels stimulated by n-6 NAEs in CHO-hCB_1 cells. Pre-incubation of cells with 100 nM AM251 for 30 min prior to agonist stimulation. Data represent mean ± SEM of four independent experiments conducted in triplicate. Data significantly different from control (absence of AM251) were determined using a paired, *t*-test **p*<0.05, ***p*<0.01,****p*<0.001, *****p*< 0.0001.

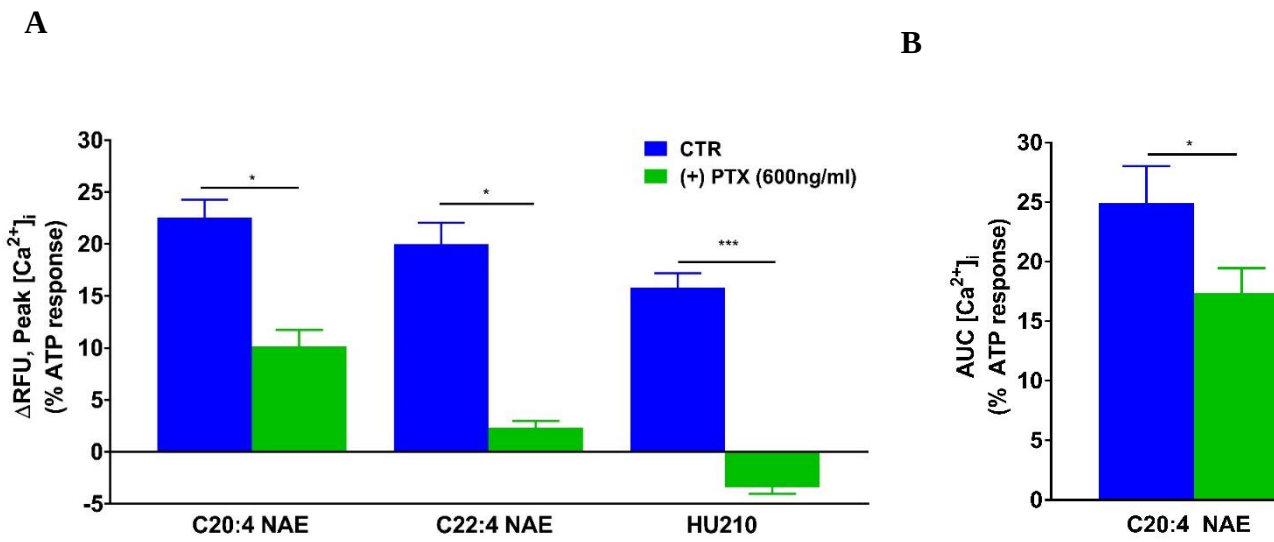


Figure 4.11 Inhibition of n-6 fatty acid ethanolamines and HU210 induced Ca^{2+} elevation by pertussis toxin in CHO-hCB_1 cells. Pre-treatment of cells with PTX (600 ng/ml) for 6 h at 37 °C preceded the measurement of Ca^{2+} peak (A) and AUC (B) influx by Fluo4 fluorescence after stimulation cells with agonist (10 µM). Data are mean± SEM were at least three separate experiments conducted in triplicate. Statistical analysis was determined using paired, two-tailed *t*-test, **p*<0.05, ****p*<0.001; agonist tested in absence of PTX (control, CTR) compared to responses in the presence of PTX.

4.3.2.1 Effect of an allosteric modulator of CB_1 receptors on intracellular calcium

The observed lack of response to the long chain n-3 fatty acids in terms of $[Ca^{2+}]_i$ elevation led us to investigate whether a positive allosteric modulator for the CB_1 receptor might enhance these responses (Baillie *et al.*, 2013, Price *et al.*, 2005).

The effect of pre-incubation of CHO-hCB_1 cells with 1 μM Org27569 for 10 min. on the HU210, AEA or n-3 PUFA ethanolamines are shown in **Figure 4.12**. The data analysis showed that Org27569 did not change either the peak or AUC intracellular calcium response to n-3 fatty acid ethanolamine ligands AEA or HU210 (paired, *t*-test two-tailed, $p > 0.05$).

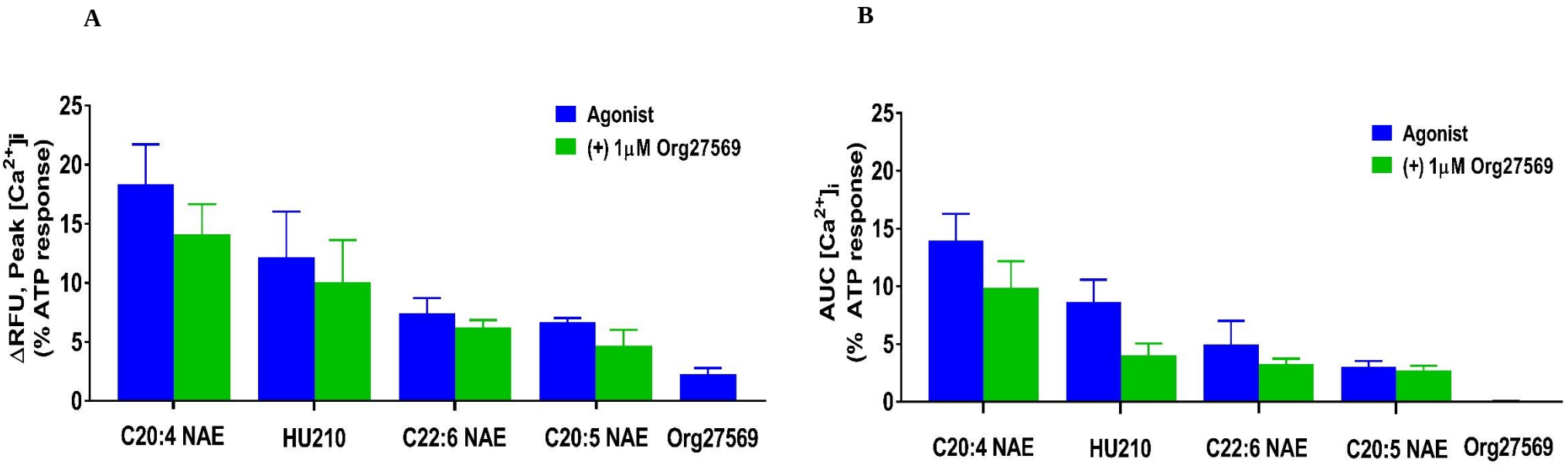


Figure 4.12 Effect of a CB_1 positive allosteric modulator on intracellular Ca^{2+} mobilisation peak (A) and area under the curve (B) responses in CHO-hCB_1. Org27569 (1 μM) was pre-incubated with cells for 10 min. at 37 °C prior to stimulation with n-3 fatty acids ethanolamine. Data are mean ± SEM relative to the positive control (ATP) from at least three independent experiments carried out in triplicate. Data were analysed using paired, two-tailed, *t*-test-tailed, $p>0.05$, comparing the presence and absence of Org27569.

4.3.3 Effect of fatty acids ethanolamine ligands on ERK phosphorylation in CHO-hCB$_2$ receptors

ERK activation in CHO cells expressing human recombinant CB_2 cannabinoid receptors in response to fatty acids ethanolamine was conducted by Wafa Hourani (PhD student, see the Appendices).

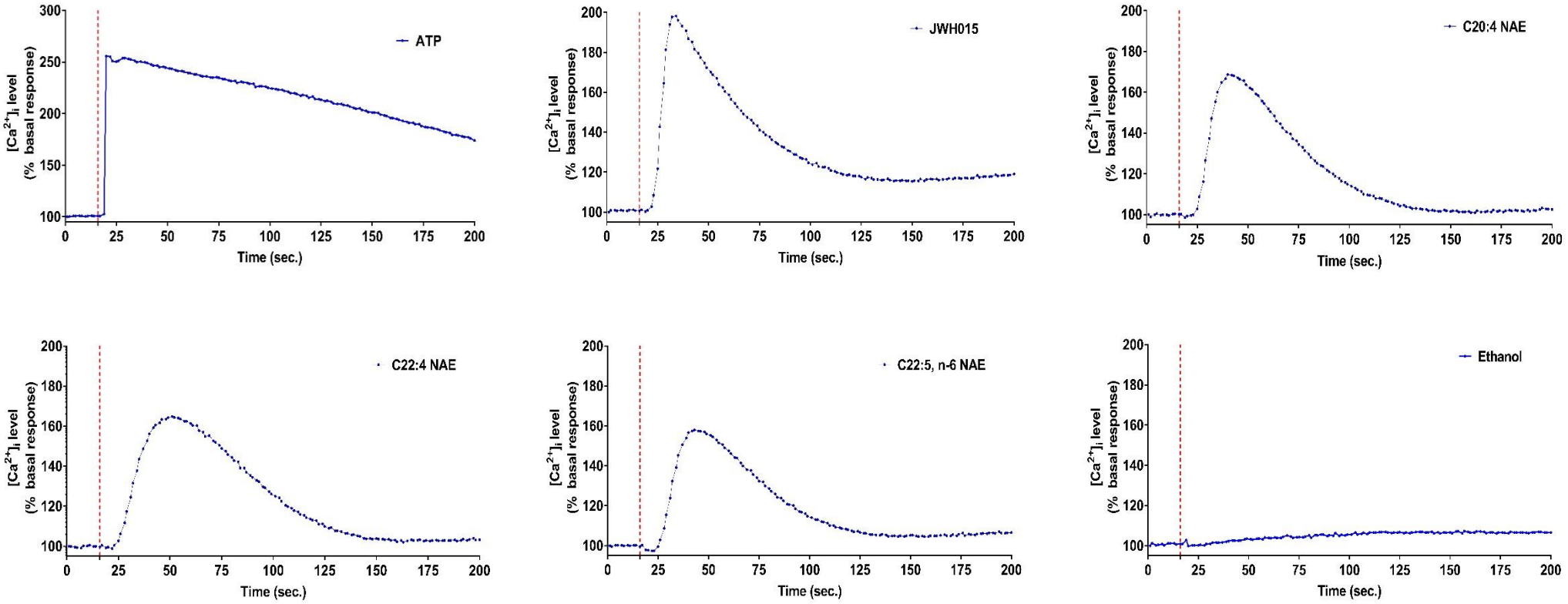
4.3.4 Effects of fatty acid ethanolamine ligands on intracellular calcium mobilisation in human CB$_2$-transfected CHO cells

A panel of fatty acid ethanolamine ligands was applied to CHO cells heterologously expressing human CB_2 receptors to examine their ability to evoke changes in intracellular calcium levels over a 3 min incubation period. The CB_2 agonist, JWH015, was included as a positive control.

Administration of 10 µM n-3 and n-6 fatty acids ethanolamine ligands or JWH015 elicited rapid rises in $[Ca^{2+}]_i$ in CHOhCB$_2$ cells, followed by decline in the response until it returned to basal levels (**Figure 4.13 A and B**). Similarly, ATP was able to elicit a $[Ca^{2+}]_i$ response within seconds and the response gradually decreased over 3 min.

Analysis of the peak response data revealed that both long chain n-3 and n-6 fatty acids ethanolamine ligands and JWH015 induced significant responses of peak intracellular calcium (**Figure 4.14**, one-way ANOVA, Dunnett's test; $p< 0.05$), while the same concentration of the mono-unsaturated and saturated fatty acid ethanolamines had a similar magnitude to the basal response.

A


ATP
JWH015
C20:4 NAE
C22:4 NAE
C22:5, n-6 NAE
Ethanol
[Ca2+]i level
(% basal response)
Time (sec.)

B

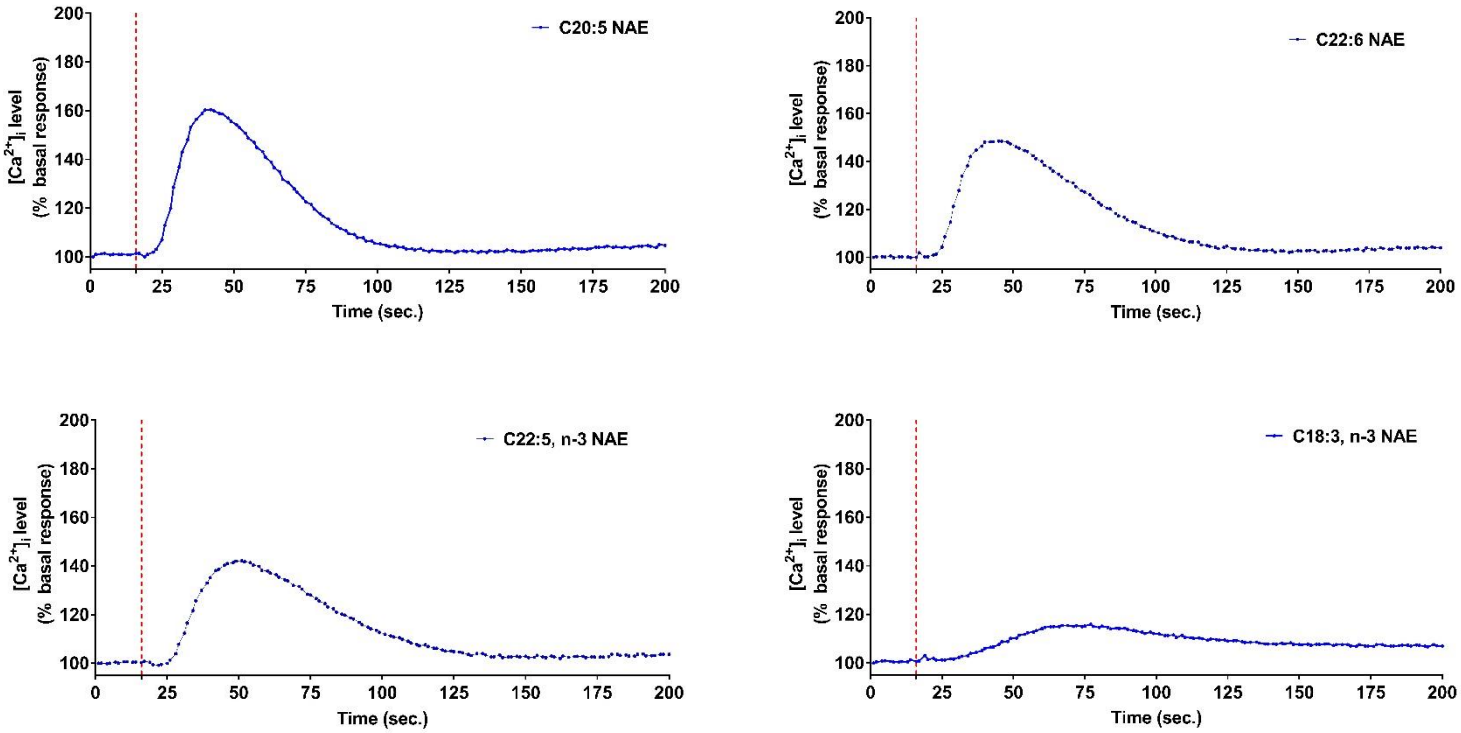


Figure 4.13 Representative curves showing the time courses of intracellular calcium mobilisation responses to the positive controls (JWH015, ATP), n-6 NAEs and ethanol as vehicle (A) and n-3 NAEs (B) measured by Fluo4 fluorescence in CHO-hCB_2 cells with red dashed line indicating the time of agonist addition.

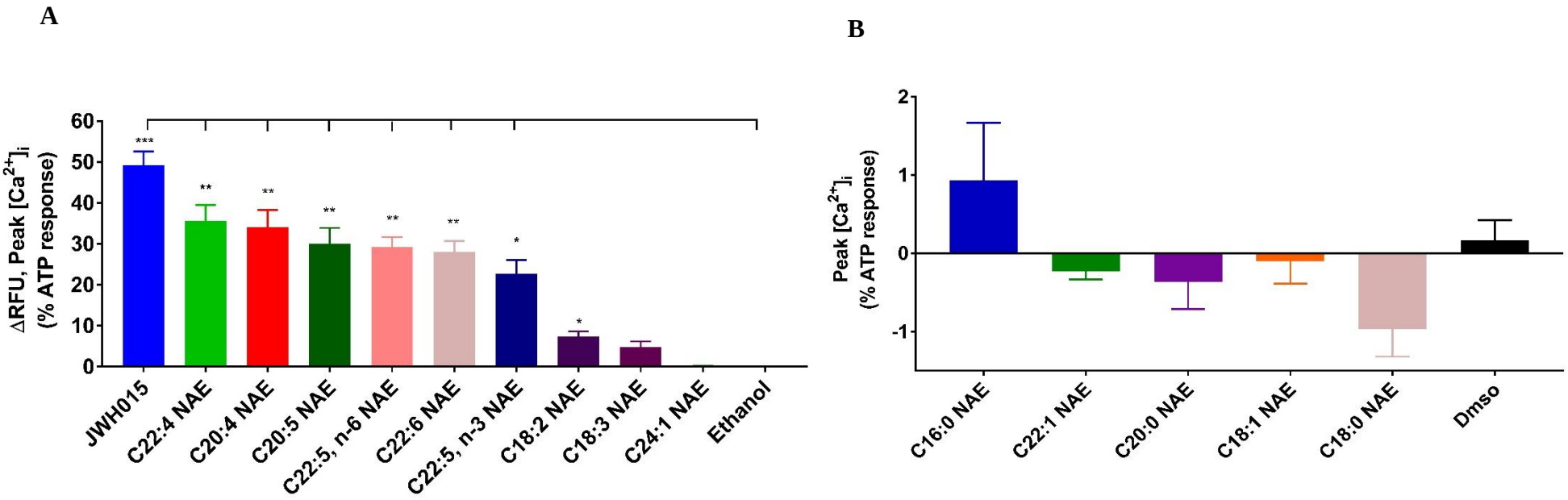


Figure 4.14 The maximum peak of intracellular Ca^{2+} mobilisation stimulation in response to fatty acid ethanolamines dissolved in ethanol (A) and DMSO (B) in CHO-hCB_2. Data are means ± SEM from at least three experiments performed in triplicate. Statistical analysis was determined using one-way ANOVA, followed by post-hoc Dunnett's test; *p<0.05, **p<0.01, ***p<0.001; comparing the peak of agonist with the vehicle.

To confirm the role of the CB_2 receptor in agonist-induced responses, experiments were repeated in the presence of the CB_2-selective competitive antagonist, AM 630 (Ross *et al.*, 1999).

Initially, a preliminary experiment was performed to determine the optimal concentration of AM630 (CB_2 antagonist) for use in subsequent calcium mobilisation assays. Pre-incubation of the cells with AM630 caused a concentration-dependent decrease in $[Ca^{2+}]_i$ levels (**Figure 4.15 A**). High concentrations of AM630 caused a clear decrease in the agonist-evoked calcium response. On the basis of these results, 10 µM AM630 was chosen for subsequent experiments.

Treatment of hCB_2-transfected CHO cells with 10µM AM630 for 30 min at 37 °C resulted in significant inhibitions of the maximum peak and AUC of intracellular calcium response induced by n-3 and n-6 fatty acid ethanolamine ligands and JWH015 (as a positive control for CB_2 receptor) over duration of 3 min (**Figure 4.15 B+C**, paired, two-tailed *t-test*, $p<0.05$).

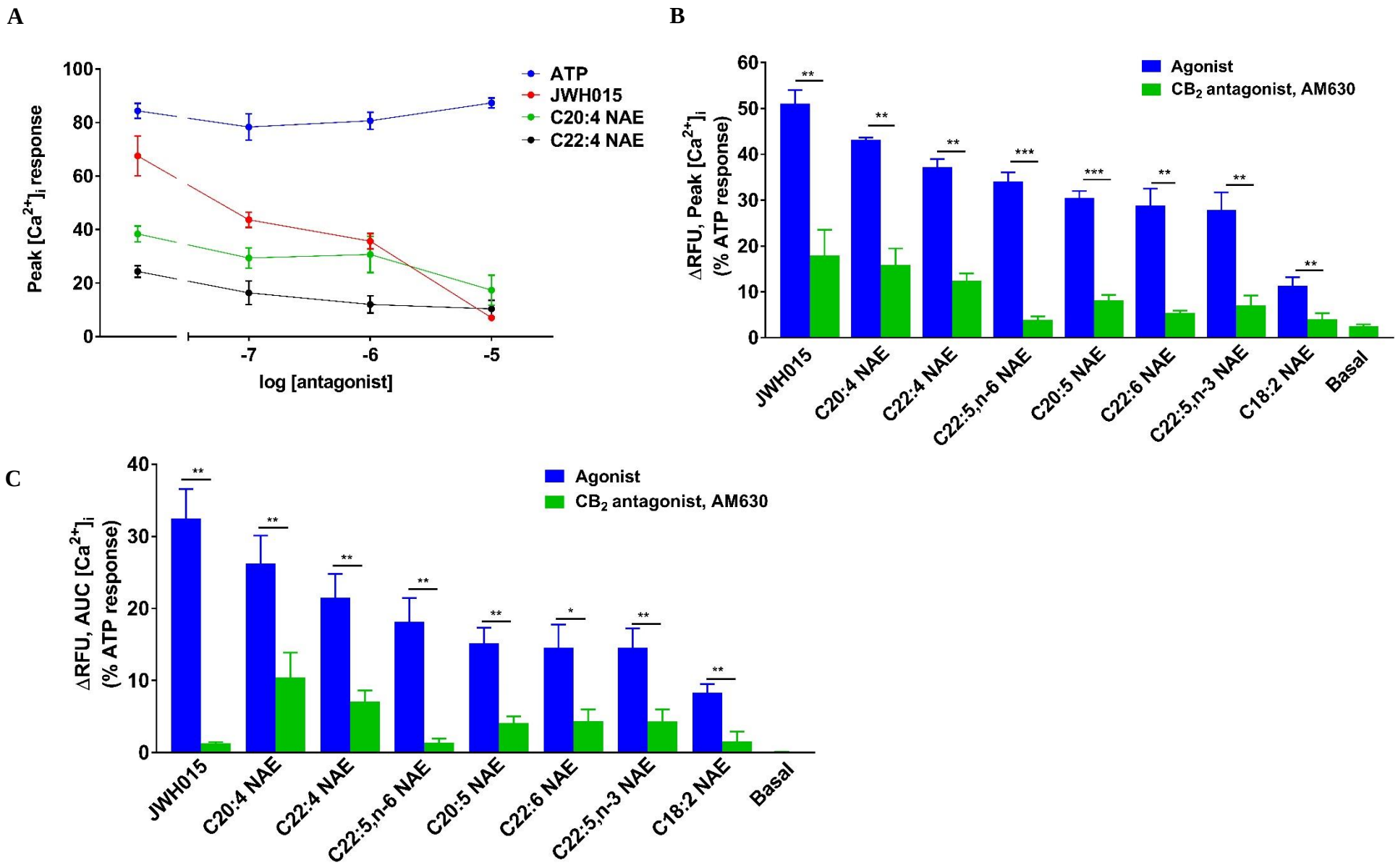

A
Peak [Ca2+]i response
100
80
60
40
20
0
-7
-6
-5
log [antagonist]
ATP
JWH015
C20:4 NAE
C22:4 NAE
B
ΔRFU, Peak [Ca2+]i
(% ATP response)
60
50
40
30
20
10
0
Agonist
CB2 antagonist, AM630
**
***
JWH015
C20:4 NAE
C22:4 NAE
C22:5,n-6 NAE
C20:5 NAE
C22:6 NAE
C22:5,n-3 NAE
C18:2 NAE
Basal
C
ΔRFU, AUC [Ca2+]i
(% ATP response)
40
30
20
10
0
Agonist
CB2 antagonist, AM630
**
*
JWH015
C20:4 NAE
C22:4 NAE
C22:5,n-6 NAE
C20:5 NAE
C22:6 NAE
C22:5,n-3 NAE
C18:2 NAE
Basal

Figure 4.15 Inhibition of fatty acid ethanolamine ligands induced intracellular calcium mobilisation using CB_2 antagonist in CHO-hCB_2 cells. Cells were pre-incubated with AM630 for 30 min at 37 °C and responses measured over 3 min by Fluo-4 fluorescence following adding agonist at 10 μM **(A)** CB_2 antagonist (AM630) produced a concentration dependent reduction in calcium mobilisation in CHO-CB_2. **(A)** The maximum peak and **(B)** area under the curve (AUC) of intracellular calcium mobilisation in presence of 10 μM AM630 stimulated by tested agonists and represent as a percentage of the ATP mobilisation. All data shown are mean ± SEM from four independent experiments. Statistical analysis was conducted on raw data by comparing change in $[Ca^{2+}]_i$ levels in presence and absence of AM630 using paired, two-tailed t-test, *p<0.05, **p<0.01, ***p<0.001.

The latency to peak for n-6 and n-3 PUFA ethanolamines ligands and JWH015 are shown in **Figure 4.16**. AM630 significantly increased the time to peak of C20:4 NAE, C22:4 NAE, C22:5, n-6 NAE and JWH015 (paired, two-tailed *t*-test, $p< 0.05$) while the CB_2 antagonist did not affect the latency to peak of C22:5, n-3 NAE and C22:6 NAE, C20:5 NAE in CHO-hCB_2 cells as seen in **Figure 4.16**.

To further investigate coupling of CB_2 receptors with G_i protein-coupled receptors, CHO-hCB_2 cells were initially treated with 600ng/ml of PTX for 6 h to inactivate susceptible G proteins. Intracellular calcium mobilisation in response to hCB_2 activation through tested ligands was blocked by 600 ng/ml of PTX for six h incubation over duration 3 min (**Figure 4.17**, paired, two-tailed t-test, $p<0.05$).

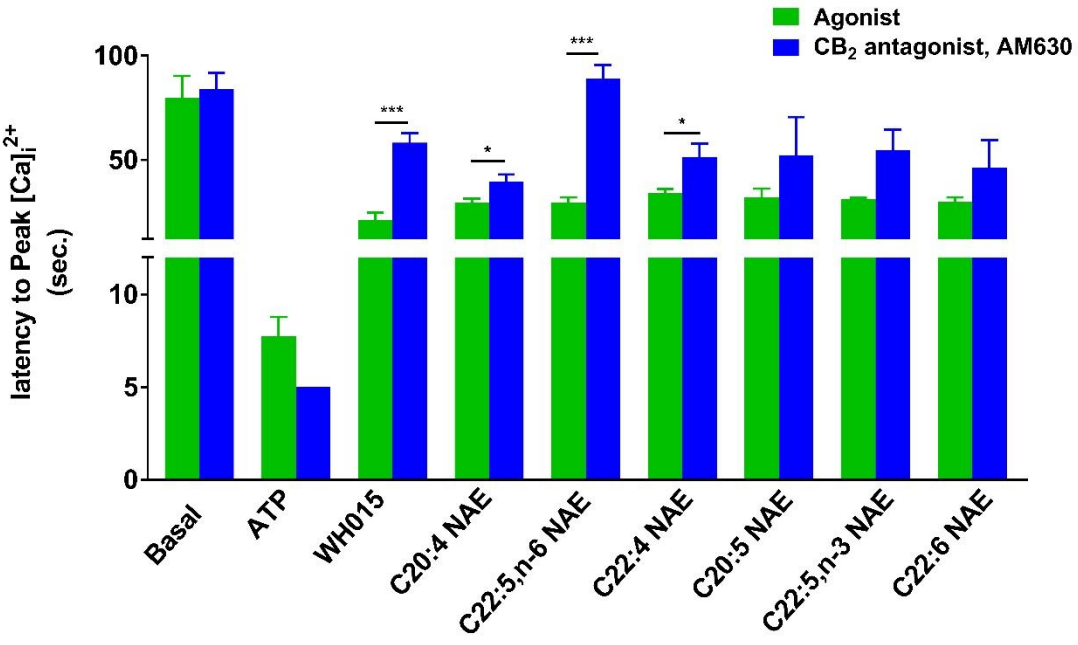


Figure 4.16 Effect of CB_2 antagonist (AM630) on the latency to peak of calcium mobilisation response to activation CHO-hCB_2 cells stimulated by tested NAEs ligands. Cells were loaded with calcium indicator Fluo-4 for 45 min and pre-treated with 10 μM AM 630 for 30 min at 37 °C. Data represent mean ± SEM calculated from 4 separate experiment. Statistical analysis was conducted on raw data and determined using paired, two-tailed t-test, *p<0.05 and ***p<0.00.

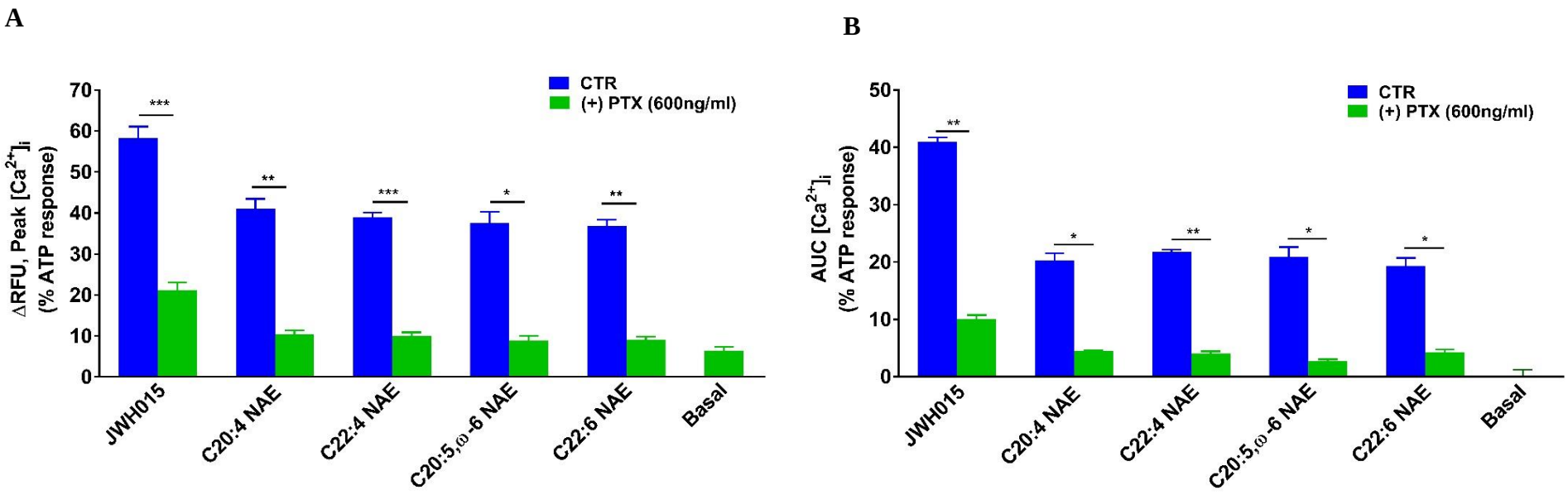


Figure 4.17 Intracellular calcium mobilisation in response to n-3 and n-6 fatty acid ethanolamines in the presence of PTX in CHO-hCB_2. Cells were pre-treated for 6 h at 37 °C and then stimulated with agonist (10 μM). The intracellular calcium response was calculated as a percentage of the ATP response (as positive control) for the maximum peak (A) AUC (B). The experiment was repeated 4 times from different cell passages. Data were compared in the absence of PTX (control, CTR) with the presence of PTX using paired, two-tailed t-test,*p<0.05, **p<0.01, ***p<0.0001.

4.3 Discussion

The CB_1 receptor has been reported to be involved in the regulation of numerous intracellular signalling pathways, for example regulation of adenylyl cyclase, ion channel and activation of MAP kinases and calcium mobilisation. One of the most ubiquitous mechanisms of signal transduction in response to environmental stimuli is the activation of mitogen- and stress-activated protein kinase (MAP kinase) cascades (Garrington and Johnson, 1999).

The first intracellular signalling to be investigated with various fatty acid derivatives of ethanolamine was extracellular signal regulated kinases phosphorylation, using a fluorescence immunocytochemical-based assay in which the target protein is detected using epitope-specific primary antibodies in fixed cultured cells in a 96 well plate (Chen *et al.*, 2005).

The maximum peak of ERK phosphorylation for HU210 and AEA at 37 °C was achieved at 5 min as seen in **Figure 4.1.** This observation was consistent with previous reports in the detection of ERK signalling mediated by CB_1 receptor (Hsu *et al.*, 2007, Liu *et al.*, 2000).

All the n-6 fatty acid ethanolamines examined in this study elicited a robust ERK phosphorylation in CHO-hCB_1 cells following 5 min incubation. The responses elicited by docosatetranoylethanolamine (C22:4 NAE) and docosapentaenoylethanolamine (C22:5 NAE) were comparable to that induced by anandamide (C20:4 NAE) response in CHO-hCB_1 cells as seen in **Figure 4.3**. Pre-incubation with the CB_1-selective antagonist AM251 or with pertussis toxin caused a significant reduction of all these

response, clearly indicating that the observed responses were mediated by CB_1-receptor in a PTX-sensitive manner. These findings were consistent with many reports describing the activation of ERK phosphorylation through CB_1 receptors in various cell lines (Graham *et al.*, 2006, BERDYSHEV *et al.*, 2001, Liu *et al.*, 2000).

In 2001, Berdyshev and co-workers reported that PEA (C16:0) and OEA (C18:1, n-9) mediated CB_1 receptor independent ERK phosphorylation (BERDYSHEV *et al.*, 2001). Comparing with our results, this finding suggests that there are other targets for monounsaturated and saturated fatty acid ethanolamines coupled to the MAP kinase transduction cascade. In terms of n-3 NAE, previous reports have shown that long chain n-3 fatty acid ethanolamines (C22:6 and C20:5 NAE) were able to competitively inhibit specific binding of the radio-ligand ([^{3}H] CP55490) in a concentration-dependent manner in MF1 mouse whole brain membranes. EPEA (C20:5, n-3 NAE) and DHEA (C22:6, n-3 NAE) have been reported to induce cell death in human prostate cancer cell lines (Brown *et al.*, 2010). The effect of CB receptor antagonists was investigated, but provided no clear-cut or consistent effect, suggesting a complex action in this extended assay. In ^{35}S-GTPγS binding assays using human recombinant CB_2 receptors in CHO cells, EPEA and DHEA evoked concentration-dependent increases (Brown *et al.*, 2010) consistent with the observations reported here. However, in conflict with the present findings (**Figure 4.3**), the authors suggested a similar potency for EPEA and DHEA in stimulating ^{35}S-GTPγS binding in mouse whole brain, a tissue expressing predominantly CB_1 receptors. This discrepancy could be related to the functional selectivity of these NAEs at CB_1 receptors. Alternatively, there may be a species difference in sensitivity to n-3 PUFA-NAEs or result from the extended periods of co-incubation required in the

published study compared to the present results. These alternatives require further investigation.

Interestingly, complete inhibition of ATP-mediated ERK activation was observed by blocking CB_1 receptor activation (**Figure 4.4)**, implying an indirect interaction between CB_1 and endogenous P2 receptors. Although a similar interaction has been described between epidermal growth factor and lysophosphatidic acid receptors (Wu and Cunnick, 2002), a similar convergence of signalling between cannabinoid and P2 receptors has not previously been reported. Further studies need to be undertaken to clarify the relationship between these two receptors in mediating ERK activation.

The other signalling pathway investigated in this study was the effect of fatty acid ethanolamines on intracellular calcium levels. Many previous studies have reported that AEA induces a rapid and transient increase in intracellular $[Ca^{2+}]_i$ levels, suggesting that this effect of AEA is mediated by the classical cannabinoid receptor, CB_1 (Sugiura *et al.*, 1997, Filipeanu *et al.*, 1997, Mombouli *et al.*, 1999). Similarly, we found that the fatty acid ethanolamines docosatetraenoylethanolamide (C22:4 NAE) and docosapentaenoylethanolamines (C22:6 NAE) can trigger calcium mobilisation in CHO-hCB_1 cell line responses. These results are in contrast to the other fatty acids ethanolamines tested, which were unable to evoke a calcium mobilisation.

The non-selective cannabinoid agonist, HU210 generated a lower response (~ 15% of maximum $[Ca^{2+}]_i$ mobilisation) compared to AEA (24%) in CB_1 calcium responses (**Figure 4.8**), which contrasts with other signalling pathways. AEA had a lower maximal response for stimulation of [^{35}S]-GTPγS binding (Glass and Northup, 1999) and

equivalent responses for inhibition of cAMP (Bonhaus *et al.*, 1998). This may be related to the phenomenon of signalling bias (Priestley *et al.*, 2017a).

Although the exact mechanism of fatty acid ethanolamines induced calcium mobilisation is yet to be determined, the essential role of G_i protein in eliciting $[Ca^{2+}]_i$ responses to C20:4 NAE ,HU210 and C22:4 NAE of ethanolamine have been demonstrated in CB_1 transfected model (**Figure 4.11**). The sensitivity to AM251 confirmed the involvement of CB_1 receptor in mediating of these responses as seen in **Figure 4.9.** It seems, however, that the concentration of AM251 used was insufficient to block the CB_1 receptor completely in this non-equilibrium assay, reflected in the lack of effect on AUC calcium responses. However, AM251 was able to reduce the peak height and delay the time to peak significantly. Interestingly, the shortening of the latency and decreasing the AUC of ATP as result of AM251 effect which suggests that ATP evokes the formation of endocannabinoids subsequently activating CB_1 receptors, which prolong and extend the duration of the calcium response. This suggestion supported by Walter and co-worker study who showed a rapid and significant production in 2-AG induced by ATP in astrocytes (Walter *et al.*, 2004). Future research should investigate this effect by using selective inhibitors of DAGL and NAPE-PLD to identify the synthetic pathway involved.

The positive allosteric modulator of CB_1 receptors (Org27569) has been shown to alter receptor activity through conformational changes to increase agonist affinity at orthosteric binding site (Price *et al.*, 2005). A study on the effect of Org 27569 on a diverse signalling pathways from CB_1 receptors demonstrated a reduced efficacy of C20:4 (AEA) in GTPγ binding and β-arrestin recruitment but no effect on ERK

signalling cascade (Baillie *et al.*, 2013). It was, therefore, investigated whether Org27569 could increase the effects of the n-3 NAEs at CB_1 receptor-evoked calcium mobilisation. In CHO-hCB_1 cells pre-treated with Org27569, there was no significant effect on responses to n-3 PUFA ethanolamine or to H210 or C20:4 NAE. Together with the results of Baillie *et al* (2013), our results suggest that the action of allosteric modulators might dependent both on the ligand and the signalling pathway being investigated.

The function of fatty acid ethanolamines acting at the CB_2 receptor was investigated using CHO cells transfected with human CB_2 receptors. It has been shown in many studies that the two classical cannabinoid receptors have in common their the intracellular signalling pathways involving $G_{i/o}$ proteins (Felder *et al.*, 1995). In hCB_2 transfected CHO cells, long chain polyunsaturated n-6 and n-3 fatty acids ethanolamine rapidly elevated intracellular Ca^{2+} levels that were sensitive to the CB_2 selective antagonist, AM630. Although this signalling pathway is not widely described, a previous report showed that C20:4 NAE induced $[Ca^{2+}]_i$ mobilisation in endothelial cells endogenously expressing CB_2 receptors (Zoratti *et al.*, 2003).

AM630 increased significantly the latency to peak for NAEs (C20:4, C22:4 and C22:5, n-6) and JWH015 (**Figure 4.15**) although it failed to alter significantly responses to the less effective agonists. This lack of effect may simply be a reflection of the smaller responses to these agonists. However, all these responses were inhibited by pre-treatment with PTX which implicates $G_{i/o}$ proteins in this $[Ca^{2+}]_i$ response. At least one report demonstrated the mechanism of calcium mobilisation which might be through phospholipase C and IP_3 (Zoratti *et al.*, 2003).

4.4 Conclusion

In conclusion, the data presented in this chapter clearly demonstrate that n-6 long chain fatty acid ethanolamine evoke both ERK phosphorylation and intracellular calcium elevation through the CB_1 receptor transfected in CHO cells. It showed a clear discrimination between n-6 polyunsaturated and other types of fatty acids in activated CB_1 receptor. At CB_2 receptors, both n-6 and n-3 PUFA ethanolamine evoked ERK activation and intracellular calcium elevation. Given the possibility of changing the profile of N-acylethanolamines through dietary intervention, this raises the possibility that the balance of tone at CB_1 vs CB_2 receptors can be changed by food choices.

Chapter 5
Functional effects of fatty acid ethanolamines at rat transient receptor potential vanilloid 1 (TRPV1) channels

5.1 Introduction

The transient receptor potential vanilloid 1 (TRPV1) channel plays a pivotal role in the development of neurogenic pain and inflammation. The location of TRPV1 predominantly in the small diameter Aδ and C peptidergic sensory nerves (Sanchez *et al.*, 2001) and its activation, as a Ca^{2+} permeable cation channels, induces a large inward current, thereby elevating intracellular Ca^{2+} concentration because of the influx of extracellular Ca^{2+} in primary sensory neurons (Caterina *et al.*, 1997).

Anandamide has been shown to activate the TRPV1 receptor directly (Zygmunt *et al.*, 1999) and to increase the possibility of initiating of inflammation (Dinis *et al.*, 2004). Several studies focused on the action of NAEs other than AEA on the TRPV1 receptor. The saturated fatty acid ethanolamines were unable to activate TRPV1 receptor, such as C16:0 NAE (Zygmunt *et al.*, 1999) and C18:0 NAE (Smart *et al.*, 2002) while C16:0 NEA enhanced the affinity and potency of AEA at TRPV1 receptors (De Petrocellis *et al.*, 2001). C18:1 NAE was also reported as a ligand, but only under 'inflamed/sensitised' conditions (Ahern, 2003). Another study reported that C18 NAEs such as C18:1 and C18:2, n-6 , C18:3, n-3 as well as C22:4, n-6 produced intracellular calcium increases in DRG neurons and mesenteric arteries that was TRPV1 receptor mediated (Movahed *et al.*, 2005), these responses were similar in profile to AEA.

An accumulation of data from previous chapters indicated that fatty acid ethanolamine ligands act as agonists at CB_1 and CB_2 receptors and are also substrates for FAAH in rat liver microsomes. A further possibility is that AEA and structurally-related lipids act as endogenous TRPV1 receptor modulators and are potentially involved in the

regulation of inflammation pain while there are no previous studies on the action of these NAEs at TRPV1 receptors.

5.2 Aim

This chapter aims to examine the ability of a series of commercially-available fatty acid ethanolamine ligands to induce functional responses in rat DRG neurons natively expressing TRPV1 receptors by measuring intracellular calcium responses using ratiometric Ca^{2+} measurement (fura-2) by microscopy.

5.3 Results

5.3.1 Effects of fatty acid ethanolamine ligands on intracellular calcium responses in DRG neuros

In Movahed *et al*., (2005) study, AEA was able to evoke a significant elevation of intracellular calcium in rat TRPV1, with pEC50 value of 6.6 as well as other NAEs such as C22:4, C18:2 and C18:3 produced responses similar in profile to AEA. Therefore, a series of fatty acid ethanolamine conjugates was investigated at a maximum concentration (10 μM) in rat DRGs that expressed native TRPV1 receptors. This was achieved by measuring evoked intracellular calcium concentrations in single cells using a ratiometric calcium dye, fura-2. The mean diameter of rat sensory neuron used in this experiment was 26.5 ± 1μm (consistent with C fibre cell bodies).

An initial experiment was conducted to confirm the effectiveness and viability of DRGs neurons for subsequent experiments. Perfusion of DRG neurons with a high concentration of a agonist to TRPV1 receptor (capsaicin) at 10 μM then, after a wash-out period and recovery, cells were stimulated with 60 mM KCl. Ninety-four per cent of neurons studied responded to the capsaicin as seen in **Figure 5.1**.

Most of the polyunsaturated ethanolamine conjugates of n-6 (C20:4, C22:5, C22:4) and n-3 (C22:5, C22:6) induced a significant rapid elevation of intracellular calcium ions (**Figure 5.2 - 5.6,** two-way ANOVA, followed by post-hoc Dunnett test, $p< 0.05$). These responses were 92 ± 12% (C20:4, n-6 NAE), 72 ± 6% (C22:5, n-6 NAE), 108 ± 27% (C22:5, n-3 NAE), 62 ± 5% (C22:6, n-3 NAE) and 96 ± 20% (C22:4 NAE) of the responses to capsaicin in the same cells.

Eicosapentaenoylethanolamine, linoleoylethanolamide (C18:2, n-6 NAE) and linolenoyl ethanolamine (C18:3, n-3 NAE) elicited significant increases in intracellular calcium levels but appeared to be less effective compared to other PUFA-ethanolamides (**Figure 5.7A**) while the monounsaturated (C22:1, C24:1 and C18:1) and saturated (C20:0, C16:0, C18:0) fatty acid ethanolamines failed to elicit a significant increase in intracellular calcium response in DRG neurons (**Figure 5.7 A, B and C,** two-way ANOVA, followed by post-hoc Dunnett test, $p > 0.05$).

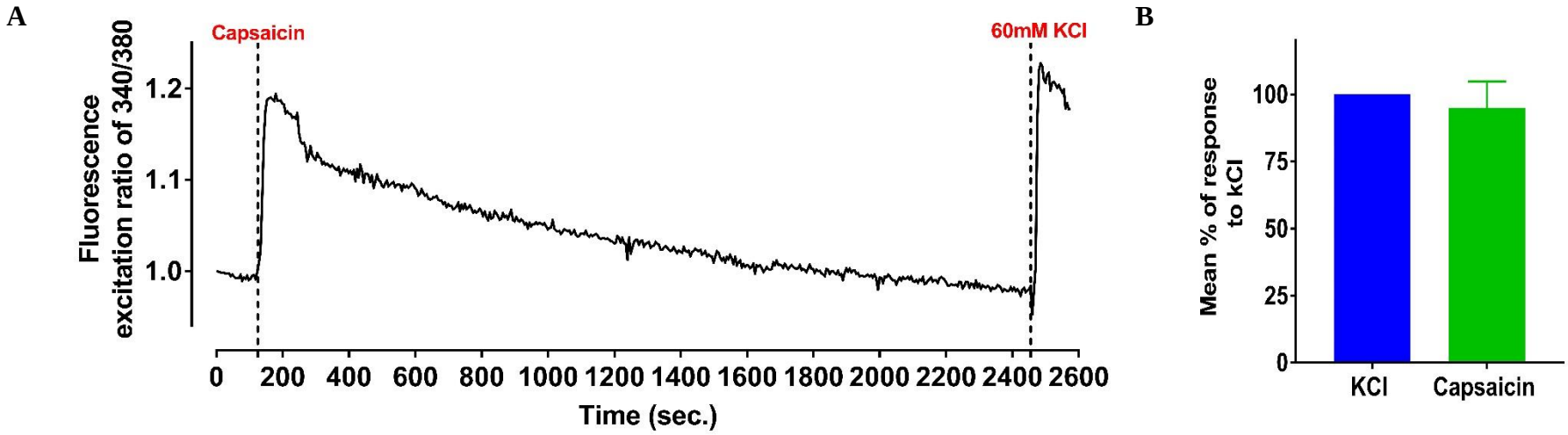


Figure 5.1 Stimulation of DRG neurons expressing TRPV1 in response to the vanilloid agonist, capsaicin. Cells were loaded with fura-2 for 45 min at 37 ºC and fluorescence was recorded (emission (510 nm), exciting at 340 and 380 nm) (A) Representative trace of intracellular calcium increase in response to 10 μM capsaicin and then after a recovery period, KCl (60mM) applied for 30 s indicated by the dashed lines. (B) Capsaicin induced increases in intracellular calcium in DRG neurons comparing to KCl response. Data (mean ± SEM values) are shown from 164 neurons of at least 3 rats. Statistical analysis comparing effects of capsaicin and KCl was conducted using unpaired, two-tailed, $p>0.05$.

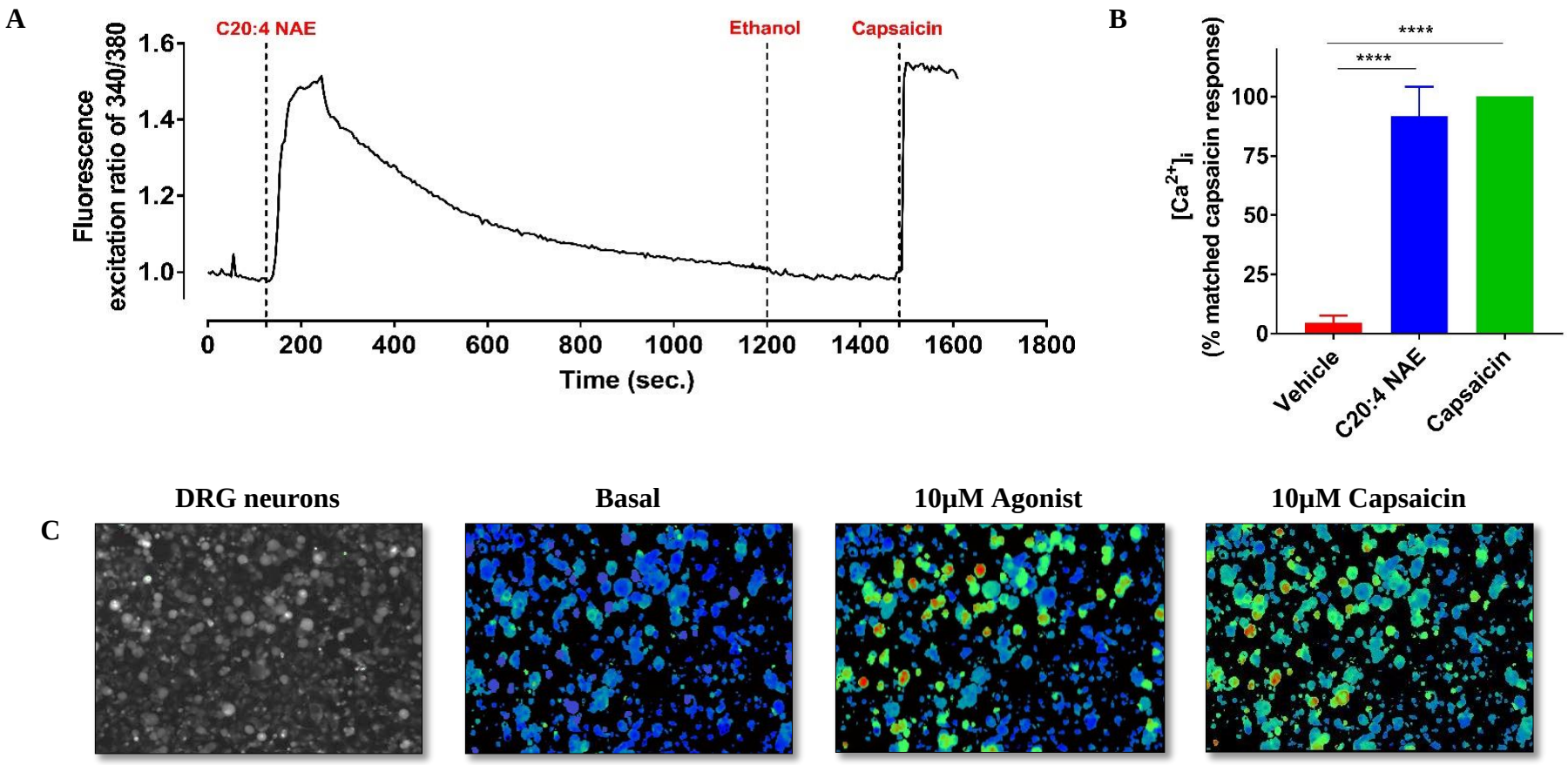


Figure 5.2 (A) C20:4 NAE (10 µM) evoked increases in intracellular calcium in DRG neurons. (B) A comparison of C20:4 NAE (10 µM) and capsaicin (10 µM) evoked increases in $[Ca^{2+}]_i$ in DRG neurons. Data are mean ± SEM values from 90 neurons of at least 3 rats. Statistical analysis was determined by comparing the agonist effects to 0.1% ethanol (%v/v) using two-way ANOVA, followed by post-hoc Dunnett test, ****p< 0.01; (C) Representative colour images showing AEA effect on intracellular calcium in neurons measured by ratiometric calcium imaging using fura-2.

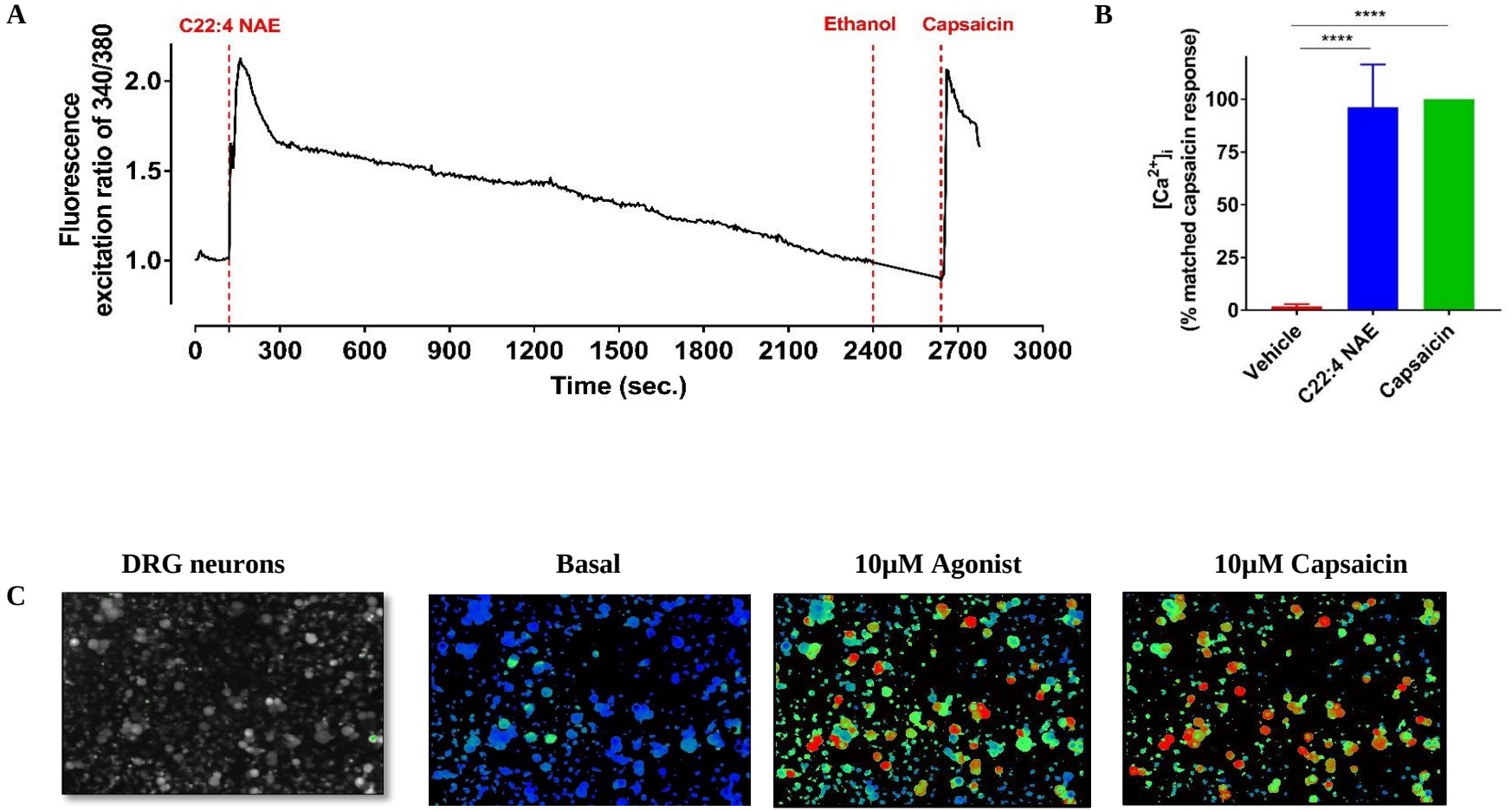


Figure 5.3 (A) C22:4 NAE evoked changes in $[Ca^{2+}]_i$ in rat DRG neurons expressing TRPV1. Cells were superfused with 10 µM C22:4 NAE (2 min) followed by a wash-out period, and stimulation with capsaicin (10 µM) for 30 s. (B) The $\Delta[Ca^{2+}]_i$ induced by agonist was normalized to the corresponding positive control. Statistical analysis was determined by comparing the agonist response with 0.1% ethanol (v/v) using two-way ANOVA, followed by post-hoc Dunnett test, ****p< 0.0001. (C) Fluorescence images reflect the effect of C22:4 NAE increase in $[Ca^{2+}]_i$ in DRG neurons measured by ratiometric dye (fura-2).

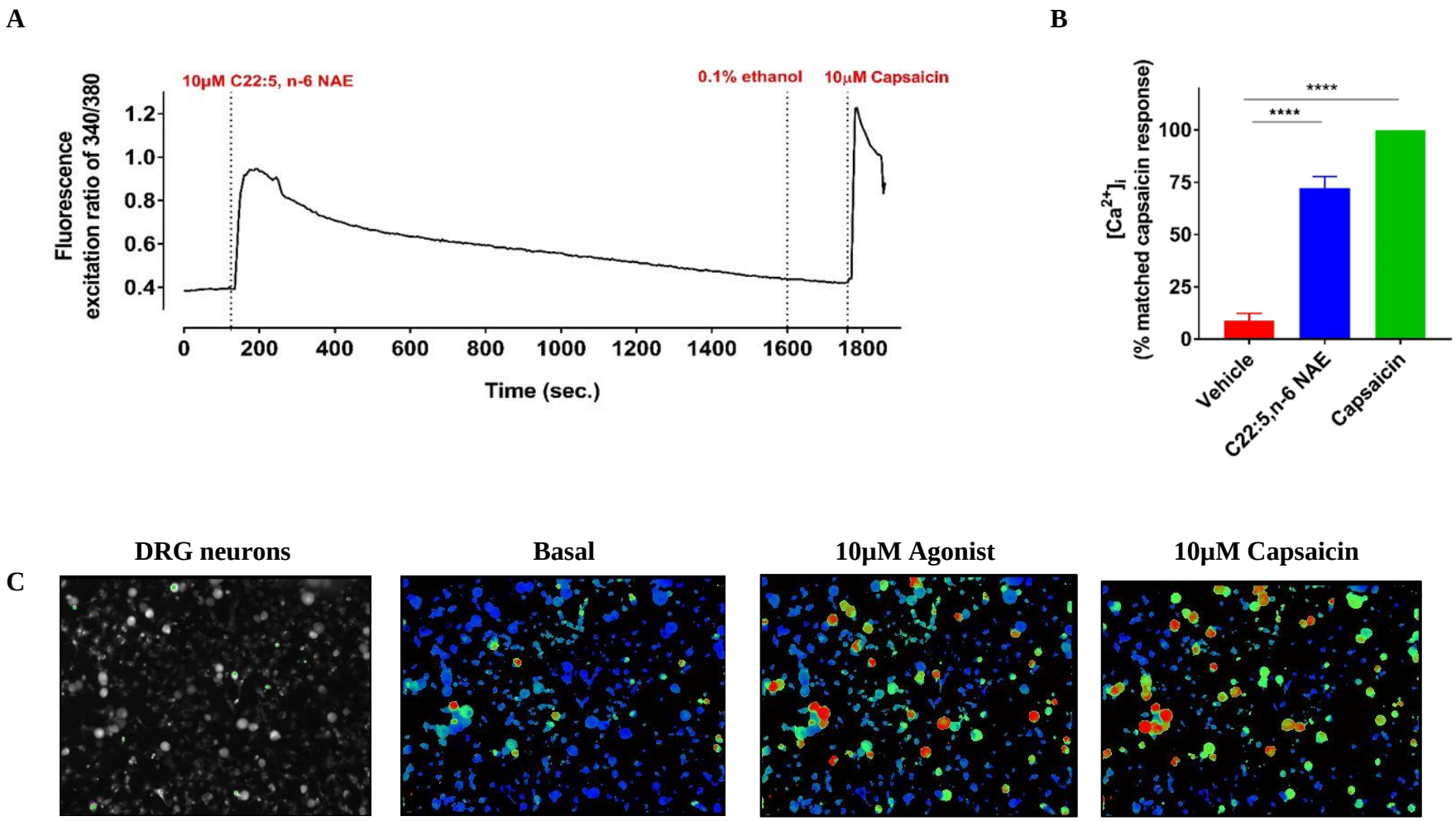


Figure 5.4 (A) C22:5, n-6 NAE (10 μM) evoked increases $[Ca^{2+}]$i in rat DRG neurons expressing TRPV1. DRG neurons were superfused with ligand for 2 min and following a wash-out period, cells were stimulated with capsaicin (10 μM) for 30 s. (B) $[Ca^{2+}]_i$ stimulation in response to agonist compared to capsaicin was performed from 3 rat (n=110 neurons). Statistical analysis was determined by comparing the effects of agonist and ethanol using two-way ANOVA, followed by post-hoc Dunnett test, ***p<0.001. (C) Fluorescence microscopy images for DRG neurons.

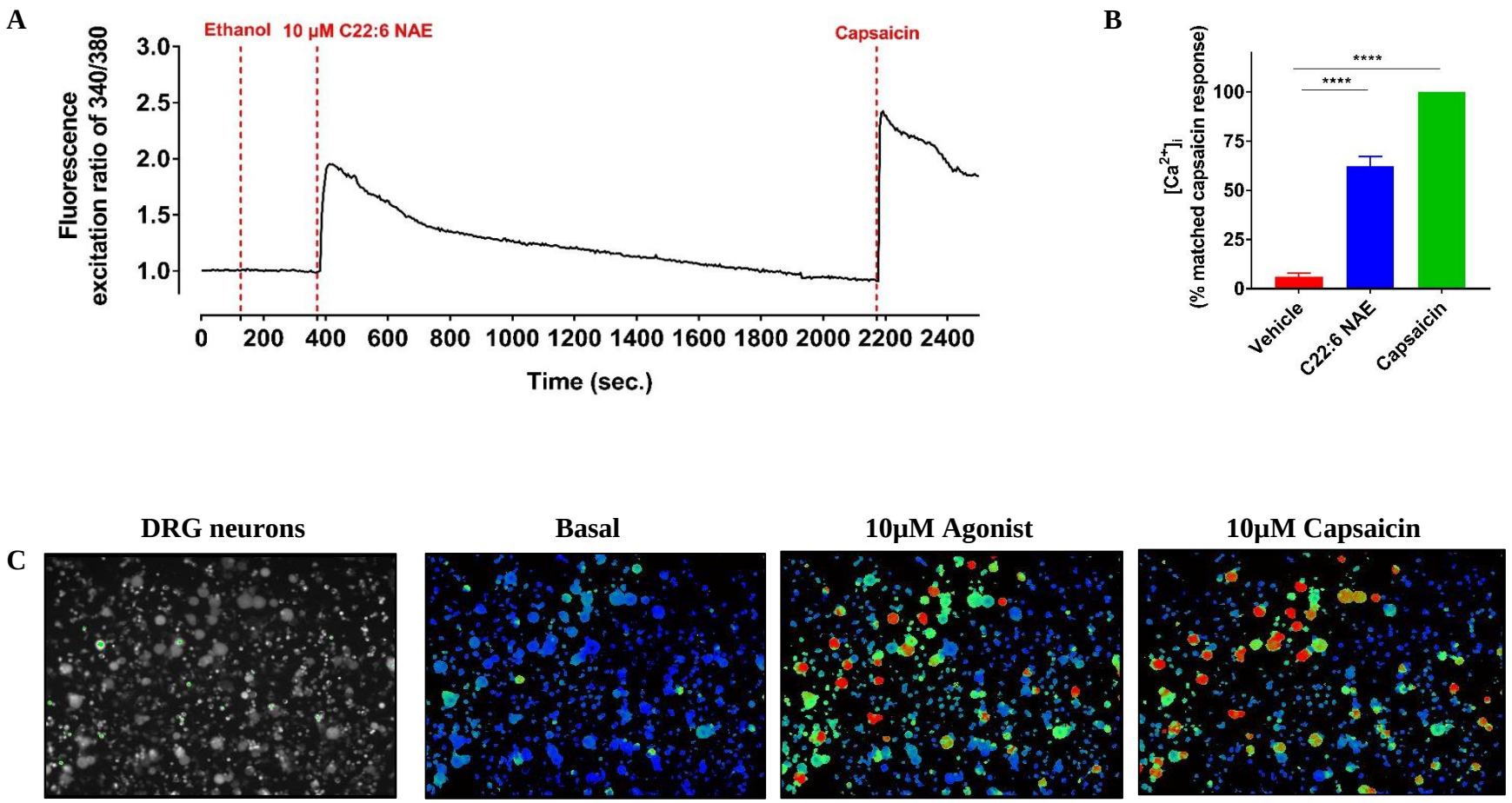


Figure 5.5 Effect of C22:6 NAE on intracellular calcium in DRG neurons expressed TRPV1. **(A)** Diagram showing the time course of intracellular calcium in response to tested NAE ligand (10 µM) comparing to capsaicin (as positive control) (B) Graph showing the percentage of tested NAE ligand comparing to positive control. Data are represented as mean ± SEM values from 205 neurons of at least 3 rats. Statistical significance was determined by comparing agonist with ethanol effects using two-way ANOVA, followed by post-hoc Dunnett test, ****p<0.0001. (C) Intracellular calcium signals were imaged by a digital camera for individual cells.

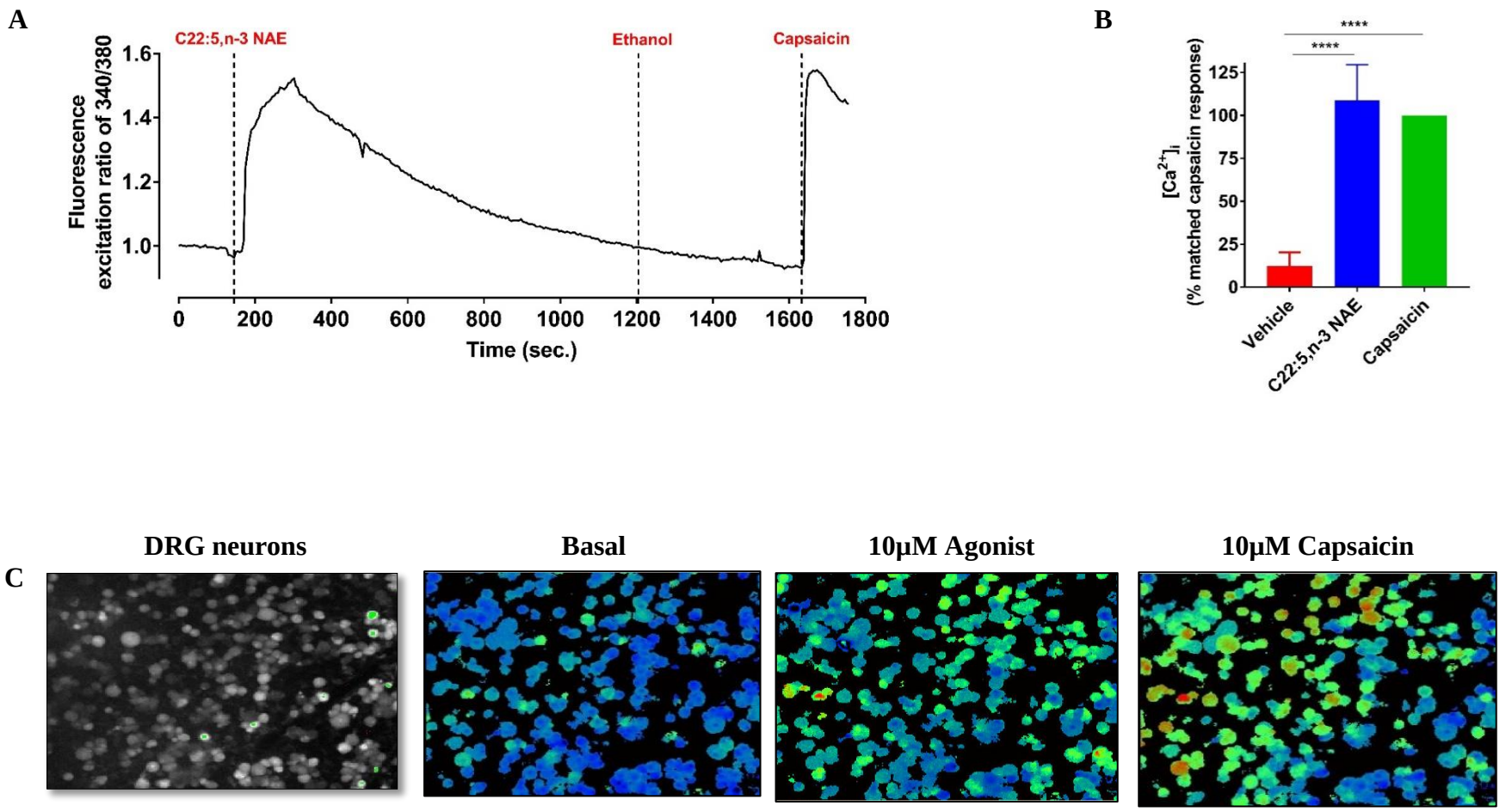


Figure 5.6 (A) C22:5 n-3 NAE elicited increase in $[Ca^{2+}]$i in DRG neurons. (B) A comparison of C22:5,n-3 NAE (10 µM) and capsaicin (10 uM) evoked increases in $[Ca^{2+}]_i$ in DRG neurons. Data are mean ± SEM values from 91 neurons of at least 3 rats. Statistical analysis was determined by comparing the agonist effects to 0.1% ethanol (%v/v) by using two-way ANOVA, followed by post-hoc Dunnett test, ****p<0.0001; **(C)** Representative pseudo colour images showing NAE ligand effect on $[Ca^{2+}]_i$ in neurons measured by ratiometric calcium imaging using fura-2.

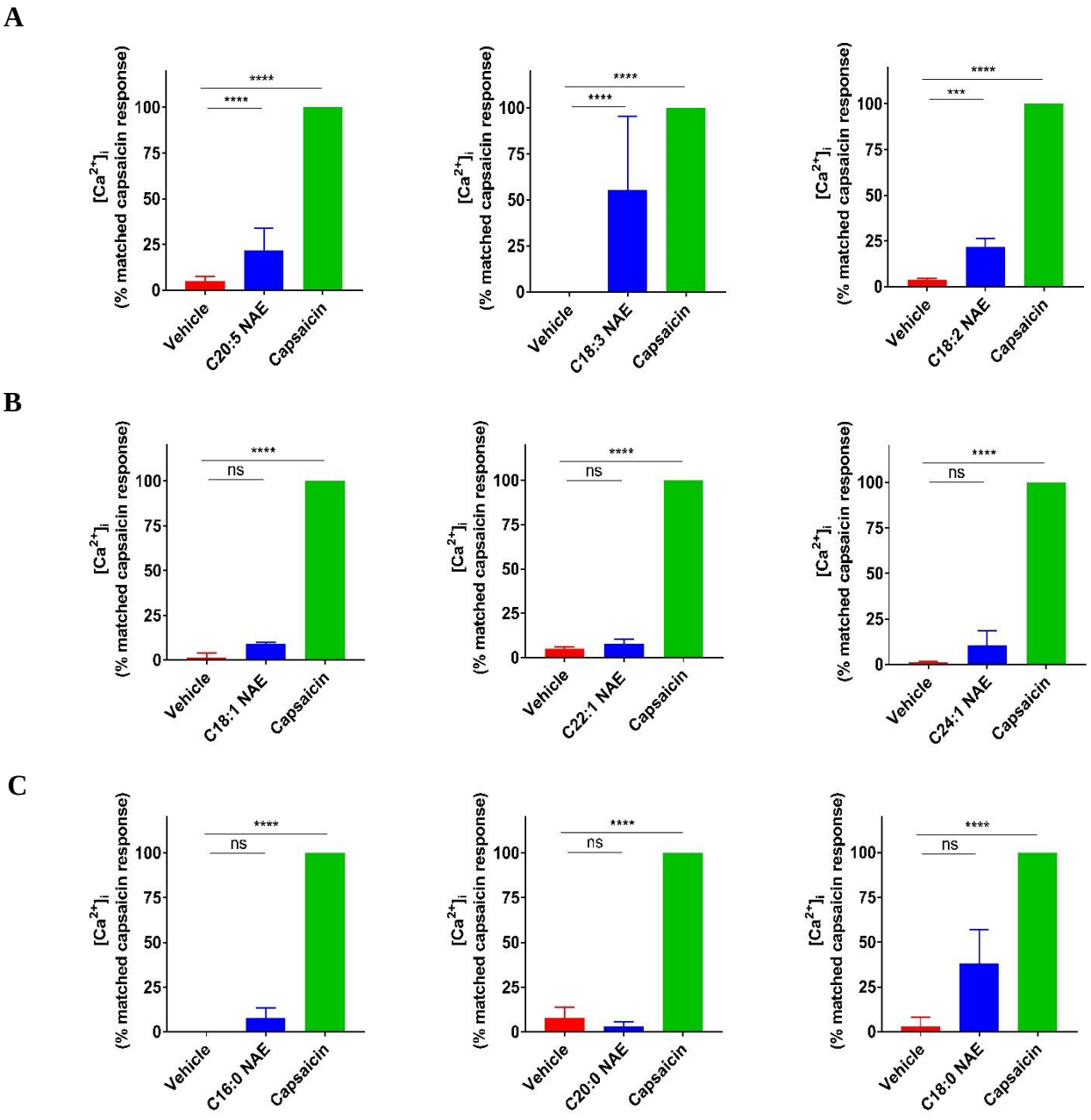


Figure 5.7 Elevation of intracellular calcium levels in rat DRG neurons using calcium imaging. DRG neuronal cells were superfused with ligands (10 μM, 2 min) followed by 10 μM capsaicin (as positive control). Data are means ± range from two (C20:0; C22-1, n-9), or means ± SEM from three (C16:0; C18:0; C18:3, n-3; C18:2, n-6), four (C18:1, n-9; C24:1, n-9), five (C22:5, n-3), six or eight (C20:5, n-3) separate rat. Statistical analysis to comparing tested ligands effects and vehicle (0.1%) determined by using two-way ANOVA, followed by post-hoc Dunnett test, ***p<0.001, ****p<0.0001.

Comparison of all NAE ligand effects on intracellular calcium response in DRG neurons with all capsaicin responses, conducted from all experiments were shown in **Figure 5.8**. C20:4 and C22:4 n-6 NAEs, or C22:5 n-3 analogues were shown to significantly elevate intracellular calcium levels similar to the capsaicin response. In addition, C22:6, n-3 NAE and C22:5,n-6 NAE increased the $[Ca^{2+}]_i$ response to about 72% of capsaicin response, while C18:3,n-3, C18:2,n-6 and C20:5,n-3 responses were less than 60% of the capsaicin response. There were no observed responses from monounsaturated and saturated NAEs in DRG neurons. The area under the curve values for the 2 min exposure to NAEs were essentially the same as the peak intracellular calcium responses (**Figure 5.9**).

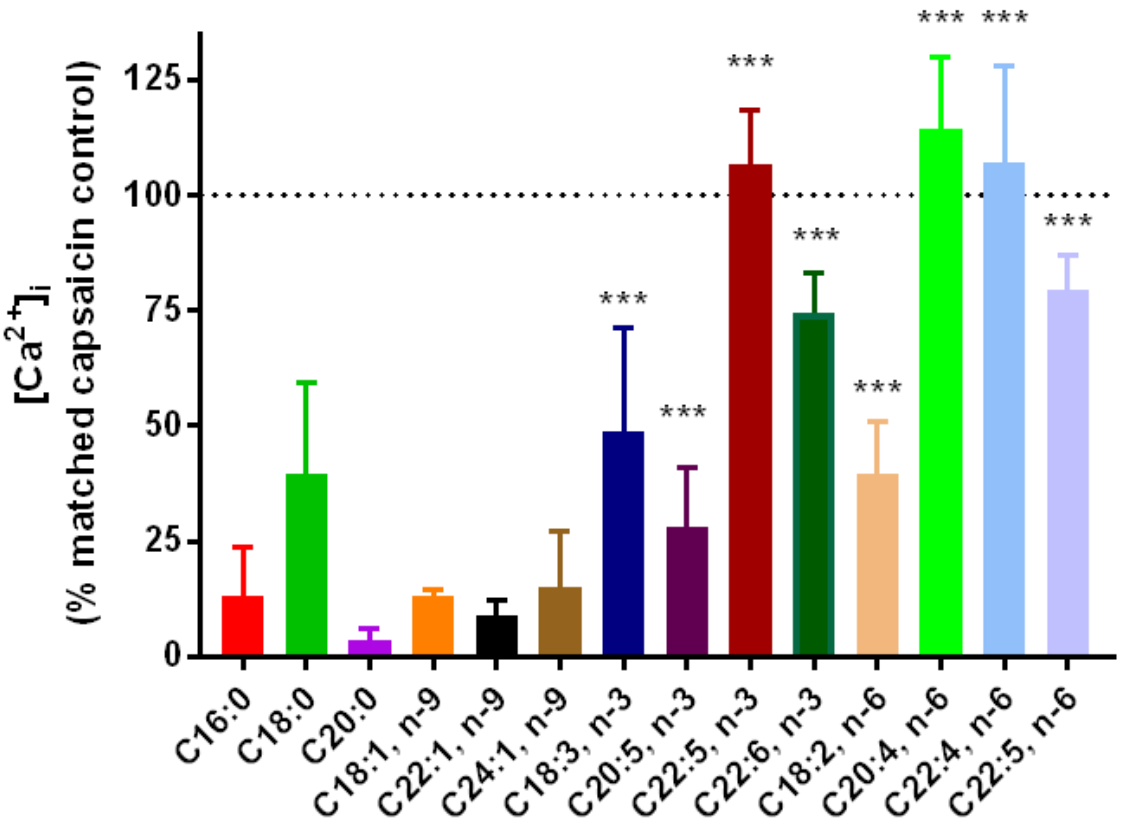


Figure 5.8 Comparison of fatty acid ethanolamine-induced intracellular calcium ion levels measured using calcium imaging, with rat dorsal root ganglion neurones in vitro. The data shown are mean ± SEM values from at least 3 different preparations. Statistical significance was determined using ***p< 0.001 vs. vehicle controls using two way ANOVA with Dunnett's multiple comparison.

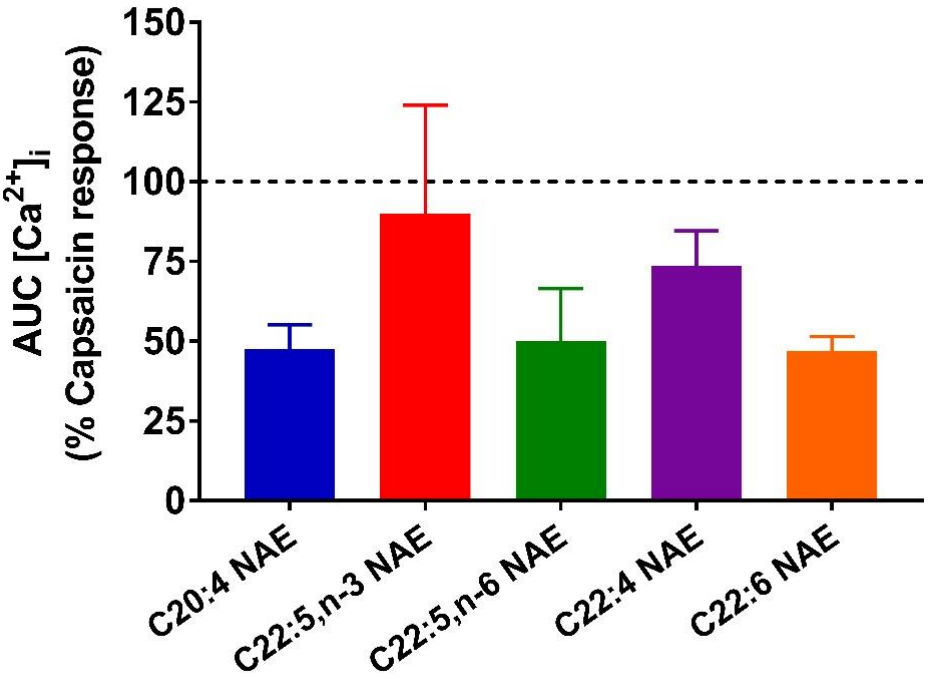


Figure 5.9 Area under the curve summaries of intracellular calcium response induced by 2 min exposure to NAE ligands. Data are mean values ± SEM from at least three separate experiments. Statistical analysis was determined using two way ANOVA, followed by post-hoc Dunnett test vs. capsaicin as control.

5.3.1.2 Effect of a TRPV1 antagonist on fatty acid ethanolamine induced increases in intracellular calcium in rat DRG neurons

The role of the TRPV1 receptor in NAE evoked changes in intracellular calcium concentrations were investigated using a TRPV1 receptor selective antagonist (capsazepine, czp).

Prior to examining whether the TRPV1 channel in sensory neurons might mediate the fatty acid ethanolamine ligands effects on intracellular calcium increase, preliminary experiments were conducted in adult rat DRG neurons to confirm the reproducibility of the NAEs effect on intracellular calcium response by exposing the cells to the same NAE concentration repeatedly. As seen in **Figure 5.10,** a reproducible effect on intracellular calcium induced by AEA (C20:4 NAE) was observed where eighty per cent of all cells sensitive to capsaicin responded to AEA at second response and 68 % to first response.

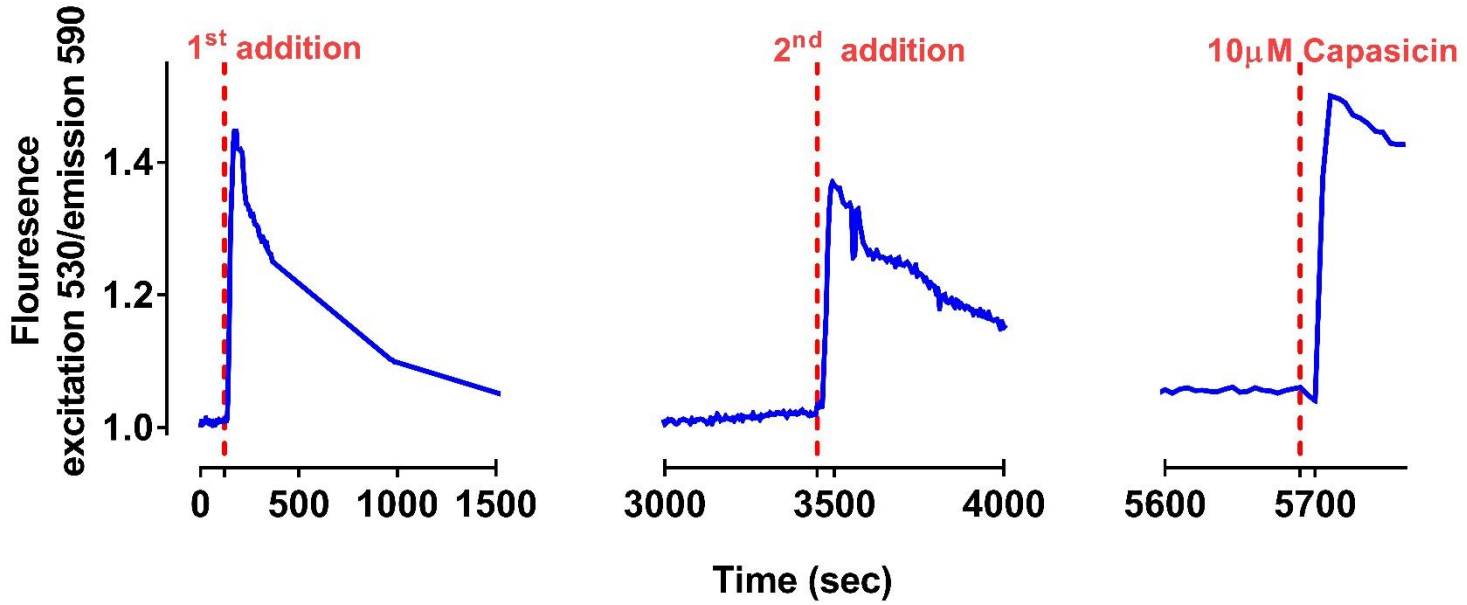


Figure 5.10 Comparison of evoked increases in $[Ca^{2+}]_i$ in adult rat DRG neurons to repeated application of C20:4 NAE. DRG neurons were superfused with C20:4 NAE (10 μM) for 2 min after which the $[Ca^{2+}]_i$ was allowed to return to basal before a second application of C20:4 NAE. Following another washout period the cells were superfused with capsaicin (10 μM) as a positive control. The diameter of DRGs used in this experiments was 28 ± 0.4 μm.

In terms of the functional involvement of TRPV1 receptors, pre-incubation of rat DRGs with 10 μM czp for 20 min evoked complete inhibition of the peak (maximum) calcium response evoked by n-3 and n-6 fatty acid ethanolamine ligands (**Figure 5.11 to 5.15,** paired, two-tailed, *t*-test, $p<0.05$), where czp reduced the peak height of C20:4 NAE from 86 ± 7% to 0.03 ± 0.3%, C22:5, n-6 NAE from 94 ± 5 to 4.3 ± 0.9% , C22:5, n-3 NAE from 90 ± 3 to13±0.8%, C22:6 NAE from 83 ± 6 to 9±1% and 92 ± 7 to 7 ± 1% of C22:4 NAE.

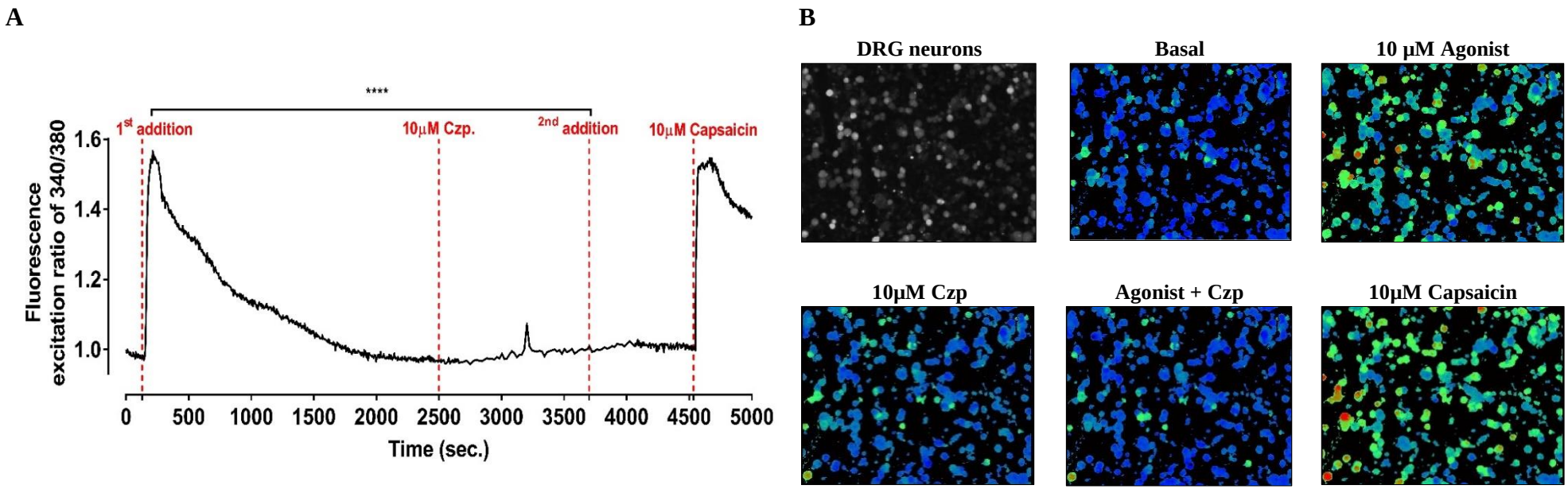


Figure 5.11 Inhibition of C20:4 ethanolamine-induced increases in intracellular calcium mediated via the TRPV1 receptor in DRG neurons. (A) DRG neurons were superfused with C20:4 NAE (10 μM) for 2 min after which the $[Ca^{2+}]_i$ was allowed to return to basal levels before the cells were superfused with czp (10 μM) for 20 minutes. The cells were then immediately superfused with C20:4 NAE (10 μM) for a second time. After a wash out, period the cells were superfused with capsaicin (10 μM) as a positive control. Data are mean ± SEM values from n= 44 neurons of at least 3 rats. Statistical significance was determined by comparing between neurons in absence and presence of czp. using paired, two-tailed, *t*-test, ****$p<0.0001$. (B) TRPV1 mediated intracellular calcium increase with agonist in DRG neurons imaged by a digital camera.

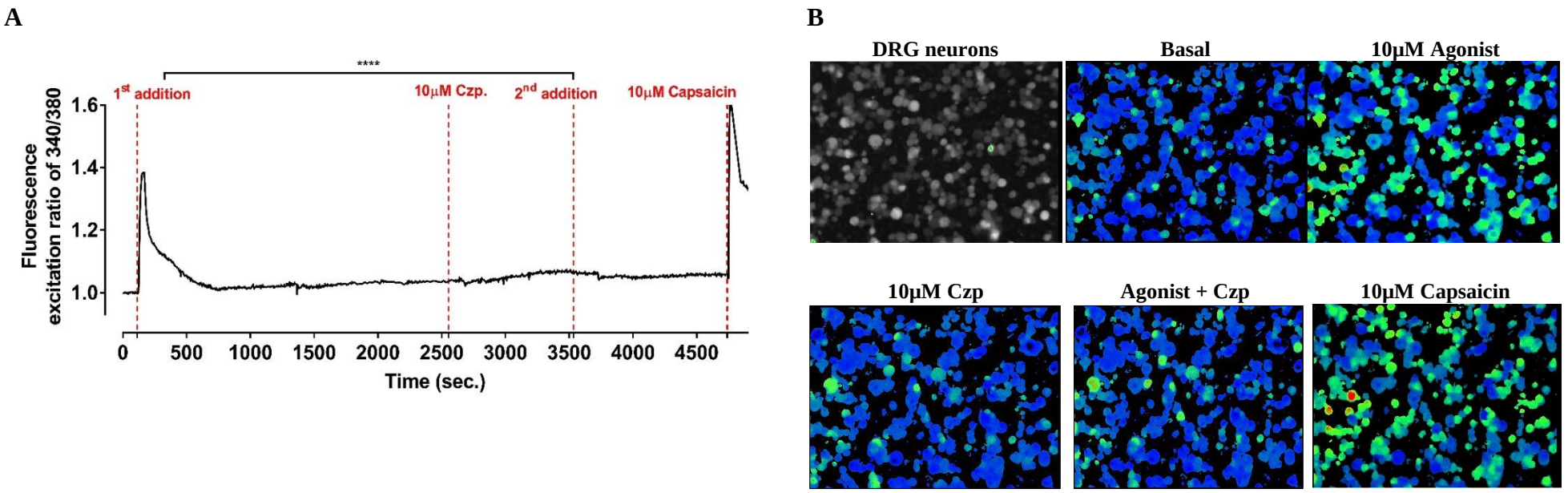


Figure 5.12 Effect of TRPV1 antagonist on C22:5, n-6 ethanolamine-induced $[Ca^{2+}]_i$ in sensory neurons. **(A)** $[Ca^{2+}]_i$ response stimulated by C22:5, n-6 NAE in presence of 10 μM czp. which are incubated for 20 minutes. Data are mean ± SEM values (n=261 neurons,3 rats) analysed using paired, two-tailed, *t*-test, ****p<0.0001 to comparing neurons treated and un treated with TRPV1 antagonist. **(B)** Functional TRPV1 receptor in $[Ca^{2+}]_i$ stimulated by C22:5,n-6 were imaged by using a digital camera.

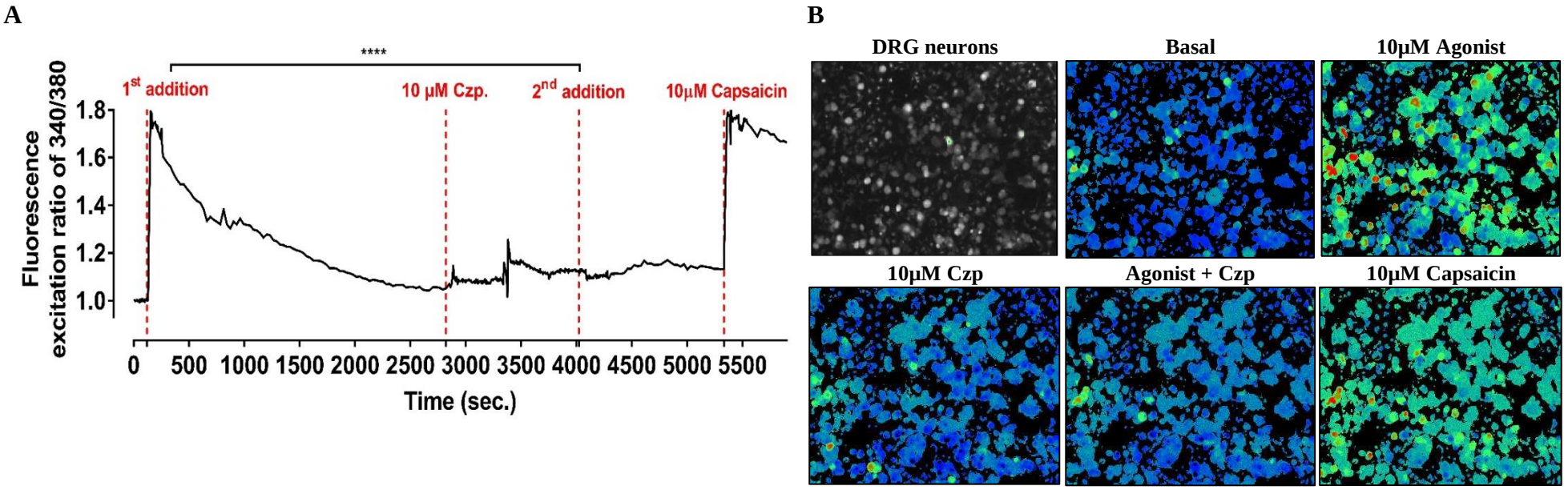


Figure 5.13 (A) TRPV1 receptor mediated intracellular calcium elevations induced by C22:4 ethanolamine. DRG neurons were perfused with agonist for 2 min and czp (10 µM) for 20 min following washing-out cells and then the agonist was re-applied for 2 min. Following another period of wash-out, capsaicin (10 µM) was added as positive control. Data are mean ± SEM values from 3 rats (261 neurons). Statistical significance by comparing the agonist in presence and absence of czp was determined using paired, two-tailed, *t*-test, ****$p<0.0001$ (B) Intracellular calcium response in rat DRGs images in response to agonist in presence of czp.

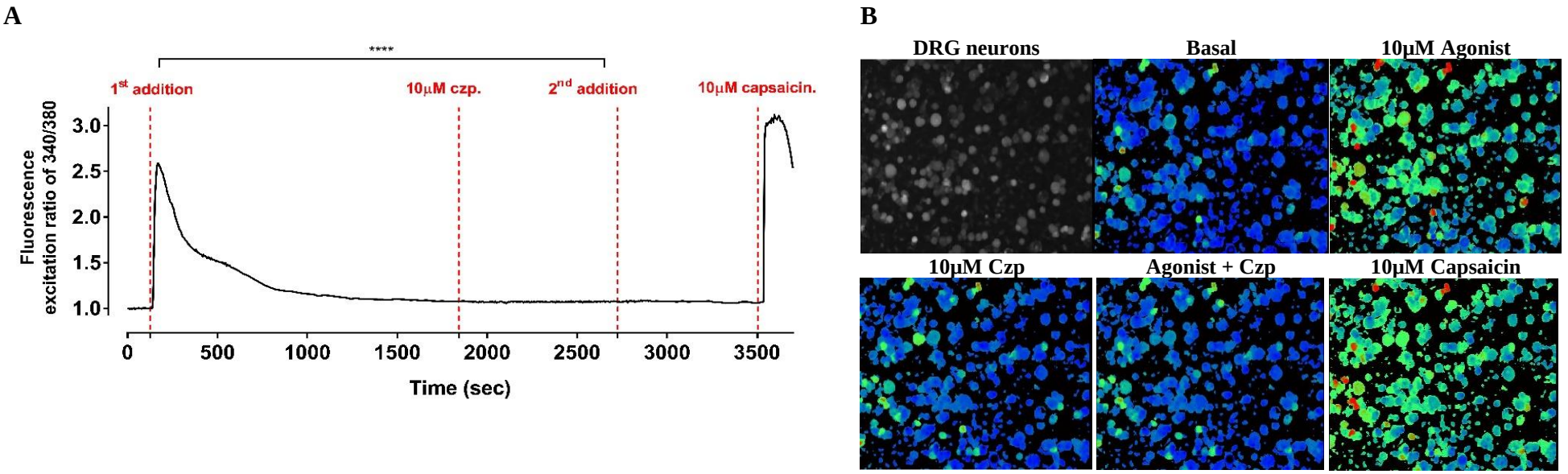


Figure 5.14 The functional activity of TRPV1 on increase in intracellular calcium stimulated by C22:6 ethanolamine ligand. (A) Time course of intracellular calcium in neurons superfused with agonist (10 µM for 2 min) and then pre-incubated with czp (10 µM) for 20 min. after wash-out. Then immediately agonist (10 µM, 2 min) was re-applied and following washout, 10 µM capsaicin was appled. Data are mean ± SEM values from 127 neurons of at least 3 rats. Statistical significance was determined by comparing between neurons in absence and presence of czp. using paired, two-tailed, *t*-test, ****$p<0.0001$. (B) TRPV1 mediated intracellular calcium increases with agonist in DRG neurons.

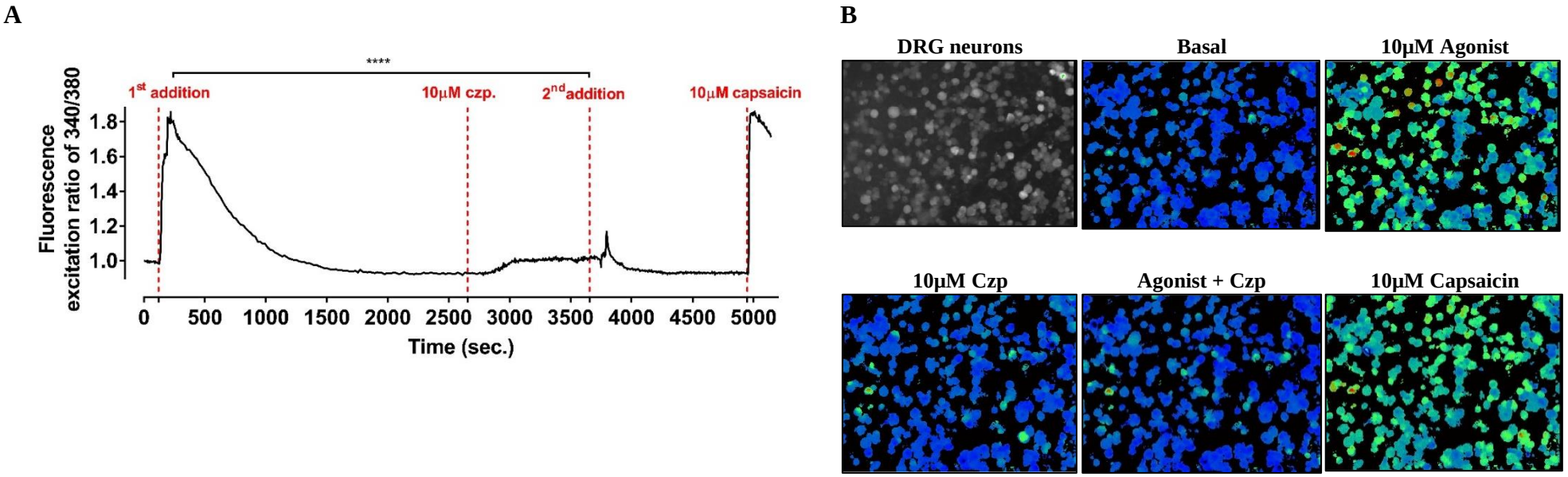


Figure 5.15 (A) TRPV1 receptor effects of C22:5, n-3 ethanolamine stimulated intracellular calcium increase in DRG neurons. Perfusion of neurons with agonist for 2 min was followed by czp (10 µM) for 20 min following washout and then add the agonist was re-applied for 2 min. Following another period of wash-out, capsaicin (10 µM) was added as positive control. Data are mean ± SEM values from 3 rats (300 neurons). Statistical significance by comparing the agonist in presence and absence of czp. was determined using paired, two-tailed, *t*-test, ****$p<0.0001$ **(B)** Intracellular calcium response in rat DRGs images in response to agonist in presence of czp. and capsaicin.

5.4 Discussion

In this chapter, we investigated the ability of a panel of fatty acids ethanolamine ligands to change intracellular calcium concentrations in adult rat neurons. The changes in intracellular calcium concentrations were measured with the calcium binding fluorophore fura-2 using for ratiometric imaging. The initial experiments in **figure 5.1** showed that capsaicin was able to elicit $[Ca^{+2}]_i$ increases in small DRG neurons. This result is in keeping with previous reports of capsaicin increasing DRG neurons $[Ca^{2+}]_i$ via the TRPV1 receptor (Caterina *et al.*, 1997, Docherty *et al.*, 1997).

A number of previous studies showed that AEA acted as an agonist on TRPV1 receptor, for example, in advanced cirrhosis (Domenicali *et al.*, 2005) or in relaxation of rat mesenteric arteries (Poblete *et al.*, 2005). In the present study, ethanolamines of n-3 and n-6 PUFA caused TRPV1 mediated intracellular calcium response in DRG neurons as shown in **Figure 5.2 to 5.6**. Amongst these lipids, docosahexaenoyl (C22:6), 7-docosapentaenoyl C22:5,n-3), 4-docosapentaenoyl (C22:5,n-6) and *N*-eicosapentaenoyl ethanolamides have not been previously been shown to interact with TRPV1 receptors. At least one report exists examining C22:4 ethanolamaine on native TRPV1 where it caused czp-sensitive relaxation in rat mesenteric arteries and evoked $[Ca^{2+}]_i$ increases in a concentration dependent-manner in HEK293-hTRPV 1(Movahed *et al.*, 2005).

Linoleoylethanolamine (C18:2, n-6) and α-linolenoylethanolamine (C18:3, n-3) are abundant in sensory neurons and blood vessels (Movahed *et al.*, 2005). All unsaturated C18 ethanolamine (C18:3, C18:2 and C18:1) produced consistent activation of TRPV1

as potent as AEA (C20:4 NAE) in blood vessels but evoked smaller TRPV1 mediated currents at nearly 55 % (C18:3, n-3) and 22 % (C18:2, n-6) of capsaicin responses in DRG neurons in the present study (as shown in **Figure 5.7 A)**. This variability in the responses may possibly be attributed to differences in levels of TRPV1 receptor expression. In vitro, nerve growth factor and glial-derived neurotrophic factor have been shown to increase levels of TRPV1 receptor mRNA and enhanced sensitivity of DRG neuron to capsaicin (Winter *et al.*, 1988, Winston *et al.*, 2001). Therefore, any changes in the expression levels might alter in the efficacy of ligands. Unlike C18:3 and C18:2, the observation that cells sensitive to capsaicin may display variation in monounsaturated C18:1 responses has been reported (Wang *et al.*, 2005, Ahern, 2003). OEA has been suggested to activate TRPV1 receptors in a protein kinase C dependent manner (Ahern, 2003). The fact that there were variations in cells sensitivity to TRPV1 activation may reflect the bioassays utilized and lead to differences in potency between different preparations in study of Movahed and co-workers.

In contrast to the polyunsaturated analogues, monosaturated (C24:1 and C22:1) and all saturated (C16:0, C18:0 and C20:0) ethanolamines failed to activate TRPV1 receptors in cultured DRG neurons. This was consistent with that previous reports with C18:0 ethanolamine (Smart *et al.*, 2002, Movahed *et al.*, 2005, Maccarrone *et al.*, 2002), failing to cause relaxation-induced calcium response through TRPV1 receptor in mesenteric arteries in any bioassay used nor displace the selective agonist TRPV1 [^{3}H]resiniferatoxin in mouse CNS. Although the saturated C16:0 NAE appeared to act with an entourage effect to potentiate the anandamide-induced relaxation response through TRPV1 receptor in rat mesenteric arteries (Ho *et al.*, 2008), it did not directly

activate TRPV1 receptors in HEK239 cells and mesenteric arteries (Zygmunt *et al.*, 1999).

Taken together, these finding strongly indicate the structure of the fatty acid ethanolamine plays a central role in activation of TRPV1 receptors. The structural features in NAEs have previously been demonstrated in activation of theTRPV1 receptor where the analysis of conformational structure showed that long chain unsaturated NAEs such as C20:4, C18:3 and C18:2 NAEs generated low energy conformations with the ends of their structures near to each other adopting U-shaped entities as seen in **Figure 5.16**. This conformational effect may allow the molecules to bind equally well to TRPV1 receptor (Movahed *et al.*, 2005). Therefore, the lack of these features in saturated NAEs might contribute to the weak effect of these lipids on TRPV1 receptors.

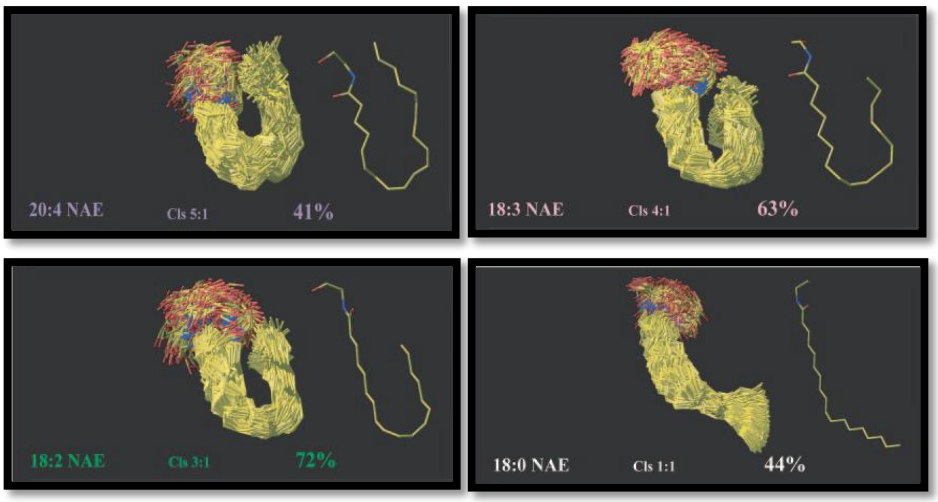


Figure 5.16 Conformational analysis of several N-acylethanolamines using MacroModel in Movahed and co-workers study (Movahed *et al.*, 2005). Monte Carlo conformational searches of lower energy NAEs structure in water, C20:4 NAE represent 41% of the conformers U-shape and 72%, 63% and 44% for C18:2, C18:3 and C18:0 NAEs respectively. All percentages were generated within 3 kcal/mol of global energy minimum of each compound (Movahed *et al.*, 2005).

Activation of the TRPV1 receptors leads to increased intracellular calcium and induces inflammatory pain; however, the receptor is readily desensitised which is likely to contribute to analgesia (Jancsó *et al.*, 1967). It has been reported that desensitisation of the TRPV1 channel is highly dependent on the agonist employed (Xu *et al.*, 2005) and calcium availability (Koplas *et al.*, 1997). In keeping with this hypothesis, our results showed that all the fatty acid ethanolamines tested showed a tendency to desensitise over the 2 min exposure and beyond similar to the vanilloid agonist capsaicin.

These findings highlight the long chain n-3 and n-6 fatty acid ethanolamines as potential analgesic agents acting through this receptor. NAEs derived from long chain n-3 PUFAs have been reported to exert antinociceptive effects in spinal cord injury (Figueroa *et al.*, 2013), however the molecular target for their action still remains

unclear. Future studies should investigate the potential role for desensitisation of TRPV1 receptors in mediating these antinociceptive effects.

5.5 Conclusion

In the present study, long chain n-3 and n-6 ethanolamines having 22 carbon have been identified as novel TRPV1 channel activators. Furthermore, it was confirmed that the degree of saturation and acyl chain length of fatty acids are important in recognition and activation of the TRPV1 channel.

Chapter 6
Expression of human recombinant peroxisome proliferator-activated receptors (PPARs)

6.1 Introduction

Three peroxisome proliferator-activated receptors (PPARs) have been identified in the human genome: α, β and γ, with specific tissue distributions. There is evidence accumulating since 2002 that *N*-acylethanolamines such as oleoylethanolamide, palmitoylethanolamide, arachidonoylethanolamine, docosahexaenoylethanolamide and eicosapentaenoylethanolamide, bind and activate PPARs (Rovito *et al.*, 2013, Sun *et al.*, 2007, Bouaboula *et al.*, 2005). This relationship has been examined via various assays, including binding studies and reporter gene assays, with blockade by selective antagonists. Aside from these ligands, the complete range of fatty acids ethanolamines previously investigated at CB_1 and CB_2 receptors or TRPV1 channels in **Chapter 4 and 5** have not been studied in terms of activating PPARs.

Protein expression and purification are central techniques in biochemistry. Recombinant protein expression in the Gram-negative bacterium *Escherichia coli* (*E.coli)* as host organism is well-used compared to other systems because of rapid growth characteristics, high density cultures inexpensive components and rapid plasmid transformation (Baneyx, 1999). Speed of protein production, its purity and large yields are also important factors to be considered.

Furthermore, codon bias can be an issue in recombinant protein expression where it can contribute to low or no expression of the protein of interest. Another case encountered in bacterial expression systems is target protein misfolding and aggregation, known as inclusion bodies that lead to inactive protein aggregation (Villaverde and Carrio, 2003).

Nevertheless, effort has been devoted to improve and overcome various challenges faced in the solubility and increase accumulation of protein expressed in *E.coli*.

Many commercial *E.coli* expression vectors are available but the effective and strong promoter system present in pET vector contributes to its widespread use for heterologous protein expression. In this system, the *lac* promoter contributes to protein expression where the gene of interest is inserted downstream of a bacteriophage T7 promoter recognised by T7 RNA polymerase. For protein expression, the pET plasmids are transformed into bacteriophage λ of DE3 derived encoding T7 RNAP under the control of a *lacUV5* promoter. Induction of this system by a lactose analogue, usually isopropyl β-D thiogalactoside (IPTG), helps in dissociation of the repressor lactose (*lacI*) from the operator which allows binding with T7 polymerase therefore permitting the production of protein (Dubendorff and Studier, 1991).

Although purification of recombinant protein can be a complex process, the pET vector includes a hexahistidine $(His)_6$ tag which facilitates the purification process. The small size of the hexapeptide, which can be eliminated after purification to prevent its interfering with target protein activity, is anticipated not to interfere with protein function (Porath and Olin, 1983).

6.2 Aim

The overall aim in this chapter was to study the affinity of ligand binding of fatty acid ethanolamine ligands to PPAR α, β and γ receptors. To achieve this goal, specific objectives were to:

1. Amplify ligand binding domains of hPPAR α, β and γ by primers designed with restriction sites.
2. Clone these fragments into pET28a (+) vector.
3. Transform the protein targets into *E. coli*.
4. Purify targets using the $(His)_6$ tag using Nickel ion affinity chromatography.

6.3 Results

6.3.1 Construction of pET28a(+)-human PPAR-LBD

The strategies for cloning the ligand binding –activation function-2 domain (LBD-AF-2) of human PPARs, α, β and γ into pET28a (+) expression vector are shown in **Figure 6.1**. The cDNA of hPPAR encoding LBD-AF-2 domain (603-1401 bp for PPARα), (519-1320bp for hPPARβ) and (627-1428bp for hPPARγ) were amplified using plasmids as template (**Figure 6.2)**. All primers were designed with two restriction sites to facilitate directional cloning (see **Table 2.1** in methods and materials section). The three LBD-AF-2 domain fragments, 987 bp, 1215 bp and 981 bp of hPPAR α, β and γ respectively were recovered from 1 % agarose gel using the Qiagen MinElute Gel Extraction Kit. These fragments were digested with restriction enzymes (NdeI and SalI) and ligated into pET28a(+) vector with the same enzymes to generate plasmids pET28a(+)-hPPARα-LBD-AF-2, pET28a(+)-hPPARβ-LBD-AF-2 and pET28a (+)-hPPARγ-LBD-AF-2 (**Figure 6.3**). The identity of the insert was confirmed by automated sequence analysis.

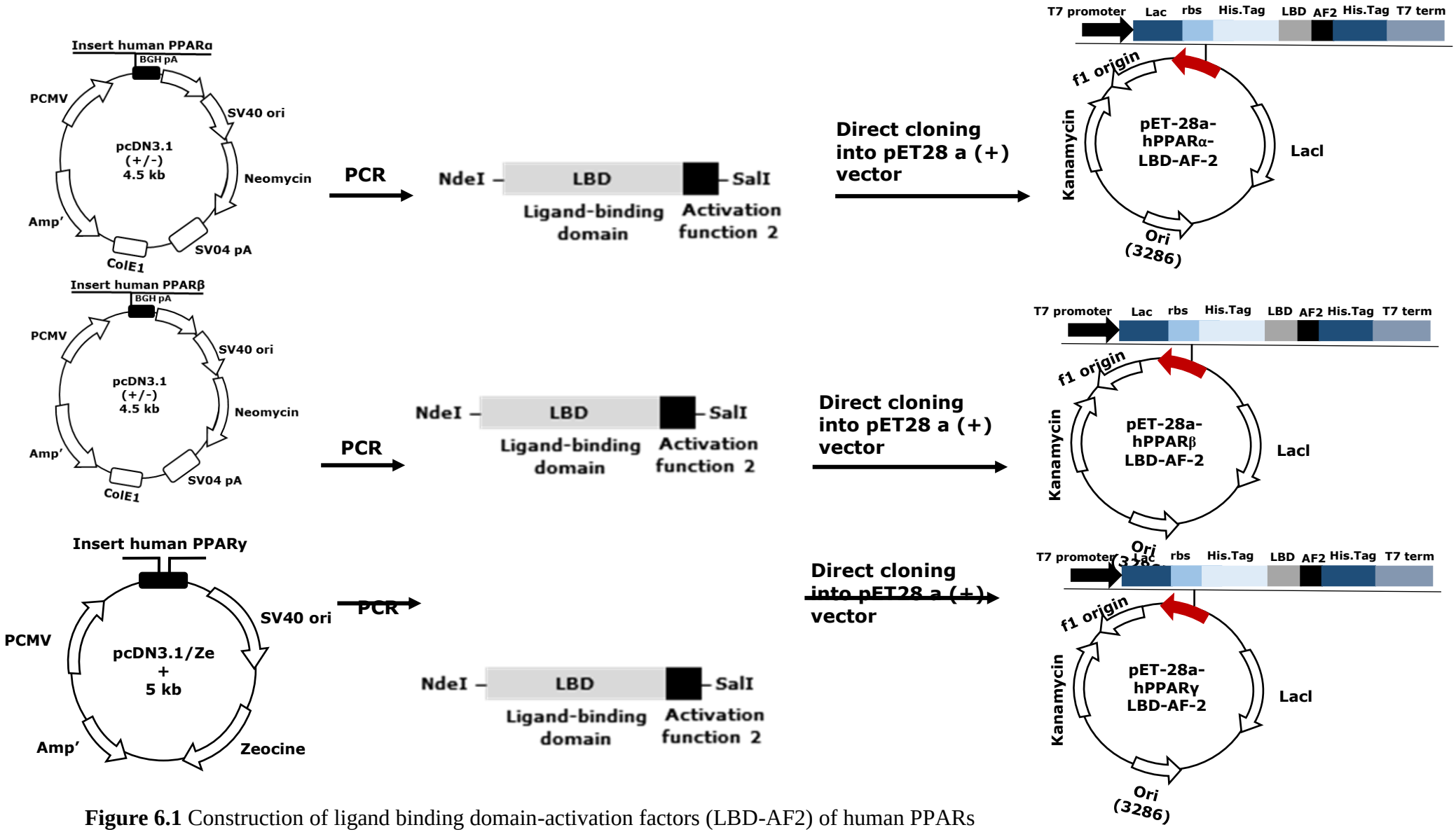


Figure 6.1 Construction of ligand binding domain-activation factors (LBD-AF2) of human PPARs into pE28a (+) vector**. Human PPARs LBD-AF-2 was amplified using plasmid as template and directly cloned into pET28 a (+) vector to generate plasmid pET28 a-hPPAR-LBD-AF-2.**

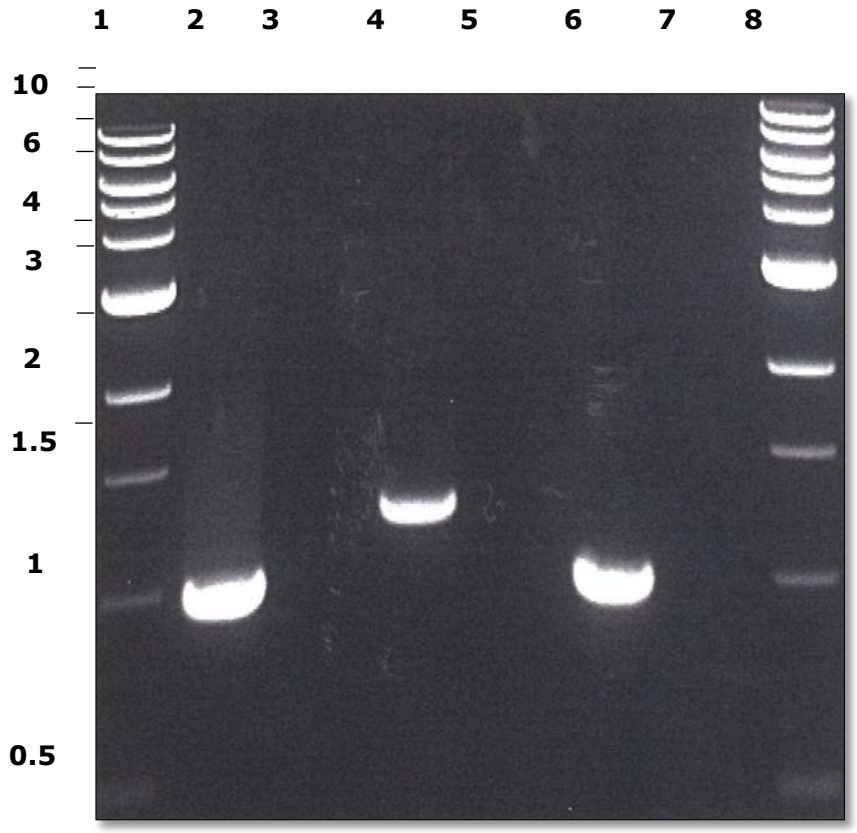


Figure 6.2 Amplification of LBD-AF2 domain of human PPAR α, β, and γ. PCR was conducted with different annealing temperatures for each gene. PCR condition: initial denaturation at 98 °C for 30 s; 30 cycles: 10 s at 98 **B**, 30 s annealing at 55 °C, 54 °C, 61 °C for PPAR α, β and γ, respectively.1 min primer extension at 72 °C; 72 °C final extension for 5 min.

Lane 1, 1 kb DNA ladder **Lane 2**, PPARα LBD-AF-2 domain

Lane 3, negative control for PPARα LBD-AF-2 **Lane 4**, PPARβ LBD-AF-2 domain

Lane 5, negative control for PPARβ LBD-AF-2 **Lane 6**, PPARγ LBD-AF-2 domain

Lane 7, negative control for PPARγ LBD-AF-2 **Lane 8**, 1 kb DNA ladder.

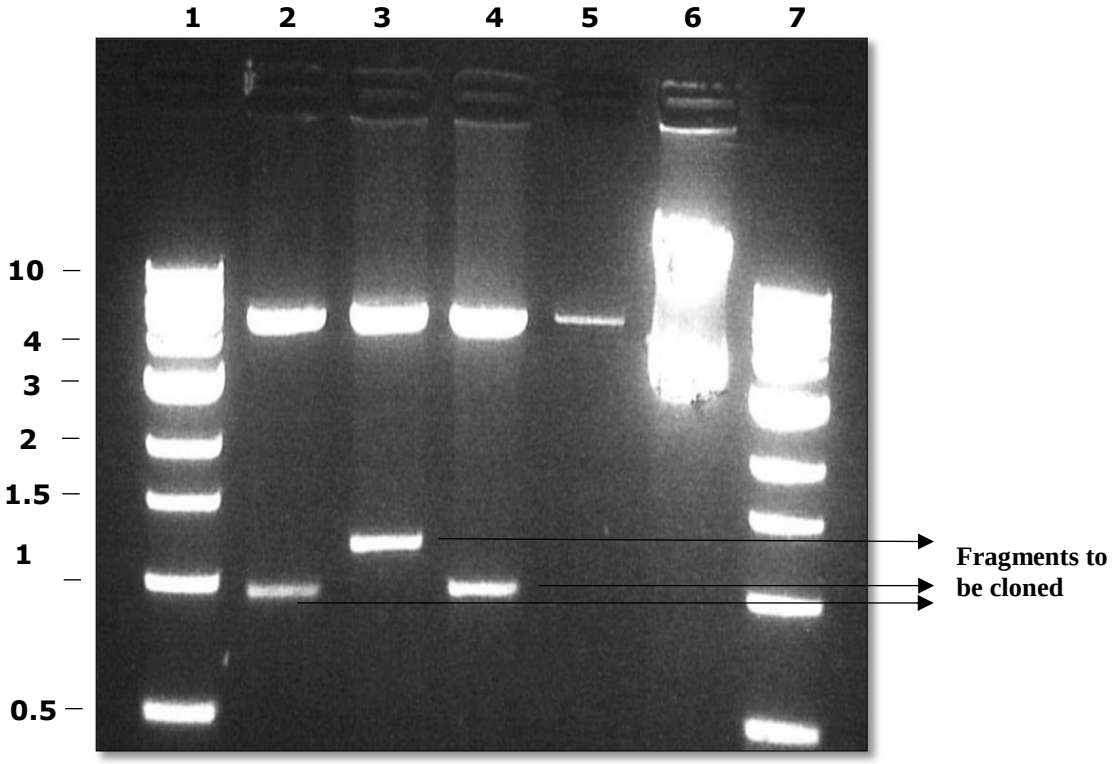


Figure 6.3 Cloning the LBD-AF-2 domain of human PPARα, β and γ into pET28 a (+) vector. The three LBD-AF-2 domains of human PPARs were cut from plasmid using restrictions enzymes. The three fragments (lane 2, 3, 4) were ligated to pET28 a (+) (lane 5) to generate pET28 a (+) -hPPARα-LBD-AF-2, pET28 a (+)-hPPARβ-LBD-AF-2 and pET28 a (+)-hPPARγ-LBD-AF-2.

Lane 1, 1 kb DNA ladder;

Lane 2, pcDNA3.1-LBD-AF-2 digested with Nde I and Sal I

Lane 3, pcDNA3.1-LBD-AF-2 digested with Nde I and Sal I

Lane 4, pcDNA3.1-LBD-AF-2 digested with Nde I and Sal I

Lane 5, pET 28 a (+) digested with Nde I and Sal I

Lane 6, pET 28 a (+) vector. **Lane 7**, 1 kb DNA ladder.

6.3.2 Protein expression and solubility test

The expression plasmids (His-tag-hPPAR LBD-AF-2 of α, β and γ) extracted by miniprep were transformed into cloning host: BL21 (D3) *E. coli* cell strain. The following day, a single colony was picked up in medium and incubated for 16 h at 25 ^{o}C. For induction, protein expression was induced with 1 mM IPTG when the optical density of bacteria reached 0.4 AU in LB medium. The samples (supernatant and pellet fractions) were loaded in polyacrylamide gels and stained with Coomassie blue dye.

The expression of target proteins are displayed in **Figure 6.4**. As shown in lane 6 of **Fig. 6.4A** high expression level of an induced protein of LBD-AF-2 PPARγ with about 0.981 kDa was achieved in *E. coli* soluble 21 (D3). Although the high expression of PPARγ LBD-AF-2 protein was observed, it was not soluble (**Figure 6.4 B**). While there was no obvious IPTG-induction of PPARα and β expression as seen in lane 2 and 4 in **Fig.6.4A**. Induction over 2, 4, 6 or 24 h also failed to show any proteins produced over time (data not shown).

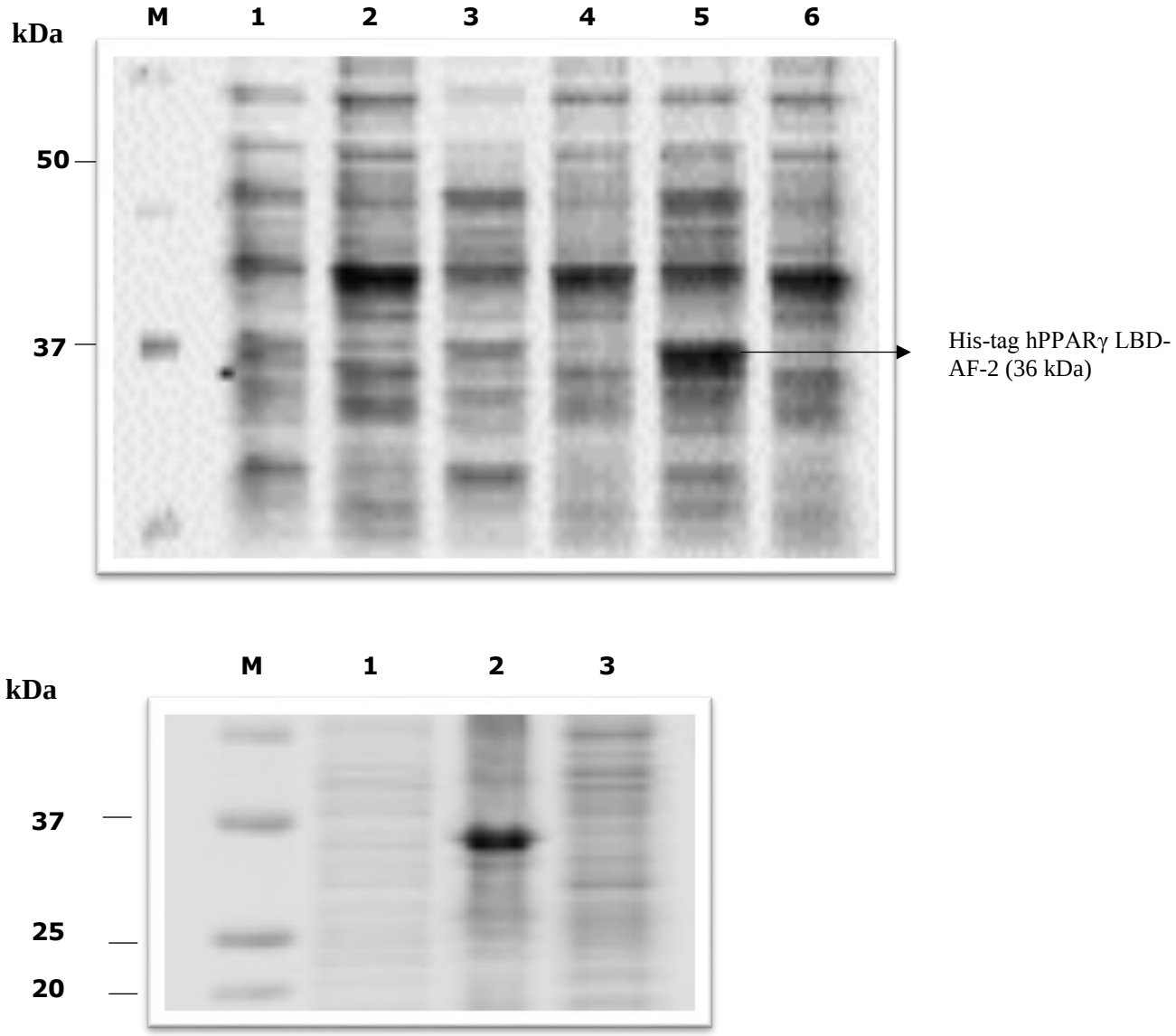


Figure 6.4 His-tagged human PPARγ LBD-AF-2 expression but not α and β, in cell lysates of E.coli stable 21 (D3). **(A) Lane 1, 3, 5,** Transformed soluble 21 cells of PPARα, β, γ induced with IPTG for 16 h at 25 °C. **Lane 2,4,6,** Transformed soluble 21 cells of PPARα,β,γ without induction; **(B)** Expressed His-tagged hPPARγ LBD-AF-2 formed inclusion bodies. **Lane 1**, Transformed soluble 21 cells without induction; **Lane 2,** pellet of cell lysate **Lane 3**, supernatant of cell lysate. 10% SDS polyacrylamide gel was run and then was stained with Coomassie blue for 1 h at room temperature and destained.

Since there are several factors such as rare codons, culture temperature and type of bacterial strains which may influence the expression and solubility of protein, the DNA sequences of hPPARα and β LBD-AF-2 domains were examined for rare codons. The sequences analysis revealed that PPARα and β had a higher frequency of rare codons (**Figure 6.5**).

Three constructs of his-tagged hPPAR α, β and γ LBD-AF-2 were transformed into different strains. BL21-CodonPlus(DE3)-RIL was chosen because it contains extra copies of genes encoding tRNA which recognise mammalian arginine, isoleucine and leucine codons. In addition, it was suggested to grow the bacteria in Terrific Broth (TB) medium for high level protein production in *E. coli* where bacteria grow in the log phase longer than when cultured in LB medium. The bacteria were cultured in TB medium and induced with 0.1 mM IPTG at OD_{600} ~1 overnight at 18 °C.

High level expression of his-tagged hPPARα and γ LBD-AF-2 was achieved (**Figure 6.6**) however, inclusion bodies were formed and soluble proteins were not produced by this system. There was no expression observed of his-tagged hPPARβ under any of these conditions.

A

rsckiqkknr nkcqycrfhk clsvgmshna irfgrmprse kaklkaeilt cehdiedset adlkslakri yeaylknfnm nkvkarvils gkasnnppfs ymiwrhcvwl rrrwwpswwp masrtrrrrs asftaasarq wrpsrssrns prpsqasqtw t*tik*hc*n tefmrpyspc cll**tktgc w*rmemgl*l vns*ka*gnr sviswnpsli lp*ssmhwnw mtvispflwl lsfaveivla f*t*dtlkkc rrvlymcsds tcrattrtis fssqnffkkw qtsgsw*rsm rswcrssrrr srmlrctryc rrstgtcte

B

flpaatqtsp gaprhphcwt ncrwavtgph aaastwsagc agtrhrastt vfmhvrgara ssvvrsa*sw strsvsaaar frrrtatsas taasrsawhw achttlsvlv gcrrlrrgsw wqg*lqtrga stthrwpt*r pspststmpt *ktst*pkrr paasspakpa trrpl*stts rhcgrqrrgw cgssw*macl ptrrsactss taasapqwrp cgsslsspra spasaassst trlpfssmac trpsspcwpl sstrtgcw*p tavalspvss caasanpsvi slslslnlls sstpwnlmtv twpyslrpsf cvetgqas*t fhgwrlsrtp scvpsnstcr pttlmpstss pscerrwltc gnwspstpr* csgsrrpkpr prctlcsrrs trtct

Figure 6.5 The sites of rare codons in the protein expression sequences of hPPAR (A) α and (B) β that are represented in red asterisks. The rare codon was detected by molbiol.ru/eng/scripts/01_11.html.

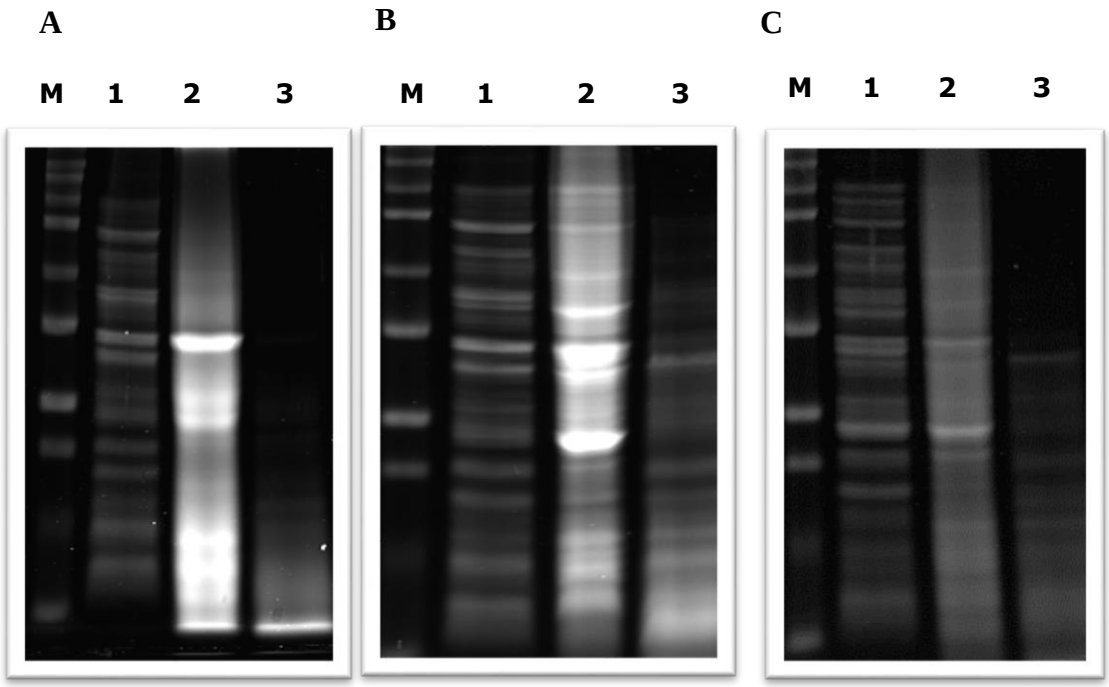


Figure 6.6 Expression of His-tagged hPPAR LBD-AF-2 formed in inclusion bodies (A) α, (B) β, (C) γ. Cells were induced with 0.1 mM IPTG in TB medium overnight at 18 °C until OD600~ 1. All samples were loaded on 10% SDS polyacrylamide gels and then stained with Coomassie blue as described in the methods section.

Lane 1, transformed BL21-codonPlus cells without induction

Lane 2, pellet of cell lysate induced with IPTG

Lane 3, supernatant of cell lysate induced with IPTG

6.4 Discussion

To study ligand binding, receptor protein is needed available in mg quantities. It is not possible to obtain large amounts of protein directly from tissues due to their trace expression. In this study, the ligand binding domain of hPPAR α (comprising amino acids 201-467), β (173-440) and γ (209-476) were PCR amplified from plasmid. After purification, these fragments were digested with NdeI and SalI and cloned into pET28a vector. Previous reports indicated that hPPARα could be expressed as a soluble and active entity in *E. coli* using pET28a (Muller *et al.*, 2008). His-tagged-LBD-AF-2 of hPPAR γ was highly expressed in *E. coli* but α and β did not express. This may result from the frequency of rare codons found in the LBD-AF-2 domain of hPPARα and β, which hamper expression and also solubility of recombinant protein. Therefore, codonPlus®RIL of modified *E. coli* strain was employed for transformation in order to increase protein expression. Furthermore, the bacteria cells were cultured in phosphate buffered medium (TB) instead of LB medium which is better for pH stability and increasing cell densities and therefore enhance protein expression.

Under all these conditions, there was high expression of hPPARα and γ, but the product lacked solubility, although it was induced at low temperature intended to reduce growth rate. Over-expression of recombinant protein might be one of the reasons that lead to protein misfolding and aggregation known as inclusion bodies, that might lead to inactive protein generation inactivation

However, there are strategies to recover active protein from inclusion bodies, which include isolating the protein and solubilisation under strong denaturing conditions and then refolding the solubilised protein. The last step may be less efficient due to the

production of inactive protein as well as aggregation, Moreover, stabilizing agents for proteins can be used to prevent protein aggregation, such as non-detergent sulfobetaines (Vuillard *et al.*, 1995, Vuillard *et al.*, 1998). Nevertheless, the final protein concentration was too low to use in a ligand binding assay.

Fusion protein partners such as glutathione-S-transferase (GST) and maltose binding protein (MBP) possess district chaperone activity which can enhance protein solubility (Kapust and Waugh, 1999). However, GST has been reported to bind fatty acids and their derivatives which might interfere with ligand binding and structure (Perron-Savard *et al.*, 2005). MBP is a large size and can lead to erroneous assessment of solubility (Costa *et al.*, 2013). The final solubility of products after the removal of these tags is unpredictable (Esposito and Chatterjee, 2006). Therefore, a small peptide tag and solubility enhancing are required in recombinant protein expression.

Recently, the calcium binding protein Fh8 has been observed to be an effective fusion partner in solubility enhancement and it has a low molecular weight compared to other tags (Costa *et al.*, 2013) and this could overcome the limitations of recombinant expression in *E.coli* in future investigations. The summary from this chapter is that LBD-AF-2 domain hPPAR α, β and γ were not successfully expressed in soluble form for subsequent use in ligand binding assays.

Chapter 7
Evaluation of fatty acid ethanolamine ligands in an immune system model *in vitro*

7.1 Introduction

The biosynthesis, uptake and degradation of endocannabinoids in macrophage and leukocytes has been reported (Schwarz *et al.*, 1994, Maccarrone *et al.*, 2001). Endocannabinoids modulate apoptosis and proliferation of lymphocytes and immune cell activation by pro-inflammatory cytokines and chemokines (Meijerink *et al.*, 2011, Berdyshev *et al.*, 1997). Other NAEs including OEA, PEA and SEA have also been reported to have anti-inflammatory properties (Dalle Carbonare *et al.*, 2008, Gabrielsson *et al.*, 2017) .

Recently, n-3 fatty acid ethanolamines have been suggested to have potential beneficial effects through anti-inflammatory properties, reduced risk of type 2 diabetes and apoptosis in cancer cells (Brown *et al.*, 2010, Brown *et al.*, 2011, Kim *et al.*, 2014). Evidence for synthesis of fatty acid ethanolamines from their equivalent PUFA precursors was provided in a study of Balvers *et al.* (2010) who showed that 3T3-L1 adipocytes were able to convert eicosapentaenoic acid (EPA) and docosahexaenoic acid (DHA) to DHEA and EPEA where they possess anti-inflammatory properties (Balvers *et al.*, 2010). Moreover, Figueroa and co-workers (2013) noted a minor NAE (docosapentanoylethanolamine) was produced from diet enriched with n-3 PUFAs in spinal cord injury with anti-inflammatory properties. However, the role of these entities in modulating immune cells was not investigated.

The n-3 and n-6 NAEs can activate CB_2 receptors as seen in **Chapter 4** and the CB_2 receptor is highly expressed in immune cells. It was logical, therefore, to investigate the role of these compounds in relation to their immune modulating effects.

7.2 Aim

The aim of this chapter was investigate the effect of NAEs in modulating an immune response. **First**, the effect of NAEs on LPS-stimulated human inducible nitric oxide synthase (iNOS) activity transfected into RAW24.7 macrophage cells was assessed.

Second, the effect of selected NAEs on nitric oxide (NO) production and gene expression of pro-inflammatory (IL-1β and TNF-α) and anti-inflammatory (IL-10) cytokines in human monocytes isolated from PBMCs and macrophages was assessed.

7.3 Results

7.3.1 Fatty acid ethanolamine ligands effects on inflammatory markers

7.3.1.1 Human iNOS activity in mouse macrophage cells

The RAW246.7 cell line was chosen due to its wide use as a macrophage model to study inflammatory responses (Dickins *et al.*, 2005). The effect of fatty acid ethanolamine ligands on LPS-stimulated hiNOS activity in RAW246.7 cells was investigated using a reporter gene assay system. This was based on hiNOS promoter driven luciferase gene transfected into RAW246.7 cells. When cells were treated with LPS, expression of the iNOS promoter was increased which was reflected in the production of luciferase activity detected by luminometry.

LPS activated hiNOS was optimised to determine the optimal concentration. RAW 264.7 cells were treated with various concentrations of LPS for 6 h The data revealed that LPS significantly increased hiNOS activity in a concentration-dependent manner (**Figure 7.1,** one-way ANOVA, followed by post-hoc Dunnett's test; *p<0.05).

On the basis of this result, 100 ng/ml LPS was chosen as an optimised condition for further experimentation. However, NAEs failed to alter hiNOS production stimulated at this concentration of LPS. Therefore, cells were treated with various concentrations of LPS following incubation with 10µM C16:0 NAE, C20:4 NAE and C22:6 NAE for 1 h. C20:4 NAE and C22:6 NAE significantly inhibited hiNOS production at 10 ng/ml LPS as seen in **Figure 7.2 and 7.4** (paired, two-tailed, t-test *p<0.05) unlike C16:0 NAE which had no effect on any concentration of LPS in RAW246.7 cells (**Figure 7.3)**.

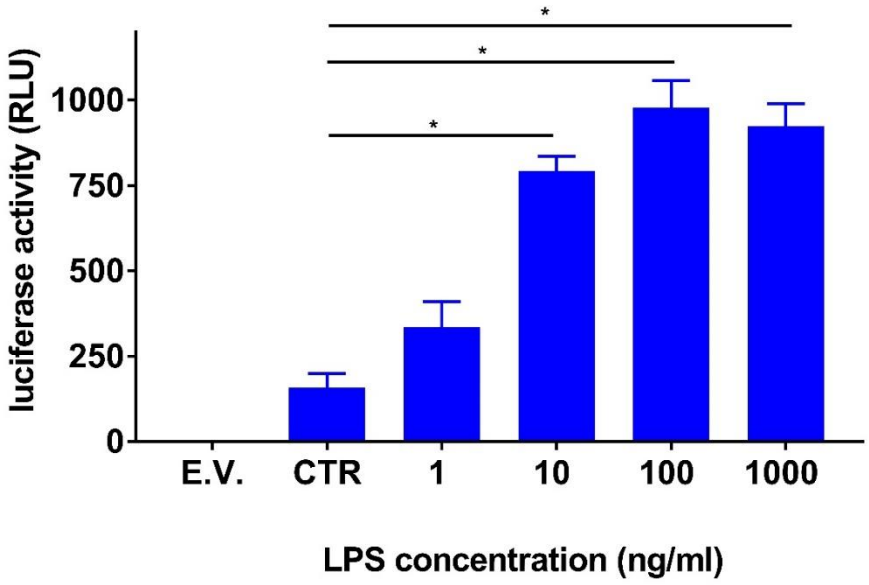


Figure 7.1 LPS effects on hiNOS production in RAW46.7 cells. Cells were transiently transfected with 1 µg of hiNOS promoter luciferase reporter plasmid or pcDNA3.1 empty vector (E.V.) for 24 h and then treated. Luciferase activity was determined 6 h after treatment with different concentrations of LPS. The figure shows mean ± SEM of triplicate determinations from three independent experiments. Untransformed data were analysed using one-way ANOVA, followed by post-hoc Dunnett's test; **p*<0.05, comparing LPS concentrations with the control (w/o LPS).

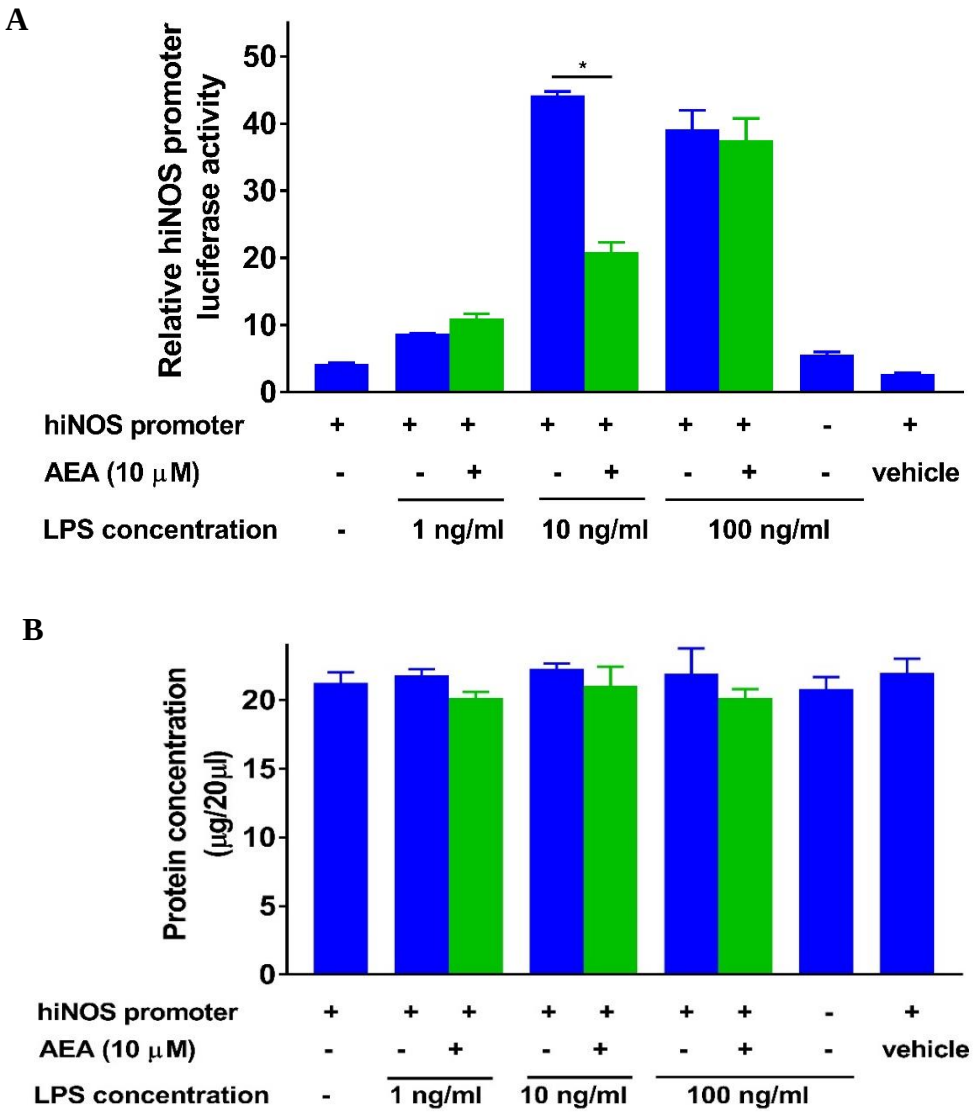


Figure 7.2 The effect of C20:4 NAE on LPS-induced production in RAW246.7 cells. Cells were seeded in 12 well plates and transiently transfected at 60% confluency with hiNOS promoter (1μg) or pcDNA3.1 empty vector (E.V.) for 24 h and then pre-treated with 10μM AEA for 1 h followed by stimulation with various concentration of LPS for 6 h. Ethanol (as vehicle) never exceeded 0.1%. (A) Luciferase activity normalised to protein concentration expressed as mean ± SEM values from 3 independent experiments. Statistical significant was determined by comparing the effect of tested ligand in presence and absence of LPS, paired, two-tailed, t-test *p<0.05 (B) Cell viability expressed as protein concentration of 20 μl cell lysate.

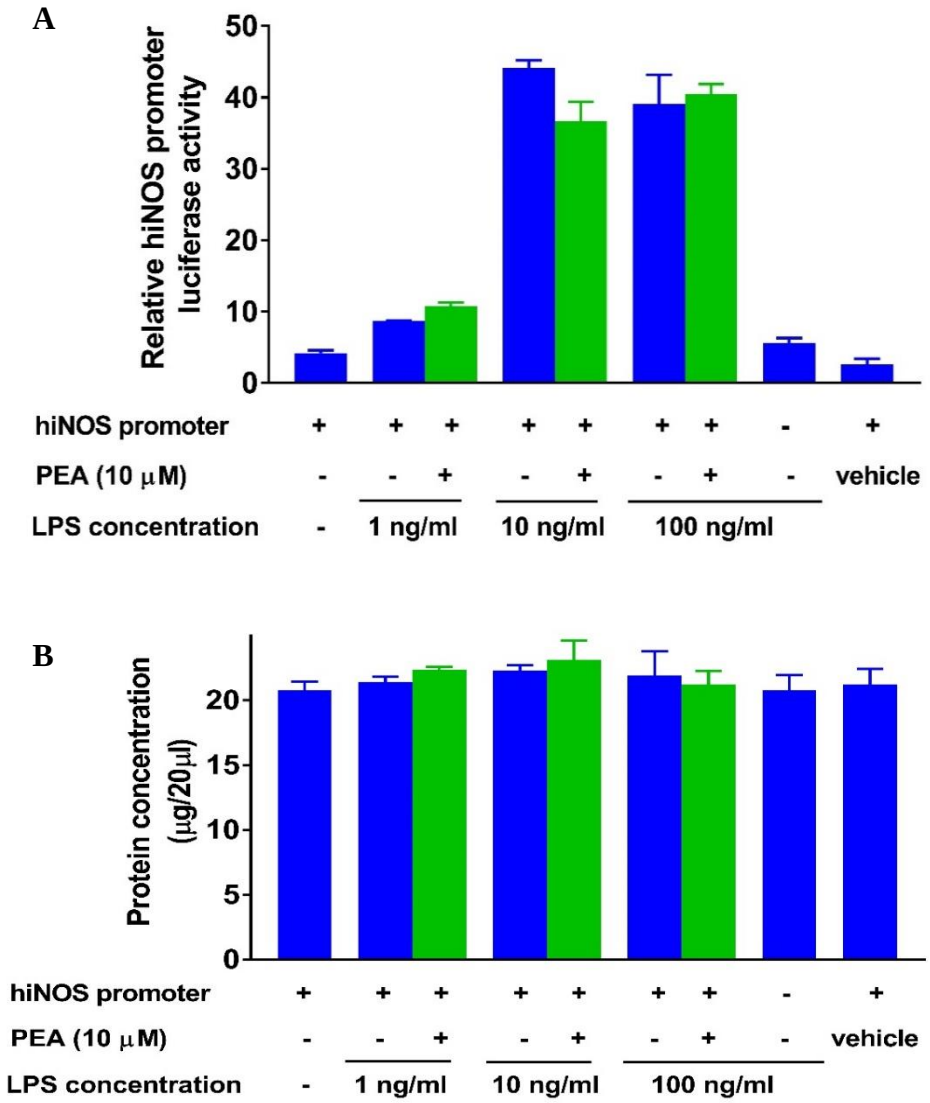


Figure 7.3 Palmitoylethanolamin (C16:0 NAE) effects on hiNOS activity stimulated by LPS in RAW246.7 cells. At 60% confluency, cells were transiently transfected with hiNOS promoter (1 µg) or pcDNA3.1 empty vector (E.V.). After 1 h. incubation with 10µM PEA, cells were treated with different concentration of LPS for 6 h. DMSO as vehicle never exceeded 0.1%. (A) Luciferase activity normalised to protein concentration expressed as mean ± SEM values from three independent experiments. Data were analysed by comparing NAE ligand in presence and absence of LPS using paired, two-tailed, t-test $p>0.05$. (B) Cell viability expressed as protein concentration of 20 µl cell lysate.

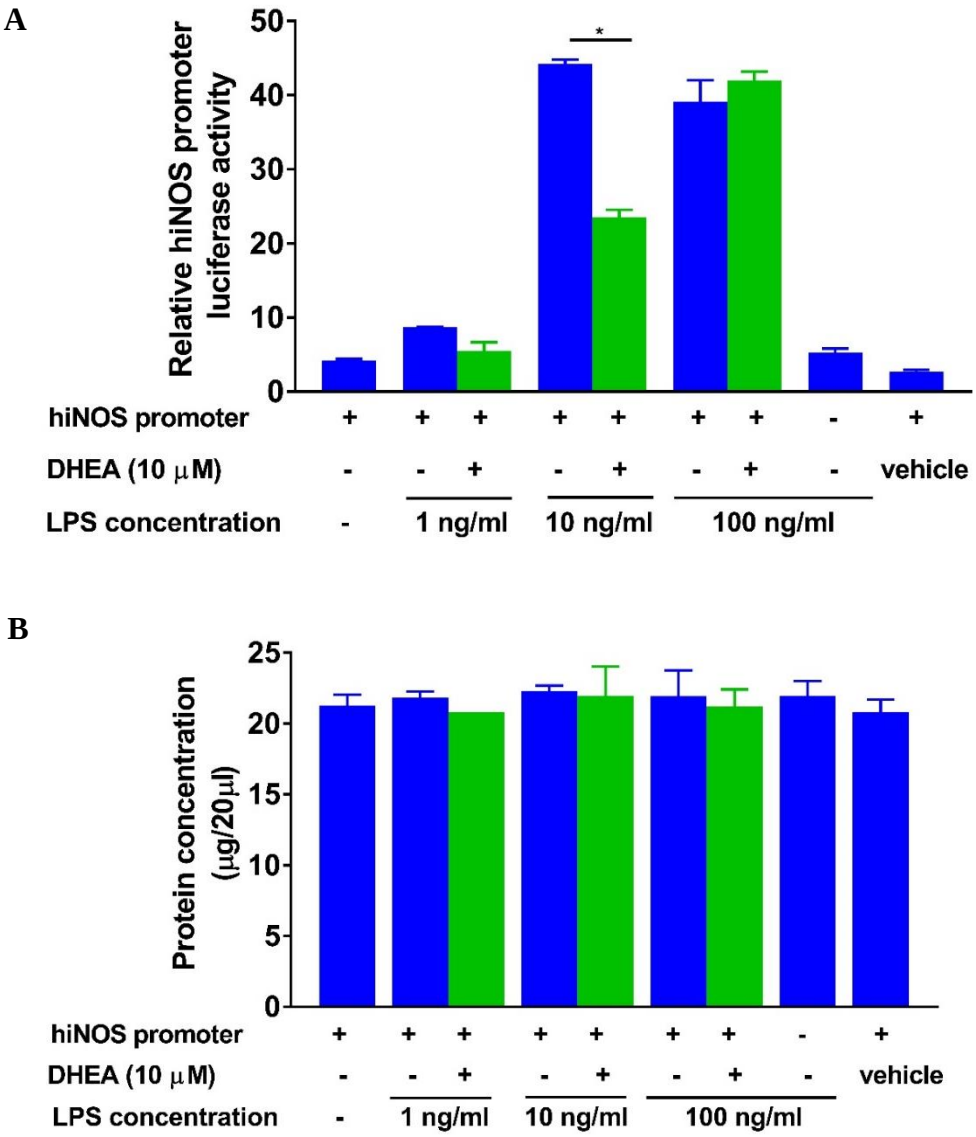


Figure 7.4 DHEA (C22:6 NAE) effects on hiNOS activity stimulated by LPS in RAW246.7 cells. At 60% confluency, cells were transiently transfected with hiNOS promoter (1μg) or pcDNA3.1 empty vector (E.V.). After 1 h. incubation with 10μM DHEA, cells were treated with different concentration of LPS for 6 h. DMSO as vehicle never exceeded 0.1%. (A) Luciferase activity normalised to protein concentration expressed as mean ± SEM values from three independent experiments. Data were analysed by comparing NAE ligand in presence and absence of LPS using paired, two-tailed, t-test $p>0.05$. (B) Cell viability expressed as protein concentration of 20 μl cell lysate.

The nature of the inhibition caused by C20:4 NAE and C22:6 NAE was investigated by testing which endogenous receptor might mediate this signalling. The effect of agonists of CB_1 and CB_2, TRPV1, PPARα, PPARβ and PPARγ receptors on LPS stimulated hiNOS activity was investigated. Pre-incubation cells with **ACEA** (0.3 μM) and **JWH015** (0.3 μM), **Capsaicin** (10 μM), **WY14643** (6 μM), **GW0742** (0.1 μM) or **GW1929** (1 μM) for 1 h before treatment with LPS were unable to alter LPS induced iNOS activity (**Figure 7.5**; one-way ANOVA, followed by post-hoc Dunnett's test; $p>0.05$).

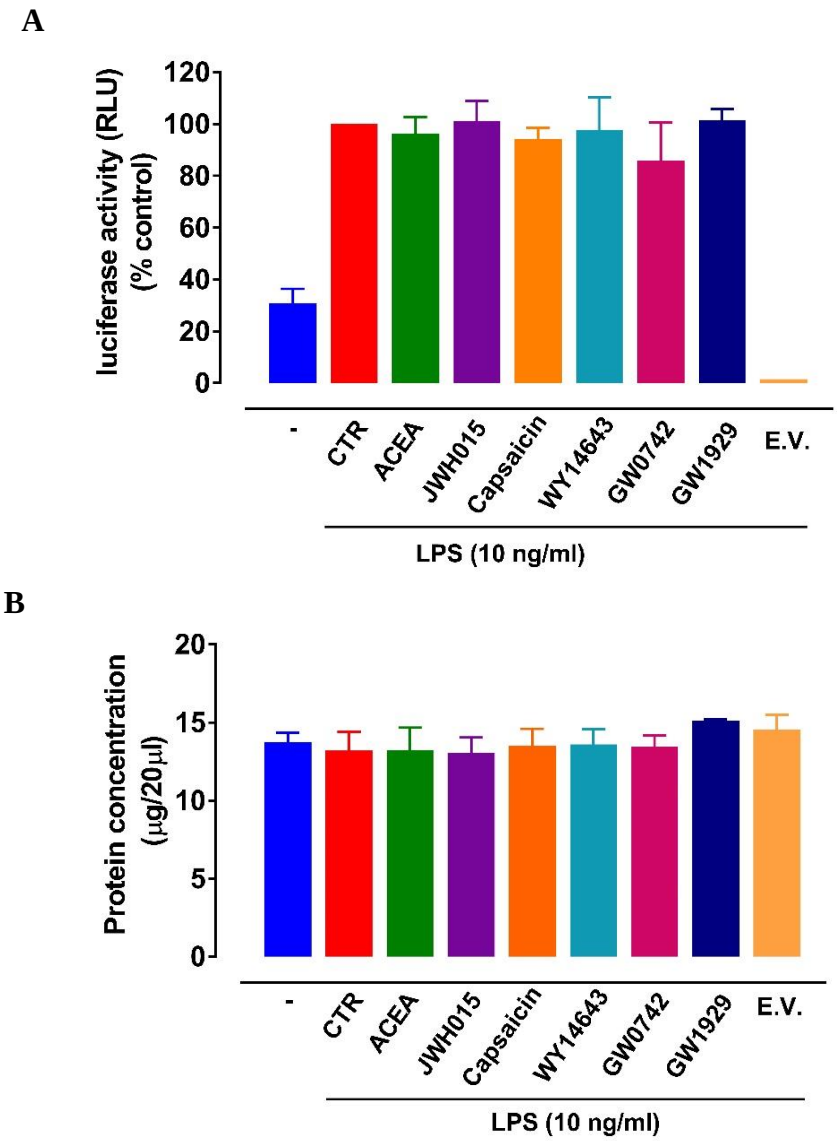


Figure 7.5 Candidate receptors effects on hiNOS activity stimulated by LPS in RAW246.7 cells. At 60% confluency, cells were transiently transfected with hiNOS promoter (1µg) or pcDNA3.1 empty vector (E.V.). After 1 h. incubation with 10 µM (Capsaicin), 0.3 µM (ACEA), 0.3 µM (JWH015), 6 µM (WY14643), 0.1 µM (GW0742), 1 µM (GW1929), cells were treated with different concentration of LPS for 6 h. Ethanol and DMSO as vehicle never exceeded 0.1%. (A) Luciferase activity normalised to protein concentration expressed as mean ± SEM values from three independent experiments. Data were analysed by comparing NAE ligand in presence and absence of LPS using paired, two-tailed, t-test $p>0.05$. (B) Cell viability expressed as protein concentration of 20 µl cell lysate.

7.3.1.2 Inflammatory markers in primary human cells

Monocytes and macrophages play an integral role in immune defence and inflammation. Here, human peripheral blood monocyte and macrophage cells were employed to investigate the effects of various fatty acids ethanolamine ligands on inflammation mediators such as NO and cytokines expression.

Human monocytes from healthy donor were isolated from peripheral blood mononuclear cell as described in method **section 2.2.7**. These cells were treated for 7 days with 50 ng/ml macrophage colony stimulating factor (M-CSF) with change culture media every three days where its help in differentiation to macrophage as seen in **Figure 7.6**.

7.3.1.2.1 Measurement of Nitric oxide

The LPS stimulated NO production in presence of NAE ligands in monocytes and macrophage were measured. Data analysis showed that there was not any significant difference in NO production in monocytes and macrophages whether cells with treated with LPS in presence of NAE derived of C20:4, C16:0 and C22:6 tested ligands or un-treated (**Figure 7.7**).

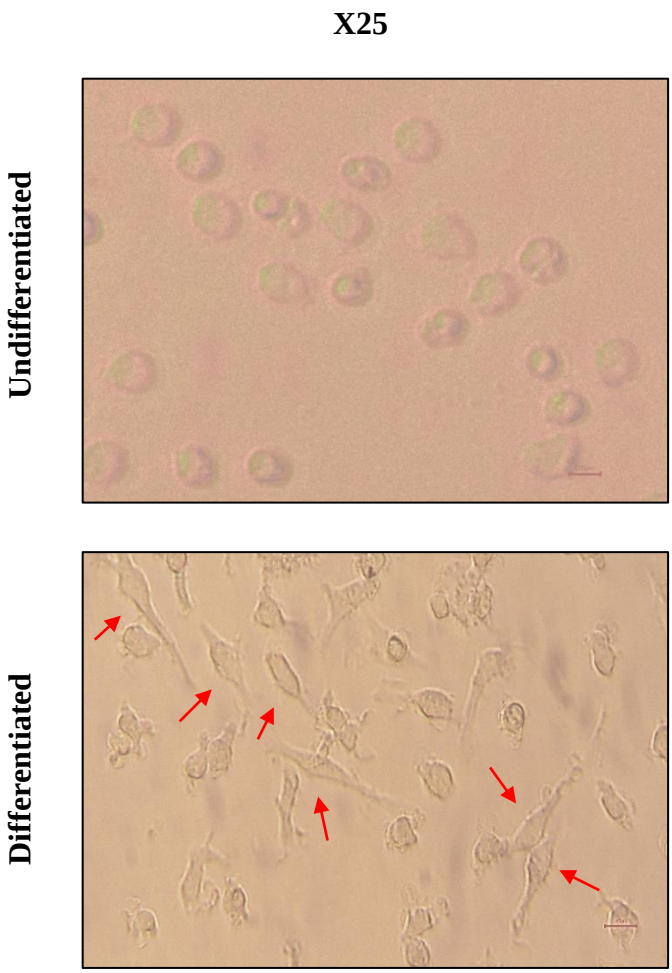


Figure 7.6 Images for primary monocytes and macrophage from human blood cultured in RPMI1460 media. Monocytes were isolated from PBMCs using CD14 microbeads. For macrophage cells, M-CSF at 50 ng/ml was added to cells and then incubated for 7 days with media change every 3 days at 37 °C and 5% CO_2. Scale Bar: at 25x 100 µm.

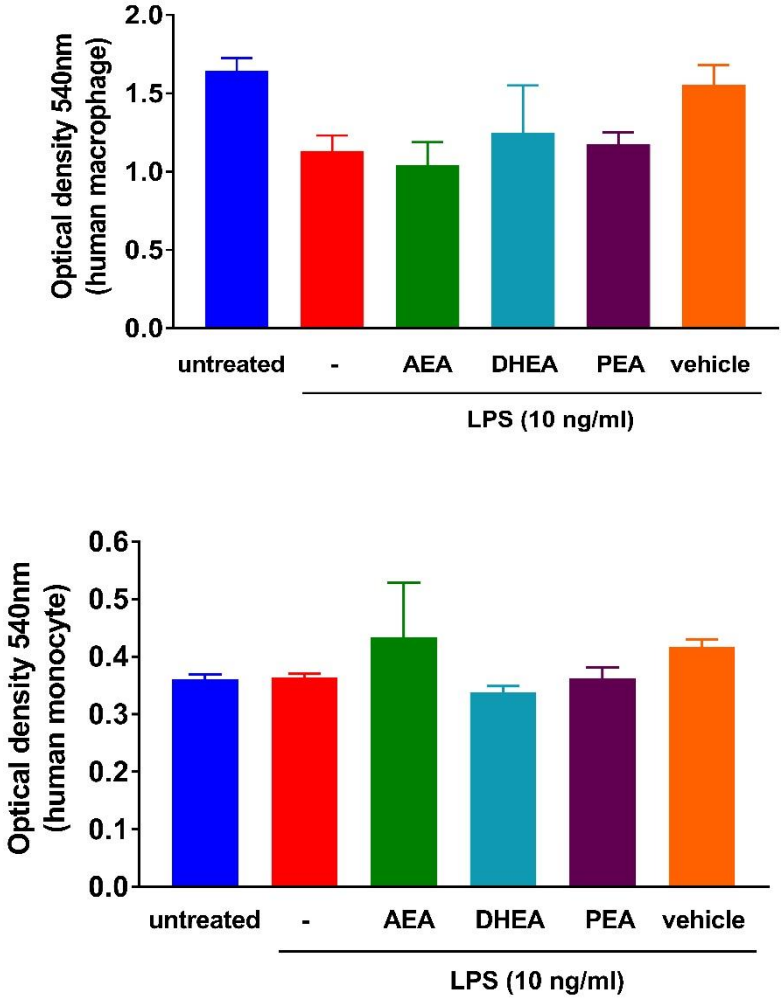


Figure 7.7 Effect of NAEs on LPS-stimulated NO production in human monocytes and macrophages. Monocytes were cultured in 96 well-plate at $5x10^4$ cells/well and $1.5x10^5$ cells/well for differentiation into macrophages with M-CSF at 50 ng/ml for at least 7 days. Cells were incubated for 1 h with tested ligands at high concentration (10µM) or ethanol never exceed 0.1% followed by treatment for 6 h with 10 ng/ml of LPS. Media was collected after incubation and NO production measured using Griess reagent. Data are mean ± SEM and analysis was determined by using one-way ANOVA, followed by post-hoc Bonferroni's test; $p>0.05$.

7.3.1.2.2 Cytokines gene expression

The quantitative real time PCR was used to investigate changes in the mRNA levels of inflammatory (IL -1β and TNF-α) and anti-inflammatory cytokines (IL-10) of fatty acids ethanolamine ligands effect in monocytes and macrophages of human blood.

Initial experiments were designed to establish the expression of cytokines at the mRNA level in human monocytes and macrophage cells. The comparison between genes expression levels require to normalize with internal reference gene or called housekeeping gene. To identify the most stably expressed candidate reference genes in LPS-stimulated monocytes, the expression levels of glyceraldehyde-3-phosphate dehydrogenase (GAPDH), actin, beta (ACTB), β-microglobulin (B2M) and TATA-binding protein (TBP) were quantified by Taq-man RT-PCR in monocytes treated with various concentration of LPS (**Figure 7.8**).

B2M was stable among LPS groups in monocytes while there were notable differences for GAPDH, β actin, TBP. Therefore, B2M was the best reference for expression gene normalisation in LPS stimulation for all subsequent experiments.

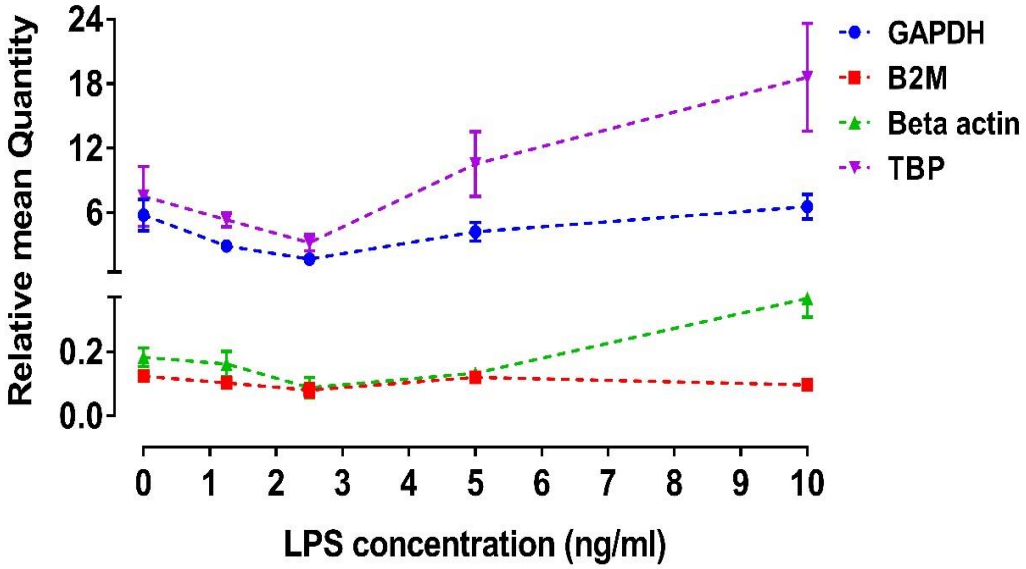


Figure 7.8 Stability of candidate reference genes expression (GAPDH, B2M, β-actin, TBP) among groups of LPS concentrations in human monocytes. Monocytes ($50x10^3$ cells/well) were plated in 96-well plate culture immediately after isolation. LPS concentrations were added in each well for 6 hr incubation and mRNA was extracted quantified and normalised to B2M expression (**see method section**).

The concentration of LPS was optimised for expression levels in cells for subsequent experiments (**Figure 7.9**). The effect of PEA on cytokine expression was clearly LPS concentration-dependent. PEA significantly decreased IL-1β expression at 5 ng/ml LPS and TNF-α expression at less than 5 ng/ml LPS while IL-10 did not change in expression. Therefore, 5 ng/ml LPS was chosen for all subsequent experiments.

The effect of NAE ligands on LPS-stimulated cytokine expression was assessed in both human monocytes and macrophages. Both PEA (C16:0 NAE) and n-3 fatty acids EPA (C20:5 NAE) and DPA (C22:5 NAE) were able to significantly decrease the level of expression of inflammatory cytokine (IL-1β) as seen in **Figure 7.10**.

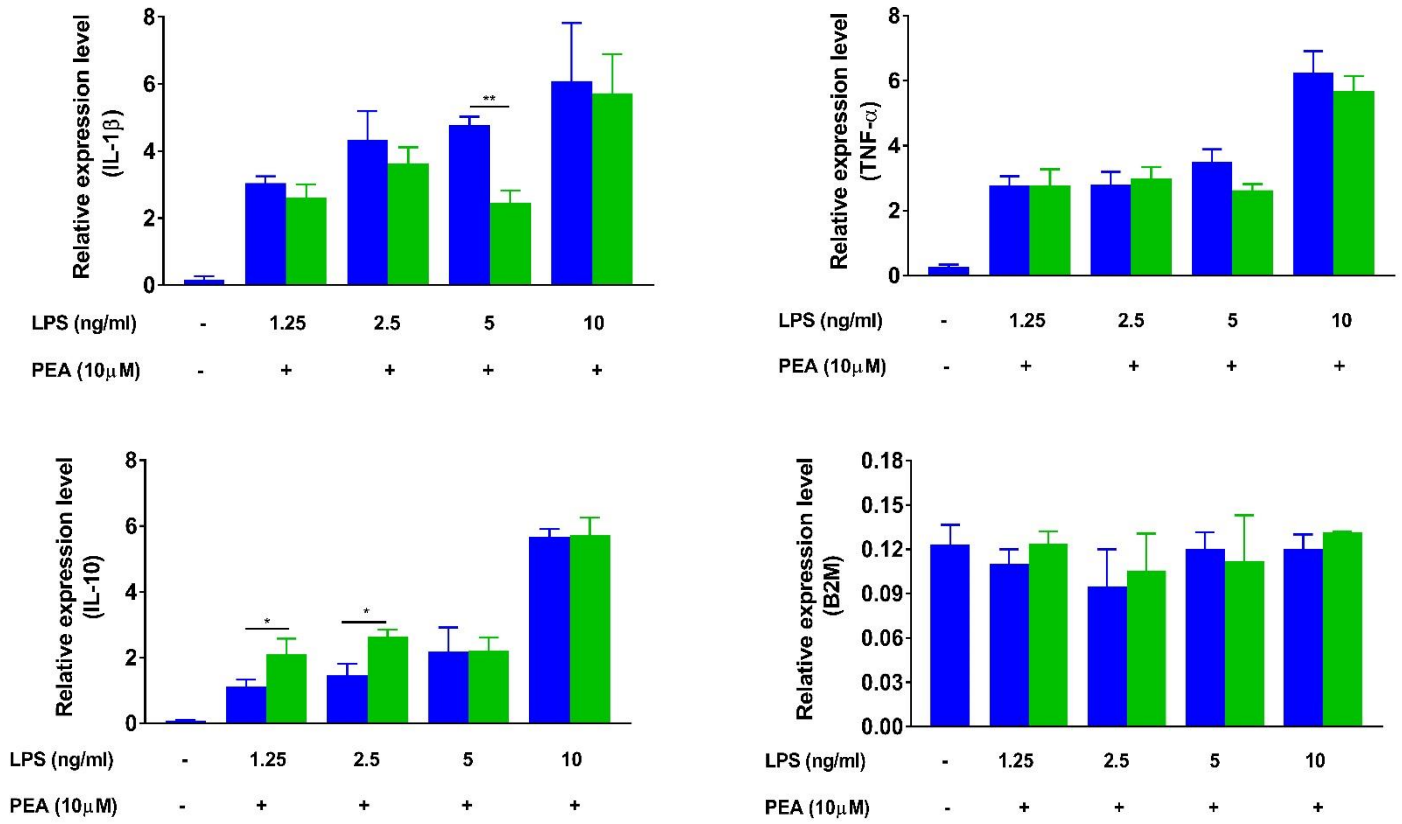


Figure 7.9 Effect of palmitoylethanolamine (PEA) on the expression levels of IL-1β, IL-10 and TNF-α in human monocytes stimulated by various LPS concentrations. Cells were pre-incubated for 30 min prior to LPS stimulation for 6 h. Gene expression levels were analysed using Taq-man RT-PCR and normalized to B2M levels. Data presented as mean ± SEM values from three experiments and analysed using paired, two-tailed t-*test*; **p*<0.05, ***p*<0.01.

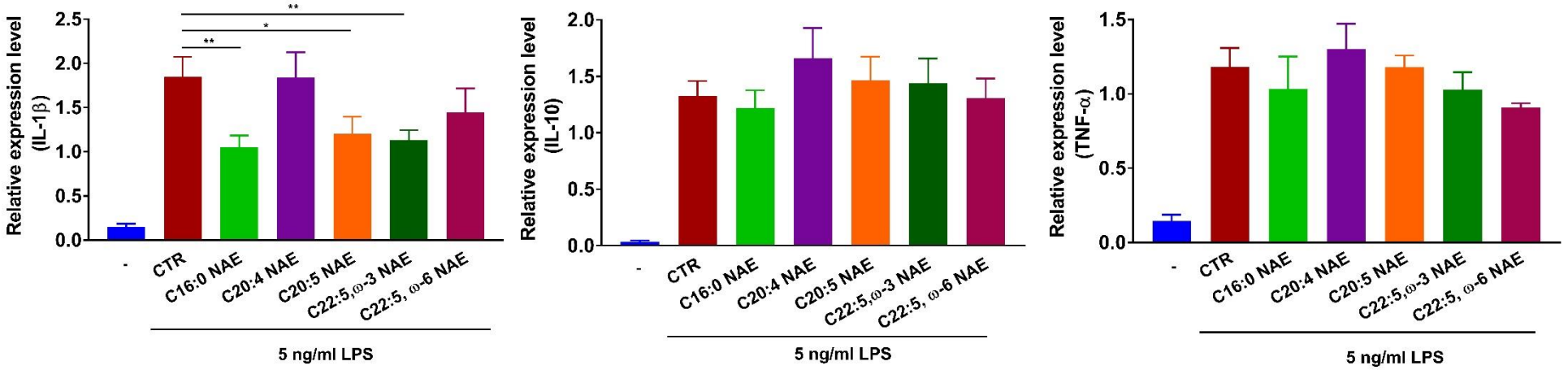


Figure 7.10 The effect of NAEs on LPS-induced inflammatory cytokine expression (IL-1β and TNF-α) and anti-inflammatory cytokine expression (interleukin-10) in human monocytes. Fresh monocytes were plated in 96 well plate culture at $50x10^3$ cell per well. Prior to cells stimulated with LPS for 6 h, NAEs were pre-treated for 30 min at 10 μM and vehicle (ethanol) never exceed 0.1%. The mRNA was extracted, quantified and expressed relative to B2M levels. Statistical significance was analysed as raw data using one-way ANOVA, followed by post-hoc Dunnett's test; $^{**}p<0.01$, $^{***}p<0.001$, by comparing NAEs effect on LPS stimulated gene expression with LPS in absence of NAEs (control, CTR). All data are mean ±SEM values from five healthy volunteers.

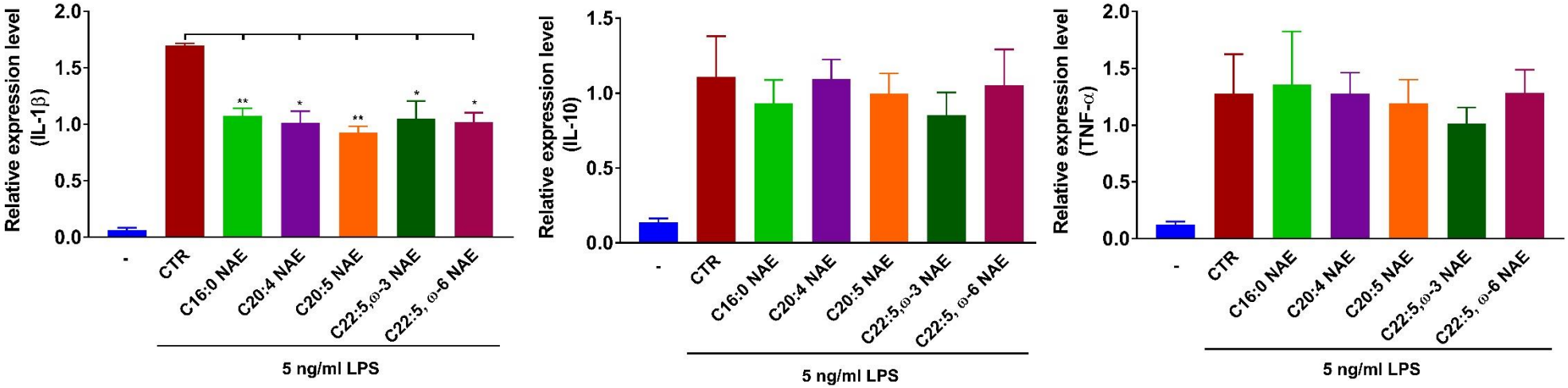


Figure 7.11 Inhibition of LPS evoked inflammatory cytokine (IL-1β) in the presence of NAEs in human macrophages. Cells were cultured in 96 well plates at $1.5x10^5$ per well for 7 days with 50 ng/ml M-CSF to differentiate to macrophages at 37 °C. Cells were pre-incubated with NAEs at 10 µM for 30 min and then stimulated with LPS (5 ng/ml) for 6 h. After mRNA extraction, it was quantified by RT-PCR and normalised to B2M levels. Data are expressed as mean ±SEM values from three healthy volunteers. Statistical analysis was conducted using one-way ANOVA, followed by post-hoc Dunnett's test; *$p<0.05$, by comparing NAE effects on LPS-stimulated cytokines expression with 5 ng/ml LPS (control, CTR) in absence of ligand.

With the human macrophages, pre-incubation of NAEs for 30 min signficanlty inhibited the expression of IL-β as well (**Figure 7.11**), while TNF-α and IL-10 expression did not change either in human monocytes and macrophage.

The potential for NAE activation of endogenous PPARα, β and γ receptors was investigated as mediators of the effects of NAEs on IL-1β expression in monocytes and macrophages. The expression of PPARs was quantified using Taq-man RT-PCR was unaltered for any PPARs in either monocytes (**Figure 7.12**) or macrophages (**Figure 7.13**).

To confirm this result, human monocytes were pre-treated with PPARα antagonist (GW6471) for 30 min at 10 μM. GW6471 was able to block the C16:0 NAE effect in monocytes but was without effect on the responses to C20:5 NAE and C20:4 NAE (**Figure 7.14**).

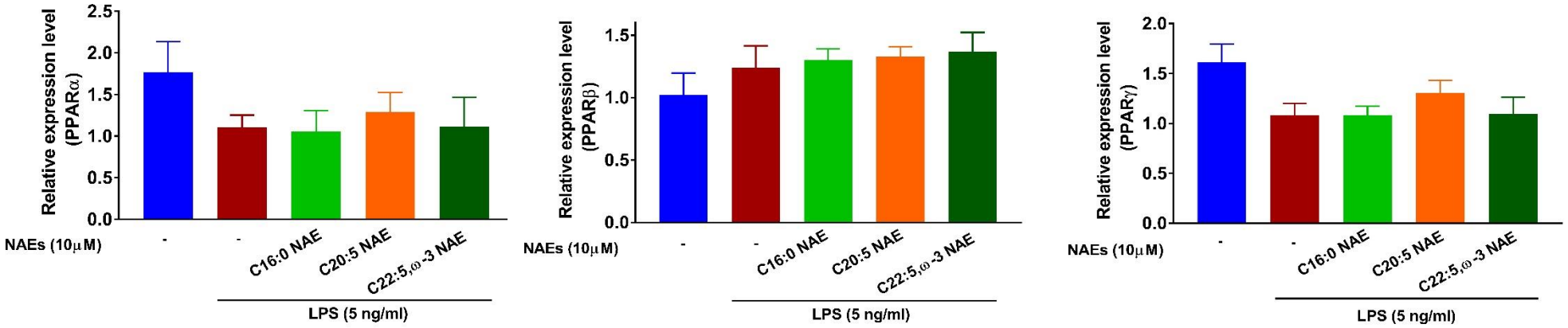


Figure 7.12 Peroxisome proliferator activated receptor (α, β, γ) expression in human monocytes. Monocytes were seeded in 96 well plate at $5x10^4$ per well and pre-treated for 30 min with NAEs at 10 μM and then stimulated with LPS (5 ng/ml) for 6 h.Data are mean ±SEM values of relative expression levels normalised to B2M expression from three healthy volunteers. No significant differences were observed using one-way ANOVA, followed by post-hoc Dunnett's test.

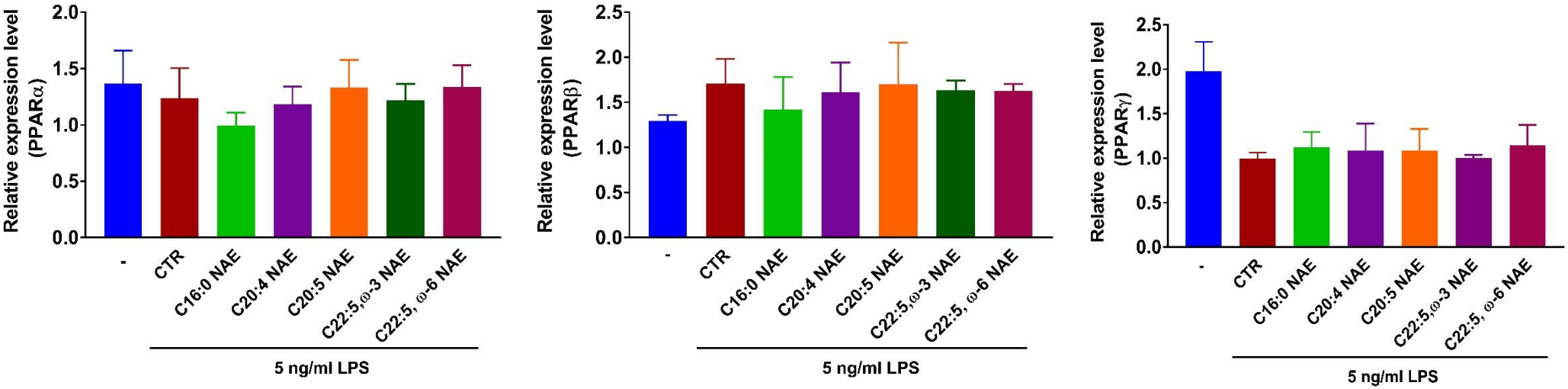


Figure 7.13 Peroxisome proliferator activated receptor (α, β, γ) expression in human macrophages. Differentiation monocytes, cells were cultured 7 days with 50 ng/ml M-CSF in 96 well plate at $1.5x10^5$ per well at 37 °C. Cells were then pre-incubated with NAEs at 10 µM for 30 min and then stimulated with LPS (5 ng/ml) for 6 h. The mRNA was quantified by Taq-man RT-PCR and normalised to B2M levels. Data are mean ± SEM values and were analysed using one-way ANOVA, followed by post-hoc Dunnett's test; $p>0.05$, by comparing PPARs expression of all condition with untreated cells.

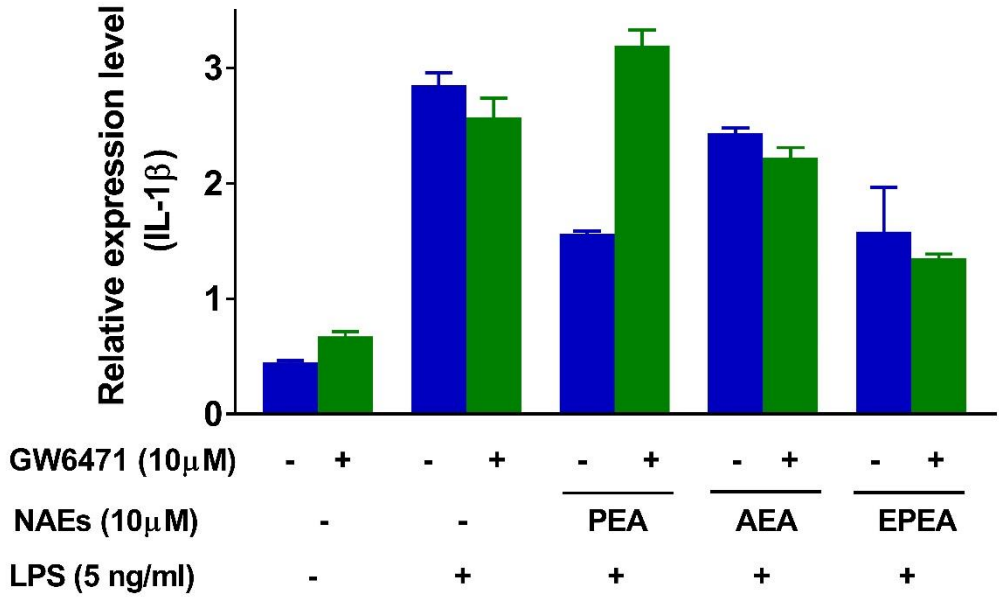


Figure 7.14 A pilot experiment for investigate the effect of PPAR α receptor antagonism on IL-1β expression stimulated by LPS in human monocytes. Fresh monocytes were isolated and cultured in 96 well plates at $50x10^4$ per well at 37 °C. Pre-incubation of cells with NAEs at 10 μM for 30 min was followed by stimulation with LPS (5 ng/ml) for 6 h. The mRNA was extracted and quantified by Taq-man RT-PCR and then normalised to B2M levels.

7.3.2 Cyclooxygenase-2 activity

COX-2 assay was designed to measure peroxidase activity using Amplex red reagent as shown in **Figure 7.15**.

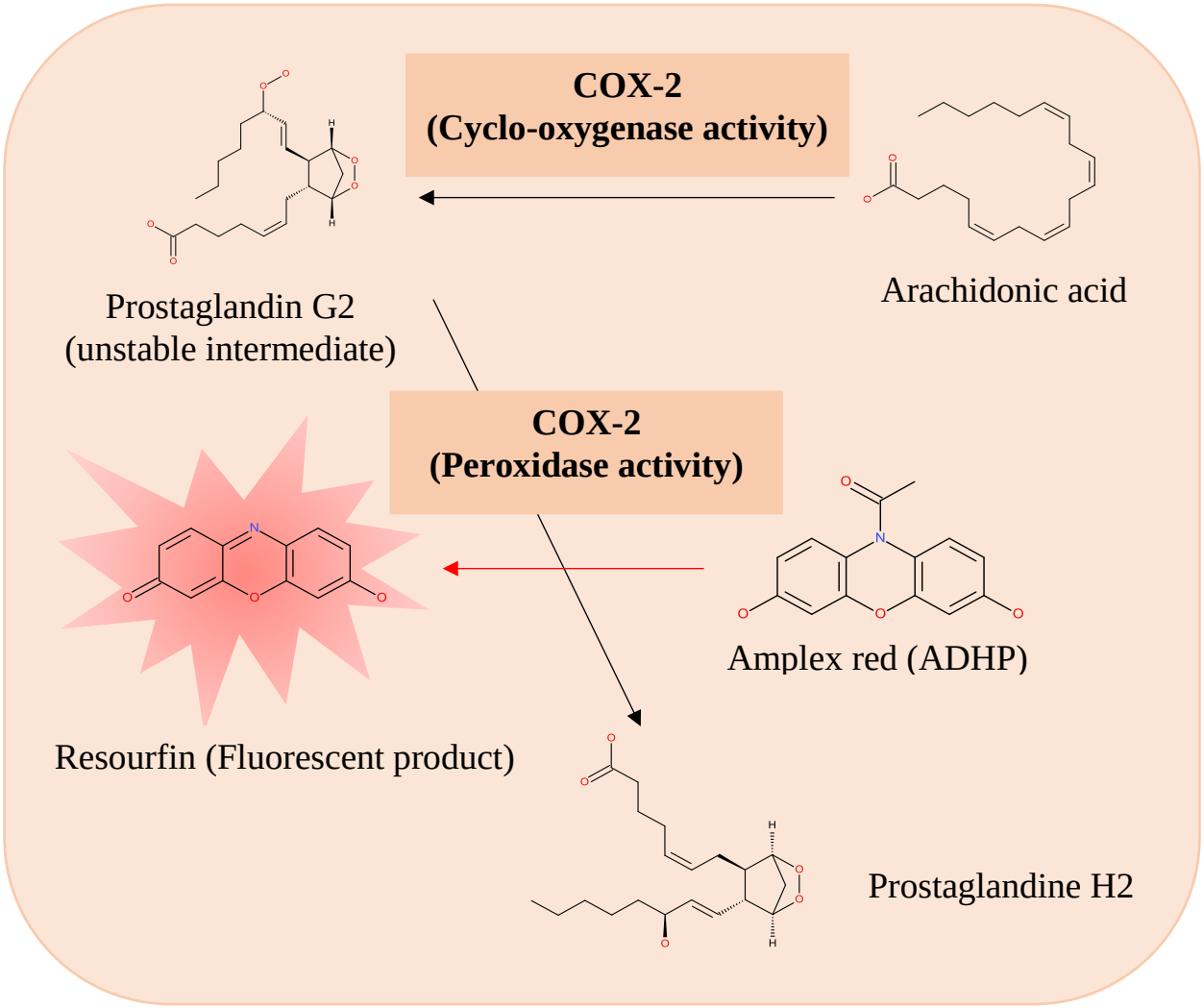


Figure 7.15 Scheme of COX activity detection using Amplex red. The cyclooxygenase reaction converts arachidonic acid to prostaglandin G2 (PGG2). PGG2 is reduced to PGH2 by peroxidase.

Initial experiments were conducted (see the Appendices) to optimise the experimental conditions and to confirm the detection of enzyme activity in BV-2 cells after stimulation with LPS (1 μg/ml). Although peroxidase activity of H_2O_2 reaction was measurable using this simple assay, it failed to measure COX-2 activity in BV-2 or COX-1 in human platelets.

7.4 Discussion

Studies of the inflammatory and immune responses to different NAEs are only limited. Here, the ability of NAEs to inhibit LPS-evoked inflammatory cytokine expression in mouse macrophage, and human monocytes and macrophages have been investigated.

7.4.1 Effect of NAEs on human iNOS activity in RAW246.7 cells

iNOS releases NO, through oxidation of L-arginine. The inducible isoform of NOS is upregulated under transcriptional control of various inflammatory cytokines, LPS or interferon-γ (Jobgen *et al.*, 2006). iNOS has been shown to be a key role in inflammatory mediators associated with several diseases including metabolic syndrome and obesity. For example, disruption of iNOS improved insulin sensitivity and glucose tolerance in obese mice (Kuhlencordt *et al.*, 2001, Dallaire *et al.*, 2008).

Of the NAEs tested, C20:4 NAE (AEA) and C22:6 NAE (DHEA) significantly inhibited hiNOS induction. This compares with results reported by Meijerink *et al.* (2011) who demonstrated that longer chain (> C18) and increased unsaturation of NAEs enhanced their effectiveness in inhibiting NO formation in RAW246.7 cells.

Inhibition of hiNOS activity in RAW246.7 macrophage was found to be dependent on the concentration of LPS used. This is consistent with data from Ross *et al*. (2000) who demonstrated cannabinoid agonists inhibited NO levels at lower concentrations of LPS (~ 2 ng/ml). However, C16:0 NAE (PEA) did not influence LPS-stimulated iNOS activity at any concentration (1, 10, 100 ng/ml).

The immunomodulatory properties of PEA have been reported since 1957. For example, PEA inhibited NO levels in RAW 246.7 cells (Ross *et al.*, 2000), in conflict with our data. PEA is also reported to reduce oxylipins oxygenated products of COX-2 activity in RAW246.7 cells (Gabrielsson *et al.*, 2017). It is possible that these effects are complicated by the activity of NAAA which hydrolyses PEA and is highly expressed and active in macrophage cells (Alhouayek *et al.*, 2017, Solorzano *et al.*, 2009).

The role of CB_2 receptors in the anti-inflammatory effects of endocannabinoids has been demonstrated in series many studies (Batkai *et al.*, 2007, Hegde *et al.*, 2008). DHEA has been shown to bind the CB_2 receptor (Brown *et al.*, 2010) while both CB_2 and PPARγ are reported to be involved in inhibition of IL-6 and MCP-1 levels by DHEA in adipocytes (Balvers *et al.*, 2010). Potentially, these molecular targets are involved in modulating immune response. There is evidence for a role of all three PPARs in modulation of inflammatory processes (Barish *et al.*, 2008, Paterniti *et al.*, 2013, Rockwell and Kaminski, 2004, LoVerme *et al.*, 2006, Thieringer *et al.*, 2000). In addition, TRPV1 expression was reported in macrophages where it has an anti-inflammatory response role (Chen *et al.*, 2003). These findings raise questions about the molecular targets of AEA and DHEA which are involved in inhibition of iNOS activity in RAW246.7 cells.

However, the use of selective ligands of six candidate receptors for AEA and DHEA on LPS induced iNOS activity in RAW246.7 cells failed to show any significant differences. It is possible that the inhibitory effects of DHEA was dependent on COX-2 derived metabolites (Meijerink *et al.*, 2015). DHEA and AEA-elicited

imumunomodulatory effects may be mediated by different mechanisms, which will require further investigation.

7.4.2 Effect of NAEs on NO production and cytokine expression in human monocytes and macrophages

NO production in human monocytes or macrophage is problematic to measure as reported in previous studies (Padgett and Pruett, 1992, Weinberg *et al.*, 1995, Zembala *et al.*, 1994). Weinberg and co-workers noted that monocytes increase expression of iNOS mRNA and produced only small amounts of NO after treatment with IFN and LPS while mouse macrophages generated a significant increase in NO release treated with LPS only (Weinberg et al., 1995). We were also unable to measure NO production in human monocytes or macrophages after activation with LPS. Potentially, the difference in detection of NO production between human and mouse macrophage might be related to expression of iNOS levels due to differences in iNOS promoter regions, suggesting different stimuli are needed for induction of iNOS and subsequent NO production (Chartrain *et al*., 1994).

Similar to NO, cytokines are key mediators of the inflammatory process in immune cells. LPS-stimulated cytokine production in monocytes was concentration-dependent where PEA reduced LPS- stimulated IL-1β at 5 ng/ml and increased IL-10 expression at concentrations below 5 ng/ml. At 5 ng/ml LPS, PEA and n-3 NAEs [(C20:5, ω-3 (EPEA) and C22:5, (7-DPEA)] inhibited significantly LPS-stimulated IL-1β expression in both human monocytes and macrophages, without altering TNF-α and IL10 mRNA levels. Berdyshev *et al.* (1997) used mixed population of peripheral mononuclear blood cell and showed that various concentrations of PEA did not change LPS-induced TNF-

α expression but decreased IL-6 expression at low concentrations AEA decreased both pro-inflammatory cytokines and both ligands were ineffective against IL-10 expression. In this study, AEA did not alter LPS-induced TNFα in both cells but inhibited LPS-induced IL-1β expression in macrophages but not in monocytes. This discrepancy dependent on cell type should be investigated further to identify whether there are distinct molecular targets for the NAEs, or whether distinct signalling pathways are activated.

Previous studies indicated high expression of PPARγ in human macrophages (Thieringer *et al.*, 2000) and PPARα in human monocytes (Chinetti *et al.*, 1998) therefore, the role of PPARs in mediating these effects of NAEs was investigated. However, the NAEs failed to change the expression of PPARs in monocytes and macrophage. A selective PPARα antagonist reversed inhibition of IL-1β in the presence of PEA but not AEA or EPEA. Further evidence that anti-inflammatory effects of PEA in vitro can be PPARα-mediated (Lo Verme *et al.*, 2005). However, these results suggest the presence of another target to mediate AEA and EPEA effects in monocytes. A recent study reported that n-3 NAEs epoxides, have anti-inflammatory properties (McDougle *et al.*, 2017). These are produced by cytochrome P450 epoxygenase which are expressed in human monocytes and macrophages (Bystrom *et al.*, 2011).

7.5 Conclusion

In conclusion, these data show for the first time the anti-inflammatory effects of novel n-3 and n-6 fatty acid ethanolamines in human monocytes and macrophage. However, the lack of identification of a molecular target means that this needs to be investigated further. The potential influence of oxidative metabolism on these NAEs is a likely candidate for future scrutiny.

Chapter 8
General Discussion

8.1 Discussion

The main of this project was to examine the hydrolysis of NAEs by FAAH and their actions on cannabinoid receptors (CB_1 and CB_2), through investigation of two rapid and robust signal transductions pathways (ERK phosphorylation and calcium mobilisation) in CHO cells expressing human CB_1 and CB_2 receptors. In addition, their action on vanilloid receptors (TRPV1) was assessed through the measuring intracellular calcium levels in DRG neurons. Finally, the effects of n-3 and n-6 PUFA-ethanolamines on inflammatory markers in macrophages and monocytes was also investigated.

As a brief over-view, the degree of saturation and chain length of fatty acids conjugated to ethanolamine were important influences on the activation of cannabinoid and TRPV1 receptors, as well as in the hydrolysis of these PUFA-ethanolamines by FAAH. Significant amounts of these fatty acids are found in the diet from sources such as green plants, nuts, soybean and vegetable and fish oils. The latter is rich in n-3 docosahexaenoic acid and eicosapentaenoic acid (Calder, 2011). Dietary fatty acids are reported to determine levels of NAEs in various tissues in that there is a link between the fatty acid precursor and formation of the cognate NAE which has been observed in human plasma and various animal tissues (Joosten *et al.*, 2010, Artmann *et al.*, 2008b, Berger *et al.*, 2001).

It is conceivable that fatty acid ethanolamines can be synthesised from similar analogous phospholipid membrane precursors (NAPEs), although it might be that different routes of synthesis may depend on the structure of these ligands. In vivo effects of AEA, PEA and OEA appear to be limited by FAAH activity, since inhibition of this enzyme prolongs the pharmacological effects of these NAEs (Desarnaud *et al.*, 1995, Fegley *et al.*, 2005).

However, AEA, PEA and OEA are not the sole endogenous substrates for FAAH. Rat liver microsomal FAAH can hydrolyse a broad range of fatty acid ethanolamines, as seen in **Chapter 3**. Quantifying the potency of URB597 indicating that all the NAEs investigated had a similar route of metabolism as they all had a similar potency when AEA was the substrate. Selective inhibitors for FAAH have been proposed to have therapeutic potential in inflammation, cancer and pain through elevation of the levels of these fatty acid ethanolamines in tissues. How much influence individual NAEs have is yet to be determined, whether interactions occur across the range of endogenous NAEs and whether dietary intake of particular fatty acids can influence NAE-mediated effects.

Differences in the maximum velocities of FAAH activity were observed in the hydrolysis of different fatty acid ethanolamines in rat liver as seen in **Chapter 3**. These findings indicate that PUFA-ethanolamines have a faster turnover than mono-unsaturated or saturated ethanolamine analogues. The majority of highly selective FAAH inhibitors are characterised as non-competitive (Mor *et al.*, 2004), therefore it is possible the mono- and saturated fatty acids ethanolamine will be less sensitive to inhibition compared to the PUFA-NAEs due to their lower V_{max} values. Clearly, this is a testable hypothesis making use of in vivo animal models to quantify PUFA, monounsaturated and saturated fatty acid ethanolamines following FAAH inhibition.

Dietary n-3 and n-6 polyunsaturated fatty acids may contribute to the progression/response/management of several diseases via multiple routes, including variation in the profile of endocannabinoids. These NAEs have been detected in the brain, a tissue enriched with CB_1 receptors (Herkenham *et al.*, 1991). However, n-6, but not n-3, PUFA ethanolamines were able to evoke ERK phosphorylation and calcium mobilisation

mediated by CB_1 receptors **as seen in Chapter 4**. These responses were shown to be $G_{i/o}$ protein-dependent through the use of pertussis toxin. DHEA (C22:6, n-3 NAE) is reported to be highly enriched in the brain and may influence brain development mechanisms such as neuritogenesis and synaptogenesis (Kim *et al.*, 2011). Although DHEA and EPEA have been reported to bind to CB_1 receptors, in these series of experiments, they failed to activate phospho-ERK and calcium mobilisation in CHO cells transfected with hCB_1 receptors.

By contrast, these experiments identified that the induction of ERK phosphorylation and intracellular calcium elevation in CHO-hCB_2 cells could be elicited by both n-3 and n-6 PUFA-ethanolamines. This profile suggests that n-3 PUFA ethanolamines, characterised as anti-inflammatory, are more likely to activate CB_2 receptors, compared to CB_1 receptors, where the CB_2 is a predominantly expressed in immune tissues (Galiegue *et al.*, 1995). Although EPA and DHA conjugates of ethanolamine bind to the CB_2 receptor, there are no publications of their role targetting CB_2 for immune-modulation. The distinct profile of CB_2 receptors binding of n-3 fatty acid ethanolamines compared with CB_1 receptors might provide a new molecular mechanism to understand the dietary modulation of inflammation process.

A previous report identified that n-3 PUFA-ethanolamides were able to inhibit NO formation in RAW246.7 mouse macrophage cells and were more effective than other types of fatty acid ethanolamines, including AEA (Meijerink *et al.*, 2011). These observations are similar to our results which showed that n-3 derivatives (C22:5 and C20:5) inhibited endotoxin-induced expression of IL-1β in human monocytes and macrophages, while the inhibitory effect of n-6 PUFA ethanolamines on IL-1β expression was observed in human macrophages only. hiNOS promoter inhibition was observed in murine macrophage cells

(RAW246.7) from NAEs of C20:4, n-6 and C22:6, n-3. It is clearly that n-3 PUFA-ethanolamide effects on macrophages and monocytes unlike ω-6 PUFA ethanolamine effects might be highlighted on the difference in mechanisms which are mediated the anti-inflammatory process from n-3 and n-6 NAEs. One previous study provided evidence of the importance of oxygenated products of n-3 NAEs metabolism which might have a significant role in exerting immune-modulating effects (McDougle *et al.*, 2017). All these observations support a role for n-3 PUFA-ethanolamides in chronic disease, particularly inflammation.

A link between n-3 fatty acids and pain associated with inflammation has been reported; however, the exact mechanism behind this relationship is still unknown (Matta *et al.*, 2007). Some of n-3 fatty acid ethanolamines were observed to activate for TRPV1 receptors in DRG neurons (**see Chapter 5**). The oxidative metabolites of these n-3 PUFA-ethanolamines might contribute to effects of these agents in vivo particularly under inflammatory conditions. There is clearly a need to know more about n-3 PUFA-ethanolamine oxidative metabolism and consequent actions in inflammation, in order to understand and generate a strategy for therapeutic use.

Previous research indicated that AEA metabolites, thorough combination of FAAH and lipoxygenases, might act as agonists at TRPV1 (Hwang *et al.*, 2000). Additionally, linoleic acid oxidative metabolites could act as endogenous regulators of TRPV1 receptors in spinal cord (Patwardhan *et al.*, 2009). TRPV1 activation by n-6 PUFA ethanolamines, which we observed in DRGs, probably is also subject to oxidative metabolism in vivo which may contribute to the development of inflammatory pain. Therefore, understanding these mechanisms could contribute to strategies for novel analgesics.

This thesis has assumed an indirect reaction between P2Y and CB_1 receptors resulting from the inhibitory effect of AM251 on the ATP-mediated intracellular calcium response and ERK pathway in CHO-hCB_1. This result needs further experiments to characterise this relationship, which includes quantifying the amount of endocannabinoids generated in these cells in the presence and absence of ATP using mass spectrometry.

8.2 Future directions and points to consider

Fatty acid amides are of considerable interest, with recent focuses on this class of lipid in nutritional and pharmacological research fields. The findings in this project have raised questions and highlighted a number of areas of further work which would greatly contribute to understanding PUFA ethanolamine actions.

A particular point was the insensitivity of mono-unsaturated and saturated fatty acid ethanolamines at CB_1 and CB_2 receptors or vanilloid receptors (TRPV1). They were also hydrolysed at a slower rate by FAAH. These observations suggest further investigations on the molecular targets which may mediate effects of this agents, of which one likely family is the PPARs.

Given the distinct profiles of n-6 PUFA-ethanolamines in activation of CB_1 receptors and also there are variety of physiological processes mediated by this receptor, therefore many therapeutic areas are possible of these n-6 long chain unsaturated ethanolamine should be considered.

Although there is evidence that FAAH-2 has a preference for primary amides, such as oleamide, it would be appropriate to compare human recombinant versions of FAAH and FAAH-2 for NAE hydrolysis.

The role of n-3 and n-6 PUFA ethanolamines in inflammation and inflammatory pain that could be mediated via TRPV1 and/or CB receptors in reducing cytokine production in immune cells would merit further mechanistic investigation. In particular, the role of CB_2 receptors and other targets, such as PPARγ, needs to be examined. In addition, the role of oxidative metabolites of PUFA-ethanolamines which are suggested to mediate these effects, at least in part, will be important to investigate. It will be important to study the kinetics of COX-2 and lipoxygenase in vitro using PUFA-ethanolamines as substrates.

A major area for future investigation would be the study of fatty acid side chain profile of analogues of 2-arachidonoylglycerol, the other major endocannabinoid. Unfortunately, PUFA mononacylglycerols are not commercially available, so this would have to involve some synthetic chemistry.

8.3 Conclusion

The thesis demonstrates the importance of structure activity relationship in hydrolysis various fatty acid conjugates (n-3, n-6, mono-unsaturated and saturated) by FAAH and in activation of multiple molecular targets such as cannabinoid receptors (CB_1 and CB_2) and vanilloid (TRPV1) receptors. The influence of dietary consumption of n-3 and n-6 PUFA on cognate ethanolamine accumulationis still uncertain.

Chapter 9
Appendices

9 Appendices

9.1 Effect of URB597 on FAAH-catalysed hydrolysis of fatty acids ethanolamine

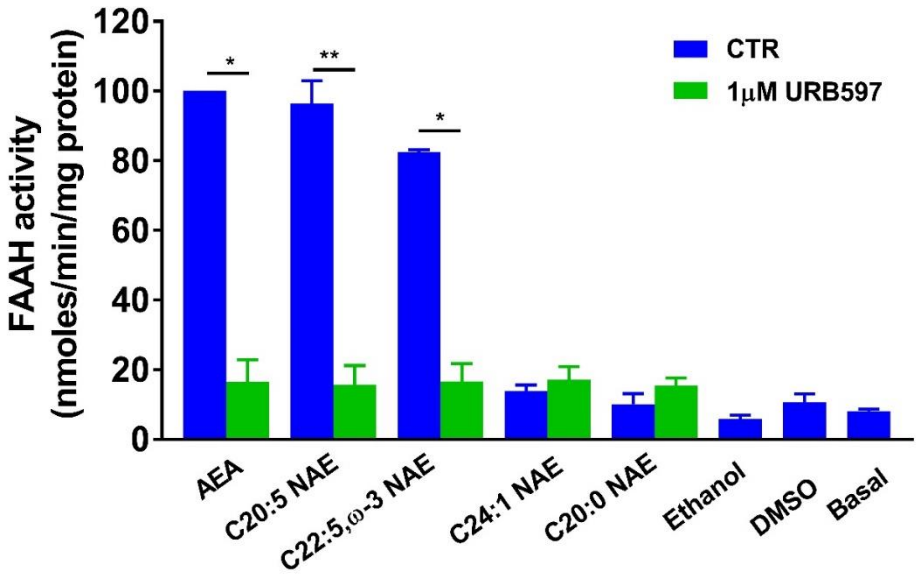


Figure 9.1 URB597-evoked inhibition of NAE hydrolysis by rat liver microsomes. Tissue (10 µg/ml) was pre-incubated with 1 µM URB597 for 15 min at 37 °C prior to addition of substrate at a concentration twice the K_m value. Data are mean ± SEM values from two independent experiments, *p<0.05, **p<0.001 paired t-test, presence vs absence of inhibitor.

9.2 ERK phosphorylation assay optimisation

- **Cell seeding density**

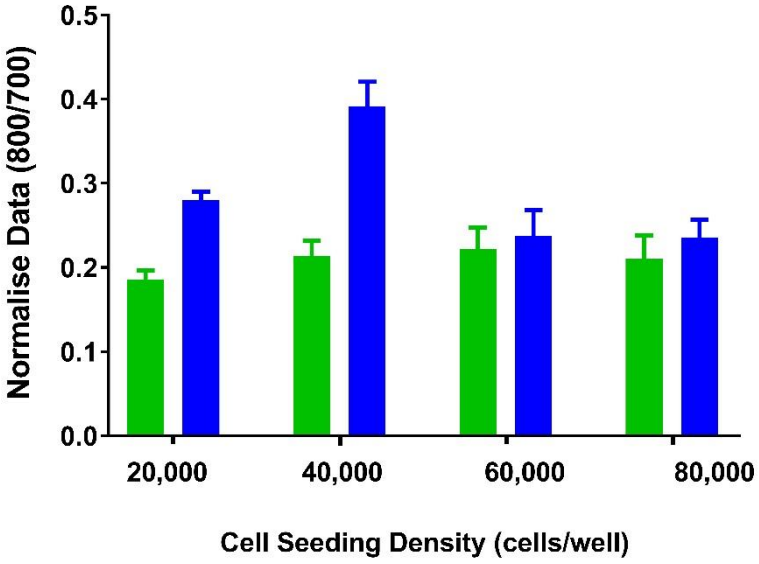


Figure 9.2.1 Effect of cell seeding density on HU210induced ERK phosphorylation. The graphs showing the basal response (green) and HU210-evoked response (blue). Cells were seeded for 24 h followed by serum starvation for 24 h and then stimulated with 1 μM HU210 for 5 min. Data are mean values ± SEM values from three independent experiments using different passages performed in triplicate.

- **Effect of apyrase on ERK phosphorylation**

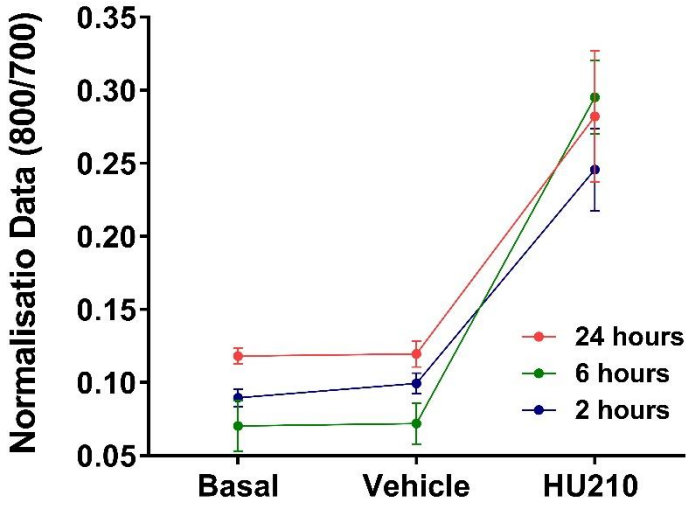


Figure 9.2.2 Effect of apyrase on HU210 stimulated ERK phosphorylation at various starvation times. Cells (40,000 cells/well) were cultured for 24 h followed by starvation at 24, 6, 2 h. Cells were then stimulated with HU210 (1 µM) for 5 min. Data represents one experiment performed in triplicate.

9.3 Investigation of ERK phosphorylation in human CB_2 receptor transfected CHO cells

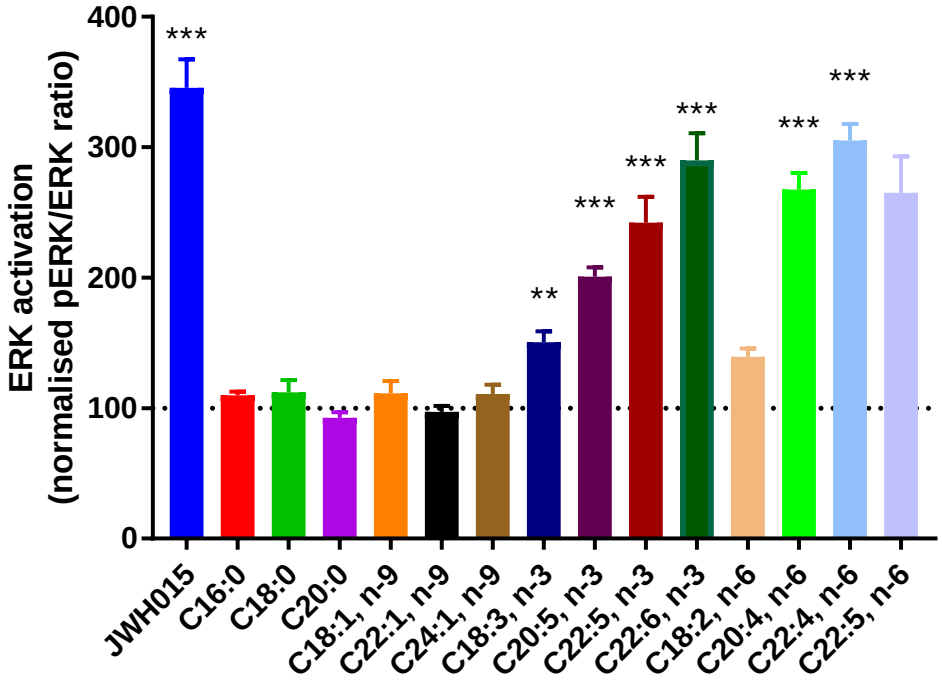


Figure 9.3 Fatty acid ethanolamine ligands on ERK phosphorylation in CHO-hCB_2 cells. Cells were cultured for 24 h followed by serum starvation Cells were stimulated with 10 µM of each ligand for 5 min at 37 °C. ERK phosphorylation values were normalized to the corresponding total-ERK values. Data are expressed as mean ± SEM values from five independent experiments performed in triplicate. Statistical analysis was conducted using one-way ANOVA followed by post-hoc Dunnett's test; ** $p<0.01$; *** $p<0.001$; compared to vehicle (either ethanol or DMSO).

9.4 COX activity assay optimisation

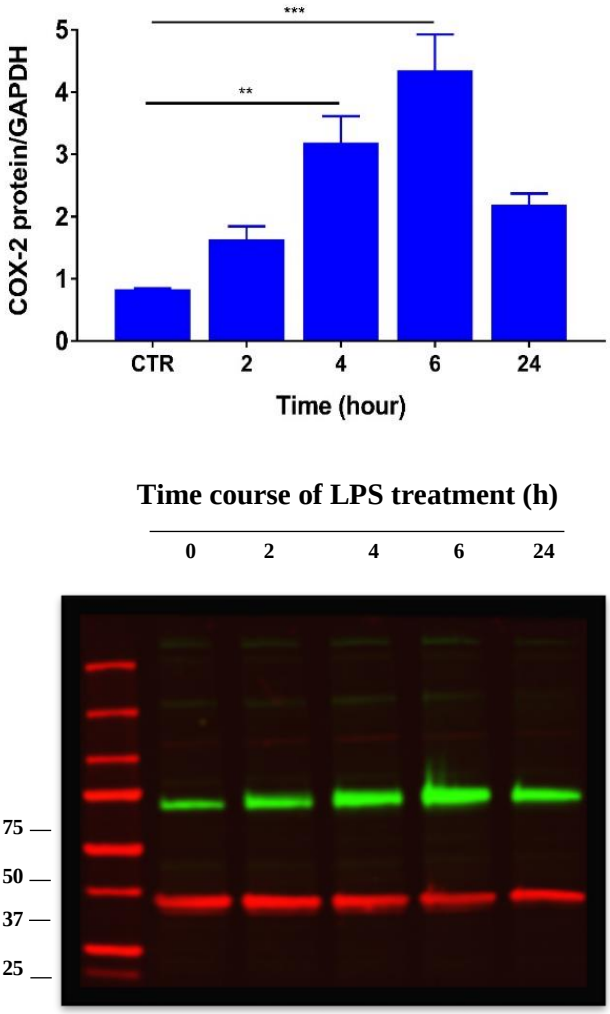


Figure 9.4 Western blot analysis showing COX-2 expression in whole cell lysates of BV-2 (20 µg protein) stimulated by 1 µg/ml LPS at various times. BV-2 cells at a density of $1.2x10^4$ were treated with LPS at 2, 4, 6 and 24 h. Blot was incubated with mouse antibody to COX-2 and GADPH followed by IRDY® conjugates goat anti-mouse and anti-rabbit IgG. (A) Bar represent mean ± SEM of COX-2 expression to GAPDH from three independent experiments. Significant analysis was determined using one-way ANOVA, followed by post-hoc Dunnett's test; $^{**}p<0.01$, $^{***}p<0.001$, LPS vs. CTR (untreated). (B) COX-2 expression at 69 kDa and 36 kDa for GAPDH.

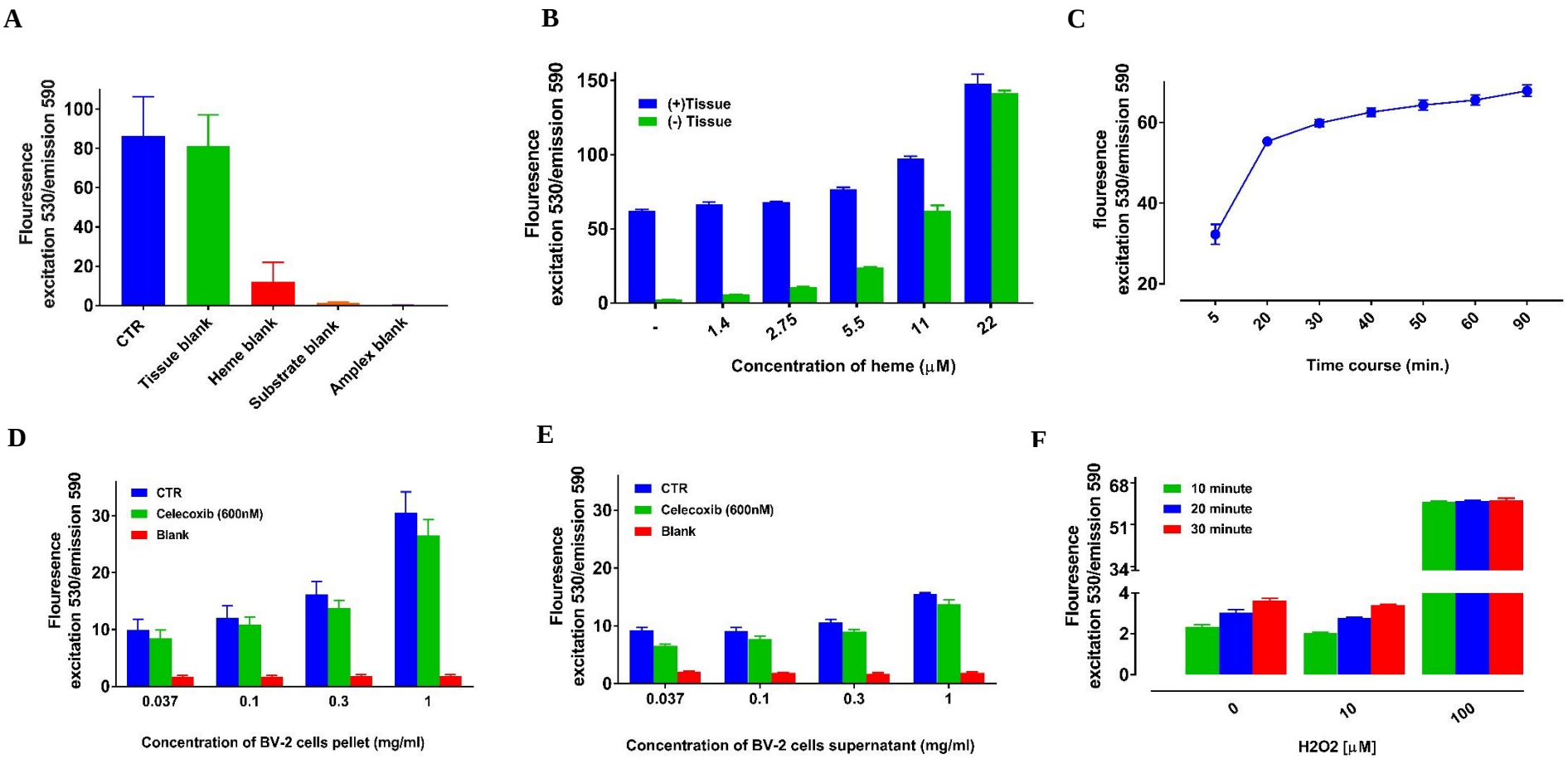


Figure 9.5 Optimisation of peroxidase activity assay in mouse microglia cells (BV-2) stimulated with 1µg/ml LPS and was applied the assay **as described in methods section.** (A) Initial experiment for measure enzyme activity (B) Effect of different dilution of heme on COX-2-catalysed oxidation of arachidonic acid (100 µM) in BV-2 cells for 90 min. (C) Time course for detection enzyme activity catalysed by arachidonic acids (100 µM) in presence of 1.4 µM heme. (D) Effect of 600nM celecoxib (COX-2 selective inhibitor) on COX-2 mediated arachidonic acid oxidation in **pellet** and **supernatant** of BV-2 cells (blank, without tissue) **(f)** Oxidation of hydrogen peroxide (H_2O_2) using Amplex red.

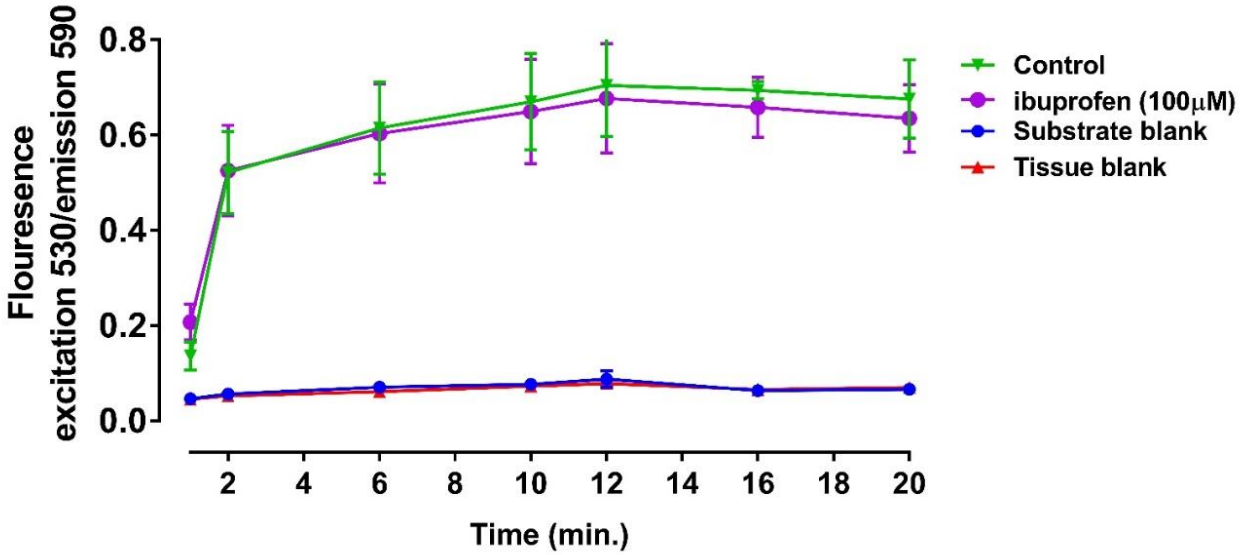


Figure 9.6 Effect of ibuprofen in inhibition COX activity in human platelet. Platelet were collected from blood of healthy donor as described in **methods section**. Cells were pre-treated with 100 µM of ibuprofen for 5 min and followed by 100 µM arachidonic acid. The activity was measure using Amplex red at different time point which indicated in figure. Data represent mean ± SEM of three independent experiment. No significant difference was observed in enzyme activity in presence or absence of ibuprofen using *TOW*-way ANOVA, followed by post-hoc *Sidak's* test, $p>0.05$.

10 References

LOWRY, O. H., ROSEBROUGH, N. J., FARR, A. L. & RANDALL, R. J. 1951. Protein measurement with the Folin phenol reagent. *J Biol Chem,* 193**,** 265-75.

JANCSÓ, N., JANCSÓ-GÁBOR, A. & SZOLCSÁNYI, J. 1967. Direct evidence for neurogenic inflammation and its prevention by denervation and by pretreatment with capsaicin. *British Journal of Pharmacology and Chemotherapy,* 31**,** 138-151.

HAMBERG, M. & SAMUELSSON, B. 1973. Detection and isolation of an endoperoxide intermediate in prostaglandin biosynthesis. *Proc Natl Acad Sci U S A,* 70**,** 899-903.

GREEN, L. C., WAGNER, D. A., GLOGOWSKI, J., SKIPPER, P. L., WISHNOK, J. S. & TANNENBAUM, S. R. 1982. Analysis of nitrate, nitrite, and [15N]nitrate in biological fluids. *Anal Biochem,* 126**,** 131-8.

PORATH, J. & OLIN, B. 1983. Immobilized metal ion affinity adsorption and immobilized metal ion affinity chromatography of biomaterials. Serum protein affinities for gel-immobilized iron and nickel ions. *Biochemistry,* 22**,** 1621-30.

HOWLETT, A. C. & FLEMING, R. M. 1984. Cannabinoid inhibition of adenylate cyclase. Pharmacology of the response in neuroblastoma cell membranes. *Mol Pharmacol,* 26**,** 532-8.

SCHMID, P. C., ZUZARTE-AUGUSTIN, M. L. & SCHMID, H. H. 1985. Properties of rat liver N-acylethanolamine amidohydrolase. *J Biol Chem,* 260**,** 14145-9.

HOWLETT, A. C., QUALY, J. M. & KHACHATRIAN, L. L. 1986. Involvement of Gi in the inhibition of adenylate cyclase by cannabimimetic drugs. *Mol Pharmacol,* 29**,** 307-13.

WINTER, J., FORBES, C. A., STERNBERG, J. & LINDSAY, R. M. 1988. Nerve growth factor (NGF) regulates adult rat cultured dorsal root ganglion neuron responses to the excitotoxin capsaicin. *Neuron,* 1**,** 973-81.

MATSUDA, L. A., LOLAIT, S. J., BROWNSTEIN, M. J., YOUNG, A. C. & BONNER, T. I. 1990. Structure of a cannabinoid receptor and functional expression of the cloned cDNA. *Nature,* 346**,** 561-4.

HERKENHAM, M., LYNN, A. B., JOHNSON, M. R., MELVIN, L. S., DE COSTA, B. R. & RICE, K. C. 1991. Characterization and localization of cannabinoid receptors in rat brain: a quantitative in vitro autoradiographic study. *J Neurosci,* 11**,** 563-83.

DUBENDORFF, J. W. & STUDIER, F. W. 1991. Controlling basal expression in an inducible T7 expression system by blocking the target T7 promoter with lac repressor. *J Mol Biol,* 219**,** 45-59.

PADGETT, E. L. & PRUETT, S. B. 1992. Evaluation of nitrite production by human monocyte-derived macrophages. *Biochem Biophys Res Commun,* 186**,** 775-81.

GÖTTLICHER, M., WIDMARK, E., LI, Q. & GUSTAFSSON, J. A. 1992. Fatty acids activate a chimera of the clofibric acid-activated receptor and the glucocorticoid receptor. *Proceedings of the National Academy of Sciences of the United States of America,* 89**,** 4653-4657.

DEVANE, W. A., HANUS, L., BREUER, A., PERTWEE, R. G., STEVENSON, L. A., GRIFFIN, G., GIBSON, D., MANDELBAUM, A., ETINGER, A. & MECHOULAM, R. 1992. Isolation and structure of a brain constituent that binds to the cannabinoid receptor. *Science,* 258**,** 1946-9.

VOGEL, Z., BARG, J., LEVY, R., SAYA, D., HELDMAN, E. & MECHOULAM, R. 1993. Anandamide, a brain endogenous compound, interacts specifically with cannabinoid receptors and inhibits adenylate cyclase. *J Neurochem,* 61**,** 352-5.

MUNRO, S., THOMAS, K. L. & ABU-SHAAR, M. 1993. Molecular characterization of a peripheral receptor for cannabinoids. *Nature,* 365**,** 61-5.

MACKIE, K., DEVANE, W. A. & HILLE, B. 1993. Anandamide, an endogenous cannabinoid, inhibits calcium currents as a partial agonist in N18 neuroblastoma cells. *Mol Pharmacol,* 44**,** 498-503.

HANUS, L., GOPHER, A., ALMOG, S. & MECHOULAM, R. 1993. Two new unsaturated fatty acid ethanolamides in brain that bind to the cannabinoid receptor. *J Med Chem,* 36**,** 3032-4.

FELDER, C. C., BRILEY, E. M., AXELROD, J., SIMPSON, J. T., MACKIE, K. & DEVANE, W. A. 1993a. Anandamide, an endogenous cannabimimetic eicosanoid, binds to the cloned human cannabinoid receptor and stimulates receptor-mediated signal transduction. *Proceedings of the National Academy of Sciences,* 90**,** 7656-7660.

FELDER, C. C., BRILEY, E. M., AXELROD, J., SIMPSON, J. T., MACKIE, K. & DEVANE, W. A. 1993b. Anandamide, an endogenous cannabimimetic eicosanoid, binds to the cloned human cannabinoid receptor and stimulates receptor-mediated signal transduction. *Proceedings of the National Academy of Sciences of the United States of America,* 90**,** 7656-7660.

DEUTSCH, D. G. & CHIN, S. A. 1993a. Enzymatic synthesis and degradation of anandamide, a cannabinoid receptor agonist. *Biochem Pharmacol,* 46**,** 791-6.

DEUTSCH, D. G. & CHIN, S. A. 1993b. Enzymatic synthesis and degradation of anandamide, a cannabinoid receptor agonist. *Biochemical Pharmacology,* 46**,** 791-796.

ZEMBALA, M., SIEDLAR, M., MARCINKIEWICZ, J. & PRYJMA, J. 1994. Human monocytes are stimulated for nitric oxide release in vitro by some tumor cells but not by cytokines and lipopolysaccharide. *Eur J Immunol,* 24**,** 435-9.

SCHWARZ, H., BLANCO, F. J. & LOTZ, M. 1994. Anadamide, an endogenous cannabinoid receptor agonist inhibits lymphocyte proliferation and induces apoptosis. *J Neuroimmunol,* 55**,** 107-15.

PINTO, J. C., POTIÉ, F., RICE, K. C., BORING, D., JOHNSON, M. R., EVANS, D. M., WILKEN, G. H., CANTRELL, C. H. & HOWLETT, A. C. 1994. Cannabinoid receptor binding and agonist activity of amides and esters of arachidonic acid. *Molecular Pharmacology,* 46**,** 516.

PERTWEE, R., GRIFFIN, G., HANUS˘, L. & MECHOULAM, R. 1994. Effects of two endogenous fatty acid ethanolamides on mouse vasa deferentia. *European Journal of Pharmacology,* 259**,** 115-120.

DI MARZO, V., FONTANA, A., CADAS, H., SCHINELLI, S., CIMINO, G., SCHWARTZ, J.-C. & PIOMELLI, D. 1994. Formation and inactivation of endogenous cannabinoid anandamide in central neurons. *Nature,* 372**,** 686.

CHILDERS, S. R., SEXTON, T. & ROY, M. B. 1994. Effects of anandamide on cannabinoid receptors in rat brain membranes. *Biochem Pharmacol,* 47**,** 711-5.

CHARTRAIN, N. A., GELLER, D. A., KOTY, P. P., SITRIN, N. F., NUSSLER, A. K., HOFFMAN, E. P., BILLIAR, T. R., HUTCHINSON, N. I. & MUDGETT, J. S. 1994. Molecular cloning, structure, and chromosomal localization of the human inducible nitric oxide synthase gene. *J Biol Chem,* 269**,** 6765-72.

YU, K., BAYONA, W., KALLEN, C. B., HARDING, H. P., RAVERA, C. P., MCMAHON, G., BROWN, M. & LAZAR, M. A. 1995. Differential activation of peroxisome

proliferator-activated receptors by eicosanoids. *J Biol Chem,* 270**,** 23975-83.

WEINBERG, J. B., MISUKONIS, M. A., SHAMI, P. J., MASON, S. N., SAULS, D. L., DITTMAN, W. A., WOOD, E. R., SMITH, G. K., MCDONALD, B., BACHUS, K. E. & ET AL. 1995. Human mononuclear phagocyte inducible nitric oxide synthase (iNOS): analysis of iNOS mRNA, iNOS protein, biopterin, and nitric oxide production by blood monocytes and peritoneal macrophages. *Blood,* 86**,** 1184-95.

VUILLARD, L., BRAUN-BRETON, C. & RABILLOUD, T. 1995. Non-detergent sulphobetaines: a new class of mild solubilization agents for protein purification. *Biochem J,* 305 (Pt 1)**,** 337-43.

UEDA, N., YAMAMOTO, K., YAMAMOTO, S., TOKUNAGA, T., SHIRAKAWA, E., SHINKAI, H., OGAWA, M., SATO, T., KUDO, I., INOUE, K., TAKIZAWA, H., NAGANO, T., HIROBE, M., MATSUKI, N. & SAITO, H. 1995a. Lipoxygenase-catalyzed oxygenation of arachidonylethanolamide, a cannabinoid receptor agonist. *Biochimica et Biophysica Acta (BBA) - Lipids and Lipid Metabolism,* 1254**,** 127-134.

UEDA, N., KURAHASHI, Y., YAMAMOTO, S. & TOKUNAGA, T. 1995b. Partial purification and characterization of the porcine brain enzyme hydrolyzing and synthesizing anandamide. *J Biol Chem,* 270**,** 23823-7.

MAURELLI, S., BISOGNO, T., DE PETROCELLIS, L., DI LUCCIA, A., MARINO, G. & DI MARZO, V. 1995. Two novel classes of neuroactive fatty acid amides are substrates for mouse neuroblastoma 'anandamide amidohydrolase'. *FEBS Lett,* 377**,** 82-6.

MACKIE, K., LAI, Y., WESTENBROEK, R. & MITCHELL, R. 1995. Cannabinoids activate an inwardly rectifying potassium conductance and inhibit Q-type calcium currents in AtT20 cells transfected with rat brain cannabinoid receptor. *J Neurosci,* 15**,** 6552-61.

HILLARD, C. J., WILKISON, D. M., EDGEMOND, W. S. & CAMPBELL, W. B. 1995. Characterization of the kinetics and distribution of N-arachidonylethanolamine (anandamide) hydrolysis by rat brain. *Biochimica et Biophysica Acta (BBA) - Lipids and Lipid Metabolism,* 1257**,** 249-256.

HAMPSON, A. J., HILL, W. A. G., ZAN-PHILLIPS, M., MAKRIYANNIS, A., LEUNG, E., EGLEN, R. M. & BORNHEIM, L. M. 1995. Anandamide hydroxylation by brain lipoxygenase:metabolite structures and potencies at the cannabinoid receptor. *Biochimica et Biophysica Acta (BBA) - Lipids and Lipid Metabolism,* 1259**,** 173-179.

GALIEGUE, S., MARY, S., MARCHAND, J., DUSSOSSOY, D., CARRIERE, D., CARAYON, P., BOUABOULA, M., SHIRE, D., LE FUR, G. & CASELLAS, P. 1995. Expression of central and peripheral cannabinoid receptors in human immune tissues and leukocyte subpopulations. *Eur J Biochem,* 232**,** 54-61.

FELDER, C. C., JOYCE, K. E., BRILEY, E. M., MANSOURI, J., MACKIE, K., BLOND, O., LAI, Y., MA, A. L. & MITCHELL, R. L. 1995. Comparison of the pharmacology and signal transduction of the human cannabinoid CB1 and CB2 receptors. *Molecular Pharmacology,* 48**,** 443-450.

DESARNAUD, F., CADAS, H. & PIOMELLI, D. 1995. Anandamide amidohydrolase activity in rat brain microsomes. Identification and partial characterization. *J Biol Chem,* 270**,** 6030-5.

BOUABOULA, M., POINOT-CHAZEL, C., BOURRIÉ, B., CANAT, X., CALANDRA, B., RINALDI-CARMONA, M., LE FUR, G. & CASELLAS, P. 1995. Activation of mitogen-activated protein kinases by stimulation of the central cannabinoid receptor CB1. *Biochemical Journal,* 312**,** 637-641.

BORNHEIM, L. M., KIM, K. Y., CHEN, B. & CORREIA, M. A. 1995. Microsomal cytochrome P450-mediated liver and brain anandamide metabolism. *Biochem Pharmacol,* 50**,** 677-86.

BARG, J., FRIDE, E., HANUS, L., LEVY, R., MATUS-LEIBOVITCH, N., HELDMAN, E., BAYEWITCH, M., MECHOULAM, R. & VOGEL, Z. 1995. Cannabinomimetic behavioral effects of and adenylate cyclase inhibition by two new endogenous anandamides. *European Journal of Pharmacology,* 287**,** 145-152.

WILLSON, T. M., COBB, J. E., COWAN, D. J., WIETHE, R. W., CORREA, I. D., PRAKASH, S. R., BECK, K. D., MOORE, L. B., KLIEWER, S. A. & LEHMANN, J. M. 1996. The structure-activity relationship between peroxisome proliferator-activated receptor gamma agonism and the antihyperglycemic activity of thiazolidinediones. *J Med Chem,* 39**,** 665-8.

SUGIURA, T., KODAKA, T., KONDO, S., TONEGAWA, T., NAKANE, S., KISHIMOTO, S., YAMASHITA, A. & WAKU, K. 1996. 2-Arachidonoylglycerol, a Putative Endogenous Cannabinoid Receptor Ligand, Induces Rapid, Transient Elevation of Intracellular Free Ca2+in Neuroblastoma × Glioma Hybrid NG108-15 Cells. *Biochemical and Biophysical Research Communications,* 229**,** 58-64.

SHOWALTER, V. M., COMPTON, D. R., MARTIN, B. R. & ABOOD, M. E. 1996. Evaluation of binding in a transfected cell line expressing a peripheral cannabinoid receptor (CB2): identification of cannabinoid receptor subtype selective ligands. *J Pharmacol Exp Ther,* 278**,** 989-99.

LANG, W., QIN, C., HILL, W. A. G., LIN, S., KHANOLKAR, A. D. & MAKRIYANNIS, A. 1996. High-Performance Liquid Chromatographic Determination of Anandamide Amidase Activity in Rat Brain Microsomes. *Analytical Biochemistry,* 238**,** 40-45.

DOCHERTY, R. J., YEATS, J. C., BEVAN, S. & BODDEKE, H. W. 1996. Inhibition of calcineurin inhibits the desensitization of capsaicin-evoked currents in cultured dorsal root ganglion neurones from adult rats. *Pflugers Arch,* 431**,** 828-37.

DI MARZO, V., DE PETROCELLIS, L., SEPE, N. & BUONO, A. 1996. Biosynthesis of anandamide and related acylethanolamides in mouse J774 macrophages and N18 neuroblastoma cells. *Biochem J,* 316 (Pt 3)**,** 977-84.

CRAVATT, B. F., GIANG, D. K., MAYFIELD, S. P., BOGER, D. L., LERNER, R. A. & GILULA, N. B. 1996. Molecular characterization of an enzyme that degrades neuromodulatory fatty-acid amides. *Nature,* 384**,** 83-7.

CHILDERS, S. R. & DEADWYLER, S. A. 1996. Role of cyclic AMP in the actions of cannabinoid receptors. *Biochem Pharmacol,* 52**,** 819-27.

YU, M., IVES, D. & RAMESHA, C. S. 1997. Synthesis of Prostaglandin E2 Ethanolamide from Anandamide by Cyclooxygenase-2. *Journal of Biological Chemistry,* 272**,** 21181-21186.

THUMSER, A. E. A., VOYSEY, J. & WILTON, D. C. 1997a. A fluorescence displacement assay for the measurement of arachidonoyl ethanolamide (anandamide) and oleoyl amide (octadecenoamide) hydrolysis. *Biochemical Pharmacology,* 53**,** 433-435.

THUMSER, A. E., VOYSEY, J. & WILTON, D. C. 1997b. A fluorescence displacement assay for the measurement of arachidonoyl ethanolamide (anandamide) and oleoyl amide (octadecenoamide) hydrolysis. *Biochem Pharmacol,* 53**,** 433-5.

SUGIURA, T., KODAKA, T., KONDO, S., NAKANE, S., KONDO, H., WAKU, K., ISHIMA, Y., WATANABE, K. & YAMAMOTO, I. 1997. Is the cannabinoid CB1 receptor a 2-arachidonoylglycerol receptor? Structural requirements for triggering a Ca2+ transient in NG108-15 cells. *J Biochem,* 122**,** 890-5.

SHESKIN, T., HANUS, L., SLAGER, J., VOGEL, Z. & MECHOULAM, R. 1997. Structural requirements for binding of anandamide-type compounds to the brain cannabinoid receptor. *J Med Chem.* 1997/02/28 ed.

SCHMID, P. C., KUWAE, T., KREBSBACH, R. J. & SCHMID, H. H. 1997. Anandamide and other N-acylethanolamines in mouse peritoneal macrophages. *Chem Phys Lipids,* 87**,** 103-10.

MIRALLES, E., PRAT, D., COMPANO, R. & GRANADOS, M. 1997. Assessment of Different Fluorimetric Reactions for Cyanide Determination in Flow Systems. *Analyst,* 122**,** 553-558.

KOPLAS, P. A., ROSENBERG, R. L. & OXFORD, G. S. 1997. The role of calcium in the desensitization of capsaicin responses in rat dorsal root ganglion neurons. *J Neurosci,* 17**,** 3525-37.

GIANG, D. K. & CRAVATT, B. F. 1997. Molecular characterization of human and mouse fatty acid amide hydrolases. *Proceedings of the National Academy of Sciences,* 94**,** 2238-2242.

FORMAN, B. M., CHEN, J. & EVANS, R. M. 1997. Hypolipidemic drugs, polyunsaturated fatty acids, and eicosanoids are ligands for peroxisome proliferator-activated receptors alpha and delta. *Proc Natl Acad Sci U S A,* 94**,** 4312-7.

FILIPEANU, C. M., DE ZEEUW, D. & NELEMANS, S. A. 1997. Delta9-tetrahydrocannabinol activates [Ca2+]i increases partly sensitive to capacitative store refilling. *Eur J Pharmacol,* 336**,** R1-3.

DOCHERTY, R. J., YEATS, J. C. & PIPER, A. S. 1997. Capsazepine block of voltage-activated calcium channels in adult rat dorsal root ganglion neurones in culture. *British Journal of Pharmacology,* 121**,** 1461-1467.

CATERINA, M. J., SCHUMACHER, M. A., TOMINAGA, M., ROSEN, T. A., LEVINE, J. D. & JULIUS, D. 1997. The capsaicin receptor: a heat-activated ion channel in the pain pathway. *Nature,* 389**,** 816-24.

BURKEY, T. H., QUOCK, R. M., CONSROE, P., EHLERT, F. J., HOSOHATA, Y., ROESKE, W. R. & YAMAMURA, H. I. 1997. Relative efficacies of cannabinoid CB1 receptor agonists in the mouse brain. *European Journal of Pharmacology,* 336**,** 295-298.

BISOGNO, T., MAURELLI, S., MELCK, D., DE PETROCELLIS, L. & DI MARZO, V. 1997. Biosynthesis, Uptake, and Degradation of Anandamide and Palmitoylethanolamide in Leukocytes. *Journal of Biological Chemistry,* 272**,** 3315-3323.

BERDYSHEV, E. V., BOICHOT, E., GERMAIN, N., ALLAIN, N., ANGER, J. P. & LAGENTE, V. 1997. Influence of fatty acid ethanolamides and delta9-tetrahydrocannabinol on cytokine and arachidonate release by mononuclear cells. *Eur J Pharmacol,* 330**,** 231-40.

VUILLARD, L., RABILLOUD, T. & GOLDBERG, M. E. 1998. Interactions of non-detergent sulfobetaines with early folding intermediates facilitate in vitro protein renaturation. *Eur J Biochem,* 256**,** 128-35.

TOMINAGA, M., CATERINA, M. J., MALMBERG, A. B., ROSEN, T. A., GILBERT, H., SKINNER, K., RAUMANN, B. E., BASBAUM, A. I. & JULIUS, D. 1998. The cloned capsaicin receptor integrates multiple pain-producing stimuli. *Neuron,* 21**,** 531-43.

STRANGMAN, N. M., PATRICK, S. L., HOHMANN, A. G., TSOU, K. & WALKER, J. M. 1998. Evidence for a role of endogenous cannabinoids in the modulation of acute and tonic pain sensitivity. *Brain Res,* 813**,** 323-8.

SÁNCHEZ, C., GALVE-ROPERH, I., RUEDA, D. & GUZMÁN, M. 1998. Involvement of Sphingomyelin Hydrolysis and the Mitogen-Activated Protein Kinase Cascade in the Δ⁹-Tetrahydrocannabinol-Induced

Stimulation of Glucose Metabolism in Primary Astrocytes. *Molecular Pharmacology,* 54**,** 834-843.
MOLINA-HOLGADO, F., MOLINA-HOLGADO, E. & GUAZA, C. 1998. The endogenous cannabinoid anandamide potentiates interleukin-6 production by astrocytes infected with Theiler's murine encephalomyelitis virus by a receptor-mediated pathway. *FEBS Lett,* 433**,** 139-42.
MACCARRONE, M., VAN DER STELT, M., ROSSI, A., VELDINK, G. A., VLIEGENTHART, J. F. & AGRO, A. F. 1998. Anandamide hydrolysis by human cells in culture and brain. *J Biol Chem,* 273**,** 32332-9.
DE PETROCELLIS, L., MELCK, D., PALMISANO, A., BISOGNO, T., LAEZZA, C., BIFULCO, M. & DI MARZO, V. 1998a. The endogenous cannabinoid anandamide inhibits human breast cancer cell proliferation. *Proceedings of the National Academy of Sciences of the United States of America,* 95**,** 8375-8380.
DE PETROCELLIS, L., MELCK, D., PALMISANO, A., BISOGNO, T., LAEZZA, C., BIFULCO, M. & DI MARZO, V. 1998b. The endogenous cannabinoid anandamide inhibits human breast cancer cell proliferation. *Proc Natl Acad Sci U S A,* 95**,** 8375-80.
CHINETTI, G., GRIGLIO, S., ANTONUCCI, M., TORRA, I. P., DELERIVE, P., MAJD, Z., FRUCHART, J. C., CHAPMAN, J., NAJIB, J. & STAELS, B. 1998. Activation of proliferator-activated receptors alpha and gamma induces apoptosis of human monocyte-derived macrophages. *J Biol Chem,* 273**,** 25573-80.
BREIVOGEL, C. S., SELLEY, D. E. & CHILDERS, S. R. 1998. Cannabinoid receptor agonist efficacy for stimulating [35S]GTPgammaS binding to rat cerebellar membranes correlates with agonist-induced decreases in GDP affinity. *J Biol Chem,* 273**,** 16865-73.
BONHAUS, D. W., CHANG, L. K., KWAN, J. & MARTIN, G. R. 1998. Dual activation and inhibition of adenylyl cyclase by cannabinoid receptor agonists: evidence for agonist-specific trafficking of intracellular responses. *J Pharmacol Exp Ther,* 287**,** 884-8.
ZYGMUNT, P. M., PETERSSON, J., ANDERSSON, D. A., CHUANG, H.-H., SORGARD, M., DI MARZO, V., JULIUS, D. & HOGESTATT, E. D. 1999. Vanilloid receptors on sensory nerves mediate the vasodilator action of anandamide. *Nature,* 400**,** 452-457.
XU, H. E., LAMBERT, M. H., MONTANA, V. G., PARKS, D. J., BLANCHARD, S. G., BROWN, P. J., STERNBACH, D. D., LEHMANN, J. M., WISELY, G. B., WILLSON, T. M., KLIEWER, S. A. & MILBURN, M. V. 1999. Molecular recognition of fatty acids by peroxisome proliferator-activated receptors. *Mol Cell,* 3**,** 397-403.
WALKER, J. M., HUANG, S. M., STRANGMAN, N. M., TSOU, K. & SANUDO-PENA, M. C. 1999. Pain modulation by release of the endogenous cannabinoid anandamide. *Proc Natl Acad Sci U S A,* 96**,** 12198-203.
SUGIURA, T., KODAKA, T., NAKANE, S., MIYASHITA, T., KONDO, S., SUHARA, Y., TAKAYAMA, H., WAKU, K., SEKI, C., BABA, N. & ISHIMA, Y. 1999. Evidence that the cannabinoid CB1 receptor is a 2-arachidonoylglycerol receptor. Structure-activity relationship of 2-arachidonoylglycerol, ether-linked analogues, and related compounds. *J Biol Chem,* 274**,** 2794-801.
ROSS, R. A., BROCKIE, H. C., STEVENSON, L. A., MURPHY, V. L., TEMPLETON, F., MAKRIYANNIS, A. & PERTWEE, R. G. 1999. Agonist-inverse agonist characterization at CB1 and CB2 cannabinoid receptors of L759633, L759656, and AM630. *Br J Pharmacol,* 126**,** 665-72.
MOMBOULI, J. V., SCHAEFFER, G., HOLZMANN, S., KOSTNER, G. M. & GRAIER, W. F. 1999. Anandamide-induced mobilization of cytosolic Ca2+ in endothelial cells. *Br J Pharmacol,* 126**,** 1593-600.

MELCK, D., RUEDA, D., GALVE-ROPERH, I., DE PETROCELLIS, L., GUZMAN, M. & DI MARZO, V. 1999. Involvement of the cAMP/protein kinase A pathway and of mitogen-activated protein kinase in the anti-proliferative effects of anandamide in human breast cancer cells. *FEBS Lett,* 463**,** 235-40.

MACCARRONE, M., BARI, M. & AGRÒ, A. F. 1999. A Sensitive and Specific Radiochromatographic Assay of Fatty Acid Amide Hydrolase Activity. *Analytical Biochemistry,* 267**,** 314-318.

LAN, R., LIU, Q., FAN, P., LIN, S., FERNANDO, S. R., MCCALLION, D., PERTWEE, R. & MAKRIYANNIS, A. 1999. Structure-activity relationships of pyrazole derivatives as cannabinoid receptor antagonists. *J Med Chem,* 42**,** 769-76.

KAPUST, R. B. & WAUGH, D. S. 1999. Escherichia coli maltose-binding protein is uncommonly effective at promoting the solubility of polypeptides to which it is fused. *Protein Sci,* 8**,** 1668-74.

HILLARD, C. J., MANNA, S., GREENBERG, M. J., DICAMELLI, R., ROSS, R. A., STEVENSON, L. A., MURPHY, V., PERTWEE, R. G. & CAMPBELL, W. B. 1999. Synthesis and Characterization of Potent and Selective Agonists of the Neuronal Cannabinoid Receptor (CB1). *Journal of Pharmacology and Experimental Therapeutics,* 289**,** 1427.

GOPARAJU, S. K., KURAHASHI, Y., SUZUKI, H., UEDA, N. & YAMAMOTO, S. 1999. Anandamide amidohydrolase of porcine brain: cDNA cloning, functional expression and site-directed mutagenesis(1). *Biochim Biophys Acta,* 1441**,** 77-84.

GLASS, M. & NORTHUP, J. K. 1999. Agonist selective regulation of G proteins by cannabinoid CB(1) and CB(2) receptors. *Mol Pharmacol,* 56**,** 1362-9.

GIUFFRIDA, A., PARSONS, L. H., KERR, T. M., RODRIGUEZ DE FONSECA, F., NAVARRO, M. & PIOMELLI, D. 1999. Dopamine activation of endogenous cannabinoid signaling in dorsal striatum. *Nat Neurosci,* 2**,** 358-63.

GEBREMEDHIN, D., LANGE, A. R., CAMPBELL, W. B., HILLARD, C. J. & HARDER, D. R. 1999. Cannabinoid CB1 receptor of cat cerebral arterial muscle functions to inhibit L-type Ca2+ channel current. *Am J Physiol,* 276**,** H2085-93.

GARRINGTON, T. P. & JOHNSON, G. L. 1999. Organization and regulation of mitogen-activated protein kinase signaling pathways. *Curr Opin Cell Biol,* 11**,** 211-8.

BISOGNO, T., DELTON-VANDENBROUCKE, I., MILONE, A., LAGARDE, M. & DI MARZO, V. 1999. Biosynthesis and inactivation of N-arachidonoylethanolamine (anandamide) and N-docosahexaenoylethanolamine in bovine retina. *Arch Biochem Biophys,* 370**,** 300-7.

BANEYX, F. 1999. Recombinant protein expression in Escherichia coli. *Curr Opin Biotechnol,* 10**,** 411-21.

UEDA, N., PUFFENBARGER, R. A., YAMAMOTO, S. & DEUTSCH, D. G. 2000. The fatty acid amide hydrolase (FAAH). *Chem Phys Lipids,* 108**,** 107-21.

THIERINGER, R., FENYK-MELODY, J. E., LE GRAND, C. B., SHELTON, B. A., DETMERS, P. A., SOMERS, E. P., CARBIN, L., MOLLER, D. E., WRIGHT, S. D. & BERGER, J. 2000. Activation of peroxisome proliferator-activated receptor gamma does not inhibit IL-6 or TNF-alpha responses of macrophages to lipopolysaccharide in vitro or in vivo. *J Immunol,* 164**,** 1046-54.

ROSS, R. A., BROCKIE, H. C. & PERTWEE, R. G. 2000. Inhibition of nitric oxide production in RAW264.7 macrophages by cannabinoids and palmitoylethanolamide. *Eur J Pharmacol,* 401**,** 121-30.

OINONEN, C. & ROUVINEN, J. 2000. Structural comparison of Ntn-hydrolases. *Protein Science,* 9**,** 2329-2337.

MACCARRONE, M., LORENZON, T., BARI, M., MELINO, G. & FINAZZI-AGRO, A. 2000. Anandamide induces apoptosis in human cells via vanilloid receptors. Evidence for a protective role of cannabinoid receptors. *J Biol Chem,* 275**,** 31938-45.

LIU, J., GAO, B., MIRSHAHI, F., SANYAL, A. J., KHANOLKAR, A. D., MAKRIYANNIS, A. & KUNOS, G. 2000. Functional CB1 cannabinoid receptors in human vascular endothelial cells. *Biochem J,* 346 Pt 3**,** 835-40.

HWANG, S. W., CHO, H., KWAK, J., LEE, S.-Y., KANG, C.-J., JUNG, J., CHO, S., MIN, K. H., SUH, Y.-G., KIM, D. & OH, U. 2000. Direct activation of capsaicin receptors by products of lipoxygenases: Endogenous capsaicin-like substances. *Proceedings of the National Academy of Sciences of the United States of America,* 97**,** 6155-6160.

HARRIS, J., DREW, L. J. & CHAPMAN, V. 2000. Spinal anandamide inhibits nociceptive transmission via cannabinoid receptor activation in vivo. *Neuroreport,* 11**,** 2817-9.

GIUFFRIDA, A., RODRIGUEZ DE FONSECA, F. & PIOMELLI, D. 2000. Quantification of bioactive acylethanolamides in rat plasma by electrospray mass spectrometry. *Anal Biochem,* 280**,** 87-93.

DI MARZO, V., HILL, M. P., BISOGNO, T., CROSSMAN, A. R. & BROTCHIE, J. M. 2000. Enhanced levels of endogenous cannabinoids in the globus pallidus are associated with a reduction in movement in an animal model of Parkinson's disease. *FASEB J,* 14**,** 1432-8.

WOODWARD, D. F., KRAUSS, A. H., CHEN, J., LAI, R. K., SPADA, C. S., BURK, R. M., ANDREWS, S. W., SHI, L., LIANG, Y., KEDZIE, K. M., CHEN, R., GIL, D. W., KHARLAMB, A., ARCHEAMPONG, A., LING, J., MADHU, C., NI, J., RIX, P., USANSKY, J., USANSKY, H., WEBER, A., WELTY, D., YANG, W., TANG-LIU, D. D., GARST, M. E., BRAR, B., WHEELER, L. A. & KAPLAN, L. J. 2001. The pharmacology of bimatoprost (Lumigan). *Surv Ophthalmol,* 45 Suppl 4**,** S337-45.

WINSTON, J., TOMA, H., SHENOY, M. & PASRICHA, P. J. 2001. Nerve growth factor regulates VR-1 mRNA levels in cultures of adult dorsal root ganglion neurons. *Pain,* 89**,** 181-6.

VARMA, N., CARLSON, G. C., LEDENT, C. & ALGER, B. E. 2001. Metabotropic glutamate receptors drive the endocannabinoid system in hippocampus. *J Neurosci,* 21**,** RC188.

UEDA, N., YAMANAKA, K. & YAMAMOTO, S. 2001. Purification and characterization of an acid amidase selective for N-palmitoylethanolamine, a putative endogenous anti-inflammatory substance. *J Biol Chem,* 276**,** 35552-7.

TUCKER, R. C., KAGAYA, M., PAGE, C. P. & SPINA, D. 2001. The endogenous cannabinoid agonist, anandamide stimulates sensory nerves in guinea-pig airways. *Br J Pharmacol,* 132**,** 1127-35.

SANCHEZ, J. F., KRAUSE, J. E. & CORTRIGHT, D. N. 2001. The distribution and regulation of vanilloid receptor VR1 and VR1 5′ splice variant RNA expression in rat. *Neuroscience,* 107**,** 373-381.

RODRIGUEZ DE FONSECA, F., NAVARRO, M., GOMEZ, R., ESCUREDO, L., NAVA, F., FU, J., MURILLO-RODRIGUEZ, E., GIUFFRIDA, A., LOVERME, J., GAETANI, S., KATHURIA, S., GALL, C. & PIOMELLI, D. 2001. An anorexic lipid mediator regulated by feeding. *Nature,* 414**,** 209-12.

PEARSON, G., ROBINSON, F., BEERS GIBSON, T., XU, B. E., KARANDIKAR, M., BERMAN, K. & COBB, M. H. 2001. Mitogen-activated protein (MAP) kinase pathways: regulation and physiological functions. *Endocr Rev,* 22**,** 153-83.

OLIVER, W. R., JR., SHENK, J. L., SNAITH, M. R., RUSSELL, C. S., PLUNKET, K. D., BODKIN, N. L., LEWIS, M. C., WINEGAR, D. A., SZNAIDMAN, M. L., LAMBERT, M. H., XU, H. E., STERNBACH, D. D., KLIEWER, S. A., HANSEN,

B. C. & WILLSON, T. M. 2001. A selective peroxisome proliferator-activated receptor delta agonist promotes reverse cholesterol transport. *Proc Natl Acad Sci U S A,* 98**,** 5306-11.

MACCARRONE, M., DE PETROCELLIS, L., BARI, M., FEZZA, F., SALVATI, S., DI MARZO, V. & FINAZZI-AGRÒ, A. 2001. Lipopolysaccharide Downregulates Fatty Acid Amide Hydrolase Expression and Increases Anandamide Levels in Human Peripheral Lymphocytes. *Archives of Biochemistry and Biophysics,* 393**,** 321-328.

KUHLENCORDT, P. J., CHEN, J., HAN, F., ASTERN, J. & HUANG, P. L. 2001. Genetic deficiency of inducible nitric oxide synthase reduces atherosclerosis and lowers plasma lipid peroxides in apolipoprotein E-knockout mice. *Circulation,* 103**,** 3099-104.

KOBAYASHI, Y., ARAI, S., WAKU, K. & SUGIURA, T. 2001. Activation by 2-arachidonoylglycerol, an endogenous cannabinoid receptor ligand, of p42/44 mitogen-activated protein kinase in HL-60 cells. *J Biochem,* 129**,** 665-9.

JAGGAR, S. I., SCOTT, H. C., JAMES, I. F. & RICE, A. S. 2001. The capsaicin analogue SDZ249-665 attenuates the hyper-reflexia and referred hyperalgesia associated with inflammation of the rat urinary bladder. *Pain,* 89**,** 229-35.

HUESTIS, M. A., GORELICK, D. A., HEISHMAN, S. J., PRESTON, K. L., NELSON, R. A., MOOLCHAN, E. T. & FRANK, R. A. 2001. Blockade of effects of smoked marijuana by the CB1-selective cannabinoid receptor antagonist SR141716. *Arch Gen Psychiatry,* 58**,** 322-8.

DE PETROCELLIS, L., DAVIS, J. B. & DI MARZO, V. 2001. Palmitoylethanolamide enhances anandamide stimulation of human vanilloid VR1 receptors. *FEBS Letters,* 506**,** 253-256.

BERGER, A., CROZIER, G., BISOGNO, T., CAVALIERE, P., INNIS, S. & DI MARZO, V. 2001. Anandamide and diet: inclusion of dietary arachidonate and docosahexaenoate leads to increased brain levels of the corresponding N-acylethanolamines in piglets. *Proc Natl Acad Sci U S A,* 98**,** 6402-6.

BERDYSHEV, E. V., SCHMID, P. C., KREBSBACH, R. J., HILLARD, C. J., HUANG, C., CHEN, N., DONG, Z. & SCHMID, H. H. O. 2001. Cannabinoid-receptor-independent cell signalling by N-acylethanolamines. *Biochemical Journal,* 360**,** 67-75.

BANTAN-POLAK, T., KASSAI, M. & GRANT, K. B. 2001. A Comparison of Fluorescamine and Naphthalene-2,3-dicarboxaldehyde Fluorogenic Reagents for Microplate-Based Detection of Amino Acids. *Analytical Biochemistry,* 297**,** 128-136.

WU, J. & CUNNICK, J. M. 2002. Trans-regulation of epidermal growth factor receptor by lysophosphatidic acid and G protein-coupled receptors. *Biochimica et Biophysica Acta (BBA) - Molecular and Cell Biology of Lipids,* 1582**,** 100-106.

SUGIURA, T., KOBAYASHI, Y., OKA, S. & WAKU, K. 2002. Biosynthesis and degradation of anandamide and 2-arachidonoylglycerol and their possible physiological significance. *Prostaglandins, Leukotrienes and Essential Fatty Acids,* 66**,** 173-192.

SMART, D., JONSSON, K. O., VANDEVOORDE, S., LAMBERT, D. M. & FOWLER, C. J. 2002. 'Entourage' effects of N-acyl ethanolamines at human vanilloid receptors. Comparison of effects upon anandamide-induced vanilloid receptor activation and upon anandamide metabolism. *Br J Pharmacol,* 136**,** 452-8.

SCHUEL, H., BURKMAN, L. J., LIPPES, J., CRICKARD, K., FORESTER, E., PIOMELLI, D. & GIUFFRIDA, A. 2002. N-Acylethanolamines in human reproductive fluids. *Chemistry and Physics of Lipids,* 121**,** 211-227.

RUEDA, D., NAVARRO, B., MARTINEZ-SERRANO, A., GUZMAN, M. & GALVE-ROPERH, I. 2002. The endocannabinoid anandamide inhibits neuronal progenitor cell differentiation through attenuation of the Rap1/B-Raf/ERK pathway. *J Biol Chem,* 277**,** 46645-50.

PAROLARO, D., MASSI, P., RUBINO, T. & MONTI, E. 2002. Endocannabinoids in the immune system and cancer. *Prostaglandins Leukot Essent Fatty Acids,* 66**,** 319-32.

MACCARRONE, M., CARTONI, A., PAROLARO, D., MARGONELLI, A., MASSI, P., BARI, M., BATTISTA, N. & FINAZZI-AGRO, A. 2002. Cannabimimetic activity, binding, and degradation of stearoylethanolamide within the mouse central nervous system. *Mol Cell Neurosci,* 21**,** 126-40.

LICHTMAN, A. H., VARVEL, S. A. & MARTIN, B. R. 2002. Endocannabinoids in cognition and dependence. *Prostaglandins Leukot Essent Fatty Acids,* 66**,** 269-85.

KIM, J., ISOKAWA, M., LEDENT, C. & ALGER, B. E. 2002. Activation of Muscarinic Acetylcholine Receptors Enhances the Release of Endogenous Cannabinoids in the Hippocampus. *The Journal of Neuroscience,* 22**,** 10182-10191.

JOOST, P. & METHNER, A. 2002. Phylogenetic analysis of 277 human G-protein-coupled receptors as a tool for the prediction of orphan receptor ligands. *Genome Biol,* 3**,** RESEARCH0063.

HOWLETT, A. C., BARTH, F., BONNER, T. I., CABRAL, G., CASELLAS, P., DEVANE, W. A., FELDER, C. C., HERKENHAM, M., MACKIE, K., MARTIN, B. R., MECHOULAM, R. & PERTWEE, R. G. 2002. International Union of Pharmacology. XXVII. Classification of cannabinoid receptors. *Pharmacol Rev,* 54**,** 161-202.

GALVE-ROPERH, I., RUEDA, D., GOMEZ DEL PULGAR, T., VELASCO, G. & GUZMAN, M. 2002. Mechanism of extracellular signal-regulated kinase activation by the CB(1) cannabinoid receptor. *Mol Pharmacol,* 62**,** 1385-92.

DI MARZO, V., BLUMBERG, P. M. & SZALLASI, A. 2002. Endovanilloid signaling in pain. *Curr Opin Neurobiol,* 12**,** 372-9.

COSTA, B., CONTI, S., GIAGNONI, G. & COLLEONI, M. 2002. Therapeutic effect of the endogenous fatty acid amide, palmitoylethanolamide, in rat acute inflammation: inhibition of nitric oxide and cyclo-oxygenase systems. *Br J Pharmacol,* 137**,** 413-20.

CONTI, S., COSTA, B., COLLEONI, M., PAROLARO, D. & GIAGNONI, G. 2002. Antiinflammatory action of endocannabinoid palmitoylethanolamide and the synthetic cannabinoid nabilone in a model of acute inflammation in the rat. *Br J Pharmacol,* 135**,** 181-7.

CHRISTOPOULOS, A. & KENAKIN, T. 2002. G protein-coupled receptor allosterism and complexing. *Pharmacol Rev,* 54**,** 323-74.

BHAVE, G., ZHU, W., WANG, H., BRASIER, D. J., OXFORD, G. S. & GEREAU, R. W. 2002. cAMP-Dependent Protein Kinase Regulates Desensitization of the Capsaicin Receptor (VR1) by Direct Phosphorylation. *Neuron,* 35**,** 721-731.

ZORATTI, C., KIPMEN-KORGUN, D., OSIBOW, K., MALLI, R. & GRAIER, W. F. 2003. Anandamide initiates Ca(2+) signaling via CB(2) receptor linked to phospholipase C in calf pulmonary endothelial cells. *British Journal of Pharmacology,* 140**,** 1351-1362.

VILLAVERDE, A. & CARRIO, M. M. 2003. Protein aggregation in recombinant bacteria: biological role of inclusion bodies. *Biotechnol Lett,* 25**,** 1385-95.

PRESCOTT, E. D. & JULIUS, D. 2003. A modular PIP2 binding site as a determinant of capsaicin receptor sensitivity. *Science,* 300**,** 1284-8.

KATHURIA, S., GAETANI, S., FEGLEY, D., VALINO, F., DURANTI, A., TONTINI, A., MOR, M., TARZIA, G., LA RANA, G., CALIGNANO, A., GIUSTINO, A., TATTOLI, M., PALMERY, M., CUOMO, V. & PIOMELLI, D. 2003. Modulation of anxiety through blockade of anandamide hydrolysis. *Nat Med,* 9**,** 76-81.

GINGOLD, A. R. & BERGASA, N. V. 2003. The cannabinoid agonist WIN 55, 212-2 increases nociception threshold in cholestatic rats: implications for the treatment of the pruritus of cholestasis. *Life Sciences,* 73**,** 2741-2747.

GAETANI, S., CUOMO, V. & PIOMELLI, D. 2003. Anandamide hydrolysis: a new target for anti-anxiety drugs? *Trends Mol Med,* 9**,** 474-8.

FU, J., GAETANI, S., OVEISI, F., LO VERME, J., SERRANO, A., RODRIGUEZ DE FONSECA, F., ROSENGARTH, A., LUECKE, H., DI GIACOMO, B., TARZIA, G. & PIOMELLI, D. 2003. Oleylethanolamide regulates feeding and body weight through activation of the nuclear receptor PPAR-[alpha]. *Nature,* 425**,** 90-93.

CHEN, C. W., LEE, S. T., WU, W. T., FU, W. M., HO, F. M. & LIN, W. W. 2003. Signal transduction for inhibition of inducible nitric oxide synthase and cyclooxygenase-2 induction by capsaicin and related analogs in macrophages. *Br J Pharmacol,* 140**,** 1077-87.

AHERN, G. P. 2003. Activation of TRPV1 by the satiety factor oleoylethanolamide. *J Biol Chem,* 278**,** 30429-34.

WALTER, L., DINH, T. & STELLA, N. 2004. ATP Induces a Rapid and Pronounced Increase in 2-Arachidonoylglycerol Production by Astrocytes, a Response Limited by Monoacylglycerol Lipase. *The Journal of Neuroscience,* 24**,** 8068-8074.

SCHICHO, R., FLORIAN, W., LIEBMANN, I., HOLZER, P. & LIPPE, I. T. 2004. Increased expression of TRPV1 receptor in dorsal root ganglia by acid insult of the rat gastric mucosa. *Eur J Neurosci,* 19**,** 1811-8.

SAGHATELIAN, A., TRAUGER, S. A., WANT, E. J., HAWKINS, E. G., SIUZDAK, G. & CRAVATT, B. F. 2004a. Assignment of Endogenous Substrates to Enzymes by Global Metabolite Profiling. *Biochemistry,* 43**,** 14332-14339.

SAGHATELIAN, A., TRAUGER, S. A., WANT, E. J., HAWKINS, E. G., SIUZDAK, G. & CRAVATT, B. F. 2004b. Assignment of endogenous substrates to enzymes by global metabolite profiling. *Biochemistry,* 43**,** 14332-9.

ROCKWELL, C. E. & KAMINSKI, N. E. 2004. A Cyclooxygenase Metabolite of Anandamide Causes Inhibition of Interleukin-2 Secretion in Murine Splenocytes. *Journal of Pharmacology and Experimental Therapeutics,* 311**,** 683-690.

OKAMOTO, Y., MORISHITA, J., TSUBOI, K., TONAI, T. & UEDA, N. 2004. Molecular characterization of a phospholipase D generating anandamide and its congeners. *J Biol Chem,* 279**,** 5298-305.

MOR, M., RIVARA, S., LODOLA, A., PLAZZI, P. V., TARZIA, G., DURANTI, A., TONTINI, A., PIERSANTI, G., KATHURIA, S. & PIOMELLI, D. 2004. Cyclohexylcarbamic acid 3'- or 4'-substituted biphenyl-3-yl esters as fatty acid amide hydrolase inhibitors: synthesis, quantitative structure-activity relationships, and molecular modeling studies. *J Med Chem,* 47**,** 4998-5008.

GUZMAN, M., LO VERME, J., FU, J., OVEISI, F., BLAZQUEZ, C. & PIOMELLI, D. 2004. Oleoylethanolamide stimulates lipolysis by activating the nuclear receptor peroxisome proliferator-activated receptor alpha (PPAR-alpha). *J Biol Chem,* 279**,** 27849-54.

FERRÉ, P. 2004. The Biology of Peroxisome Proliferator-Activated Receptors. *Diabetes,* 53**,** S43.

DINIS, P., CHARRUA, A., AVELINO, A., YAQOOB, M., BEVAN, S., NAGY, I. & CRUZ, F. 2004. Anandamide-evoked activation of vanilloid receptor 1 contributes

to the development of bladder hyperreflexia and nociceptive transmission to spinal dorsal horn neurons in cystitis. *J Neurosci,* 24**,** 11253-63.
CONTASSOT, E., WILMOTTE, R., TENAN, M., BELKOUCH, M. C., SCHNURIGER, V., DE TRIBOLET, N., BURKHARDT, K. & DIETRICH, P. Y. 2004a. Arachidonylethanolamide induces apoptosis of human glioma cells through vanilloid receptor-1. *J Neuropathol Exp Neurol,* 63**,** 956-63.
CONTASSOT, E., TENAN, M., SCHNURIGER, V., PELTE, M. F. & DIETRICH, P. Y. 2004b. Arachidonyl ethanolamide induces apoptosis of uterine cervix cancer cells via aberrantly expressed vanilloid receptor-1. *Gynecol Oncol,* 93**,** 182-8.
BOLDRUP, L., WILSON, S. J., BARBIER, A. J. & FOWLER, C. J. 2004. A simple stopped assay for fatty acid amide hydrolase avoiding the use of a chloroform extraction phase. *Journal of Biochemical and Biophysical Methods,* 60**,** 171-177.
XU, H., BLAIR, N. T. & CLAPHAM, D. E. 2005. Camphor activates and strongly desensitizes the transient receptor potential vanilloid subtype 1 channel in a vanilloid-independent mechanism. *J Neurosci,* 25**,** 8924-37.
WANG, X., MIYARES, R. L. & AHERN, G. P. 2005. Oleoylethanolamide excites vagal sensory neurones, induces visceral pain and reduces short-term food intake in mice via capsaicin receptor TRPV1. *The Journal of Physiology,* 564**,** 541-547.
SUN, Y.-X., TSUBOI, K., ZHAO, L.-Y., OKAMOTO, Y., LAMBERT, D. M. & UEDA, N. 2005. Involvement of N-acylethanolamine-hydrolyzing acid amidase in the degradation of anandamide and other N-acylethanolamines in macrophages. *Biochimica et Biophysica Acta (BBA) - Molecular and Cell Biology of Lipids,* 1736**,** 211-220.
SMITH, K. R., PINKERTON, K. E., WATANABE, T., PEDERSEN, T. L., MA, S. J. & HAMMOCK, B. D. 2005. Attenuation of tobacco smoke-induced lung inflammation by treatment with a soluble epoxide hydrolase inhibitor. *Proceedings of the National Academy of Sciences of the United States of America,* 102**,** 2186-2191.
RAMARAO, M. K., MURPHY, E. A., SHEN, M. W., WANG, Y., BUSHELL, K. N., HUANG, N., PAN, N., WILLIAMS, C. & CLARK, J. D. 2005. A fluorescence-based assay for fatty acid amide hydrolase compatible with high-throughput screening. *Anal Biochem,* 343**,** 143-51.
PRICE, M. R., BAILLIE, G. L., THOMAS, A., STEVENSON, L. A., EASSON, M., GOODWIN, R., MCLEAN, A., MCINTOSH, L., GOODWIN, G., WALKER, G., WESTWOOD, P., MARRS, J., THOMSON, F., COWLEY, P., CHRISTOPOULOS, A., PERTWEE, R. G. & ROSS, R. A. 2005. Allosteric modulation of the cannabinoid CB1 receptor. *Mol Pharmacol,* 68**,** 1484-95.
POBLETE, I. M., ORLIAC, M. L., BRIONES, R., ADLER-GRASCHINSKY, E. & HUIDOBRO-TORO, J. P. 2005. Anandamide elicits an acute release of nitric oxide through endothelial TRPV1 receptor activation in the rat arterial mesenteric bed. *J Physiol,* 568**,** 539-51.
PERTWEE, R. G. 2005. Pharmacological actions of cannabinoids. *Handb Exp Pharmacol***,** 1-51.
PERRON-SAVARD, P., DE CRESCENZO, G. & MOUAL, H. L. 2005. Dimerization and DNA binding of the Salmonella enterica PhoP response regulator are phosphorylation independent. *Microbiology,* 151**,** 3979-3987.
PACHER, P., BÁTKAI, S. & KUNOS, G. 2005. Cardiovascular Pharmacology of Cannabinoids. *Handbook of experimental pharmacology***,** 599-625.
OZ, M., ALPTEKIN, A., TCHUGUNOVA, Y. & DINC, M. 2005. Effects of saturated long-chain N-acylethanolamines on voltage-dependent Ca2+ fluxes in rabbit T-tubule membranes. *Arch Biochem Biophys,* 434**,** 344-51.

MOVAHED, P., JONSSON, B. A., BIRNIR, B., WINGSTRAND, J. A., JORGENSEN, T. D., ERMUND, A., STERNER, O., ZYGMUNT, P. M. & HOGESTATT, E. D. 2005. Endogenous unsaturated C18 N-acylethanolamines are vanilloid receptor (TRPV1) agonists. *J Biol Chem,* 280**,** 38496-504.

LO VERME, J., FU, J., ASTARITA, G., LA RANA, G., RUSSO, R., CALIGNANO, A. & PIOMELLI, D. 2005. The nuclear receptor peroxisome proliferator-activated receptor-alpha mediates the anti-inflammatory actions of palmitoylethanolamide. *Mol Pharmacol,* 67**,** 15-9.

LIU, B., ZHANG, C. & QIN, F. 2005. Functional recovery from desensitization of vanilloid receptor TRPV1 requires resynthesis of phosphatidylinositol 4,5-bisphosphate. *J Neurosci,* 25**,** 4835-43.

LAUCKNER, J. E., HILLE, B. & MACKIE, K. 2005. The cannabinoid agonist WIN55,212-2 increases intracellular calcium via CB1 receptor coupling to Gq/11 G proteins. *Proc Natl Acad Sci U S A,* 102**,** 19144-9.

HOLT, S., COMELLI, F., COSTA, B. & FOWLER, C. J. 2005. Inhibitors of fatty acid amide hydrolase reduce carrageenan-induced hind paw inflammation in pentobarbital-treated mice: comparison with indomethacin and possible involvement of cannabinoid receptors. *Br J Pharmacol,* 146**,** 467-76.

FEGLEY, D., GAETANI, S., DURANTI, A., TONTINI, A., MOR, M., TARZIA, G. & PIOMELLI, D. 2005. Characterization of the fatty acid amide hydrolase inhibitor cyclohexyl carbamic acid 3'-carbamoyl-biphenyl-3-yl ester (URB597): effects on anandamide and oleoylethanolamide deactivation. *J Pharmacol Exp Ther,* 313**,** 352-8.

DOMENICALI, M., ROS, J., FERNANDEZ-VARO, G., CEJUDO-MARTIN, P., CRESPO, M., MORALES-RUIZ, M., BRIONES, A. M., CAMPISTOL, J. M., ARROYO, V., VILA, E., RODES, J. & JIMENEZ, W. 2005. Increased anandamide induced relaxation in mesenteric arteries of cirrhotic rats: role of cannabinoid and vanilloid receptors. *Gut,* 54**,** 522-7.

DICKINS, R. A., HEMANN, M. T., ZILFOU, J. T., SIMPSON, D. R., IBARRA, I., HANNON, G. J. & LOWE, S. W. 2005. Probing tumor phenotypes using stable and regulated synthetic microRNA precursors. *Nature Genetics,* 37**,** 1289.

DE BANK, P. A., KENDALL, D. A. & ALEXANDER, S. P. 2005. A spectrophotometric assay for fatty acid amide hydrolase suitable for high-throughput screening. *Biochem Pharmacol,* 69**,** 1187-93.

CHEN, H., KOVAR, J., SISSONS, S., COX, K., MATTER, W., CHADWELL, F., LUAN, P., VLAHOS, C. J., SCHUTZ-GESCHWENDER, A. & OLIVE, D. M. 2005. A cell-based immunocytochemical assay for monitoring kinase signaling pathways and drug efficacy. *Anal Biochem,* 338**,** 136-42.

BOUABOULA, M., HILAIRET, S., MARCHAND, J., FAJAS, L., LE FUR, G. & CASELLAS, P. 2005. Anandamide induced PPARgamma transcriptional activation and 3T3-L1 preadipocyte differentiation. *Eur J Pharmacol,* 517**,** 174-81.

WEI, B. Q., MIKKELSEN, T. S., MCKINNEY, M. K., LANDER, E. S. & CRAVATT, B. F. 2006. A second fatty acid amide hydrolase with variable distribution among placental mammals. *J Biol Chem,* 281**,** 36569-78.

PIOMELLI, D., TARZIA, G., DURANTI, A., TONTINI, A., MOR, M., COMPTON, T. R., DASSE, O., MONAGHAN, E. P., PARROTT, J. A. & PUTMAN, D. 2006. Pharmacological profile of the selective FAAH inhibitor KDS-4103 (URB597). *CNS Drug Rev,* 12**,** 21-38.

PERTWEE, R. G. 2006. Cannabinoid pharmacology: the first 66 years. *British Journal of Pharmacology,* 147**,** S163-S171.

OVERTON, H. A., BABBS, A. J., DOEL, S. M., FYFE, M. C. T., GARDNER, L. S., GRIFFIN, G., JACKSON, H. C., PROCTER, M. J., RASAMISON, C. M., TANG-CHRISTENSEN, M., WIDDOWSON, P. S., WILLIAMS, G. M. & REYNET, C. 2006. Deorphanization of a G protein-coupled receptor for

oleoylethanolamide and its use in the discovery of small-molecule hypophagic agents. *Cell Metabolism,* 3**,** 167-175.
LOVERME, J., RUSSO, R., LA RANA, G., FU, J., FARTHING, J., MATTACE-RASO, G., MELI, R., HOHMANN, A., CALIGNANO, A. & PIOMELLI, D. 2006. Rapid broad-spectrum analgesia through activation of peroxisome proliferator-activated receptor-alpha. *J Pharmacol Exp Ther,* 319**,** 1051-61.
LIZANECZ, E., BAGI, Z., PÁSZTOR, E. T., PAPP, Z., ÉDES, I., KEDEI, N., BLUMBERG, P. M. & TÓTH, A. 2006. Phosphorylation-Dependent Desensitization by Anandamide of Vanilloid Receptor-1 (TRPV1) Function in Rat Skeletal Muscle Arterioles and in Chinese Hamster Ovary Cells Expressing TRPV1. *Molecular Pharmacology,* 69**,** 1015-1023.
LEUNG, D., SAGHATELIAN, A., SIMON, G. M. & CRAVATT, B. F. 2006. Inactivation of N-acyl phosphatidylethanolamine phospholipase D reveals multiple mechanisms for the biosynthesis of endocannabinoids. *Biochemistry,* 45**,** 4720-6.
KIM, S. R., KIM, S. U., OH, U. & JIN, B. K. 2006. Transient receptor potential vanilloid subtype 1 mediates microglial cell death in vivo and in vitro via Ca2+-mediated mitochondrial damage and cytochrome c release. *J Immunol,* 177**,** 4322-9.
JOBGEN, W. S., FRIED, S. K., FU, W. J., MEININGER, C. J. & WU, G. 2006. Regulatory role for the arginine-nitric oxide pathway in metabolism of energy substrates. *J Nutr Biochem,* 17**,** 571-88.
GRAHAM, E. S., BALL, N., SCOTTER, E. L., NARAYAN, P., DRAGUNOW, M. & GLASS, M. 2006. Induction of Krox-24 by endogenous cannabinoid type 1 receptors in Neuro2A cells is mediated by the MEK-ERK MAPK pathway and is suppressed by the phosphatidylinositol 3-kinase pathway. *J Biol Chem,* 281**,** 29085-95.
ESPOSITO, D. & CHATTERJEE, D. K. 2006. Enhancement of soluble protein expression through the use of fusion tags. *Curr Opin Biotechnol,* 17**,** 353-8.
DEMUTH, D. G. & MOLLEMAN, A. 2006. Cannabinoid signalling. *Life Sci,* 78**,** 549-63.
CLAPPER, J. R., DURANTI, A., TONTINI, A., MOR, M., TARZIA, G. & PIOMELLI, D. 2006. The fatty-acid amide hydrolase inhibitor URB597 does not affect triacylglycerol hydrolysis in rat tissues. *Pharmacological Research,* 54**,** 341-344.
ZHAO, L.-Y., TSUBOI, K., OKAMOTO, Y., NAGAHATA, S. & UEDA, N. 2007. Proteolytic activation and glycosylation of N-acylethanolamine-hydrolyzing acid amidase, a lysosomal enzyme involved in the endocannabinoid metabolism. *Biochimica et Biophysica Acta (BBA) - Molecular and Cell Biology of Lipids,* 1771**,** 1397-1405.
SUN, Y., ALEXANDER, S. P., GARLE, M. J., GIBSON, C. L., HEWITT, K., MURPHY, S. P., KENDALL, D. A. & BENNETT, A. J. 2007. Cannabinoid activation of PPAR alpha; a novel neuroprotective mechanism. *Br J Pharmacol,* 152**,** 734-43.
SUARDÍAZ, M., ESTIVILL-TORRÚS, G., GOICOECHEA, C., BILBAO, A. & RODRÍGUEZ DE FONSECA, F. 2007. Analgesic properties of oleoylethanolamide (OEA) in visceral and inflammatory pain. *PAIN®,* 133**,** 99-110.
SAUNDERS, C. I., KUNDE, D. A., CRAWFORD, A. & GERAGHTY, D. P. 2007. Expression of transient receptor potential vanilloid 1 (TRPV1) and 2 (TRPV2) in human peripheral blood. *Mol Immunol,* 44**,** 1429-35.
O'SULLIVAN, S. E. 2007. Cannabinoids go nuclear: evidence for activation of peroxisome proliferator-activated receptors. *Br J Pharmacol,* 152**,** 576-82.
MATTA, J. A., MIYARES, R. L. & AHERN, G. P. 2007. TRPV1 is a novel target for omega-3 polyunsaturated fatty acids. *J Physiol,* 578**,** 397-411.

HSU, S. S., HUANG, C. J., CHENG, H. H., CHOU, C. T., LEE, H. Y., WANG, J. L., CHEN, I. S., LIU, S. I., LU, Y. C., CHANG, H. T., HUANG, J. K., CHEN, J. S. & JAN, C. R. 2007. Anandamide-induced Ca2+ elevation leading to p38 MAPK phosphorylation and subsequent cell death via apoptosis in human osteosarcoma cells. *Toxicology,* 231**,** 21-9.

HORSWILL, J. G., BALI, U., SHAABAN, S., KEILY, J. F., JEEVARATNAM, P., BABBS, A. J., REYNET, C. & WONG KAI IN, P. 2007. PSNCBAM-1, a novel allosteric antagonist at cannabinoid CB(1) receptors with hypophagic effects in rats. *British Journal of Pharmacology,* 152**,** 805-814.

BORTOLATO, M., MANGIERI, R. A., FU, J., KIM, J. H., ARGUELLO, O., DURANTI, A., TONTINI, A., MOR, M., TARZIA, G. & PIOMELLI, D. 2007. Antidepressant-like activity of the fatty acid amide hydrolase inhibitor URB597 in a rat model of chronic mild stress. *Biol Psychiatry,* 62**,** 1103-10.

BATKAI, S., OSEI-HYIAMAN, D., PAN, H., EL-ASSAL, O., RAJESH, M., MUKHOPADHYAY, P., HONG, F., HARVEY-WHITE, J., JAFRI, A., HASKO, G., HUFFMAN, J. W., GAO, B., KUNOS, G. & PACHER, P. 2007. Cannabinoid-2 receptor mediates protection against hepatic ischemia/reperfusion injury. *FASEB J,* 21**,** 1788-800.

WOOD, J. A. T., WILLIAMS, J. S., PANDARINATHAN, L., COURVILLE, A., KEPLINGER, M. R., JANERO, D. R., VOUROS, P., MAKRIYANNIS, A. & LAMMI-KEEFE, C. J. 2008. Comprehensive profiling of the human circulating endocannabinoid metabolome: clinical sampling and sample storage parameters. *Clin Chem Lab Med,* 46**,** 1289-95.

SVIZENSKA, I., DUBOVY, P. & SULCOVA, A. 2008. Cannabinoid receptors 1 and 2 (CB1 and CB2), their distribution, ligands and functional involvement in nervous system structures--a short review. *Pharmacol Biochem Behav,* 90**,** 501-11.

MULLER, M. Q., ROTH, C., STRATER, N. & SINZ, A. 2008. Expression and purification of the ligand-binding domain of peroxisome proliferator-activated receptor alpha (PPARalpha). *Protein Expr Purif,* 62**,** 185-9.

HORVATH, G., KEKESI, G., NAGY, E. & BENEDEK, G. 2008. The role of TRPV1 receptors in the antinociceptive effect of anandamide at spinal level. *Pain,* 134**,** 277-84.

HO, W. S., BARRETT, D. A. & RANDALL, M. D. 2008. 'Entourage' effects of N-palmitoylethanolamide and N-oleoylethanolamide on vasorelaxation to anandamide occur through TRPV1 receptors. *British Journal of Pharmacology,* 155**,** 837-846.

HEGDE, V. L., HEGDE, S., CRAVATT, B. F., HOFSETH, L. J., NAGARKATTI, M. & NAGARKATTI, P. S. 2008. Attenuation of experimental autoimmune hepatitis by exogenous and endogenous cannabinoids: involvement of regulatory T cells. *Mol Pharmacol,* 74**,** 20-33.

DALLE CARBONARE, M., DEL GIUDICE, E., STECCA, A., COLAVITO, D., FABRIS, M., D'ARRIGO, A., BERNARDINI, D., DAM, M. & LEON, A. 2008. A Saturated N-Acylethanolamine Other than N-Palmitoyl Ethanolamine with Anti-inflammatory Properties: a Neglected Story…. *Journal of Neuroendocrinology,* 20**,** 26-34.

DALLAIRE, P., BELLMANN, K., LAPLANTE, M., GELINAS, S., CENTENO-BAEZ, C., PENFORNIS, P., PEYOT, M. L., LATOUR, M. G., LAMONTAGNE, J., TRUJILLO, M. E., SCHERER, P. E., PRENTKI, M., DESHAIES, Y. & MARETTE, A. 2008. Obese mice lacking inducible nitric oxide synthase are sensitized to the metabolic actions of peroxisome proliferator-activated receptor-gamma agonism. *Diabetes,* 57**,** 1999-2011.

DAIGLE, T. L., KEARN, C. S. & MACKIE, K. 2008. Rapid CB1 cannabinoid receptor desensitization defines the time course of ERK1/2 MAP kinase signaling. *Neuropharmacology,* 54**,** 36-44.

BISOGNO, T. 2008. Endogenous cannabinoids: structure and metabolism. *J Neuroendocrinol.* 2008/05/09 ed.

BARISH, G. D., ATKINS, A. R., DOWNES, M., OLSON, P., CHONG, L. W., NELSON, M., ZOU, Y., HWANG, H., KANG, H., CURTISS, L., EVANS, R. M. & LEE, C. H. 2008. PPARdelta regulates multiple proinflammatory pathways to suppress atherosclerosis. *Proc Natl Acad Sci U S A,* 105**,** 4271-6.

ASTARITA, G., AHMED, F. & PIOMELLI, D. 2008. Identification of biosynthetic precursors for the endocannabinoid anandamide in the rat brain. *J Lipid Res,* 49**,** 48-57.

ARTMANN, A., PETERSEN, G., HELLGREN, L. I., BOBERG, J., SKONBERG, C., NELLEMANN, C., HANSEN, S. H. & HANSEN, H. S. 2008a. Influence of dietary fatty acids on endocannabinoid and N-acylethanolamine levels in rat brain, liver and small intestine. *Biochim Biophys Acta,* 1781.

ARTMANN, A., PETERSEN, G., HELLGREN, L. I., BOBERG, J., SKONBERG, C., NELLEMANN, C., HANSEN, S. H. & HANSEN, H. S. 2008b. Influence of dietary fatty acids on endocannabinoid and N-acylethanolamine levels in rat brain, liver and small intestine. *Biochim Biophys Acta,* 1781**,** 200-12.

SOLORZANO, C., ZHU, C., BATTISTA, N., ASTARITA, G., LODOLA, A., RIVARA, S., MOR, M., RUSSO, R., MACCARRONE, M., ANTONIETTI, F., DURANTI, A., TONTINI, A., CUZZOCREA, S., TARZIA, G. & PIOMELLI, D. 2009. Selective N-acylethanolamine-hydrolyzing acid amidase inhibition reveals a key role for endogenous palmitoylethanolamide in inflammation. *Proceedings of the National Academy of Sciences of the United States of America,* 106**,** 20966-20971.

SCHILLING, T. & EDER, C. 2009. Importance of the non-selective cation channel TRPV1 for microglial reactive oxygen species generation. *J Neuroimmunol,* 216**,** 118-21.

RAJALINGAM, D., LOFTIS, C., XU, J. J. & KUMAR, T. K. S. 2009. Trichloroacetic acid-induced protein precipitation involves the reversible association of a stable partially structured intermediate. *Protein Sci,* 18**,** 980-93.

PATWARDHAN, A. M., SCOTLAND, P. E., AKOPIAN, A. N. & HARGREAVES, K. M. 2009. Activation of TRPV1 in the spinal cord by oxidized linoleic acid metabolites contributes to inflammatory hyperalgesia. *Proceedings of the National Academy of Sciences of the United States of America,* 106**,** 18820-18824.

UEDA, N., TSUBOI, K. & UYAMA, T. 2010. N-acylethanolamine metabolism with special reference to N-acylethanolamine-hydrolyzing acid amidase (NAAA). *Prog Lipid Res,* 49**,** 299-315.

LORÍA, F., PETROSINO, S., HERNANGÓMEZ, M., MESTRE, L., SPAGNOLO, A., CORREA, F., DI MARZO, V., DOCAGNE, F. & GUAZA, C. 2010. An endocannabinoid tone limits excitotoxicity in vitro and in a model of multiple sclerosis. *Neurobiology of Disease,* 37**,** 166-176.

KACZOCHA, M., GLASER, S. T., CHAE, J., BROWN, D. A. & DEUTSCH, D. G. 2010. Lipid droplets are novel sites of N-acylethanolamine inactivation by fatty acid amide hydrolase-2. *J Biol Chem,* 285**,** 2796-806.

JOOSTEN, M. M., BALVERS, M. G., VERHOECKX, K. C., HENDRIKS, H. F. & WITKAMP, R. F. 2010. Plasma anandamide and other N-acylethanolamines are correlated with their corresponding free fatty acid levels under both fasting and non-fasting conditions in women. *Nutrition & Metabolism,* 7**,** 1-6.

BROWN, I., CASCIO, M. G., WAHLE, K. W., SMOUM, R., MECHOULAM, R., ROSS, R. A., PERTWEE, R. G. & HEYS, S. D. 2010. Cannabinoid receptor-dependent and -independent anti-proliferative effects of omega-3 ethanolamides in androgen receptor-positive and -negative prostate cancer cell lines. *Carcinogenesis,* 31**,** 1584-91.

BALVERS, M. G., VERHOECKX, K. C., PLASTINA, P., WORTELBOER, H. M., MEIJERINK, J. & WITKAMP, R. F. 2010. Docosahexaenoic acid and eicosapentaenoic acid are converted by 3T3-L1 adipocytes to N-acyl ethanolamines with anti-inflammatory properties. *Biochim Biophys Acta,* 1801**,** 1107-14.

MEIJERINK, J., PLASTINA, P., VINCKEN, J. P., POLAND, M., ATTYA, M., BALVERS, M., GRUPPEN, H., GABRIELE, B. & WITKAMP, R. F. 2011. The ethanolamide metabolite of DHA, docosahexaenoylethanolamine, shows immunomodulating effects in mouse peritoneal and RAW264.7 macrophages: evidence for a new link between fish oil and inflammation. *Br J Nutr,* 105**,** 1798-807.

KIM, H. Y., MOON, H. S., CAO, D., LEE, J., KEVALA, K., JUN, S. B., LOVINGER, D. M., AKBAR, M. & HUANG, B. X. 2011. N-Docosahexaenoylethanolamide promotes development of hippocampal neurons. *Biochem J,* 435**,** 327-36.

JOHNSON, D. S., STIFF, C., LAZERWITH, S. E., KESTEN, S. R., FAY, L. K., MORRIS, M., BEIDLER, D., LIIMATTA, M. B., SMITH, S. E., DUDLEY, D. T., SADAGOPAN, N., BHATTACHAR, S. N., KESTEN, S. J., NOMANBHOY, T. K., CRAVATT, B. F. & AHN, K. 2011. Discovery of PF-04457845: A Highly Potent, Orally Bioavailable, and Selective Urea FAAH Inhibitor. *ACS Medicinal Chemistry Letters,* 2**,** 91-96.

CALDER, P. C. 2011. Fatty acids and inflammation: the cutting edge between food and pharma. *Eur J Pharmacol,* 668 Suppl 1**,** S50-8.

BYSTROM, J., WRAY, J. A., SUGDEN, M. C., HOLNESS, M. J., SWALES, K. E., WARNER, T. D., EDIN, M. L., ZELDIN, D. C., GILROY, D. W. & BISHOP-BAILEY, D. 2011. Endogenous Epoxygenases Are Modulators of Monocyte/Macrophage Activity. *PLoS ONE,* 6**,** e26591.

BROWN, I., WAHLE, K. W., CASCIO, M. G., SMOUM-JAOUNI, R., MECHOULAM, R., PERTWEE, R. G. & HEYS, S. D. 2011. Omega-3 N-acylethanolamines are endogenously synthesised from omega-3 fatty acids in different human prostate and breast cancer cell lines. *Prostaglandins Leukot Essent Fatty Acids,* 85**,** 305-10.

BRAILOIU, G. C., OPREA, T. I., ZHAO, P., ABOOD, M. E. & BRAILOIU, E. 2011. Intracellular cannabinoid type 1 (CB1) receptors are activated by anandamide. *J Biol Chem,* 286**,** 29166-74.

ASIMAKI, O. & MANGOURA, D. 2011. Cannabinoid receptor 1 induces a biphasic ERK activation via multiprotein signaling complex formation of proximal kinases PKCε, Src, and Fyn in primary neurons. *Neurochemistry International,* 58**,** 135-144.

AHN, K., SMITH, S. E., LIIMATTA, M. B., BEIDLER, D., SADAGOPAN, N., DUDLEY, D. T., YOUNG, T., WREN, P., ZHANG, Y., SWANEY, S., VAN BECELAERE, K., BLANKMAN, J. L., NOMURA, D. K., BHATTACHAR, S. N., STIFF, C., NOMANBHOY, T. K., WEERAPANA, E., JOHNSON, D. S. & CRAVATT, B. F. 2011. Mechanistic and pharmacological characterization of PF-04457845: a highly potent and selective fatty acid amide hydrolase inhibitor that reduces inflammatory and noninflammatory pain. *J Pharmacol Exp Ther,* 338**,** 114-24.

MERIGHI, S., GESSI, S., VARANI, K., SIMIONI, C., FAZZI, D., MIRANDOLA, P. & BOREA, P. A. 2012. Cannabinoid CB(2) receptors modulate ERK-1/2 kinase

signalling and NO release in microglial cells stimulated with bacterial lipopolysaccharide. *Br J Pharmacol,* 165**,** 1773-1788.
LI, G. L., WINTER, H., ARENDS, R., JAY, G. W., LE, V., YOUNG, T. & HUGGINS, J. P. 2012. Assessment of the pharmacology and tolerability of PF-04457845, an irreversible inhibitor of fatty acid amide hydrolase-1, in healthy subjects. *British Journal of Clinical Pharmacology,* 73**,** 706-716.
HUGGINS, J. P., SMART, T. S., LANGMAN, S., TAYLOR, L. & YOUNG, T. 2012. An efficient randomised, placebo-controlled clinical trial with the irreversible fatty acid amide hydrolase-1 inhibitor PF-04457845, which modulates endocannabinoids but fails to induce effective analgesia in patients with pain due to osteoarthritis of the knee. *Pain,* 153**,** 1837-46.
HIMI, N., HAMAGUCHI, A., HASHIMOTO, K., KOGA, T., NARITA, K. & MIYAMOTO, O. 2012. Calcium influx through the TRPV1 channel of endothelial cells (ECs) correlates with a stronger adhesion between monocytes and ECs. *Adv Med Sci,* 57**,** 224-9.
ADHIKARY, S., KOCIEDA, V. P., YEN, J. H., TUMA, R. F. & GANEA, D. 2012. Signaling through cannabinoid receptor 2 suppresses murine dendritic cell migration by inhibiting matrix metalloproteinase 9 expression. *Blood,* 120**,** 3741-9.
ROVITO, D., GIORDANO, C., VIZZA, D., PLASTINA, P., BARONE, I., CASABURI, I., LANZINO, M., DE AMICIS, F., SISCI, D., MAURO, L., AQUILA, S., CATALANO, S., BONOFIGLIO, D. & ANDO, S. 2013. Omega-3 PUFA ethanolamides DHEA and EPEA induce autophagy through PPARgamma activation in MCF-7 breast cancer cells. *J Cell Physiol,* 228**,** 1314-22.
PATERNITI, I., IMPELLIZZERI, D., CRUPI, R., MORABITO, R., CAMPOLO, M., ESPOSITO, E. & CUZZOCREA, S. 2013. Molecular evidence for the involvement of PPAR-delta and PPAR-gamma in anti-inflammatory and neuroprotective activities of palmitoylethanolamide after spinal cord trauma. *J Neuroinflammation,* 10**,** 20.
ISHIDA, T., NISHIUMI, S., TANAHASHI, T., YAMASAKI, A., YAMAZAKI, A., AKASHI, T., MIKI, I., KONDO, Y., INOUE, J., KAWAUCHI, S., AZUMA, T., YOSHIDA, M. & MIZUNO, S. 2013. Linoleoyl ethanolamide reduces lipopolysaccharide-induced inflammation in macrophages and ameliorates 2,4-dinitrofluorobenzene-induced contact dermatitis in mice. *European Journal of Pharmacology,* 699**,** 6-13.
FONSECA, B. M., COSTA, M. A., ALMADA, M., CORREIA-DA-SILVA, G. & TEIXEIRA, N. A. 2013. Endogenous cannabinoids revisited: a biochemistry perspective. *Prostaglandins Other Lipid Mediat,* 102-103**,** 13-30.
FIGUEROA, J. D., CORDERO, K., SERRANO-ILLAN, M., ALMEYDA, A., BALDEOSINGH, K., ALMAGUEL, F. G. & DE LEON, M. 2013. Metabolomics uncovers dietary omega-3 fatty acid-derived metabolites implicated in anti-nociceptive responses after experimental spinal cord injury. *Neuroscience,* 255**,** 1-18.
COSTA, S. J., ALMEIDA, A., CASTRO, A., DOMINGUES, L. & BESIR, H. 2013. The novel Fh8 and H fusion partners for soluble protein expression in Escherichia coli: a comparison with the traditional gene fusion technology. *Appl Microbiol Biotechnol,* 97**,** 6779-91.
BAILLIE, G. L., HORSWILL, J. G., ANAVI-GOFFER, S., REGGIO, P. H., BOLOGNINI, D., ABOOD, M. E., MCALLISTER, S., STRANGE, P. G., STEPHENS, G. J., PERTWEE, R. G. & ROSS, R. A. 2013. CB(1) receptor allosteric modulators display both agonist and signaling pathway specificity. *Mol Pharmacol,* 83**,** 322-38.
YU, S., LEVI, L., CASADESUS, G., KUNOS, G. & NOY, N. 2014. Fatty acid-binding protein 5 (FABP5) regulates cognitive function both by decreasing

anandamide levels and by activating the nuclear receptor peroxisome proliferator-activated receptor beta/delta (PPARbeta/delta) in the brain. *J Biol Chem,* 289**,** 12748-58.

KIM, J., CARLSON, M. E. & WATKINS, B. A. 2014. Docosahexaenoyl ethanolamide improves glucose uptake and alters endocannabinoid system gene expression in proliferating and differentiating C2C12 myoblasts. *Front Physiol,* 5**,** 100.

HYE KHAN, M. A., PAVLOV, T. S., CHRISTAIN, S. V., NECKAR, J., STARUSCHENKO, A., GAUTHIER, K. M., CAPDEVILA, J. H., FALCK, J. R., CAMPBELL, W. B. & IMIG, J. D. 2014. Epoxyeicosatrienoic acid analogue lowers blood pressure through vasodilation and sodium channel inhibition. *Clin Sci (Lond),* 127**,** 463-74.

TSUBOI, K., OKAMOTO, Y., RAHMAN, I. A., UYAMA, T., INOUE, T., TOKUMURA, A. & UEDA, N. 2015. Glycerophosphodiesterase GDE4 as a novel lysophospholipase D: a possible involvement in bioactive N-acylethanolamine biosynthesis. *Biochim Biophys Acta,* 1851**,** 537-48.

MEIJERINK, J., POLAND, M., BALVERS, M. G., PLASTINA, P., LUTE, C., DWARKASING, J., VAN NORREN, K. & WITKAMP, R. F. 2015. Inhibition of COX-2-mediated eicosanoid production plays a major role in the anti-inflammatory effects of the endocannabinoid N-docosahexaenoylethanolamine (DHEA) in macrophages. *Br J Pharmacol,* 172**,** 24-37.

ERDOZAIN, A. M., RUBIO, M., VALDIZAN, E. M., PAZOS, A., MEANA, J. J., FERNANDEZ-RUIZ, J., ALEXANDER, S. P. & CALLADO, L. F. 2015. The endocannabinoid system is altered in the post-mortem prefrontal cortex of alcoholic subjects. *Addict Biol,* 20**,** 773-83.

PAWSEY, S., WOOD, M., BROWNE, H., DONALDSON, K., CHRISTIE, M. & WARRINGTON, S. 2016. Safety, Tolerability and Pharmacokinetics of FAAH Inhibitor V158866: A Double-Blind, Randomised, Placebo-Controlled Phase I Study in Healthy Volunteers. *Drugs R D,* 16**,** 181-91.

O'SULLIVAN, S. E. 2016. An update on PPAR activation by cannabinoids. *Br J Pharmacol,* 173**,** 1899-910.

KAUR, R., SIDHU, P. & SINGH, S. 2016. What failed BIA 10–2474 Phase I clinical trial? Global speculations and recommendations for future Phase I trials. *Journal of Pharmacology & Pharmacotherapeutics,* 7**,** 120-126.

ENDO, J. & ARITA, M. 2016. Cardioprotective mechanism of omega-3 polyunsaturated fatty acids. *J Cardiol,* 67**,** 22-7.

DELGADO-PERAZA, F., AHN, K. H., NOGUERAS-ORTIZ, C., MUNGRUE, I. N., MACKIE, K., KENDALL, D. A. & YUDOWSKI, G. A. 2016. Mechanisms of Biased beta-Arrestin-Mediated Signaling Downstream from the Cannabinoid 1 Receptor. *Mol Pharmacol,* 89**,** 618-29.

VAN ESBROECK, A. C. M., JANSSEN, A. P. A., COGNETTA, A. B., 3RD, OGASAWARA, D., SHPAK, G., VAN DER KROEG, M., KANTAE, V., BAGGELAAR, M. P., DE VRIJ, F. M. S., DENG, H., ALLARA, M., FEZZA, F., LIN, Z., VAN DER WEL, T., SOETHOUDT, M., MOCK, E. D., DEN DULK, H., BAAK, I. L., FLOREA, B. I., HENDRIKS, G., DE PETROCELLIS, L., OVERKLEEFT, H. S., HANKEMEIER, T., DE ZEEUW, C. I., DI MARZO, V., MACCARRONE, M., CRAVATT, B. F., KUSHNER, S. A. & VAN DER STELT, M. 2017. Activity-based protein profiling reveals off-target proteins of the FAAH inhibitor BIA 10-2474. *Science,* 356**,** 1084-1087.

PRIESTLEY, R., GLASS, M. & KENDALL, D. 2017a. Chapter Six - Functional Selectivity at Cannabinoid Receptors. *In:* KENDALL, D. & ALEXANDER, S. P. H. (eds.) *Advances in Pharmacology.* Academic Press.

PRIESTLEY, R., GLASS, M. & KENDALL, D. 2017b. Functional Selectivity at Cannabinoid Receptors. *Adv Pharmacol,* 80**,** 207-221.
MCDOUGLE, D. R., WATSON, J. E., ABDEEN, A. A., ADILI, R., CAPUTO, M. P., KRAPF, J. E., JOHNSON, R. W., KILIAN, K. A., HOLINSTAT, M. & DAS, A. 2017. Anti-inflammatory omega-3 endocannabinoid epoxides. *Proc Natl Acad Sci U S A,* 114**,** E6034-E6043.
GABRIELSSON, L., GOUVEIA-FIGUEIRA, S., HAGGSTROM, J., ALHOUAYEK, M. & FOWLER, C. J. 2017. The anti-inflammatory compound palmitoylethanolamide inhibits prostaglandin and hydroxyeicosatetraenoic acid production by a macrophage cell line. *Pharmacol Res Perspect,* 5**,** e00300.
ALHOUAYEK, M., BOTTEMANNE, P., MAKRIYANNIS, A. & MUCCIOLI, G. G. 2017. N-acylethanolamine-hydrolyzing acid amidase and fatty acid amide hydrolase inhibition differentially affect N-acylethanolamine levels and macrophage activation. *Biochim Biophys Acta,* 1862**,** 474-484.
LAYE, S., NADJAR, A., JOFFRE, C. & BAZINET, R. P. 2018. Anti-Inflammatory Effects of Omega-3 Fatty Acids in the Brain: Physiological Mechanisms and Relevance to Pharmacology. *Pharmacol Rev,* 70**,** 12-38.